The Origin of Intraplate Volcanism on the New Zealand micro-continent Zealandia

Dissertation
zur Erlangung des Doktorgrades
an der Mathematischen-Naturwissenschaftlichen Fakultät
der Christian-Albrechts-Universität
zu Kiel

vorgelegt von
Christian Timm

Kiel
2008

Hiermit erkläre ich, dass ich die vorliegende Doktorarbeit selbständig und ohne unerlaubte Hilfen erstellt habe. Ferner habe ich weder diese noch eine ähnliche Arbeit an einer anderen Abteilung oder Hochschule im Rahmen eines Prüfungsverfahrens vorgelegt, veröffentlicht oder zur Veröffentlichung vorgelegt.

……..
Christian Timm

Referent/in……Prof. Dr. Kaj Hoernle, Ph.D.

Koreferent/in……Prof. Dr. Colin Devey

Tag der mündlichen Prüfung……04.07.2008

Zum Druck genehmigt: Kiel, ……

Prof. Dr. J. Grotemeyer (Dekan)

Kurzfassung

Der Ursprung von Intraplatten-Vulkanismus wird hauptsächlich mittels einer stationären thermalen Anomalie unterhalb der Lithosphäre (Mantel Plume), oder durch kontinentales „Rifting“ erklärt. Diese beiden Prozesse sind oftmals mit voluminösem Vulkanismus assoziiert. Der langlebige und diffus auftretende Vulkanismus auf dem Neuseeländischen Mikro-Kontinent, Zealandia, hingegen kann nicht durch diese Theorien erklärt werden und wird in dieser Dissertation genauer untersucht. Bis in die mittlere Kreidezeit (~ 100 Mio. Jahre) stellte Zealandia einen Teil im NW des ehemaligen Superkontinents Gondwana dar und lag über einer aktiven Subduktionszone. Subduktionbezogener Vulkanismus endete allerdings zwischen 100 – 90 Mio Jahren mit der beginnenden Separation Zealandias von Gondwana. Das beginnende Auseinanderdriften der beiden Landmassen ging einher mir voluminösem Intraplatten-Vulkanismus. Seitdem ist Zealandia ca. 6000 km im Bezug auf den darunter liegenden Mantel nach NW zur heutigen Position gedriftet. Das gesamte Känozoikum hindurch trat diffus über das Plateau Zealandias verteilt Intraplatten-Vulkanismus in Form von monogenetischen vulkanischen Feldern und Schildvulkanen auf. Die mafische Känozoischen Vulkangesteine (MgO > 5 Gew %) ähneln Ozean Insel Basalten und liegen auf Isotopendiagrammen zwischen den Mantelendgliedern MORB, EMII, und HIMU, was auf fundamental unterschiedliche Bildungsgeschichten dieser vulkanischen Gesteine hindeutet. Anhand der seismischen Tomographie ist unterhalb des östlichen Teils von Zealandia ein Bereich mit niedrigeren seismischen Wellengeschwindigkeiten (höchstwahrscheinlich heiß) zwischen ~600 und 1450 km entdeckt worden, die sich bis in die Antarktis verfolgen lässt. Die Isotopensignaturen der Känozoischen Vulkangesteine lassen sich durch eine Mischung der HIMU-artigen kreidezeitlichen vulkanischen Gesteine mit der verarmten (MORB-ähnlichen) oberen Asthenosphäre erklären. Daher liegt die Vermutung nahe, dass der unterhalb von 600 km auftretende Plume, der zur Separation Zealandias von Gondwana beitrug, den oberen Mantel mit primitiven

„Plume-Domänen“ versehen hat und die Känozoischen Vulkangesteine demnach höchstwahrscheinlich Mischschmelzen aus diesen beiden Endgliedern darstellen. Die EMII-typ Isotopensignaturen hingegen deuten auf die Interaktion der tief gebildeten asthenosphärischen Schmelzen mit der darüber liegenden kontinentalen Lithosphäre (Mantel, metasomatiert durch Subduktion im Mesozoikum und Kruste) hin. Ein möglicher Prozess zur eigentlichen Schmelzbildung unterhalb Zealandias ist jedoch lithosphärische Delamination durch Rayleigh-Taylor Instabilitäten. Die Bildung von Rayleigh-Taylor Instabilitäten entlang des Übergangs von dichterer unterer Lithosphäre und weniger dichter oberer Asthenosphäre führt zum Aufströmen von warmen asthenosphärischem Mantel und dadurch zur Bildung dekompressiver Schmelzen.

Abstract

The origin of intraplate volcanism has been predominately attributed to a stationary thermal anomaly beneath the lithosphere (mantle plume) or to continental rifting. Both mechanisms generally result in voluminous volcanic activity. However, diffusely and continuously occurring low-volume intraplate volcanism on the New Zealand micro-continent, Zealandia is inconsistent with these processes. Until the mid-Cretaceous Zealandia was part of the former super-continent Gondwana, situated at its NW margin above an active subduction zone. Subduction ended at ~ 100 Ma and volcanism changed from subduction- to rift-related as Zealandia started to separate from Gondwana, which was associated with voluminous eruptions until ~ 90 Ma. Since the final separation of Zealandia from Gondwana, the micro-continent drifted ~ 6000 km to the NW with respect to the upper asthenosphere to its recent position. During the Cenozoic diffuse intraplate volcanism occurred randomly distributed on the continental plateau, forming two volcanic endmembers: 1) monogenetic volcanic fields and 2) composite shield volcanoes. The mafic Cenozoic volcanic rocks of these volcanic centers (MgO > 5wt %) are strongly akin to ocean island basalts and plot between three isotopic endmembers: MORB, HIMU and EMII, suggesting fundamental differences in the formation of these volcanic rocks.

Seismic tomography reveals a low velocity zone (most likely hot) between ~600 and 1450 km beneath Zealandia, which can be traced to Antarctica. Since mixing of the HIMU-type Cretaceous volcanic rocks with depleted MORB can explain most of the isotopic compositions of the Cenozoic lavas, the deep-seated plume (which possibly contributed to the separation Zealandias from Gondwana) polluted the depleted upper asthenospheric mantle (MORB) with fertile (HIMU-type) domains. The EMII-type isotopic signature in some of the volcanic reflects interaction (partly extensively) of the asthenospheric melts with continental lithospheric (mantle, metasomatized by subduction during the Mesozoic and crust). A possible mechanism to trigger partial melts, however is lithospheric removal by Rayleigh-

Taylor instabilities. The downwelling of a dense lower lithosphere allowed the warm and less dense upper asthenosphere to stream into the resulting cavities and form partial melts by decompression.

Vorwort

Diese Arbeit stellt in Ihrer Gesamtheit eine monographische Dissertation dar, die aus vier unabhängigen Kapiteln besteht (Chapter I-IV).

Diese Arbeit entstand auf Anregung durch Prof. Dr. Kaj Hoernle, welche im Rahmen der durch die Deutsche Forschungsgemeinschaft geförderten Projekte HO1833/12-1 und HO1833/12-2 durchgeführt wurden. Ihm gilt mein besonderer Dank für die Vergabe dieser Arbeit, seine Unterstützung, progressive Diskussionen und wichtige Denkanstösse und vor allem, den roten Faden nicht zu verlieren!
Prof. Dr. Colin Devey möchte ich für die Übernahme des Koreferats danken.

Ein Weiterer besonderer Dank gilt Dr.F. Hauff, Dr. J. Fietzke, Dr. P vd Bogaard und Dipl.-Ing. J. Sticklus, S. Hauff für Ihre Assistenz und unschätzbarer Hilfe bei der Isotopenanalytik, ohne deren Unterstützung von technischer Seite, wie auch bei der Datenauswertung, die Durchführung der Dissertation nicht möglich gewesen wäre. Dagmar Rau danke ich für die RFA Analytik. Außerdem bin ich dem IFM-GEOMAR für die Kostenübernahme der “In-House” Analytik (Hauptelement- und Sr-Nd-Pb-Hf Isotopenanalytik) zu großem Dank verpflichtet, denn ohne die Übernahme dieser Kosten wäre diese Arbeit nicht möglich gewesen.

Dr. J. Geldmachen, Dr. S. Duggen und Dr. M. Portnyagin danke ich für Ihre Diskussionsbereitschaft und hilfreichen und stimulierenden Kommentare.

Desweiteren danke ich Dieter Garbe-Schönberg und seinem Team, insbesondere Ulrike Westernströer, Petra Fiedler, Heidi Blaschek und Inge Dold für Ihre Unterstützung bei der Probenaufbereitung für die ICP-MS Analytik.

Spezieller Dank geht an das PGP Team und Prof. Yuri Podlachikov in Oslo, welches mir zu einem tollen Aufenthalt in Oslo (März/April 2007) ermöglicht hat und hier insbesondere and die Doktoranden WG (Karthik, Christoph, Marcin und Karen), genauso wie Lars Rüpke und Timm John. Ebenso bin ich dankbar für den tollen Neuseelandaufenthalt (Februar-April 2005) und hier insbesondere Andrea Todt für die nette Beherbergung in Dunedin und Dr. James White von der University of Otago für die Reparatur des defekten Getriebes...

Für Ihre Hilfe als Hiwis möchte ich mich bei Christoph Marshall, David Rose, Jochen Kollofrath und Anna Erichsen bedanken.

Ken Heydolph, Nikolaus Bigalke, Jens Schneider, Rieka Harders, Mathias Marquardt, Sebastian Münn, Brian Haley und Gerd Lube (und natürlich allen anderen die dabei waren auch) gilt mein Dank für die vielen netten Stunden in der Mensa, die guten und unterhaltsamen Gespräche, Kaffeepausen etc.. Hier sei insbesondere der SFB Kaffee hervorgehoben...

Mein größter Dank allerdings geht an meine Eltern und insbesondere an meine werdende eigene Familie und hier natürlich an meine Jule, die mir unendlich viel Kraft gegeben und meine Launen zum Ende der Arbeit hin geduldig ertragen hat. Vielen Dank!

Content

Kurzfassung……I

Abstract…….III

Vorwort……..V

List of Figures……...XI

List of Tables……...XII

Chapter I

1.1 Geological frame..…….1

1.2. Brief overview of the mantle structure and composition…….3

1.3 Outline of the thesis and future perspectives…..……...4

Chapter II

Geochemical Evolution of Intraplate Volcanism at Banks Peninsula, New Zealand: Mantle Melts versus Crustal Contamination

Abstract…..……...12

2.1 Introduction..……...13

2.2 Geological Background……...14

2.3. Analytical Methods……17

2.4 Results…….19

2.4.1 Age Determinations…….19

2.4.2 Geochemistry……...21

2.5 Discussion……...35

2.5.1 Temporal and Geochemical
Evolution of the Banks Peninsula Volcanoes……..35

2.5.2 General Geochemical Characteristics of Banks Peninsula Volcanic Rocks……37

2.5.3 Akaroa low-silica group: Eclogite/Pyroxenite melting in upwelling asthenosphere……...38

2.5.4 Low-silica Diamond Harbour Volcanic Group Rocks: Evidence for Eclogite/Pyroxenite melting beneath both volcanoes……..42

2.5.5 Lyttelton high-silica group: Lithospheric Contamination……...43

2.5.6 High-silica Diamond Harbour Volcanic Group Rocks: Strongest lithospheric signature……..47

2.6 Dynamic model for the magmatic evolution of Banks Peninsula……..47

2.7 Conclusion……..51

Acknowledgements……..52

References……..……..52

Chapter III

Magmatic Evolution of Intraplate Volcanism on the New Zealand Micro-continent Zealandia

Abstract……..……..59

3.1 Introduction……..…..60

3.2 Tectonic Background of Zealandia since the Cretaceous……..……60

3.3 Evolution of Cenozoic Magmatism and Sample Background……...……64

3.4 Sampling and Analytical Methods…..……70

3.5 Results……72

3.5.1 Age Dating……..72

3.5.2 Geochemistry of Cenozoic intraplate volcanic rocks from Zealandia……77

3.5.2.1 Major and Trace elements……..……..77

3.5.2.2 Sr - Nd - Hf - Pb Isotope Data…..……81

3.6 Discussion……..…….....87

3.6.1 Late Cretaceous Volcanism on Zealandia……...87

3.6.2 Cenozoic Volcanism……..…….88

3.6.3 Source characteristics of intraplate volcanic rocks from Zealandia……..…….……..91

3.6.3.1 Low-Silica Mafic Volcanic Rocks - Partial melting of upwelling heterogeneous asthenosphere…….94

3.6.3.2 High-Silica Mafic volcanic rocks – contribution of the lithosphere (mantle and crust) …….....97

3.6.4 Evaluation of previously proposed models for the origin of the Cenozoic intraplate volcanism……..101

3.6.5 Towards a combined Model to explain the Cenozoic intraplate volcanism on Zealandia…….....105

3.7 Conclusion……..108

Acknowledgments……110

References……110

Chapter IV

Melting processes by Rayleigh-Taylor instabilities beneath Continents: Evidence from Cenozoic intraplate volcanism on Zealandia, SW Pacific

Abstract……136

4.1 Introduction……....136

4.2 Geological and Geochemical Background…….137

4.3 Lithospheric delamination…….....140

4.4 Model Setup……...143

4.5 Results……....144

4.5.1 Temporal and spatial evolution of the Rayleigh-Taylor instabilities…….....144

4.5.2 Partial melting by Raleigh-Taylor instabilities and the influence of H_2O……146

4.6 Discussion…….....152

4.6.1 Melting beneath continents triggered by Rayleigh-Taylor instabilities: the Zealandia synthesis……..152

4.7 Conclusion…….....155

Acknowledgement…….....156

References…….....156

Appendices……i

I.I XRF Standards……..i

I.II ICPMS Standards……ii

II Selceted Conference Abstracts…….……iii

III CV……...vii

List of Figures

1.1 Schematic cartoon of the mantle…….....2

2.1 Schematic map of Banks Peninsula……...14
2.2 Total Alkalies (Na_2O+K_2O wt%) vs. SiO_2 (wt%) diagram….……..22
2.3 Selected major and trace elements versus MgO (wt%).……....32
2.4 Multi-element diagrams……....33
2.5 Sr-Nd-Pb-Hf and O isotopic relationships……....34
2.6 Temporal evolution of the Banks Peninsula…….....36
2.7 SiO_2 (wt%) versus FeO^t (wt%)..……..39
2.8 Selected trace element ratios…….....40
2.9 Selected trace element and isotope ratios versus SiO_2 (wt%).……...41
2.10 Sr-Nd and O isotope relationships……..44
2.11 $^{206}Pb/^{204}Pb$ vs. $^{207}Pb/^{204}Pb$ and 1/Pb versus $^{207}Pb/^{204}Pb$…….…...46
2.12 Schematic model…….....49

3.1 Bathymetric map of Zealandia……..61
3.2 Age distribution of intraplate volcanic centers of Zealandia……64
3.3 Bathymetric maps of selected submarine Cenozoic volcanic centers……...69
3.4 Histogram of our $^{40}Ar/^{39}Ar$ database…….....73
3.5 Total Alkalies (Na_2O+K_2O wt%) vs. SiO_2 (wt%) diagram ……..78
3.6 Selected major elements versus MgO (wt%).……...79
3.7 Multi-element diagram…….....80
3.8 Sr-Nd-Hf isotope diagram……..…..82
3.9 Age distribution of the intraplate volcanic centers……...90
3.10 Pb, Sr and Nd versus $^{206}Pb/^{204}Pb$ isotope correlation diagrams..……....91
3.11 $(Sm/Yb)_N$ versus Zr/Hf…….....96
3.12 Selected trace element ratios……..98
3.13 Calculated age profiles……..103
3.14 Schematic box model……107

4.1 Schematic map of Zealandia……...138

4.2 Rayleigh-Taylor growth rates…….142
4.3 Model setup…….144
4.4 Model run with peridotite melting……..148
4.5 Model run with pyroxenite melting…….....150
4.6 Age versus $^{143}Nd/^{144}Nd_{initial}$…….153

List of Tables

2.1 $^{40}Ar/^{39}Ar$ age determinations of Banks Peninsula volcanic rocks……....20
2.2 Major and trace element analyses of Banks Peninsula volcanic rocks……....23
2.3 Isotope analyses Banks Peninsula volcanic rocks……....31
2.4 EC-AFC modeling parameter……..45

3.1 $^{40}Ar/^{39}Ar$ determinations from Zealandia……..……....75
3.2 Isotope analyses from Zealandia…….83
3.3 Major and trace element analyses from Zealandia……....120

Appendices

1. Analytical accuracy of major and trace element analyses…….....i
2. Conference Abstracts……...iii
3. CV (in German)…….....vii

Chapter I

Introduction

1.1 Geological frame

Areas of volcanic activity represent windows to the deeper earth, where volcanic and magma forms through partial melting of the upper mantle and is subsequently transported to the surface. The study of volcanic and magmatic rocks gives the possibility to better understand the processes related to volcanism and magmatism and therefore to get an insight of the earths dynamics.

Three different settings where melts are generated in the mantle are known. The most prominent and productive area of volcanic activity (in terms of erupted volumes) are the world spanning mid ocean ridges, having a total length of ~60,000km and add ~3 km^3yr^{-1} of new basaltic lava to the oceanic crust (plus ~18 km^3yr^{-1} of new plutonic rocks; Wilson, 1989). At mid ocean ridges partial melts are generated along an active diverging plate boundary in response to adiabatic decompression of mostly depleted peridotite in a narrow zone of upwelling. The partial melts, when cooled, form new oceanic crust. The second areas, where major volcanism occurs are above subduction zones (production rate of ~0.4–8 km^3yr^{-1}; Wilson, 1989). Along subduction zones an oceanic plate dives beneath another, forming in response the deepest areas on the ocean floor, such as the Mariana and Tonga trench. Magmatic activity at subduction zones occur predominantly through dehydration of the sinking slab, releasing its fluids to the mantle wedge, which lowers the solidus and subsequently form partial melts. Characteristic surface expression of a subduction zone are arcuate or linear chains of islands or volcanoes parallel to the trench, such as the Tongan Islands and the volcanic front in America, extending from Alaska to southern Chile. These two major processes are directly coupled to plate tectonics, where new plate is formed at the mid ocean ridges and older plates are recycled back into the mantle at subduction zones. Nevertheless, a considerable amount of volcanism (0.03–2 km^3yr^{-1}; Wilson, 1989) is not confined to plate boundaries and occurs within the plate interiors. Prominent examples for intraplate (within plate) volcanism are the large Hawaiian (~80,000 km^3) and Canary Islands

(~20,000 km^3) volcanoes, which rise up to ~10,000m above the seafloor (Schmincke, 2000). Besides large prominent volcanoes, numerous smaller seamounts exist on the ocean floor below sealevel. Only for the Pacific a total of 22,000 – 55,000 seamounts are estimated (Batiza, 1982).

Based on the time progressive alignment of the Hawaiian Islands, Wilson (1963) suggested that they were formed by a stationary hot anomaly over which the lithosphere moved. Around a decade later, Morgan (1971) developed the classical plume theory, which assumes a stationary hot anomaly originated at a thermal boundary layer, such as the core-mantle boundary and leads to partial melting beneath a lithosphere through decompression and temperature increase.

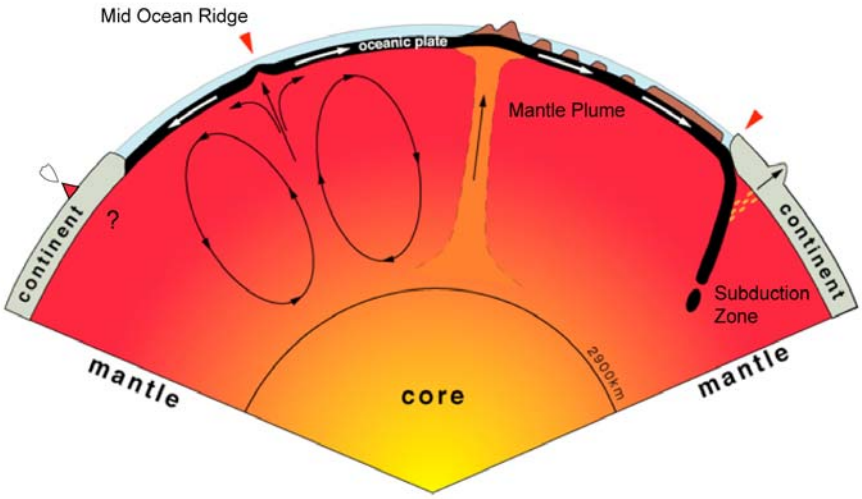

Fig. 1.1 Schematic and simplified cartoon of the upper mantle.

Since then intraplate volcanism in many areas, also on continents has been attributed to the classical plume theory (e.g. Coffin and Eldholm, 1992; Clouard and Bonneville, 2001; Richardson et al., 1989). Some intracontinental volcanic provinces however are clearly associated with extensional tectonics and rifting (often associated with plume activity), such as the East African Rift system and the Basin and Range province (USA) (e.g. Gans and Bohrson, 1998; Mechie et al., 1998). Major continental rifting result in substantial thinning of the lithosphere and thus allows the upper mantle to stream up and subsequently form partial melts by decompression (e.g. Weaver et al., 1994).

Diffusely occurring and low-volume intraplate volcanism, mostly of alkaline character, in many continental areas, however cannot be explained by the classical plume theory and/or through continental rifting. Here, alternative models are required to explain the intraplate volcanism. One of these areas is the New Zealand micro-continent, Zealandia, which has been studied in this thesis.

1.2 Brief overview of the structure and composition of the upper mantle

The upper mantle comprises the outer 670 km of the earth, including the crust, lithosphere and the upper asthenosphere and is separated from the lower mantle by a seismic discontinuity, corresponding to major changes in the structure of silicate minerals. The outer shell of the earth is the crust, above the Mohorovicic discontinuity (MOHO), which ranges in thickness on average from ~6 km beneath the oceans to about 35-40 km beneath continents (Turcotte and Schubert, 1982). The lithosphere (including the crust) is the strong outer layer, ranging from ~50–200 km in thickness. The asthenosphere underlies the lithosphere and has much lower seismic velocities than the lithosphere, which may suggests the presence of small amounts of melts. This layer represents the least rigid portion of the mantle and can easily deform, which overlies the remaining part of the upper mantle. Beneath ~400 km major changes in the structure of silicate mineral occur, such as the change from olivine to spinel structure, which changes again from spinel to perovskite structure at ~670 km. The mineral structure change between 400 km and 670 km marks the transition zone. Nevertheless, since material of the lower lithosphere and asthenosphere can flow over geological time scales (e.g. through extension or compression) they can be treated as viscous fluids (e.g. Ranalli, 1995; Conrad and Jones, 2004).

In general, the upper mantle is composed of lherzolite (mainly consisting of olivine and (ortho- and clino-) pyroxene), which contains garnet, or spinel or plagioclase, depending on the pressure conditions. Additional mantle rocks are pyroxenites and eclogites. The latter formed through a metamorphic transition of the subducting oceanic plates, whereas pyroxenite can occur beneath continents as residue after interacion between a high silica melt and peridotite (e.g. Sobolev et al., 2007). Direct evidence for such mantle rocks come from xenoliths transported to the surface through deep derived melts (e.g. kimberlites), which collected them on the way up.

The mantle (as already suggested by the occurrence of different mantle xenoliths), however is chemically heterogeneous (e.g. Rubin et al., 2001; Morgan and Morgan, 1999). In order to better understand the chemical composition of the mantle, isotopic tracers (Sr-Nd-Pb-Hf-O etc) can be used, since partial melting do not change their ratios. The isotopic composition, therefore, give an idea about the mantle source (as long as the influence of fractional crystallization, assimilation of other components can be minimized). Based on this, Zindler and Hart (1986) defined several mantle components, each having a distinct isotopic composition, where the most used components are MORB (mid ocean ridge basalts), EM (enriched mantle) and HIMU (high time integrated μ (U/Pb)).

Major and trace elements, instead are dependent on (additional to the source composition) the conditions under which a volcanic rock was formed (pressure, temperature and thus degree of partial melting etc.). E.g. a volcanic rock can be termed as depleted, enriched or fertile. MORB display generally a depleted source composition, whereas EM mantle has presumably experienced later enrichment (e.g. sediment and fluid input, crustal contamination, mantle metasomatism). HIMU-type isotopic mantle compositions, instead may have formed by recycling of old oceanic lithosphere with a high initial U/Pb ratio, which develops to high Pb isotopic ratios by radioactive decay. All of these mantle endmembers are present in the volcanic rocks from the New Zealand micro-continent, Zealandia, revealing a complex story for the origin of intraplate volcanism on this micro-continent.

1.3 Outline of the thesis and future perspectives

Aim of this study was to investigate the geochemical evolution of a volcanic center in more detail and to reconstruct the geologic history of Zealandia by $^{40}Ar/^{39}Ar$ dating and to further develop the origin of this diffuse volcanism by the geochemistry of emplaced intraplate volcanics. Furthermore geodynamic modeling based on the findings of the geochemistry was performed to test the developed qualitative model. The thesis therefore combines geochemistry with geophysics and contributes to the understanding of non-plume and non-rifting intraplate volcanism.

The work is presented in three independent chapters (II, III, IV), in which the origin of intraplate volcanism on Zealandia is investigated in more detail and which are prepared as manuscripts for publication.

Chapter II

Authors: Christian Timm, Kaj Hoernle, Paul van den Bogaard, Ilya Bindemann and Steve Weaver

Status: in review at Journal of Petrology

The *second chapter* focuses on the geochemical and temporal evolution of the most prominent volcanic landform on the South Island of New Zealand: the two composite shield volcanoes of the Banks Peninsula. This study therefore represents a case study of intraplate volcanism on Zealandia. Volcanism at Banks Peninsula started at ~ 12.5 Ma with the formation of the Lyttelton Volcano (~ 350 cm^3) continuing until ~ 10 Ma. A second pulse of volcanism formed the much larger Akaroa Volcano (~ 1200 cm^3), located adjacent to the Lyttelton Volcano in the SW, from ~ 9.6 - 8.6 Ma. Here, late stage activity continued until ~ 7 Ma. The shields of both volcanoes, the older Lyttelton and the younger Akaroa Volcano, formed within 1 - 2 Ma with late stage activity proceeding for ~ 2 Ma having an overall duration of volcanic activity of ~ 7 Ma. All mafic volcanics (MgO > 4 wt%) emplaced at Banks Peninsula resemble ocean island basalts on multi-element diagrams and can be grouped into a high-silica Lyttelton group (SiO_2 > 48.5 wt%) and a low-silica Akaroa group (SiO_2 < 48.5 wt%). Compared to the low-silica Akaroa group volcanics, the high-silica group volcanic rocks generally have lower incompatible element concentrations as well as an enriched EMII-type isotopic composition. This is accompanied by decreased ratios of less fluid-mobile to fluid-mobile and more to less incompatible trace element ratios (e.g. Nb/(U, Th), (La, Sm)/Yb, Zr/Y (Ce, Nd)/Pb), which suggests a subduction-related and/or crustal imprint. High FeOt, Zr/Hf, Sr/Y, as well as a HIMU-type isotopic signature instead, indicate the presence of pyroxenite and/or eclogite in form of recycled oceanic crust in the source and characterize the low-silica Akaroa group volcanic rock. In order to produce two adjacent shield volcanoes, with each having a different geochemical composition, two delamination events are necessary. A

relatively smaller delamination event caused the partial melting within the upper heterogeneous asthenosphere (containing recycled oceanic crust). These melts interacted extensively with a lower lithosphere, modified by prior subduction-related volcanism, and subsequently assimilated up to ~ 7 % of the local continental crust. A second, relatively bigger delamination event caused the formation of the much larger Akaroa Volcano, those magmas formed within a similar heterogeneous asthenosphere and ascended much faster, showing therefore insignificant modifications by the continental lithosphere.

Chapter III

Authors: Christian Timm, Kaj Hoernle, Reinhard Werner, Paul van den Bogaard, Folkmar Hauff, James White, Nick Mortimer and Dieter Garbe-Schönberg

Status: in review at Earth Science Reviews

The *third chapter* expands the findings of the first chapter to magma generation on the entire New Zealand micro-continent Zealandia (submarine and subarial). Since separating from Gondwana (involving plume activity), Zealandia drifted ~6000 km until its present position. Throughout the Cenozoic (while drifting) continuous and diffusely intraplate volcanism occurred as 1) monogenetic volcanic fields (e.g. Waipiata Volcanic Field, central Chatham Rise, Pukaki Bank and Alpine Dike Swarm) and 2) composite shield volcanoes (e.g. Banks Peninsula, Dunedin Volcano and Auckland and Campbell Islands). Mafic volcanic rocks (MgO > 5wt%) from Zealandia are similar to those of ocean island basalts (OIB) and can be grouped into a high (SiO_2 > 46 wt%) and a low silica group (SiO_2 < 46wt%). On isotope correlation diagrams all Cenozoic volcanic rocks plot between the Cretaceous volcanic rocks and Pacific MORB, which can be explained by mixing these two endmembers. The presence of MORB and HIMU-type isotopic signature in volcanic rocks from the Osbourne crust seamount, which formed on thin oceanic crust, far away from the continental plateau, underline the formation of the HIMU and MORB-type volcanic rocks in heterogeneous asthenosphere, containing plume-related domains. This is consistent with the presence of a deep-seated thermal anomaly between ~600 and 1450 km, which extends to Antarctica (e.g. Montelli et al., 2006;

Nolet et al., 2006 Li et al., 2008) and presumable exist since the Late Cretaceous, polluting the upper asthenosphere with plume-related material. The enriched mantle (EMII-type) isotopic signature instead indicates the interaction of the asthenospheric melts with the continental lithosphere (mantle and crust). A possible mechanism, however, to adequately explain continuously and widespread occurring intraplate volcanism on Zealandia is lithospheric removal by Rayleigh-Taylor instabilities. The formation of gravitational instabilities along the interface between a dense lower lithosphere and a less dense asthenosphere results in upwelling of warmer asthenospheric mantle, which consequently melts by decompression.

Chapter IV

Authors: Christian Timm, Lars Rüpke, and Kaj Hoernle

Status: in preparation for Earth and Planetary Science Letters

The *fourth chapter* focuses on the geodynamical aspect of the Cenozoic intraplate volcanism on Zealandia. Two-dimensional numerical modeling using the finite element method was performed to test the developed qualitative model. A four-layer box model, representing the Zealandia micro-continent, with a lower lithosphere being 1.5% denser than the underlying asthenosphere was developed. In order to achieve a more realistic scenario, temperature-dependent viscosity for the asthenosphere (cooling from the top; 1400°C for the upper asthenosphere), a thermal anomaly (T = 1700°C; as identified by Nolet et al., 2006) beneath 600 km and edge-driven convection were involved in the model. Since Zealandia was situated above an active subduction zone during the Mesozoic, the lower lithosphere presumably contains small amounts of H_2O. In order to generate partial melts beneath Zealandia, the dense lower lithosphere (containing ~300-600 ppm H_2O) forms “intracontinental” Rayleigh-Taylor instabilities within the first 30 million years. Due to continuous downwelling of the lower lithosphere and the resulting upwelling partial melting can be sustained throughout the Cenozoic. Furthermore, local upwelling of hot mantle material from beneath 600 km contributes to the formation of magmatism. Our model shows that lithospheric removal by Rayleigh-Taylor instabilities can explain the

intraplate volcanism on Zealandia and contributes to the global understanding of mantle dynamics beneath continents.

Our model shows that lithospheric delamination generally provides a mechanism, which can explain intraplate volcanism on Zealandia, but is certainly too simplified. More information about the structure of the lithosphere (such as elasticity, different rheologies) is needed to explain lithospheric removal by Rayleigh-Taylor instabilities more realistic. Furthermore the model does not include dynamic melting, which involves the change of the physical and chemical properties of the residue after melt extraction. Also the influence of CO_2 in melt generation, which is an important factor, needs to be included, as well as melting of eclogite. But in order to justify the developed model more high-resolution seismic tomographic imaging of the upper mantle beneath Zealandia is required, to resolve whether small-scale upwelling of hot mantle material beneath the lithosphere is present. There are certainly many more aspects, which need to be considered to make the model more realistic, but this thesis gives an approach contributing to better understand the origin of intraplate volcanism.

Besides the main written contributions I am co-author on a paper entitled: "Cenozoic intraplate volcanism on New Zealand: Upwelling induced by lithospheric removal" by K. Hoernle, J.D.L. White, P. van den Bogaard, F. Hauff, D.S. Coombs, R. Werner, C. Timm, D. Garbe-Schönberg, A. Reay, A.F. Cooper, published in Earth and Planetary Science Letters (2006) 248, 335-352. Furthermore different aspects of this study were presented at several conferences:

DMG Tagung Geochemie, 2006 (Talk)

Timm C., K. Hoernle, F. Hauff, P. van den Bogaard and S. Weaver (2006) Enriched Isotopic Signatures in Shield Basalts from Banks Peninsula, South Island, New Zealand, DMG Tagung, Sektion Geochemie, Kiel, 2006.

Goldschmidt Conference, Melbourne, 2006 (Talk)

Timm C., K. Hoernle, F. Hauff, P. van den Bogaard and S. Weaver (2006) A Mantle Origin for the Enriched Signature in Basalts from Banks Peninsula, New Zealand. In: Geochimica et Cosmochimica Acta, Goldschmidt Abstracts, v. 70, August-September, p. A650.

EGU, Wien, 2007 (Talk)

Timm, C.; Hoernle, K.; Hauff, F.; van den Bogaard, P.; Weaver, S. (2007): Crustal Assimilation vs. Mantle Melts in Lavas from Banks Peninsula, NZ; In: European Geosciences Union General Assembly, Vienna, April 15-20, Geophysical Research Abstracts, Vol. 9, Abstract 04990, SRef-ID: 1607-7962/gra/EGU2007-A-04990.

Invited Talk at PGP, University of Oslo, 2007

Timm, C.; Hoernle, K.; Hauff, F.; van den Bogaard, P.; White, J.; Weaver, S. (2007): The Origin of Intraplate Volcanism in New Zealand? ; In: Seminar presentation at the PGP, University of Oslo, March 22.

Goldschmidt Conference, Cologne, 2007 (Poster)

Timm, C.; Rüpke, L.; Hoernle, K. (2007): Melting processes by Rayleigh-Taylor instabilities beneath Continents: Evidence from Cenozoic intraplate volcanism on Zealandia, SW Pacific; In: Geochimica et Cosmochimica Acta, Goldschmidt Abstracts, v. 71, p. A1022, http://www.sciencedirect.com/science/article/B6V66-4P8C87H-N/2/dc7c62db0baf255469389796d30412bd.

EGU, Wien, 2008 (Invited Talk)

Timm, C.; Hoernle, K.; Hauff, F.; van den Bogaard, P. (2007): The Origin of Intraplate Volcanism on Zealandia; In: European Geosciences Union General Assembly, Vienna, April 13-18, Geophysical Research Abstracts, Vol. 9, Abstract 04990, SRef-ID: 1607-7962/gra/EGU2007-A-04990.

References:

Batiza, R., 1982. Abundances, distribution and sizes of volcanoes in the Pacific Ocean and implications for the origin of non-hotspot volcanoes. Earth and Planetary Science Letters 60, 195-206.

Clouard, V., and Bonneville, A., 2001. How many Pacific hotspots are fed by deep-mantle plumes? Geology 29 (8), 695-698.

Coffin, M.F., and Eldholm, O., 1993. Large igneous provinces, Scientific American 269 (4): 42-49.

Conrad, C.P., and Jones, C., 2004. A testof laboratory based rheological parameters of olivine from an analysis of late Cenozoic convective removal of mantle lithosphere beneath the Sierra Nevada, Calofornia, USA. Geophysical Journal International 156, 555-564.

Elkins-Tanton, L.T., 2005. Continental magmatism caused by lithospheric delamination, in: G.R. Foulger, J.H. Natland, D.C. Presnall, D.L. Anderson (Eds.), Plates, Plumes, and Paradigms, Geological Society of America Special Paper 388, Geological Society of America, 449–461.

Gans, P.B., and Bohrson, W.A., 1998. Suppression of Volcanism During Rapid Extension in the Basin and Range Province, United States. Science 279, 66-68.

Hoernle, K., White, J.D.L., Bogaard, P.v.d., Hauff, F., Coombs, D.S., Werner, R., Timm, C., Garbe-Schönberg, C.-D., Reay. A., Cooper, A.F., 2006. Cenozoic Intraplate Volcanism on New Zealand: Upwelling Induced by Lithospheric Removal. Earth and Planetary Science Letters 248, 335-352.

Kay, R.W. and Kay, S.M., 1993. Delamination and delamination magmatism. Tectonophysics 219, 177-189.

Li, C., van der Hilst, R.D., Engdahl, E.R., Burdick, S., 2008. A new global model for P wave speed variations in Earth's mantle. Geochemistry Geophysics Geosystems 9(5), Q05018, doi:10.1029/2007GC001806

Mechie, J., Keller, G.R., Prodehl, C., Khan, M.A., Gaciri, S.J., 1997. A model for the structure, composition and evolution of the Kenya rift. Tectonophysics 278, 95-119.

Montelli, R., Nolet, G., Dahlen, R.A., Masters, G., 2006. A catalogue of deep mantle plumes: New results from finite frequency tomography. Geochemistry Geophysics Geosystems 7(11), Q11007, doi:10.1029/2006GC001248.

Morgan, W.J., 1971. Convection plumes in the lower mantle, Nature 230, 42–43.

Morgan, J.P., and Morgan, W.J., 1999. Two-stage melting and the geochemical evolution of the mantle: a recipe for mantle plum-pudding. Earth and Planetary Science Letters 170, 215-239.

Nolet, G., Karato, S.-I., Montelli, R., 2006. Plume fluxes from seismic tomography. Earth and Planetary Science Letters 248, 685-699.

Ranalli, G., 1995. Rheology of the earth. Chapman & Hall, second edition. 436pp.

Richards, M.A., R.A. Duncan, and V.E. Courtillot, 1989. Flood basalts and hotspot tracks: Plume heads and tails. Science, 246, 103-107.

Rubin, K.H., Smith, M.C., Bergmanis, E.C., Perfit, M.R., Sinton, J.M., Batiza, R., 2001. Geochemical heterogeneity within mid-ocean ridge lava flows: insights into eruption, emplacement and global variations in magma generation. Earth and Planetary Science Letters 188, 349-367.

Schmincke, H.U., 2000. Volcanism. Springer Verlag, 324 pp.

Sobolev, A.V., Hofmann, A.W. Kuzmin, D.V., Yaxley, G.M., Arndt, N.T., Chung, S.-L., Danyushevsky, L.V., Elliott, T., Frey, F.A., Garcia, M.O., Gurenko, A.A., Kamenetsky, V.S., Kerr, A.C., Krivolutskaya, N.A., Matvienkov, V.V., Nikogosian, I.K., Rocholl, A., Sigurdsson, I.A., Sushchevskaya, N.M., Teklay, M., 2007. The Amount of Recycled Crust in Sources of Mantle-Derived Melts. Science 10.1126/science.1138113.

Turcotte, D.L., and Schubert, G., 1982. Geodynamics. Cambridge University Press, 456 pp.

Weaver, S.D., Storey, B.C., Pankhurst, R.J., Mukasa, S.B., DiVenere, V.J., Bradshaw, J.D., 1994. Antarctica-New Zealand rifting and Marie Byrd Land lithospheric magmatism linked to ridge subduction and mantle plume activity. Geology 22, 811-814.

Wilson, J.T., 1963. A possible origin of the Hawaiian islands. Canadian Journal of Physics 41, 863-870.

Wilson, M., 1989. Igneous Petrogenesis. Kluwer Academic Publishers, 466pp.

Zindler, A., and Hart, S., 1986. Chemical Geodynamics. Annual Review of Earth and Planetary Science 14. 493-571.

Chapter II

Geochemical Evolution of Intraplate Volcanism at Banks Peninsula, New Zealand: Mantle Melts versus Crustal Contamination

Abstract

Intraplate volcanism was widespread and occurred continuously throughout the Cenozoic on the New Zealand micro-continent, Zealandia, forming two volcanic endmembers: 1) monogenetic volcanic fields and 2) composite shield volcanoes. The most prominent volcanic landforms on the South Island of New Zealand are the two composite shield volcanoes (Lyttelton and Akaroa) forming Banks Peninsula. We present new $^{40}Ar/^{39}Ar$ age and geochemical (major and trace elements and Sr-Nd-Pb-Hf-O isotopes) data from this Miocene volcanism, which persisted for ~ 7 Ma. Both volcanoes primarily formed over a ~ 1 Ma interval with small volumes of late-stage volcanism continuing for ~ 1.5 Ma after formation of the shields. The Banks Peninsula volcanoes have distinct chemical compositions. The Akaroa volcanic rocks have low SiO_2, high incompatible element abundances, low $\partial^{18}O$ (4.6-4.9) and high time integrated $^{238}U/^{204}Pb$ (HIMU)-type isotopic signatures, consistent with their derivation from a heterogeneous upper asthenosphere containing recycled oceanic lithosphere. In contrast, the Lyttelton volcanics have higher SiO_2 and fluid mobile to fluid immobile element ratios, together with generally lower contents of incompatible elements and enriched (EMII-type) signatures, indicating formation through extensive interaction of low-silica Akaroa - type melts with the continental lithosphere of the former Gondwana convergent margin.

We propose decompression melting resulting from lithospheric delamination in the form of Rayleigh-Taylor instabilities as a possible mechanism for producing partial melts over ~ 7 Ma with two major pulses of volcanism. Accordingly a small delamination event removed some of the lower lithosphere leading to the formation of

the Lyttelton Volcano. A larger delamination event then removed most of the modified lithosphere resulting in the formation of the much larger Akaroa Volcano.

2.1 Introduction

In the Early Cretaceous, the New Zealand micro-continent, Zealandia, was part of the former super-continent Gondwana, located at its northern to northwestern margin. Throughout the Mesozoic, before separating from Gondwana, Zealandia experienced voluminous, subduction-related magmatism (Muir et al., 1998). After continental separation ~ 84 Ma ago (Davy, 2006; Waight et al., 1998), Zealandia drifted ~ 6000 km (~ 70 km/Ma) towards the NW to its present position. The products of intraplate volcanism are ubiquitous in New Zealand and occurred nearly continuously throughout the Cenozoic. One endmember type of volcanism is widely dispersed monogenetic volcanic fields, defining broad areas where volcanic activity took place over tens of millions of years (Coombs et al., 1986; Hoernle et al., 2006; Weaver & Smith, 1989). These fields are characterized by highly to moderately undersaturated volcanic rocks (with small proportions of more evolved differentiates) occurring as small cones, dike intrusions or pillow lavas. The second volcanic endmember is represented by shield volcanoes, such as the Dunedin and Banks Peninsula volcanoes (Fig.2.1). The origin of these volcanoes however remains enigmatic. On Banks Peninsula, there are two isolated large adjacent composite shield volcanoes not associated with a larger age progressive trend of volcanism in the direction of plate motion. In addition, the seismic tomography shows no evidence for a plume-like thermal anomaly beneath Banks Peninsula. Major extension associated with continental break-up and rifting ceased in the late Cretaceous and therefore cannot be involved to explain the origin of the Banks volcanism. In order to better understand the temporal, petrological and geochemical evolution of the Banks Peninsula volcanism, we have conducted a case study on Banks Peninsula volcanic rocks, generating new $^{40}Ar/^{39}Ar$ ages, major and trace element and Sr-Nd-Pb-Hf-O isotope data. The results of our study are consistent with the Banks volcanism being related to two major lithosphere detachment events.

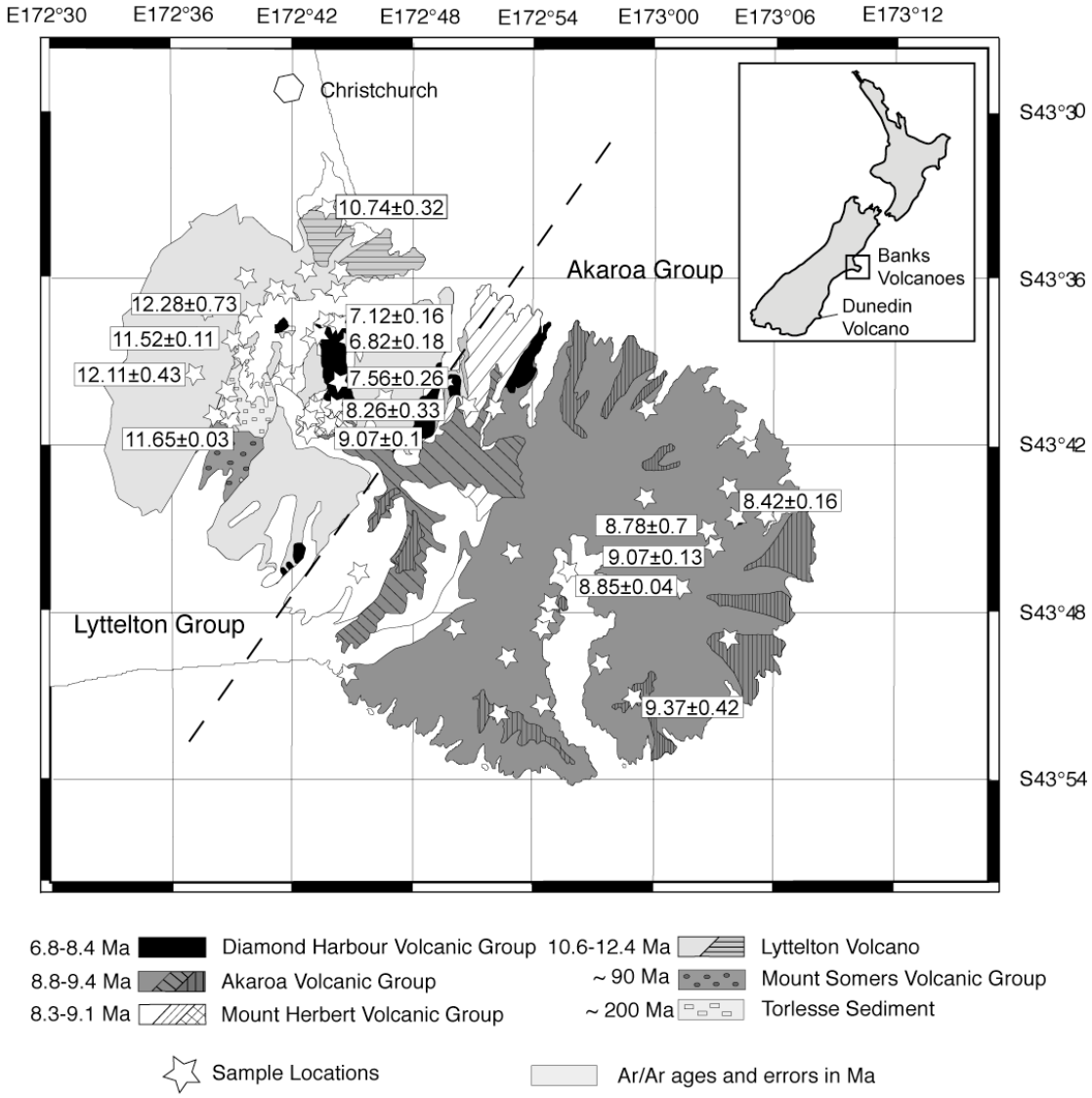

Fig.2.1: Simplified geological map of Banks Peninsula, showing the units of Lyttelton Volcano in the NW and the units of Akaroa Volcano in the SE. The Mount Herbert Volcanic Group overlies the Lyttelton volcanics but has a similar age to the Akaroa volcanic rocks. The Diamond Harbour Volcanic Group scatters over the flanks of Lyttelton Volcano with exception of two occurrences on the slopes of Akaroa volcano. Stars mark sample locations and the numbers are $^{40}Ar/^{39}Ar$ ages in Ma (see Table 1). The dashed line separates the two composite shield volcanoes, the Lyttelton and Akaroa volcanoes and also represents a chemical boundary between high-silica Lyttelton and low-silica Akaroa lavas.

2.2 Geological Background

The most prominent volcanic feature of the South Island of New Zealand is Banks Peninsula formed by the two shield volcanoes Lyttelton and Akaroa, ~ 25 km^2 and ~ 35 km^2 in diameter, respectively. Located on the east coast of the South Island of New Zealand (Fig.2.1), the Banks Peninsula volcanoes were active during the Mid to Late

Miocene (~ 11 - 6 Ma, based on K/Ar ages; Sewell, 1988) and represent highly eroded remnants of much larger volcanoes. Sector collapse and erosion has allowed the sea to reach the central parts of both shield volcanoes, forming well-protected natural harbours. The Lyttelton Volcano is located on the NW portion of Banks Peninsula and sits on Permian - Triassic Torlesse sedimentary rocks of the Rakaia Terrane and on intermediate to silicic Late Cretaceous volcanic rocks of the Mount Somers Volcanic Group. Drilled lavas, offshore of Banks Peninsula and beneath the surrounding Canterbury Plains, suggest that the shield volcanoes had original diameters of ~35 km for Lyttelton and ~50 km for Akaroa (Weaver and Smith, 1989). A minimum estimate for the volume of the Banks Peninsula volcanic rocks is ~1600 km^3: ~ 350 km^3 for Lyttelton and ~ 1200 km^3 for Akaroa Volcanoes, respectively. During the early years of activity, the two coalescing volcanoes formed an island, which became connected to the mainland of the South Island through accumulation of gravel outwash from the nearby mountain ranges forming the Canterbury Plains (Liggett et al., 1965; Weaver and Smith, 1989).

Volcanic activity associated with these shield volcanoes began ~ 11 Ma ago with eruptions at Lyttelton Volcano. The main cone of the Lyttelton Volcano probably reached a height of ~ 1500 m above sea level (Stipp and Mc Dougall, 1968). During the eruption of the shield-building lavas, a radial dike swarm of mafic to felsic rock types was emplaced (Shelley, 1988). At ~ 10 Ma volcanic activity ceased at the Lyttelton Volcano and shifted towards the SE. The eruption of the transitional Mount Herbert lavas took place initially through vents in the crater of the Lyttelton Volcano in subaqueous to water-saturated conditions as indicated by crater-lake deposits within the crater of Lyttelton Volcano (Weaver and Smith, 1989). Although the Mount Herbert Volcanic Group lavas constitute relatively minor extrusive volumes compared with the volcanoes of Lyttelton and Akaroa, they presently form the highest elevations of the Banks Peninsula with Mount Herbert reaching a height of ~920 m. Volcanic activity at Akaroa Volcano began at ~ 9 Ma. The shield of the Akaroa Volcano probably reached a height of > 1800 m above sea level (Liggett et al., 1965). Mafic and felsic dikes also occur in the intrusive core of the volcano at the northern end of the Akaroa Harbour, and radiate out from the geometric centre of the Akaroa Volcano cutting the lava shield. The youngest volcanic unit on Banks Peninsula is the Diamond Harbour Volcanic Group with scattered outcrops on both volcanoes but predominantly along the NE flank of the Lyttelton Volcano and above the northward

directed flows of the Mount Herbert Volcanic Group. Small eruption centers of the Diamond Harbour Volcanic Group are also present on the northern to north-eastern flanks of the Akaroa Volcano (Fig.2.1).

Typical explanations for continental intraplate volcanism include the plume hypothesis (Morgan, 1971) and/or major continental extension and thinning. No morphologic or geophysical indications of a thermal anomaly exist beneath Banks Peninsula, although there is evidence for a deep-seated low velocity zone between 600 and 1450 km depth (Montelli et al., 2006) beneath the entire Chatham Rise, which ends at Banks Peninsula. A sub-lithospheric mantle plume would be expected to be associated with a long-lived linear age progressive chain of volcanoes in the direction of plate motion, as is for example observed with the Louisville seamount chain to the northwest of New Zealand. There is however no evidence for such volcanism associated with Banks Peninsula. In addition it is difficult to explain the presence of volcanism over ~ 5 Ma since the plate should have drifted ~ 500 km in this time (assuming a plate motion of ~ 70 mm/yr). Therefore it is unlikely that > 1600 km^3 of lava would have been erupted from a relatively stationary sub lithospheric source forming two coalescing shield volcanoes.

In respect to continental extension, the predominant tectonic stress regime in the late Miocene was compressional (Sutherland, 1995), allowing only mild local extension (Weaver and Smith, 1989). Although an increased rate of rotational deformation and crustal thinning was recognized in the Miocene between 25 and 8 Ma by (Hall et al., 2004; Eberhart-Phillips and Bannister, 2002), which may also have caused mild extension, there is no evidence for major lithospheric extension and rifting during the Cenozoic, which could account for the generation of the voluminous magma required to form the shield volcanoes. Lithospheric melting has been proposed as a mechanism for generating intraplate volcanism on Zealandia and surrounding regions (Finn et al., 2005; Panter et al., 2006). In order to generate extensive melting (in order to form shield volcanoes) solely within the lithospheric mantle, a large amount of thermal energy would need to be applied to the base of the lithosphere. In the absence of evidence for a mantle plume or other large thermal anomalies beneath the Banks Peninsula, we do not consider lithospheric melting to be the sole mechanism for generating the Banks volcanism.

In order to produce the inferred volume of magmas forming the shield volcanoes, there must be another process besides major lithospheric extension or plume activity

involved. A possibility to generate large amounts of melt (> 1600 km^3) is lithospheric removal (Hoernle et al., 2006). This in turn could explain the fairly thin continental lithosphere (including crust and mantle) beneath Zealandia, which ranges between 70 - 100 km and thickens to > 150 km beneath the Southern Alps (Liu and Bird, 2006; Stern et al., 2002). Although volcanic activity at the Banks Peninsula ceased ca. 6 Ma ago, there is still a slightly elevated heat flow of ~ 70 mW/m^2 with 28 % mantle helium being emitted (Godfrey et al., 2001, Hoke et al., 2000).

2.3 Analytical Methods

Only the freshest parts of the volcanic rocks were selected for analyses. In order to remove easily soluble material (e.g. dustcover, salt, etc.), the samples were cleaned in deionised water in an ultrasonic bath and dried overnight at 50°C. After sieving the clean grains into several fractions, the samples were carefully hand-picked under a binocular microscope and then reduced to powder in an agate ball mill for major and trace element and isotope analyses.

Major element analyses were carried out on fused glass beads using a Phillips X'Unique PW 1480 X-ray fluorescence spectrometer using a Rh-tube at the Leibniz Institute of Marine Sciences (IFM-GEOMAR). To produce homogenous glass beads, 0.6mg of dry sample powder, lithium tetraborate and ammonium nitrate were mixed in platinum cups and then fused in four heat-steps.

For trace element analyses, an Agilent 7500c/s Quadropol Inductively Coupled Mass Spectrometer (ICP-MS) at the Institute for Geosciences of the University of Kiel was used. The samples were prepared following the pressurized mixed acid (Aqua Regia + $HCLO_4$) digestion method, as described by Garbe-Schönberg (1993).

Major element contents in internal rock standards (JB-2, JB-3, JA-1) measured with the samples are generally within 6 %, except for MnO (6.3 – 12.5%) and P_2O_5 (6.7 – 6.9 %), of the expected values (Govindaraju 1994). H_2O and CO_2 concentrations were determined by means of an infrared photometer (Rosemount CSA 5003). Replicate digestions and analyses were used to determine accuracy. The external accuracy of the determined trace elements is better than 6 %, except for Cr, Zn, Sn, Tl (< 7%) and Li, Sb, Cd (< 15.5%). Trace element compositions of BHVO-2

and AGV-1 measured along with the samples were within 7% of the USGS working values, except for Nb, Ta, Pr (11-15%) and Li, Cr, Mo, Tm (20-28%).

Sr, Nd, Pb and Hf isotope measurements were conducted at IFM-GEOMAR. For isotope determination, ~ 200 mg of sample powder was dissolved in hot HF-HNO_3 mixture followed by ion exchange procedure of Hoernle et al. (2008) to separate Sr, Nd and Pb from the matrix. Sr isotopes were analyzed on ThermoFinnigan Triton and Finnigan MAT262 RPQ^{2+} thermal ionization mass spectrometers operating in static mode; Nd isotope measurements were conducted on a ThermoFinnigan Triton thermal ionization mass spectrometer running in multidynamic mode; and Pb isotopes were determined on a Finnigan MAT262 RPQ^{2+} thermal ionization mass spectrometer operating in static mode. Sr and Nd isotopic ratios were normalized within run to $^{86}Sr/^{88}Sr = 0.1194$ and $^{146}Nd/^{144}Nd = 0.7219$ respectively. All stated errors are given as 2σ. The average values of standards are: for NBS 987 $^{87}Sr/^{86}Sr = 0.710228 \pm 0.000023$ (N=23), for La Jolla $^{143}Nd/^{144}Nd = 0.511858 \pm 0.000013$ (N=6) and for an in-house Nd monitor SPEX = 0.511724 ± 0.000010 (N=20). Sr and Nd isotope ratios were normalized to 0.71025 for $^{87}Sr/^{86}Sr$ and 0.511850 for $^{143}Nd/^{144}Nd$ for La Jolla and 0.511715 for Nd SPEX. Pb standard NBS 981 (N=19) gave $^{208}Pb/^{204}Pb = 36.527 \pm 0.0022$, $^{207}Pb/^{204}Pb = 15.591 \pm 0.007$, $^{206}Pb/^{204}Pb = 16.900 \pm 0.005$ and were corrected to the value given by Todt et al. (1996). Pb chemistry blanks are below 400 pg and can therefore be considered as negligible. Hafnium isotopes were determined on the same rock powders used for Sr, Nd, and Pb isotope measurements. Hafnium was separated following a slightly modified two-column procedure as described by Blichert-Toft et al. (1997). Hafnium isotope ratio measurements were carried out on a VG Axiom multi-collector ICPMS (MC-ICPMS). After two days of measuring the in-house SPEX Hf monitor to stabilize the signal, standards were determined repeatedly every two or three samples to verify the machine performance. To correct for the instrumental mass bias, $^{176}Hf/^{177}Hf$ was normalized to $^{179}Hf/^{177}Hf = 0.7325$. $^{176}Hf/^{177}Hf$ isotope ratios were normalized to 0.282163 for JMC.

For O isotope analyses, 2 - 4 mg pristine olivine grains were carefully hand-picked under a binocular microscope. Analyses were carried out at the University of Oregon's stable isotope lab using CO_2 laser fluorination, BrF_5 as a reagent, followed by conversion to CO_2 gas and analysis on a Finnigan MAT 253 gas source mass spectrometer. San Carlos olivine and garnet standards were measured along with the

samples. Day-to-day variability was corrected to standard working values with the variability lying within ± 0.1 ‰. Duplicates (n = 6) deviate less than 0.2 ‰ from each other.

$^{40}Ar/^{39}Ar$ dating was conducted on K-bearing mineral phases, such as feldspar, biotite, and microcrystalline matrix, by laser step-heating at the Geochronology laboratory at IFM-GEOMAR using a 20 W Spectra Physics argon laser and a MAP 216 noble gas mass spectrometer. After hand-picking ~ 20 mg of 250 - 500 µm chips for matrix and 250 µm - 1 mm sized crystals, the samples were cleaned by using deionised water and an ultrasonic disintegrator. Feldspar and amphibole crystals were etched for ~ 15 and 5 - 10 min in 5% diluted hydrofluoric acid, respectively. The clean samples were loaded in aluminum trays, wrapped in cadmium foil and neutron irradiated at the 5 MW reactor of the GKSS Reactor Centre in Geesthacht, Germany. Raw mass spectrometer peaks were corrected for mass discrimination, background noise and blanks were measured every fifth analyses. To monitor the neutron flux, the TCR-1 (Taylor Creek Rhyolite, 27.92 Ma; Duffield and Dalrymple, 1990) sanidine standard and an internal standard SAN6165 (0.47 Ma; Bogaard, 1995) were used. High purity KSO_4 and CaF_2 salt crystals run at the same time as the samples were used to correct for Ca and K interferences.

Single fusion analyses were carried out on 0.1 - 2.5 mg of crystals or matrix chips by determining the $^{40}Ar/^{39}Ar$ ratios after every single heating step. To conduct step-heat analyses, 3.8 - 7.7 mg of sample material (phenocrysts or matrix) were needed. Incrementally increasing laser output from 20 MW to 20 W allows continuous determination of the $^{40}Ar/^{39}Ar$ isotope ratio. An age is derived from the plateau proportion of the measured age spectra. All errors are given as 2σ.

2.4 Results

2.4.1 Age Determinations

Fourteen new $^{40}Ar/^{39}Ar$ ages on volcanic rocks from Banks Peninsula volcanoes are presented in Table 1 with errors stated as 2 σ. Three samples from the Lyttelton Volcano yield an age range from 12.3 - 10.7 Ma.

Table 1: $^{40}Ar/^{39}Ar$ age determinations

Sample	Phase	Unit	Sample Locality	Plateau age		2σ	MSWD	%^{39}Ar Plateau
Lyttelton Volcano (including Governors Bay Formation and Allandale Rhyolite)								
MSI13	fsp	Lyttelton Volcano (l)	S43°36'41.5" E172°40'20.0"	12.28	±	0.72	0.93	90.2
MSI107	fsp	Lyttelton Volcano (l)	S43°39'39.2" E172°37'15.2"	12.11	±	0.43	1.11	84.1
MV-4	fsp	Allandale Rhyolite (ra)	S43°41'25.6" E172°38'18.4"	11.65	±	0.03	0.45	n=12
MSI114	fsp	Governors Bay Formation (gd)	S43°37'59.7" E172°38'56.9"	11.52	±	0.11	0.61	91.3
MSI9A	fsp	Lyttelton Volcano (lp)	S43°33'24.30" E172°43'55.20"	10.74	±	0.32	1.80	80.7
Akaroa Volcano (including Mount Herbert and Diamond Harbour Volcanic Groups)								
MSI144	fsp	Akaroa Volcano (ae)	S43°50'59.0" E172°58'11.3"	9.37	±	0.42	1.03	82.6
MSI18	fsp	Akaroa Volcano (af)	S43°45'39.2" E173°03'22.6"	9.07	±	0.13	0.70	100
MSI117	mx	Mount Herbert Volcanic Group (hh)	S43°41'22.7" E172°44'30.0"	9.07	±	0.20	0.79	80.2
N36C3602	bt	Akaroa Volcano (ao)	S43°46'20.46" E172°55'38.06"	8.85	±	0.08	0.65	62.8
UC13809	mx	Akaroa Volcano (af)	S43°43'34.56" E173°02'55.91"	8.78	±	1.40	1.08	75.2
MSI20E	mx	Diamond Harbour Volcanic Group (ds) - LBPI	S43°44'20.8" E173°04'14.1"	8.42	±	0.16	1.00	86.9
CD103	fsp	Mount Herbert Volcanic Group (ho)	S43°41'08.35" E172°44'26.49"	8.26	±	0.66	1.30	100.0
CD112	fsp	Diamond Harbour Volcanic Group (ds)	S43°40'15.61" E172°44'03.96"	7.56	±	0.52	0.55	87.1
CD77	mx	Diamond Harbour Volcanic Group (ds)	S43°38'10.03" E172°43'22.52"	7.12	±	0.32	1.60	64.8
CD77	mx duplicate	Diamond Harbour Volcanic Group (ds)	S43°38'10.03" E172°43'22.52"	6.82	±	0.36	1.70	83.6

The ages from the undifferentiated Lyttelton Volcanic Group (following the classification of Sewell et al., 1993) are 12.28 ± 0.72 and 12.11 ± 0.43 Ma, whereas the stratigraphically younger Mount Pleasant Formation produced an age of 10.74 + 0.32 Ma. Samples from the Allandale Rhyolite and Governors Bay Formation gave ages of 11.65 ± 0.03 and 11.52 ± 0.11 Ma, respectively, and therefore are within two sigma errors of the basaltic volcanism from the Lyttelton Group, suggesting that these rocks were largely erupted contemporaneously. Previous Rb/Sr and K/Ar age dating, produced slightly younger ages for the Lyttelton shield (11.9 – 11.1 Ma) and the Governors Bay Formation and Allandale Rhyolite (10.8 Ma; Barley et al., 1988, Stipp & McDougall, 1968). The Mount Herbert Volcanic Group generated Ar/Ar ages of 9.07 ± 0.20 and 8.26 ± 0.66 Ma extending the K/Ar range (8.5 – 8 Ma; (Stipp & Mc Dougall, 1968) by ~ 0.6 Ma to older ages. Our ages confirm that the Mount Herbert lavas were erupted after the formation of the Lyttelton Volcano, but fall into the age range of the Akaroa Volcano, for which $^{40}Ar/^{39}Ar$ ages of 9.37 ± 0.42, 9.07 ± 0.13, 8.85 ± 0.08 and 8.78 ± 1.4 Ma were determined. An age of 8.85 ± 0.08 Ma was obtained on biotite from a syenite intrusion on the Onawe Peninsula within the age range of the Akaroa shield lavas and significantly younger than the former age of 11.8 Ma determined by the K/Ar technique (Stipp and Mc Dougall, 1968). Two samples from the Diamond Harbour Volcanic Group gave ages of 7.56 ± 0.52 and 6.97 ± 0.34 Ma (average of two determinations). One sample from the Le Bons Peak basanite intrusion (Sewell et al., 1993) on the western flank of Akaroa volcano yielded an age of 8.42 ± 0.16, which is significantly older than the other analyzed samples of the Diamond Harbour Volcanic Group but identical within error with the age determined on the younger Mount Herbert Group basalt. Therefore, the new $^{40}Ar/^{39}Ar$ ages give a revised picture of the temporal evolution of Miocene volcanism on Banks Peninsula, with both the Lyttelton Volcano and Akaroa Volcano being slightly older than previously believed. The Mount Herbert Volcanic Group lavas and the Le Bons Peak intrusion were emplaced contemporaneously with the activity at Akaroa volcano.

2.4.2 Geochemistry

New major element, trace element and Sr, Nd, Pb, Hf and O isotope data are presented in Tables 2 - 3. Lyttelton volcanics (including Governors Bay Formation and Allandale Rhyolite) range from transitional tholeiites to alkali basalts to rhyolites,

whereas lavas from Akaroa Volcano are generally more undersaturated in silica and fractionate along a trend from picrite to basanite/alkali basalt to trachyte. Mount Herbert lavas have similar compositions to Akaroa lavas ranging from alkali basalt to tephrite. The similarity in age and geochemistry suggests that the Mount Herbert lavas are associated with the formation of the Akaroa volcano. Volcanics from the Diamond Harbour Volcanic Group show the widest range of mafic compositions, varying from basanites through alkali basalts to tholeiites and mugearites (Fig.2. 2).

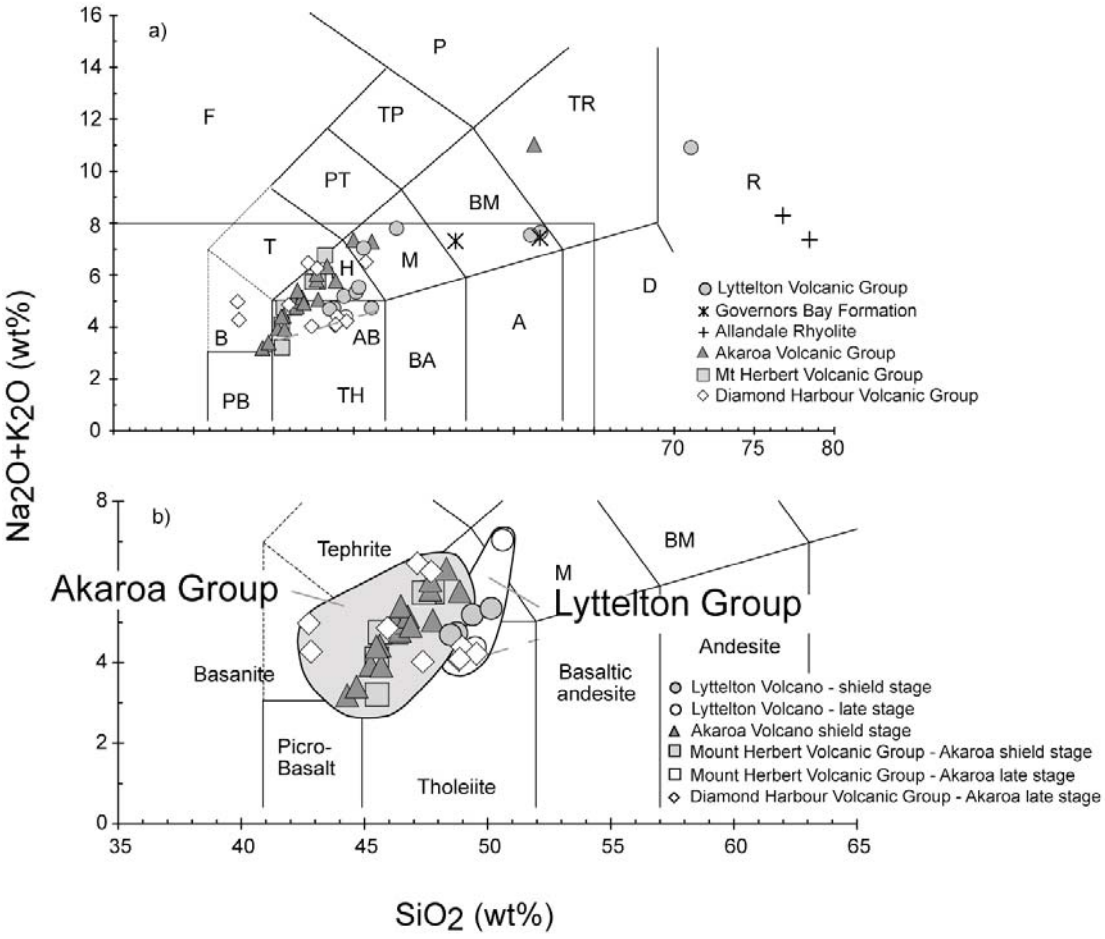

Fig.2.2: Total Alkalies (Na_2O+K_2O) vs. SiO_2 normalised to 100% on a volatile-free basis according to rock type classification (LeMaitre, 1989). Fig. 2.2a shows all samples from Banks Peninsula. Rock types range from basanite to transitional tholeiites through trachyte to rhyolite. Each symbol represents the assigned volcanic unit (Lyttelton, Mount Herbert, Akaroa and Diamond Harbour Volcanic groups and the Governors Bay Formation and Allandale Rhyolite) with closed symbols representing shield stage and open symbols representing late-stage volcanic activity in all figures. Fig.2.2b shows only mafic Banks Peninsula volcanic rocks (MgO > 4wt%). Based on the SiO_2 saturation and on the spatial distribution, mafic Banks Peninsula lavas are grouped into a high-silica Lyttelton and a low-silica Akaroa Group. Abbr.: F = foidite, PB = picrobasalt, B = basanite, T = tephrite, PT = phono-tephrite, TP = tephri-phonolite, P = phonolite, TH = tholeiite, AB = alkali basalt, H = hawaiite, M = mugearite, BM = benmoreite, TR = trachyte, BA = basaltic andesite, A = andesite, D = dacite, R = rhyolite

Table 2: Major and trace element compositions the Lyttelton Group:

Sample	MSI 9A	MSI 10	MSI 12B	MSI 13	MSI 15	MSI 100A	MSI 102
Location	S43°33'24.3" E172°43'55.2"	S43°35'44.0" E172°44'53.2"	S43°36'22.5" E172°41'25.4"	S43°36'41.5" E172°40'20.0"	S43°38'57.5" E172°39'30.4"	S43°36'02.6" E172°44'26.5"	S43°34'54.0" E172°43'31.2"
Unit (Sewell, 1993)	lp	l	gd	l	ra	l	l
Major elements (wt %; determined by XRF)							
SiO_2	49.87	48.65	55.45	50.39	74.99	61.26	52.23
TiO_2	2.20	2.83	3.44	3.66	0.04	1.28	2.00
Al_2O_3	16.07	16.67	18.24	15.32	13.44	15.55	17.52
FeO^t	10.30	10.99	4.78	12.42	0.75	7.35	9.48
MnO	0.14	0.17	0.05	0.14	0.02	0.11	0.17
MgO	5.05	4.54	1.54	3.39	0.09	1.65	2.74
CaO	7.14	8.76	6.46	7.85	0.09	4.02	6.30
Na_2O	4.89	3.83	5.20	3.37	3.60	4.26	5.41
K_2O	2.05	1.28	1.97	1.30	4.48	3.34	2.32
P_2O_5	0.60	0.62	1.00	0.58	0.01	0.34	0.77
CO_2	0.01	0.10	0.03	0.04	0.01	0.07	0.02
H_2O	0.71	1.45	1.25	1.24	1.09	1.13	0.61
Total	99.03	99.89	99.41	99.70	98.61	100.36	99.57
Trace elements (ppm; determined by ICPMS)							
Li	11.2	8.88	n.a.	7.03	175	n.a.	n.a.
Sc	14.6	18.6	n.a.	24.7	0.50	n.a.	n.a.
V	163	187	n.a.	307	2.20	n.a.	n.a.
Cr	129	52.9	n.a.	15.1	1.16	n.a.	n.a.
Co	38.8	33.0	n.a.	33.3	0.91	n.a.	n.a.
Ni	101	39.7	n.a.	24.8	0.65	n.a.	n.a.
Cu	48.9	44.0	n.a.	35.7	3.43	n.a.	n.a.
Zn	154	129	n.a.	154	84.8	n.a.	n.a.
Ga	27.4	24.3	n.a.	25.9	54.2	n.a.	n.a.
Rb	52.9	28.4	n.a.	37.3	694	n.a.	n.a.
Sr	723.	565	n.a.	482	5.11	n.a.	n.a.
Y	27.7	33.2	n.a.	39.1	41.2	n.a.	n.a.
Zr	358	245.	n.a.	272	62.8	n.a.	n.a.
Nb	72.8	50.5	n.a.	48.4	108	n.a.	n.a.
Mo	3.93	2.30	n.a.	2.21	0.38	n.a.	n.a.
Cd	n.a.	n.a.	n.a.	n.a.	n.a.	n.a.	n.a.
Sn	3.02	2.32	n.a.	2.26	36.9	n.a.	n.a.
Sb	0.12	0.06	n.a.	0.06	0.77	n.a.	n.a.
Cs	1.14	0.44	n.a.	0.67	8.56	n.a.	n.a.
Ba	532	309	n.a.	361	22.4	n.a.	n.a.
La	54.5	36.3	n.a.	39.9	13.9	n.a.	n.a.
Ce	102	73.9	n.a.	75.7	31.8	n.a.	n.a.
Pr	12.6	9.53	n.a.	10.8	4.77	n.a.	n.a.
Nd	47.7	38.7	n.a.	44.5	18.9	n.a.	n.a.
Sm	9.36	8.41	n.a.	9.83	6.25	n.a.	n.a.
Eu	3.02	2.77	n.a.	3.06	0.10	n.a.	n.a.
Gd	8.46	8.15	n.a.	9.67	7.02	n.a.	n.a.
Tb	1.17	1.21	n.a.	1.43	1.48	n.a.	n.a.
Dy	5.98	6.63	n.a.	7.88	10.4	n.a.	n.a.
Ho	1.03	1.23	n.a.	1.45	2.26	n.a.	n.a.
Er	2.30	3.02	n.a.	3.54	6.89	n.a.	n.a.
Tm	0.32	0.41	n.a.	0.49	1.19	n.a.	n.a.
Yb	1.89	2.51	n.a.	2.95	8.03	n.a.	n.a.
Lu	0.26	0.36	n.a.	0.42	1.05	n.a.	n.a.
Hf	7.97	5.76	n.a.	6.68	4.63	n.a.	n.a.
Ta	4.35	2.87	n.a.	2.78	21.4	n.a.	n.a.
W	n.a.	0.45	n.a.	0.89	13.9	n.a.	n.a.
Tl	n.a.	0.02	n.a.	0.03	3.11	n.a.	n.a.
Pb	4.80	3.09	n.a.	4.83	14.4	n.a.	n.a.
Th	8.32	4.23	n.a.	5.50	40.9	n.a.	n.a.
U	2.19	1.06	n.a.	1.37	8.81	n.a.	n.a.
Abbr.	n.a. = not analysed						

Table 2: Major and trace element compositions the Lyttelton Group (continued):

Sample	MSI 103	MSI 105	MSI 107	MSI 108	MSI 112	MSI 113	MSI 114
Location	S43°35'42.9" E172°39'58.5"	S43°37'47.4" E172°37'31.6"	S43°39'39.2" E172°37'15.2"	S43°41'17.9" E172°38'29.8"	S43°41'26.6" E172°38'17.2"	S43°40'08.5" E172°37'31.4"	S43°37'59.7" E172°38'56.9"
Unit after Sewell, 1993	l	l	l	t	ra	l	gd
Major elements (wt %; determined by XRF)							
SiO_2	48.76	69.83	47.86	77.85	77.04	47.26	60.10
TiO_2	3.32	0.22	2.69	0.08	0.08	2.94	1.43
Al_2O_3	14.49	13.51	17.49	11.89	11.62	15.80	14.24
FeO^t	12.51	3.34	10.55	0.96	1.65	12.17	6.59
MnO	0.16	0.07	0.15	0.01	0.01	0.15	0.09
MgO	3.76	0.03	4.88	0.12	0.18	4.69	2.95
CaO	7.73	0.32	9.17	0.29	0.27	9.10	4.39
Na_2O	3.86	5.81	3.51	3.26	2.87	3.40	3.84
K_2O	1.50	4.91	1.14	4.60	4.34	1.17	3.40
P_2O_5	0.65	0.05	0.58	0.01	0.02	0.59	0.29
CO_2	0.11	0.02	0.08	0.02	0.05	0.58	1.11
H_2O	1.82	0.50	1.18	0.69	1.06	1.56	0.97
Total	98.67	98.61	99.28	99.78	99.19	99.41	99.40
Trace elements (ppm; determined by ICPMS)							
Li	6.00	50.5	7.85	49.2	n.a.	6.32	14.2
Sc	22.2	0.61	18.2	1.24	n.a.	19.4	12.2
V	215	3.13	211	2.42	n.a.	231	116
Cr	1.55	1.04	93.6	0.85	n.a.	85.6	77.0
Co	35.1	0.04	34.9	0.41	n.a.	44.8	21.9
Ni	3.01	0.59	57.6	0.63	n.a.	88.6	42.3
Cu	17.3	5.79	42.9	1.60	n.a.	50.1	17.6
Zn	160	175	108	58.8	n.a.	124	101
Ga	25.9	36.5	23.8	29.3	n.a.	23.2	25.2
Rb	34.0	202	29.6	321	n.a.	29.1	116
Sr	489	5.06	635	11.0	n.a.	541	288
Y	39.0	73.3	24.0	41.7	n.a.	27.8	36.8
Zr	275	953	234	141	n.a.	239	204
Nb	54.9	134	42.4	61.3	n.a.	44.7	42.2
Mo	2.42	1.15	n.a.	0.72	n.a.	n.a.	3.03
Cd	n.a.	n.a.	n.a.	0.40	n.a.	n.a.	n.a.
Sn	2.57	9.91	1.96	11.1	n.a.	2.07	3.87
Sb	0.07	0.41	0.03	0.97	n.a.	0.07	0.31
Cs	0.39	0.76	0.98	9.71	n.a.	0.55	3.44
Ba	331	17.1	262	25.1	n.a.	274	462
La	39.8	101	32.1	31.3	n.a.	32.6	50.8
Ce	82.2	138	66.6	65.0	n.a.	67.9	99.3
Pr	10.7	23.4	8.27	7.95	n.a.	8.52	12.2
Nd	43.9	83.6	33.7	28.1	n.a.	35.0	45.6
Sm	9.74	16.6	7.30	7.12	n.a.	7.68	9.33
Eu	3.16	0.78	2.45	0.18	n.a.	2.49	1.73
Gd	9.71	15.3	7.07	6.72	n.a.	7.48	8.62
Tb	1.44	2.45	1.02	1.24	n.a.	1.09	1.31
Dy	7.98	14.2	5.58	7.79	n.a.	5.99	7.22
Ho	1.48	2.75	1.00	1.55	n.a.	1.08	1.34
Er	3.66	7.27	2.46	4.40	n.a.	2.65	3.38
Tm	0.50	1.09	0.33	0.69	n.a.	0.35	0.47
Yb	3.08	7.00	1.99	4.51	n.a.	2.16	2.94
Lu	0.43	1.01	0.27	0.61	n.a.	0.30	0.41
Hf	6.85	24.3	5.20	6.78	n.a.	5.37	6.01
Ta	3.33	8.32	2.59	5.33	n.a.	2.73	2.70
W	0.69	2.46	0.60	n.a.	n.a.	1.02	2.39
Tl	0.03	0.52	0.03	1.39	n.a.	0.03	0.34
Pb	2.97	17.4	3.33	28.1	n.a.	3.11	12.6
Th	5.28	30.2	3.93	39.2	n.a.	4.18	13.4
U	1.34	2.44	1.04	8.53	n.a.	0.98	3.01
Abbr.	n.a. = not analysed						

Table 2: Major and trace element compositions the Lyttelton and Akaroa Group:

Sample	MSI 125A	MSI 126	MSI 130	MSI 131B	CD103	M36B 2259	N36C 3069
Location	S43°33'24.3" E172°43'55.2"	S43°35'44.0" E172°44'53.2"	S43°36'22.5" E172°41'25.4"	S43°36'41.5" E172°40'20.0"	S43°41'08.4" E172°44'26.5"	S43°41'41.0" E172°44'26.5"	S43°46'23.0" E172°54'46.5"
Unit after Sewell, 1993	l	ec	l	l	hh	ho	af
Major elements (wt %; determined by XRF)							
SiO_2	49.08	92.79	60.29	49.35	45.70	44.74	47.30
TiO_2	1.99	0.11	1.40	2.96	3.36	3.13	2.86
Al_2O_3	14.54	2.59	15.61	14.59	15.84	14.12	16.86
FeO^t	10.64	0.14	7.47	12.87	13.00	12.92	11.82
MnO	0.15	0.00	0.12	0.18	0.18	0.16	0.20
MgO	8.50	0.12	1.56	4.27	6.23	9.13	4.09
CaO	9.29	0.05	4.28	8.05	8.92	10.30	7.49
Na_2O	3.26	<0,01	4.15	3.90	3.50	2.28	4.49
K_2O	1.08	0.67	3.30	1.36	1.19	0.87	1.69
P_2O_5	0.46	0.01	0.39	0.70	0.58	0.42	0.82
CO_2	0.11	0.00	0.21	0.06	0.54	0.70	1.30
H_2O	0.89	0.64	0.96	1.35	0.01	1.70	0.08
Total	99.99	97.12	99.74	99.64	99.05	100.47	99.00
Trace elements (ppm; determined by ICPMS)							
Li	8.48	5.65	23.4	6.67	8.98	7.97	11.0
Sc	20.4	1.44	11.5	22.8	27.3	38.9	17.6
V	198	21.4	93.6	234	305	424	150
Cr	248	16.7	7.55	60.3	141	407	2.37
Co	44.7	0.17	15.8	37.0	56.1	78.6	36.5
Ni	179	0.46	12.1	33.7	88.1	232	4.01
Cu	54.7	0.49	17.3	41.6	60.0	103	28.5
Zn	99.5	2.04	114	177	150	141	163
Ga	19.1	2.82	26.1	26.0	n.a.	n.a.	n.a.
Rb	25.8	34.2	113	31.9	28.6	26.2	45.1
Sr	512	3.75	374	493	796	688	963
Y	21.5	1.99	41.1	37.7	31.6	25.2	38.7
Zr	157	5.61	411	247.6	221	176	312
Nb	36.5	1.56	44.6	50.2	54.4	41.7	78.8
Mo	1.56	0.06	2.78	2.51	n.a.	n.a.	n.a.
Cd	0.13	0.02	0.26	n.a.	n.a.	n.a.	n.a.
Sn	1.61	0.37	4.50	2.23	1.72	1.43	2.06
Sb	0.08	0.11	0.20	0.09	0.06	0.05	0.09
Cs	0.35	3.56	4.28	0.48	0.29	0.29	0.46
Ba	306	56.9	705	334.7	322	242	427
La	26.5	2.76	57.2	38.6	31.3	24.5	46.2
Ce	54.2	7.21	118	79.4	64.5	50.3	94.1
Pr	6.75	0.68	13.9	10.4	7.82	6.02	11.1
Nd	27.8	2.45	53.5	42.7	31.9	24.4	43.6
Sm	6.02	0.48	10.8	9.46	7.02	5.44	9.07
Eu	1.99	0.07	2.56	3.07	2.30	1.78	2.85
Gd	5.91	0.41	10.2	9.37	6.33	4.92	7.80
Tb	0.85	0.06	1.50	1.38	0.98	0.76	1.18
Dy	4.56	0.35	8.18	7.63	5.26	4.12	6.26
Ho	0.82	0.07	1.52	1.41	0.94	0.73	1.12
Er	2.01	0.20	3.97	3.44	2.38	1.83	2.84
Tm	0.27	0.03	0.55	0.47	0.31	0.23	0.36
Yb	1.63	0.21	3.53	2.85	1.89	1.45	2.26
Lu	0.23	0.03	0.50	0.40	0.26	0.20	0.31
Hf	3.76	0.22	10.3	6.20	4.27	3.37	5.46
Ta	2.09	0.12	2.70	2.93	2.70	1.98	3.66
W	n.a.	n.a.	n.a.	0.88	n.a.	n.a.	n.a.
Tl	0.04	0.08	0.54	0.03	n.a.	n.a.	n.a.
Pb	3.69	0.61	16.9	5.16	2.20	1.61	3.14
Th	3.95	1.13	14.5	5.02	3.66	3.14	5.57
U	0.98	0.19	3.59	1.27	0.93	0.78	1.38
Abbr.	n.a. = not analysed						

Table 2: Major and trace element compositions the Akaroa Group:

Sample	N36C 3072	N36C 3602	UC 13809	MSI 18	MSI 117	MSI 120	MSI 123
Location	S43°47'45.8' E172°54'29.9"	S43°46'20.46" E172°55'38.06"	S43°43'34.56" E173°02'55.91"	S43°45'39.2" E173°03'22.6"	S43°41'22.7" E172°44'30.0"	S43°41'42.1" E172°43'24.6"	S43°41'00.4" E172°43'24.6"
Unit after Sewell, 1993	af	ao		af	hh	ho	ho
Major elements (wt %; determined by XRF)							
SiO_2	43.67	42.09	44.52	45.12	47.71	45.07	46.72
TiO_2	2.85	4.11	3.57	3.50	2.65	3.73	2.58
Al_2O_3	13.01	15.27	15.98	15.99	17.28	15.36	17.10
FeO^t	13.22	13.31	12.90	12.91	11.66	13.34	12.03
MnO	0.18	0.16	0.17	0.18	0.19	0.17	0.21
MgO	10.28	5.02	6.24	6.39	3.91	6.95	3.97
CaO	10.56	11.62	10.40	9.63	7.69	9.72	8.07
Na_2O	2.35	2.66	2.85	3.25	4.99	3.20	4.02
K_2O	0.96	0.36	1.01	1.11	1.69	0.85	1.79
P_2O_5	0.39	0.23	0.50	0.59	0.98	0.46	1.45
CO_2	1.94	0.87	0.04	0.08	0.02	0.05	0.06
H_2O	0.06	3.45	1.43	1.54	0.59	0.83	1.90
Total	99.47	99.15	99.61	100.29	99.36	99.73	99.90
Trace elements (ppm; determined by ICPMS)							
Li	7.26	5.54	5.92	5.24	8.21	3.95	5.68
Sc	42.1	49.0	33.2	21.8	9.60	24.1	9.42
V	468	583	430	271	112	318	108
Cr	497	2.47	177	117	1.59	173	3.29
Co	87.4	61.2	62.9	47.4	29.6	56.2	31.5
Ni	263	20.4	82.5	61.1	8.60	114	8.78
Cu	87.0	64.8	58.5	53.3	32.2	79.0	30.5
Zn	144	142	154	126	135	132	152
Ga	n.a.	n.a.	n.a.	22.2	23.3	22.6	25.3
Rb	32.7	9.38	30.7	23.2	37.5	17.2	42.1
Sr	548	614	801	726	901	676	1052
Y	25.0	16.3	27.5	28.0	33.7	25.9	36.7
Zr	167	79.6	206.7	208	283	194	361
Nb	38.0	22.8	50.1	52.4	75.7	43.1	83.7
Mo	n.a.	n.a.	n.a.	2.14	3.01	1.91	4.14
Cd	n.a.	n.a.	n.a.	n.a.	n.a.	n.a.	n.a.
Sn	1.44	0.90	1.61	1.75	2.11	1.70	2.01
Sb	0.05	0.03	0.05	0.06	0.09	0.04	0.11
Cs	0.26	0.29	0.24	0.24	0.42	0.27	0.47
Ba	217	113	268	313	457	271	484
La	22.2	9.98	28.3	32.3	48.8	27.2	64.5
Ce	46.6	21.7	58.0	66.4	98.4	56.1	129
Pr	5.62	2.80	6.92	8.61	12.4	7.24	16.1
Nd	23.2	12.4	28.0	35.3	48.8	29.9	62.5
Sm	5.27	3.09	6.17	7.66	9.78	6.64	12.0
Eu	1.71	1.29	2.03	2.57	3.13	2.28	3.76
Gd	4.83	3.05	5.52	7.39	8.96	6.58	10.6
Tb	0.75	0.49	0.85	1.07	1.26	0.96	1.46
Dy	4.10	2.70	4.53	5.79	6.71	5.28	7.59
Ho	0.74	0.48	0.80	1.06	1.22	0.96	1.35
Er	1.82	1.20	1.98	2.49	2.95	2.34	3.27
Tm	0.23	0.16	0.26	0.34	0.40	0.32	0.43
Yb	1.41	0.94	1.53	2.07	2.45	1.88	2.59
Lu	0.19	0.13	0.21	0.29	0.34	0.27	0.37
Hf	3.28	1.73	3.87	4.89	6.05	4.61	7.70
Ta	1.81	1.16	2.39	3.08	4.19	2.53	4.42
W	n.a.	n.a.	n.a.	0.68	0.70	0.42	1.18
Tl	n.a.	n.a.	n.a.	0.03	0.03	0.03	0.06
Pb	1.91	0.82	1.72	1.99	2.94	1.65	3.44
Th	2.74	0.98	3.48	3.63	5.58	3.24	7.30
U	0.71	0.23	0.88	0.96	1.49	0.89	1.98
Abbr.	n.a. = not analysed						

Table 2: Major and trace element compositions the Akaroa Group:

Sample	MSI 134	MSI 137	MSI 141	MSI 144	MSI 148	MSI 150	MSI 151
Location	S43°40'21.3" E172°49'57.7"	S43°40'50.2" E172°51'12.1"	S43°49'30.0" E172°56'49.7"	S43°50'59.0" E172°58'11.3"	S43°40'08.0" E172°59'40.5"	S43°43'02.4" E172°58'23.8"	S43°41'46.9" E173°03'53.7"
Unit after Sewell, 1993	hp	hp	af	ae	af	af	af
Major elements (wt %; determined by XRF)							
SiO_2	44.37	46.63	45.92	44.93	47.09	45.29	49.24
TiO_2	3.66	2.98	3.28	3.59	3.09	3.59	2.25
Al_2O_3	16.03	16.72	16.34	16.01	17.10	16.09	17.28
FeO^t	13.18	12.36	11.42	12.90	11.73	13.15	10.91
MnO	0.17	0.19	0.15	0.18	0.18	0.17	0.21
MgO	5.54	4.55	5.02	4.94	4.62	6.24	2.90
CaO	8.94	7.61	8.99	8.71	8.12	10.00	7.08
Na_2O	3.46	4.12	3.22	3.34	4.15	2.89	5.21
K_2O	1.15	1.49	1.21	1.27	1.57	0.98	2.02
P_2O_5	0.51	0.76	0.60	0.61	0.85	0.49	1.14
CO_2	0.09	0.02	1.15	0.05	0.05	0.07	0.21
H_2O	1.85	1.30	1.61	1.47	1.66	1.12	0.58
Total	98.95	98.73	98.91	98.00	100.21	100.08	99.03
Trace elements (ppm; determined by ICPMS)							
Li	5.82	6.15	n.a.	5.77	6.69	n.a.	n.a.
Sc	17.5	13.2	n.a.	17.5	12.5	n.a.	n.a.
V	260	143	n.a.	214	157	n.a.	n.a.
Cr	31.8	16.0	n.a.	27.0	12.3	n.a.	n.a.
Co	48.3	34.7	n.a.	38.7	31.3	n.a.	n.a.
Ni	37.5	13.0	n.a.	21.1	11.9	n.a.	n.a.
Cu	41.2	32.9	n.a.	24.3	23.5	n.a.	n.a.
Zn	136	136	n.a.	138	141	n.a.	n.a.
Ga	23.7	23.3	n.a.	22.3	24.1	n.a.	n.a.
Rb	29.8	32.7	n.a.	27.5	33.2	n.a.	n.a.
Sr	741	807	n.a.	1080	835	n.a.	n.a.
Y	26.0	32.0	n.a.	31.6	33.3	n.a.	n.a.
Zr	202	270	n.a.	246	304	n.a.	n.a.
Nb	49.2	65.5	n.a.	56.6	73.4	n.a.	n.a.
Mo	2.06	2.68	n.a.	2.26	3.15	n.a.	n.a.
Cd	n.a.	n.a.	n.a.	n.a.	n.a.	n.a.	n.a.
Sn	1.87	2.25	n.a.	1.99	2.36	n.a.	n.a.
Sb	0.05	0.07	n.a.	0.04	0.07	n.a.	n.a.
Cs	0.75	0.29	n.a.	0.16	0.28	n.a.	n.a.
Ba	311	388	n.a.	348	409	n.a.	n.a.
La	31.9	43.4	n.a.	36.2	47.3	n.a.	n.a.
Ce	64.1	87.0	n.a.	72.7	94.2	n.a.	n.a.
Pr	8.17	11.0	n.a.	9.47	11.9	n.a.	n.a.
Nd	33.4	43.9	n.a.	38.5	47.2	n.a.	n.a.
Sm	7.17	9.08	n.a.	8.36	9.68	n.a.	n.a.
Eu	2.43	3.00	n.a.	2.78	3.15	n.a.	n.a.
Gd	6.91	8.47	n.a.	8.04	8.97	n.a.	n.a.
Tb	1.00	1.21	n.a.	1.16	1.27	n.a.	n.a.
Dy	5.38	6.52	n.a.	6.26	6.70	n.a.	n.a.
Ho	0.97	1.20	n.a.	1.14	1.20	n.a.	n.a.
Er	2.31	2.92	n.a.	2.77	2.90	n.a.	n.a.
Tm	0.31	0.40	n.a.	0.37	0.39	n.a.	n.a.
Yb	1.84	2.42	n.a.	2.21	2.32	n.a.	n.a.
Lu	0.26	0.35	n.a.	0.31	0.33	n.a.	n.a.
Hf	4.82	6.37	n.a.	5.61	6.58	n.a.	n.a.
Ta	2.85	3.88	n.a.	3.20	4.09	n.a.	n.a.
W	0.52	0.56	n.a.	0.40	0.66	n.a.	n.a.
Tl	0.02	0.02	n.a.	0.02	0.03	n.a.	n.a.
Pb	2.47	2.86	n.a.	2.01	2.88	n.a.	n.a.
Th	4.10	5.08	n.a.	4.05	5.67	n.a.	n.a.
U	1.07	1.34	n.a.	1.01	1.53	n.a.	n.a.
Abbr.	n.a. = not analysed						

Table 2: Major and trace element compositions the Akaroa Group:

Sample	MSI 154	MSI 157	MSI 161	MSI 164	MSI 167B	MSI 169	MSI 171
Location	S43°44'21.9" E173°05'26.7"	S43°48'03.2" E173°00'21.1"	S43°47'33.8" E173°01'15.5"	S43°45'10.7" E172°52'23.6"	S43°47'39.7" E172°54'31.0"	S43°50'51.7" E172°53'42.3"	S43°50'19.4" E172°52'14.5"
Unit after Sewell, 1993	af	ae	af	af	af	af	ae
Major elements (wt %; determined by XRF)							
SiO_2	47.14	50.44	46.26	45.90	58.81	46.14	46.45
TiO_2	3.08	2.20	3.78	3.36	0.65	3.60	3.62
Al_2O_3	17.26	16.78	15.96	16.28	17.41	16.74	16.48
FeO^t	11.70	10.81	12.87	11.41	5.59	12.88	13.05
MnO	0.18	0.24	0.20	0.17	0.15	0.19	0.19
MgO	4.30	3.09	4.73	4.41	0.60	4.86	4.74
CaO	8.07	6.63	9.13	8.80	1.74	8.57	8.79
Na_2O	4.40	5.08	3.80	3.51	6.25	4.07	3.57
K_2O	1.55	2.09	1.27	1.33	4.32	1.27	1.29
P_2O_5	0.92	1.04	0.69	0.66	0.20	0.70	0.67
CO_2	0.07	0.04	0.52	2.10	2.22	0.09	0.68
H_2O	1.45	0.71	1.21	1.60	0.73	0.69	1.12
Total	100.12	99.15	100.42	99.53	98.67	99.80	100.65
Trace elements (ppm; determined by ICPMS)							
Li	6.54	n.a.	5.60	6.66	11.5	n.a.	n.a.
Sc	12.1	n.a.	17.1	18.1	3.60	n.a.	n.a.
V	142	n.a.	231	212	2.71	n.a.	n.a.
Cr	2.85	n.a.	4.37	37.4	0.94	n.a.	n.a.
Co	30.7	n.a.	38.5	37.6	2.81	n.a.	n.a.
Ni	5.12	n.a.	9.19	24.6	0.83	n.a.	n.a.
Cu	27.7	n.a.	19.7	34.0	9.34	n.a.	n.a.
Zn	139	n.a.	140	134	150.6	n.a.	n.a.
Ga	24.0	n.a.	23.5	23.2	28.7	n.a.	n.a.
Rb	33.5	n.a.	25.6	31.1	71.7	n.a.	n.a.
Sr	846	n.a.	748	767	207	n.a.	n.a.
Y	34.8	n.a.	32.4	32.1	36.6	n.a.	n.a.
Zr	284	n.a.	243	244	591	n.a.	n.a.
Nb	72.3	n.a.	57.8	58.5	103	n.a.	n.a.
Mo	3.12	n.a.	2.09	1.99	2.73	n.a.	n.a.
Cd	n.a.	n.a.	n.a.	n.a.	n.a.	n.a.	n.a.
Sn	1.92	n.a.	2.02	2.02	5.20	n.a.	n.a.
Sb	0.07	n.a.	0.08	0.04	0.49	n.a.	n.a.
Cs	0.33	n.a.	0.23	0.39	0.77	n.a.	n.a.
Ba	434	n.a.	336	365	1100	n.a.	n.a.
La	47.4	n.a.	36.2	38.0	56.4	n.a.	n.a.
Ce	94.7	n.a.	73.9	78.1	106	n.a.	n.a.
Pr	12.0	n.a.	9.56	10.1	12.6	n.a.	n.a.
Nd	48.0	n.a.	39.2	41.1	44.6	n.a.	n.a.
Sm	9.82	n.a.	8.54	8.81	8.55	n.a.	n.a.
Eu	3.20	n.a.	2.83	2.92	2.50	n.a.	n.a.
Gd	9.19	n.a.	8.27	8.51	7.59	n.a.	n.a.
Tb	1.30	n.a.	1.20	1.23	1.17	n.a.	n.a.
Dy	6.94	n.a.	6.49	6.66	6.69	n.a.	n.a.
Ho	1.26	n.a.	1.18	1.22	1.30	n.a.	n.a.
Er	3.03	n.a.	2.84	2.94	3.51	n.a.	n.a.
Tm	0.41	n.a.	0.38	0.40	0.53	n.a.	n.a.
Yb	2.49	n.a.	2.31	2.40	3.50	n.a.	n.a.
Lu	0.35	n.a.	0.33	0.34	0.51	n.a.	n.a.
Hf	6.23	n.a.	5.55	5.90	12.7	n.a.	n.a.
Ta	3.90	n.a.	3.28	3.44	6.03	n.a.	n.a.
W	0.86	n.a.	0.35	0.39	1.37	n.a.	n.a.
Tl	0.08	n.a.	0.04	0.03	0.14	n.a.	n.a.
Pb	2.68	n.a.	2.16	2.46	9.44	n.a.	n.a.
Th	5.38	n.a.	4.14	4.45	13.9	n.a.	n.a.
U	1.41	n.a.	1.27	1.16	2.02	n.a.	n.a.
Abbr.	n.a. = not analysed						

Table 2: Major and trace element compositions the Akaroa and Diamond Harbour Volcanic Groups:

Sample	MSI 174	MSI 177	MSI 179	CD77	CD112	UC13790	MSI 16
Location	S43°48'22.0" E172°47'30.4"	S43°49'33.9" E172°42'52.9"	S43°45'37.9" E172°43'33.7"	S43°38'10.03" E172°43'22.52"	S43°40'15.61" E172°44'03.96"	S43°43'34.56" E173°02'55.91"	S43°37'50.2" E172°44'35.9"
Unit after Sewell, 1993	af	af	ho	sb	sb	sb - LBPI	sb
Major elements (wt %; determined by XRF)							
SiO_2	44.77	45.95	46.49	48.06	45.53	41.86	47.56
TiO_2	3.50	2.94	3.15	1.94	3.22	2.79	2.91
Al_2O_3	16.35	16.24	16.62	13.82	15.81	12.13	17.68
FeO^t	12.60	12.43	12.10	11.34	12.89	12.94	11.92
MnO	0.17	0.18	0.17	0.15	0.18	0.18	0.18
MgO	5.85	6.15	4.93	9.24	6.32	11.99	4.23
CaO	9.95	9.49	7.96	9.24	9.50	10.66	7.97
Na_2O	3.17	3.83	4.17	2.95	3.53	2.95	4.67
K_2O	1.14	1.11	1.45	1.03	1.27	1.21	1.55
P_2O_5	0.67	0.77	0.76	0.39	0.60	0.69	0.74
CO_2	0.14	0.04	0.07	0.59	0.56	0.07	0.04
H_2O	1.80	0.75	1.24	0.05	0.04	2.06	0.62
Total	100.11	99.88	99.11	98.80	99.45	99.53	100.07
Trace elements (ppm; determined by ICPMS)							
Li	5.36	5.31	6.00	13.2	8.73	10.4	6.46
Sc	21.5	20.3	15.8	33.3	29.7	32.4	9.56
V	276	229	193	295	348	380	131
Cr	56.1	152	33.6	457	155	660	7.74
Co	46.7	48.1	38.4	67.1	58.4	87.5	30.7
Ni	52.2	79.3	25.5	302	95.5	426	13.3
Cu	60.6	60.5	41.7	84.4	63.6	97.8	32.0
Zn	129	137	141	129	149	169	114
Ga	23.1	23.8	25.8	n.a.	n.a.	n.a.	20.7
Rb	24.0	25.9	32.3	30.9	32.5	52.3	34.6
Sr	810	779	984	494	776	860	970
Y	28.9	28.8	31.7	23.7	30.5	25.2	28.4
Zr	230	215	283	138.8	242	235	260
Nb	57.8	55.7	65.4	33.6	58.3	73.5	67.4
Mo	2.40	2.57	2.83	n.a.	n.a.	n.a.	2.84
Cd	n.a.	n.a.	n.a.	n.a.	n.a.	n.a.	0.17
Sn	2.06	1.72	2.42	1.33	1.86	1.74	1.98
Sb	0.04	0.06	0.07	0.08	0.07	0.08	0.07
Cs	0.22	0.31	0.31	0.59	0.30	0.31	0.49
Ba	342	342	412	257	324	389	439
La	37.1	37.6	44.4	20.9	34.7	44.3	43.9
Ce	75.4	75.8	88.5	43.5	70.0	88.6	89.6
Pr	9.66	9.72	11.2	5.24	8.22	10.2	10.6
Nd	39.3	39.5	44.8	21.7	32.8	39.8	42.0
Sm	8.29	8.34	9.24	4.86	6.91	7.99	8.54
Eu	2.75	2.81	3.03	1.54	2.22	2.42	2.82
Gd	7.85	8.03	8.69	4.49	6.09	6.58	8.07
Tb	1.13	1.14	1.23	0.71	0.95	0.94	1.14
Dy	6.13	6.05	6.62	3.90	5.03	4.58	5.99
Ho	1.10	1.09	1.20	0.71	0.91	0.74	1.07
Er	2.66	2.62	2.88	1.80	2.28	1.70	2.65
Tm	0.35	0.35	0.39	0.24	0.30	0.20	0.35
Yb	2.14	2.07	2.35	1.46	1.80	1.15	2.14
Lu	0.30	0.29	0.33	0.20	0.25	0.15	0.30
Hf	5.50	5.07	6.49	2.79	4.50	4.24	5.79
Ta	3.48	3.29	3.85	1.63	2.87	3.36	3.94
W	0.41	0.69	0.66	n.a.	n.a.	n.a.	n.a.
Tl	0.02	0.03	0.02	n.a.	n.a.	n.a.	0.03
Pb	2.37	2.10	2.71	3.26	2.24	2.45	3.04
Th	4.22	4.24	5.11	3.43	4.20	5.40	5.40
U	1.15	1.12	1.40	0.79	1.06	1.35	1.40
Abbr.	n.a. = not analysed						

Table 2: Major and trace element compositions the Akaroa and Diamond Harbour Volcanic Groups:

Sample	MSI 17	MSI 20 B	MSI 20E	MSI 127A	MSI 128B	MSI 129A	NZS 8
Location	S43°38'04.7" E172°44'42.3"	S43°44'20.8" E173°04'14.1"	S43°44'20.8" E173°04'14.1"	S43°38'03.5" E172°43'22.3"	S43°37'35.3" E172°44'15.7"	S43°38'04.7" E172°44'42.3"	
Unit after Sewell, 1993	cd	sb - LBPI	sb - LBPI	sb	sb	cb	cd
Major elements (wt %; determined by XRF)							
SiO_2	49.44	42.29	48.73	48.77	46.06	47.56	42.27
TiO_2	2.34	2.85	1.92	1.98	2.89	2.91	2.99
Al_2O_3	17.94	12.26	14.10	14.08	17.01	17.68	14.33
FeO^t	12.07	13.17	11.25	11.21	12.00	11.92	12.55
MnO	0.18	0.18	0.16	0.16	0.18	0.18	0.17
MgO	2.02	11.51	9.54	8.91	4.40	4.23	7.58
CaO	5.64	10.74	9.35	9.51	7.88	7.97	10.76
Na_2O	4.30	3.77	3.02	3.29	4.75	4.67	2.69
K_2O	2.02	1.13	1.05	1.07	1.55	1.55	1.03
P_2O_5	1.20	0.71	0.37	0.39	0.71	0.74	0.49
CO_2	0.04	0.05	0.01	0.06	0.04	0.04	2.42
H_2O	3.04	0.78	0.50	0.64	0.77	0.62	0.86
Total	100.23	99.44	100.00	100.07	98.24	100.07	98.14
Trace elements (ppm; determined by ICPMS)							
Li	8.17	6.23	8.60	7.48	7.36	6.46	14.1
Sc	7.67	24.1	22.2	24.1	9.79	9.56	21.1
V	51.8	284	205	223	136	131	286
Cr	0.52	517	310	352	9.35	7.74	203
Co	18.3	69.7	49.5	53.5	34.2	30.7	54.9
Ni	2.57	329	228	225	13.4	13.3	136
Cu	17.9	80.9	65.7	65.8	29.2	32.0	59.6
Zn	172	154	105	116	116	114	114
Ga	26.2	22.8	18.4	20.2	21.8	20.7	20.7
Rb	44.6	28.8	26.7	28.5	35.4	34.6	26.3
Sr	814	740	431	443	1091	967	672
Y	39.4	24.5	21.8	23.8	28.6	28.4	22.6
Zr	371	235	137	144	283	259.5	189
Nb	89.1	70.2	31.6	33.2	66.7	67.4	44.2
Mo	3.70	2.69	0.96	1.20	3.19	2.84	2.10
Cd	n.a.	n.a.	0.12	n.a.	n.a.	0.17	n.a.
Sn	2.63	1.88	1.38	1.54	1.96	1.98	1.61
Sb	0.06	0.07	0.06	0.06	0.08	0.07	0.06
Cs	0.32	0.64	0.57	0.40	0.45	0.49	3.36
Ba	619	438	270	268	349	439	542
La	62.3	48.4	22.2	23.0	42.8	43.9	30.4
Ce	112	95.3	45.3	46.1	83.2	89.6	61.9
Pr	15.6	12.0	5.79	6.01	10.5	10.6	7.62
Nd	60.4	47.3	24.1	24.5	40.8	42.0	31.0
Sm	11.9	9.50	5.36	5.49	8.26	8.54	6.68
Eu	3.90	2.99	1.76	1.79	2.74	2.82	2.22
Gd	10.8	8.52	5.43	5.46	7.66	8.07	6.43
Tb	1.52	1.15	0.81	0.81	1.08	1.14	0.93
Dy	8.08	5.67	4.43	4.51	5.74	5.99	4.96
Ho	1.47	0.93	0.81	0.84	1.03	1.07	0.89
Er	3.59	2.06	2.05	2.06	2.52	2.65	2.16
Tm	0.49	0.26	0.27	0.28	0.34	0.35	0.28
Yb	2.99	1.45	1.72	1.74	2.02	2.14	1.72
Lu	0.42	0.20	0.24	0.25	0.28	0.30	0.24
Hf	8.22	5.69	3.40	3.41	5.41	5.79	4.43
Ta	5.06	4.12	1.84	1.84	3.73	3.94	2.60
W	0.61	0.89	n.a.	0.15	1.06	n.a.	0.36
Tl	0.02	0.02	0.06	0.02	0.03	0.03	0.23
Pb	3.65	2.61	3.54	3.38	3.29	3.04	1.88
Th	7.12	5.67	3.46	3.50	5.73	5.40	3.35
U	1.90	1.46	0.80	0.78	1.50	1.40	0.92
Abbr.	n.a. = not analysed						

Table 3: Sr - Nd - Pb - Hf and $\partial^{18}O$ isotope data (errors are in 2 σ)

Sample	$^{87}Sr/^{86}Sr$		$^{143}Nd/^{144}Nd$		$^{206}Pb/^{204}Pb$		$^{207}Pb/^{204}Pb$		$^{208}Pb/^{204}Pb$		$^{176}Hf/^{177}Hf$		$\partial^{18}O$ in ‰ (dupl)
Lyttelton Volcano													
MSI 9A	0.703041	3	0.512934	3	19.575	1	15.564	1	39.146	2	-	-	-
MSI 10	0.703048	3	0.512918	3	19.496	3	15.550	2	39.060	5	-	-	4.76
MSI 107	0.703030	2	0.512934	2	19.365	1	15.542	1	38.979	2	0.283052	8	5.05
MSI 113	0.703220	4	0.512919	2	19.326	1	15.613	1	39.153	3	-	-	-
MSI 114	0.704461	2	0.512787	2	19.067	1	15.591	1	38.793	2	-	-	-
MSI 125A	0.703629	3	0.512877	3	19.087	1	15.577	1	38.760	2	0.282972	9	5.19
MSI 130	0.704996	2	0.512755	3	19.024	1	15.583	1	38.718	2	-	-	-
MSI 131B	0.703332	3	0.512906	3	19.336	2	15.592	2	39.032	4	-	-	-
Mount Herbert Volcanic Group													
CD103	0.703091	3	0.512966	3	19.587	1	15.549	1	39.136	2	-	-	4.81 (4.63)
M36B 2259	0.703015	2	0.512966	2	19.402	2	15.543	2	38.982	4	-	-	4.76
MSI 117	0.702999	3	0.512964	2	19.653	2	15.543	1	39.196	3	-	-	-
MSI 120	0.702982	2	0.512974	2	19.523	1	15.529	1	39.058	3	-	-	4.73 (4.61)
MSI 134	0.703059	3	0.512950	3	19.413	1	15.549	1	38.976	3	-	-	-
Akaroa Volcano													
N36C 3072	0.702991	3	0.512958	2	19.552	1	15.545	1	39.067	3	-	-	4.74
N36C 3602	0.703006	3	0.512964	2	19.457	1	15.546	1	39.008	2	-	-	-
UC 13809	0.702970	5	0.512972	3	19.576	2	15.531	2	39.080	4	-	-	-
MSI 18	0.703020	3	0.512963	3	19.579	2	15.540	2	39.100	5	-	-	4.86
MSI 144	0.703097	3	0.512973	2	19.676	1	15.539	1	39.199	2	-	-	-
MSI 177	0.703004	3	0.512975	2	19.570	1	15.529	1	39.081	1	0.283048	6	4.65 (4.84)
Diamond Harbour Volcanic Group													
CD77	0.703605	3	0.512880	2	19.096	2	15.580	1	38.794	3	-	-	-
CD112	0.703029	3	0.512965	3	19.669	1	15.543	1	39.198	3	-	-	4.76
UC13790	0.702958	2	0.512957	3	19.860	1	15.551	1	39.360	3	-	-	4.90
MSI 16	0.703637	2	0.512864	3	19.061	1	15.578	1	38.761	2	-	-	-
MSI 17	0.703027	3	0.512953	2	19.662	1	15.566	0	39.251	3	-	-	-
MSI 20E	0.702972	3	0.512951	3	19.843	2	15.560	1	39.362	4	0.283036	5	4.80
MSI 127A	0.703592	3	0.512876	3	19.077	4	15.572	3	38.770	8	0.282991	8	5.02
MSI 128B	0.703558	3	0.512878	3	19.058	1	15.570	1	38.732	2	-	-	-
NZS8	0.703027	6	0.512955	3	19.648	1	15.590	1	39.317	2	-	-	-

Based on the SiO_2 content, the moderately mafic (> 4 wt% MgO) volcanic rocks can be grouped into a high-silica group (> 48 wt % SiO_2) and a low-silica group (< 48 wt % SiO_2; Fig. 2.2 and Fig. 2.3). The more SiO_2 - saturated volcanics occur on the Lyttelton Volcano (NW part of the Banks Peninsula), whereas the more SiO_2 - undersaturated lavas occur on the Akaroa Volcano (SE part of the Banks Peninsula). Two exceptions are Diamond Harbour volcanic rocks, which erupted on the Lyttelton shield, but have geochemical characteristics of the low-silica Akaroa group volcanics. In comparison to the high-silica Lyttelton volcanics, the low-silica Akaroa volcanics generally have higher contents of FeO^t, TiO_2, CaO, Sr and Nb but lower Pb for a given MgO content (Fig. 2.3a-d).

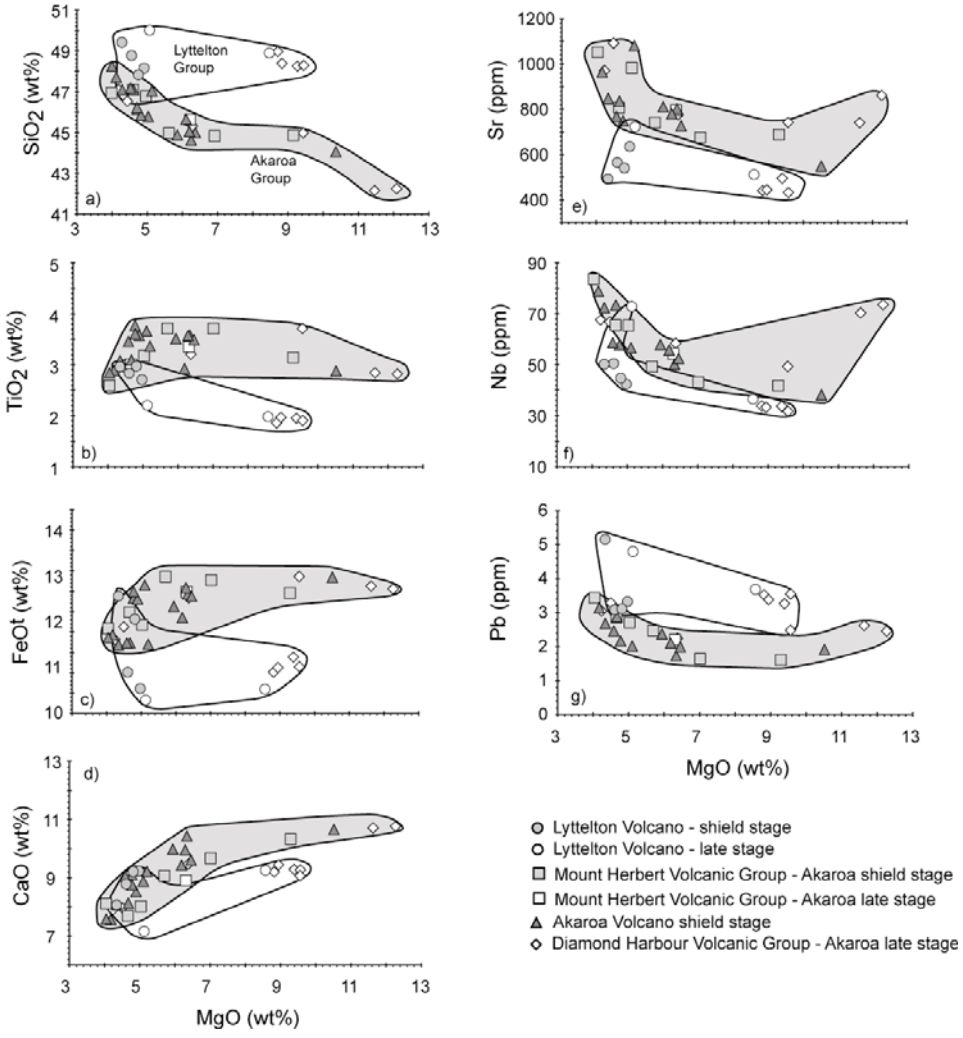

Fig.2.3a-g: Diagrams showing selected major and trace elements versus MgO for mafic samples (MgO > 4wt%) of the Banks Peninsula volcanic rocks. The two groups for Lyttelton and Akaroa volcanoes define almost parallel trends, with the Lyttelton group having higher SiO_2 and Pb, but lower TiO_2, FeO^t, CaO, Sr and Nb concentrations relative to MgO. The grey field represent the low-silica Akaroa lavas, whereas the white field represents the high-silica Lyttelton volcanics.

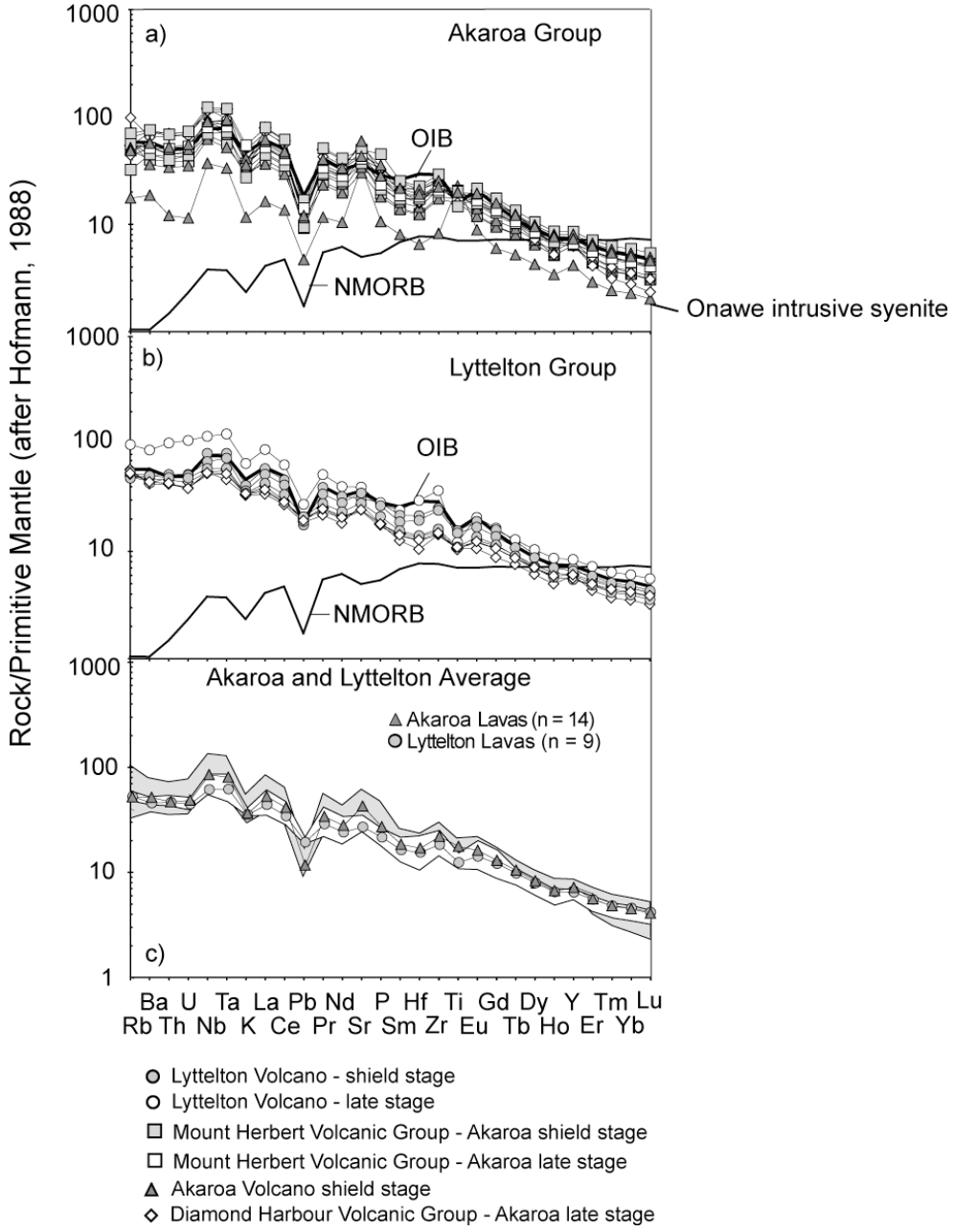

Fig.2.4: Primitive mantle normalised (after Hofmann, 1988) incompatible element patterns of mafic lavas (MgO > 4 wt%) on multi-element diagrams. All volcanics show incompatible element patterns similar to those of ocean island basalts and show enrichment in incompatible elements compared to MORB. Black lines represent typical OIB and NMORB incompatible element patterns after Sun and McDonough (1989). Dark and light grey fields in Fig. 2.4c represent all mafic Akaroa and Lyttelton group lavas, respectively. The Akaroa group lavas have the most pronounced peaks for Nb, Ta and troughs for K and Pb, which become less pronounced within the Lyttelton lavas. Although there is considerable overlap between Akaroa and Lyttelton group incompatible element patterns, the Akaroa Group trends towards slightly higher incompatible element contents compared to the Lyttelton rocks with similar MgO.

Incompatible element patterns of all mafic Banks Peninsula volcanic rocks on multi-element diagrams are strongly akin to ocean island basalts (Fig. 2.4), showing pronounced peaks in Nb-Ta and troughs for Pb and K. All samples are enriched in incompatible elements (LILE, LREE, Sr, U, Th, etc.) compared to mid ocean ridge basalts and have steep, negative rare earth element patterns ($(La/Yb)_N$ > 6.5, $(Sm/Yb)_N$ > 3.5 and $(Er/Yb)_N$ > 1; N = Normalized to primitive mantle after Hofmann, 1988)) on multi-element diagrams. Akaroa lavas with low SiO_2 concentrations (basanites) have more pronounced peaks in Nb, Ta, Zr (higher Nb/La, Zr/Hf, Nb/Ta) and more prominent troughs for Pb and K. Ratios of fluid mobile elements to less fluid mobile incompatible elements (U/(Nb, La), (Rb, Ba)/Zr) are higher and ratios of more to less incompatible elements (such as Nb/Zr, (La, Sm)/Yb, Zr/Y etc.) are lower in the more silica-saturated Lyttelton volcanics. Exceptions are the late-stage high-silica lavas from Lyttelton Volcano (Mount Pleasant Formation) with a more pronounced incompatible element pattern (Fig. 2.4b).

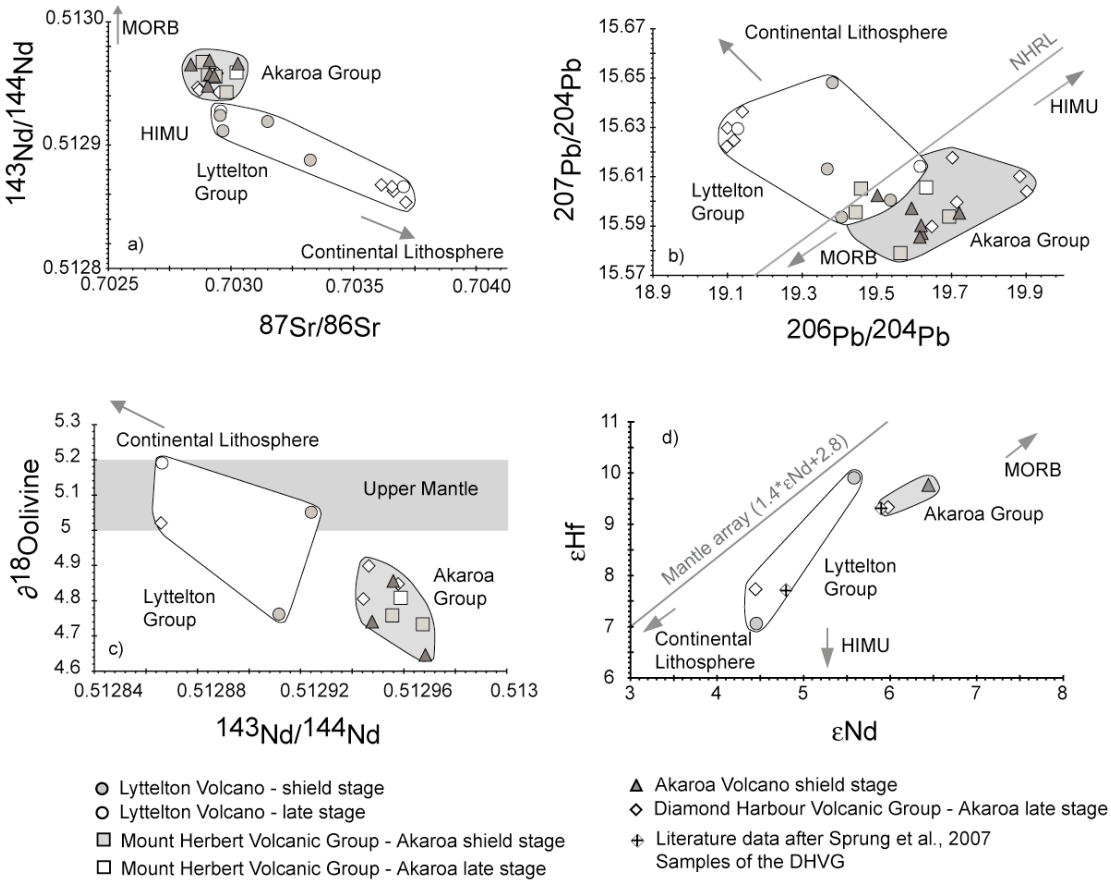

Fig. 2.5: Sr, Nd, Pb, Hf and O isotopic relationships of mafic (MgO > 4%) volcanic rocks from Banks Peninsula. Both Lyttelton and Akaroa volcanoes form isotopically distinct fields with minor overlap in Pb isotopic composition. The Lyttelton group lavas trend towards an enriched (EMII-type) endmember, which is represented by continental lithosphere (crust and mantle), whereas the Akaroa group lavas plot on an array between HIMU and Pacific MORB. The grey rectangle in the Nd-O isotope space represents common peridotitic mantle as defined by Mattey, 1994. The mantle array in the Nd-Hf space is after Geldmacher *et al.*, 2003. Two additional data points (black crosses) in the Nd-Hf isotope diagram are taken from Sprung *et al.*, 2007.

The low-silica Akaroa group has isotopic compositions intermediate between mid ocean ridge basalts (MORB) and HIMU mantle endmembers with $^{87}Sr/^{86}Sr$ = 0.70297 - 0.70312, $^{143}Nd/^{144}Nd$ = 0.51294 - 0.51297, $^{206}Pb/^{204}Pb$ = 19.44 - 19.90, $^{207}Pb/^{204}Pb$ = 15.58 - 15.61, $^{208}Pb/^{204}Pb$ = 39.17 - 39.55, $^{176}Hf/^{177}Hf$ = 0.283036 - 0.283048 and $\partial^{18}O$ values of olivine (4.65 - 4.90) below those common for mantle peridotite and MORB (Mattey *et al.*, 1994; Fig. 2.5). The high-silica Lyttelton group has higher $^{87}Sr/^{86}Sr$ = 0.70307 - 0.70366, $^{207}Pb/^{204}Pb$ = 15.59 - 15.65 and $\partial^{18}O$ values of 4.76 - 5.19 and generally lower $^{143}Nd/^{144}Nd$ = 0.51278 - 0.51293, $^{206}Pb/^{204}Pb$ = 19.10 - 19.62, $^{208}Pb/^{204}Pb$ = 38.91 - 39.33 and $^{176}Hf/^{177}Hf$ = 0.282972 - 0.283052 ratios (Fig.2.5a-2.5d) compared to the low-silica Akaroa volcanics. Isotopic compositions extending from the Akaroa array towards an enriched (EMII-type) endmember.

2.5 Discussion

2.5.1 Temporal and geochemical evolution of Banks Peninsula volcanoes

The temporal framework of volcanism on Banks Peninsula was previously based on K/Ar age determinations and stratigraphy (Sewell, 1993; Stipp and Mc Dougall, 1968; Weaver and Smith, 1989). The new $^{40}Ar/^{39}Ar$ ages presented here suggest that both volcanoes, Lyttelton and Akaroa, formed in two phases: 1) a voluminous shield phase and 2) a low-volume late stage phase (Fig.2.6). Volcanic activity at Lyttelton presumably started with a fairly voluminous pulse of magmatism immediately forming most of the Lyttelton Volcano within ~ 1 Ma (12.5 - 11.5 Ma, including the Governors Bay Formation and the Allandale Rhyolite) by erupting a minimum of ~ 350 km^3 shield building lavas. After the shield-building phase, late-stage volcanic activity continued until 10.5 Ma through the eruption of much lower volumes of mafic

lavas focused at the N flank of Lyttelton Volcano (the Mount Pleasant Formation), as well as dike intrusions varying from mafic to felsic composition (Shelley, 1988).

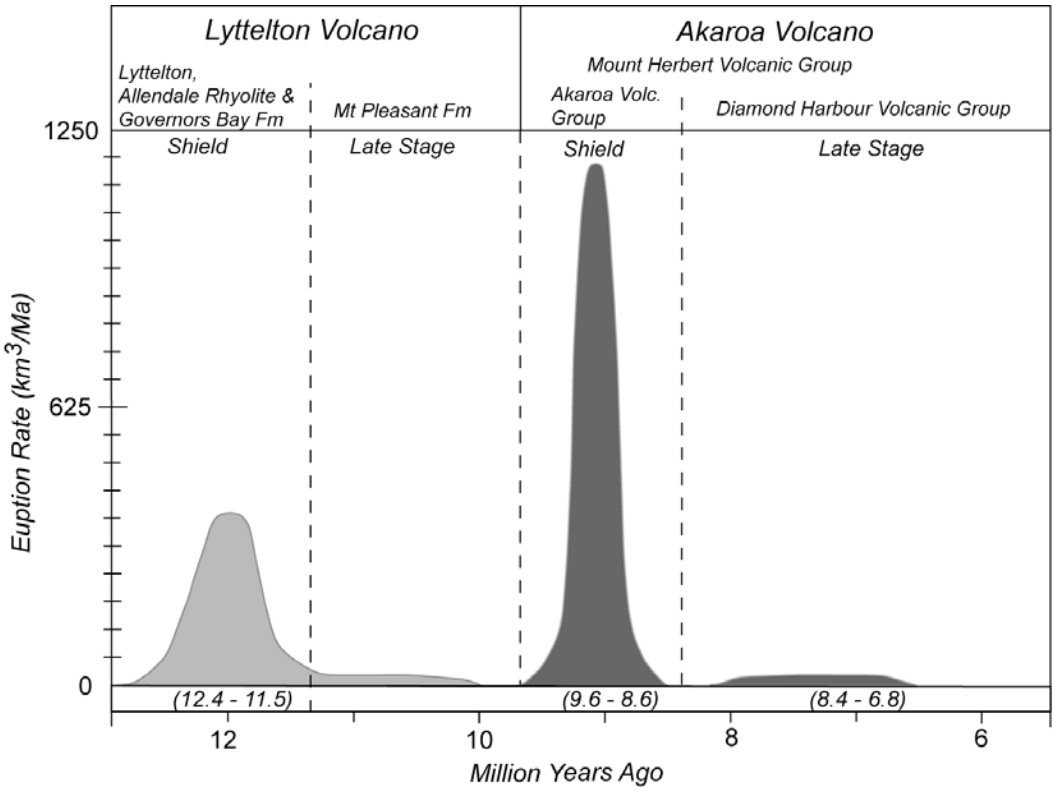

Fig. 2.6: Temporal evolution of the Banks Peninsula showing eruption rate versus $^{40}Ar/^{39}Ar$ age. Both volcanoes of Banks Peninsula, the older Lyttelton and the younger Akaroa volcano, formed rapidly (within ~1 Ma) during a voluminous shield-building stage (350 and 1200 km^3, respectively) followed by more protracted late-stage volcanism. Dashed lines divide the volcanic activity into a shield and late stages. Peak volcanic activity occurred at ~ 12 Ma at Lyttelton and at ~ 9 Ma at Akaroa volcano.

After a period of ~ 0.5 Ma of relative volcanic quiescence, volcanism shifted to the SE at ~ 9.6 Ma with the initiation of Akaroa Volcano eruptions. The main volcanic edifice of the Akaroa Volcano was formed within ~ 1 Ma (9.6 - 8.6 Ma) with more than three times the volume (~ 1200 km^3) of the Lyttelton Volcano (~350 km^3). Eruption products of the Akaroa shield-building stage were concentrated in the SE where the Akaroa Volcano formed; however, lower volumes of lava erupted from a centre situated on the deeply eroded SE flanks of the Lyttelton Volcano forming the Mount Herbert Volcanic Group. After the shield stage of Akaroa Volcano (including most of the Mount Herbert Group volcanics), late stage volcanism (Diamond Harbour

Volcanic Group) was maintained for ~ 1.4 Ma (8.4 - 7 Ma; or 8.4 - 6 Ma, if the lower limit is based on the K/Ar ages of Sewell, 1988).

In summary, both shield-building phases of the Lyttelton and Akaroa volcanoes took place within ~ 1 Ma with peak activities at ~ 12 and 9 Ma (Fig. 2.6). The shield phases of the Lyttelton and the Akaroa volcanoes are characterized by high magma eruption rates (~ 350 and 1200 km^3/Ma, respectively) yielding geochemically distinct mafic lavas. Late-stage volcanism of similar composition occurred on both volcanoes for ~1.5 - 2.5 Ma after the shield stage volcanism. The eruption of geochemically contrasting volcanic rocks in both the shield and late stages on both volcanoes indicates fundamental differences in the petrogenetic history of Lyttelton and Akaroa volcanoes.

2.5.2 General geochemical characteristics of Banks Peninsula volcanic rocks

As noted above, the mafic volcanic rocks (MgO > 4 wt%) from Banks Peninsula can be divided into a low-silica Akaroa group with SiO_2 < ~ 48 wt% (including low-silica lavas from Mount Herbert and Diamond Harbour Volcanic Groups) and a high-silica Lyttelton group with SiO_2 > ~ 48 wt% (including high-silica lavas from Diamond Harbour Volcanic Group; Fig.2.2). Within the two groups increasing SiO_2, Al_2O_3, alkalies (not shown) and decreasing CaO, FeO^t and TiO_2 with decreasing MgO are consistent with fractionation of the observed phenocryst phases olivine, clinopyroxene, plagioclase and Fe-Ti oxides.

A number of geochemical differences between the two groups at similar MgO content however cannot be explained by fractional crystallization. These differences are summarized here. Compared to the Lyttelton shield phase volcanic rocks, the Akaroa volcanics have: 1) lower SiO_2, but higher FeO^t, CaO, TiO_2, 2) generally higher abundances of highly to moderately incompatible trace elements (e. g. Nb, Ta, Sr etc.), but lower Pb (and Cs; not shown), 3) higher ratios of more to less incompatible elements (e.g. (La, Sm)/Yb, Sr/Y, Ta/Ce) and of Nb/Ta, 4) higher ratios of more to less fluid mobile elements (e.g. Pb/Ce, U/Nb, Ba/La) and 5) generally higher $^{206}Pb/^{204}Pb$, $^{143}Nd/^{144}Nd$ and $^{176}Hf/^{177}Hf$ and lower $^{87}Sr/^{86}Sr$ and $\partial^{18}O$. In summary, the geochemical data for the Banks Peninsula volcanics are akin to those of ocean island basalts (OIB). The Akaroa Group volcanics show a HIMU-like

geochemical flavor, whereas the Lyttelton Group volcanics tend towards a more enriched EMII-type geochemical composition.

To evaluate the geochemical evolution of Banks Peninsula, each volcano will be discussed separately below.

2.5.3 Akaroa low-silica group: Eclogite/Pyroxenite melting in upwelling asthenosphere

The content of both FeO^t and SiO_2 in mantle partial melt is pressure sensitive and hence indirectly an indicator of melting depth (Hirose and Kushiro, 1993). The alkali basalts of the Akaroa group can be explained by partial melting of dry peridotite at depths of ~ 80 - 100 km (see Fig. 2.7) at temperatures ranging from 1425 to 1500°C (Hirose and Kushiro, 1993). These exceed common upper mantle temperature estimates for mid-ocean-ridge basalts by ≥ 100 °C (Green et al., 2001; McKenzie and O´Nions, 1995). Melting experiments showed, that carbonated eclogitic and/or a garnet-bearing pyroxenitic components can lower the melting temperature by ~ 100°C to 1350 – 1450°C at melting depths of ~ 70 - 100 km (Dasgupta et al., 2005; Hirschmann et al., 2003). Experiments on the melting of eclogite and pyroxenite produced basanites with similar SiO_2 and FeO^t contents as observed in the lavas from Banks Peninsula (Dasgupta et al., 2005; Hirschmann et al., 2003) and result in higher melt productivity at a given depth of melting compared to a pure dry peridotite melting experiments. The temperature estimate of ~ 1350°C derived by eclogite melting at 30 kbar (Dasgupta, 2006) is supported by the calculated potential temperature based on the MgO content of T = ~ 1313°C for the most MgO-rich (Ni = 263 (ppm) and Cr = 497 (ppm)) sample of the Akaroa shield stage lavas (MgO = 10.4 wt% (N36C3072); after Herzberg & O'Hara, 2002). Additional support for eclogite as a residual source component comes from the high CaO/Al_2O_3 (0.44-0.88), $(Sm/Yb)_N$ (3.5-7.6), Zr/Hf (39.9-57.1; Fig. 2.8c) and Nb/Ta (16.7-21.5), indicating residual clinopyroxene and Ca-rich garnet in the source. Ca-rich (eclogitic) garnet incorporates Yb and Ta preferentially to Sm and Nb, resulting in increased Sm/Yb and Nb/Ta in the melts derived from such a source (Pfänder et al., 2007).

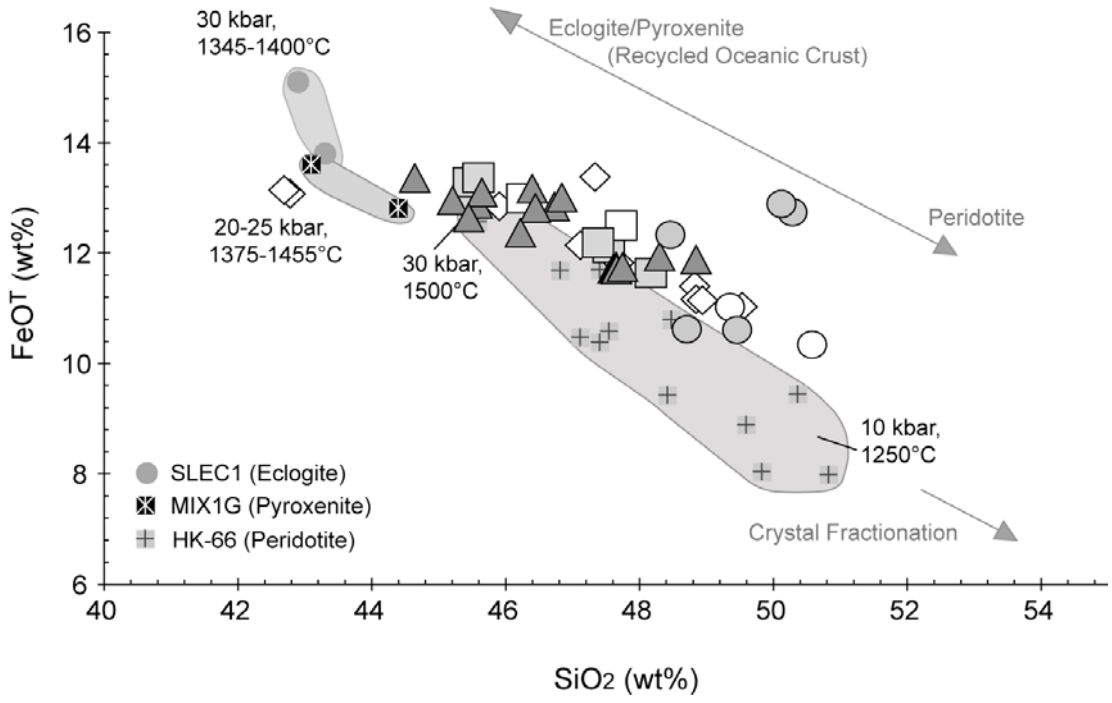

Fig.2.7: SiO_2 wt% versus FeO^t wt% showing mafic (MgO > 4 wt%) lavas from Banks Peninsula. Fields represent experimental results for partial melts of dry peridotite (Hirose and Kushiro, 1993), grt-pyroxenite (Hirschman, 2003) and carbonated eclogite (Dasgupta, 2005). Symbols are the same as in previous figures.

Following Pertermann et al., 2004, high Zr/Hf ratios are controlled by the presence of clinopyroxene in the source incorporating preferentially Hf to Zr. High Sr/Y (> 21, Fig. 2.8b), which is high in adakitic magma derived from eclogite melting (Bindeman et al., 2005) is also consistent with eclogite melting. The high FeO^t, TiO_2 and Nb/Ta also suggest the presence of residual rutile and/or titanite, which are common phases in eclogite (Rudnick et al., 2000; Yaxley and Green, 1994; Schmidt et al., 2004). The question of generating SiO_2 undersaturated ocean island basalt (OIB) by partial melts of pyroxenite and eclogite is discussed in many recent publications (Dasgupta et al., 2006; Hirschmann et al., 2003; Kogiso and Hirschmann, 2006; Kogiso et al., 2003; Pertermann and Hirschmann, 2003). It is therefore well established that partial melts of pyroxenite and eclogite can act as sources for silica-deficient oceanic island basalts The HIMU-type signature observed in the Sr – Nd – Hf – Pb isotopes is commonly interpreted to reflect the presence of hydrothermally-altered recycled oceanic crust in the mantle source (e.g. Hofmann and White, 1982; Hoernle et al., 1991; Hoernle et al., 2006). Hydrothermally-altered recycled oceanic crust in the form of eclogite could also explain the low $\delta^{18}O$ measured in olivine (4.6 - 4.9) compared to the averaged mantle value of 5.2 ± 0.2 ‰ (Mattey and Lowry, 1994).

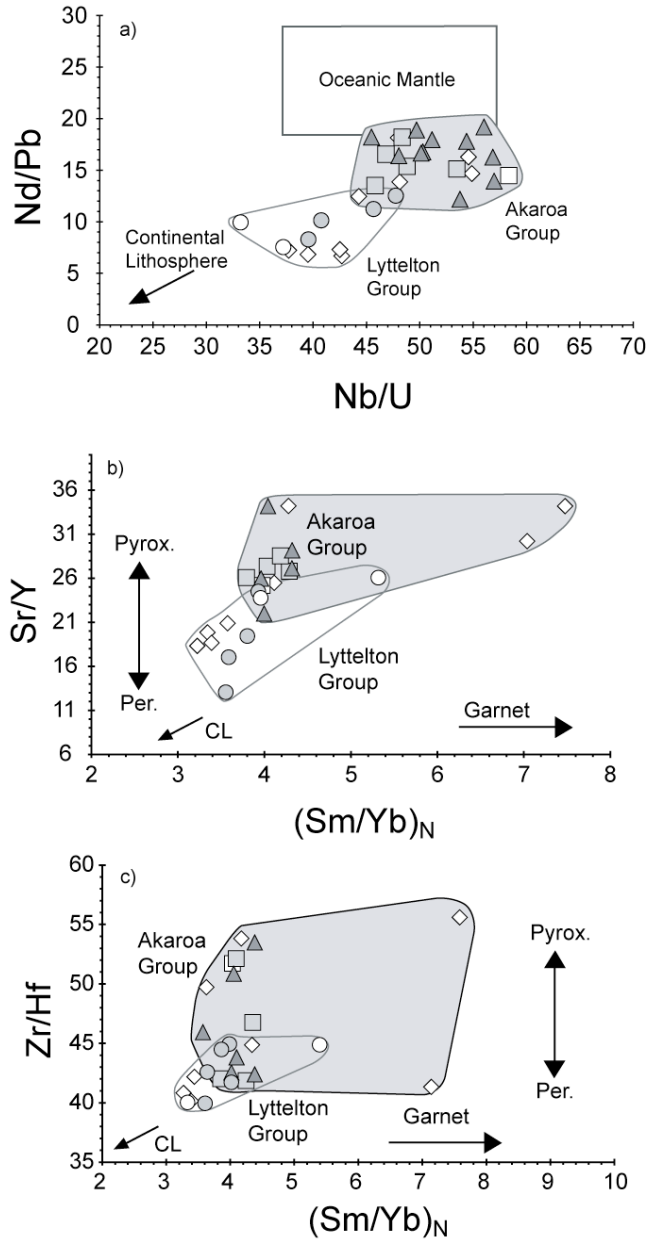

Fig.2.8a-c: Selected trace element ratios. $(Sm/Yb)_N$ displays the increasing garnet signature with decreasing SiO_2 (wt%). Sr/Y and Zr/Hf indicate an increasing influence of eclogite/pyroxenite (as recycled oceanic crust) in the source, but imply that pyroxenite/eclogite was involved in melt generation of all samples (because of superchondritic values). Nd/Pb versus Nb/U indicates the involvement of at least two different mantle sources for the low and high silica groups. The dark grey field of the 'oceanic mantle' represents the Nd/Pb and Nb/U taken from Rehkämper and Hofmann, 1997 and Hofmann, 1986, respectively. The lower Nd/Pb commonly found in mantle rocks suggests that both Akaroa and Lyttelton volcanic rocks have experienced some contamination by enriched lithosphere, but the Lyttelton lavas have been affected more than the Akaroa lavas.

Similar evidence of the presence of hydrothermally-altered oceanic crust in the source was identified beneath the Azores (Turner et al., 2007). Pb isotopic compositions between HIMU and N-MORB in the Akaroa volcanics could reflect relatively young

HIMU recycling ages for the oceanic crust (e.g. Hoernle et al., 2006) or mixing between HIMU and DM sources. Therefore, it appears likely that hydrothermally-altered oceanic crust is present in the upper asthenosphere beneath Banks Peninsula. The fact that SiO_2 forms broad negative trends in the most mafic Banks Peninsula volcanics with $^{206}Pb/^{204}Pb$, $^{143}Nd/^{144}Nd$, Nb/La, Nb/Th (Fig.2.9a-2.9d) and broad positive trends with $^{87}Sr/^{86}Sr$, and $\delta^{18}O$ (not shown) is consistent with the suggestion that the Akaroa group represents low degree partial melts of eclogite-bearing asthenospheric mantle (Hoernle et al., 2006). Compared to typical oceanic mantle with Nd/Pb = 24±5 (Rehkämper & Hofmann 1997), Nb/U=47±10 (Hofmann et al., 1986), Nb/Th = ~19; (Hofmann, 1988) and Nb/La ~1 (Hofmann, 1988), almost all lavas erupted at Akaroa Volcano however generally have lower Nd/Pb, Nb/(U,Th) (Fig.2.8a and 2.9c), possibly reflecting interaction with the continental lithosphere (subduction-modified lithospheric mantle and continental crust).

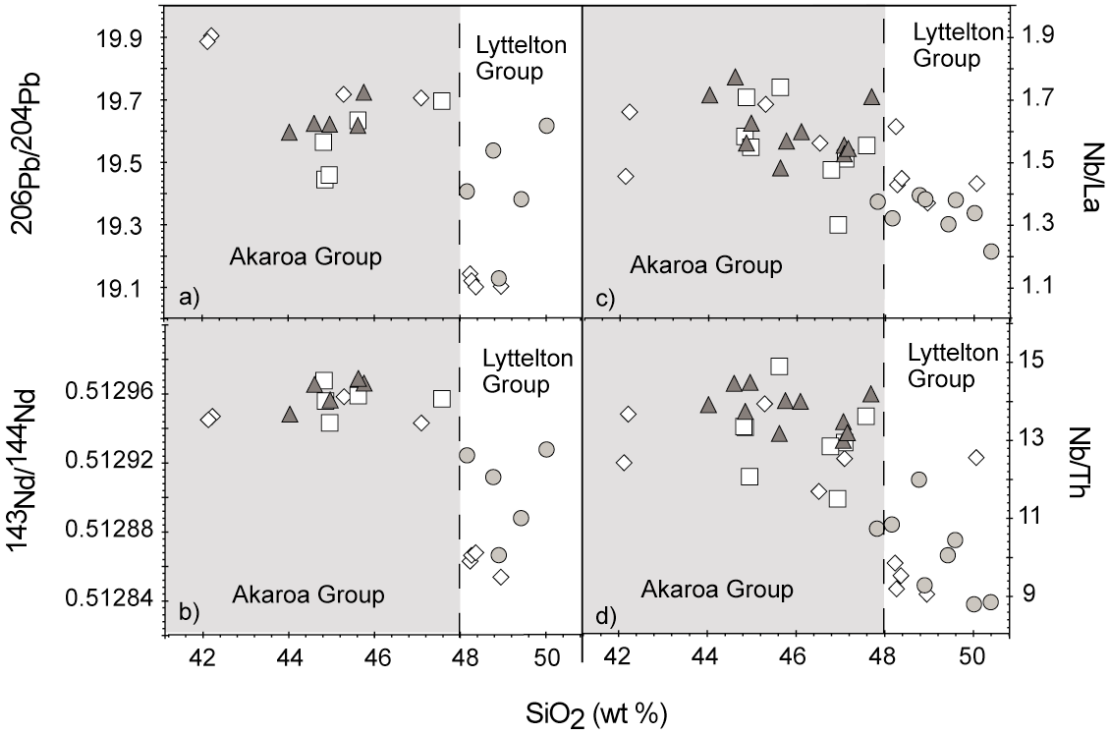

Fig.2.9a-d: $^{206}Pb/^{204}Pb$ (a), $^{143}Nd/^{144}Nd$ (b), Nb/La (c) and Nb/Th (d) versus SiO_2 (wt%). Grey field encompass the low-silica Akaroa group lavas, whereas the white field encloses the high-silica Lyttelton group lavas. Pb and Nd isotope ratios as well as Nb/La and Nb/Th decrease with increasing SiO_2 (wt%), which can be explained by the increasing influence of the continental lithosphere.

Nb/La instead is higher compared to common oceanic mantle, which may have been increased due to the presence of eclogite in the mantle source (John et al., 2004).

2.5.4 Low-silica Diamond Harbour Volcanic Group Rocks: Evidence for Eclogite/Pyroxenite melting beneath both volcanoes

Mafic volcanics of the Diamond Harbour Volcanic Group show the widest range in composition of the Banks Peninsula volcanic units, including the most primitive volcanics on Banks Peninsula with the lowest SiO_2 (42.7 wt%), and highest MgO (12.3 wt%). These variations are accompanied by the most enriched incompatible element pattern, the highest $^{206}Pb/^{204}Pb$ and the lowest $^{143}Nd/^{144}Nd$ (most HIMU-like compositions) within the low-silica Akaroa group pointing to the greatest role of eclogite in melt generation. A progressive decrease in degree of partial melting during the evolution of the Akaroa Volcano, reflecting an increased contribution of eclogite to the melts, could explain the most HIMU-like composition in the Diamond Harbour Volcanic Group. Based on the high FeO^t and the low SiO_2 concentrations, the two basanites (MSI20E, UC13790) of the Diamond Harbour volcanic rocks at 'Le Bons Peak' could represent partial melts of pure carbonated eclogite or silica undersaturated pyroxenite at ~ 100 km depth within the asthenosphere. The steepest HREE pattern (e.g. $(Sm/Yb)_N > 7$) suggests more garnet in the source, which is consistent with the presence of eclogite, containing typically higher quantities of garnet than garnet peridotite. Calculated potential melting temperature estimates are ~ 1380°C (Herzberg and O'Hara, 2002) and in good agreement with partial melting of carbonated eclogite (Dasgupta et al., 2005). The mafic low-silica lavas of the Diamond Harbour Volcanic Group located on or near the Lyttelton Volcano display similar geochemical compositions to the Akaroa shield stage lavas, suggesting derivation from a similar source as for the Akaroa volcano. Based on the relationship of FeO^t with SiO_2 (Fig.2.7) and the high Zr/Hf (~ 53), Sr/Y (~ 24) ratios (Fig.2.8), the 'low-silica Diamond Harbour lavas' erupted at Lyttelton Volcano also formed at depths of ~ 80 - 100 km by partial melting of garnet peridotite and pyroxenite (eclogite). In conclusion, the low-silica Diamond Harbour volcanics at the Lyttelton Volcano erupted contemporaneous with, and are geochemically similar to, the Akaroa group and therefore are most likely derived from the same melting event as the Akaroa volcanics.

2.5.5 Lyttelton high-silica group: Lithospheric Contamination

As summarized above, the Lyttelton group volcanic rocks show different major and trace element and Sr-Nd-Hf-Pb and O isotope signatures, compared to the Akaroa group.The predominant mafic rock-types range from transitional tholeiites through alkali basalts to mugearites. Higher Pb and Cs concentrations in the Lyttelton group volcanics could imply crustal or sedimentary contamination. Generally lower Nd/Pb, support this assumption, whereas lower (Nb,Ta)/La, (Nb,Ta)/(U, Th, Ba, Rb point towards increasing influence of a subduction-related or crustal components low in Nb and Ta. These observations are consistent with the generally higher $^{207}Pb/^{204}Pb$, $^{87}Sr/^{86}Sr$ and $\partial^{18}O_{olivine}$ and lower $^{206}Pb/^{204}Pb$, $^{143}Nd/^{144}Nd$ and $^{176}Hf/^{177}Hf$ tending towards enriched (EMII or crustal-type) endmembers.

These potential enriched endmembers could either be local continental crust (Tappenden, 2003), which crops out at Lyttelton volcano, and/or Cretaceous EMII-type lavas emplaced as mafic dikes in Marie Byrd Land (MBL) in West Antarctica, which are believed to characterize the lithospheric mantle composition beneath MBL (Storey *et al.,* 1999). The MBL dikes may also reflect the composition of the lithospheric mantle beneath New Zealand (Hoernle *et al.,* 2006), because Zealandia was joined to West Antarctica prior to mid-Cretaceous break-up and was therefore also exposed to Gondwana margin subduction.

As indicated by Weaver & Sewell (1986) and Barley & Weaver (1988), magmas from Lyttelton volcano may have interacted with old continental crust. Both, the Cretaceous Mount Somers Volcanic Group (McQueen's Andesites and Gebbies Pass Rhyolite) and the Permian-Triassic Torlesse Group sedimentary rocks outcrop on the NW part of the Banks Peninsula and could be potential contaminants. The combined low Sr and CaO/AL_2O_3 (Al_2O_3 is constant throughout the mafic Lyttelton lavas) within some Lyttelton lavas could reflect the retention of CaO and Sr in a plagioclase-rich continental crustal rock (such as the quartzofelspathic Torlesse sediments and the Gebbies Pass rhyolite). The quantitative calculation of fractional crystallization and assimilation for Sr-Nd-Pb and O isotopes was conducted by means of the **e**nergy **c**onstraint - **a**ssimilation **f**ractional **c**rystallization (EC-AFC) model of Spera & Bohrson (2001) and Bohrson & Spera (2002; Fig. 2.10a-c).

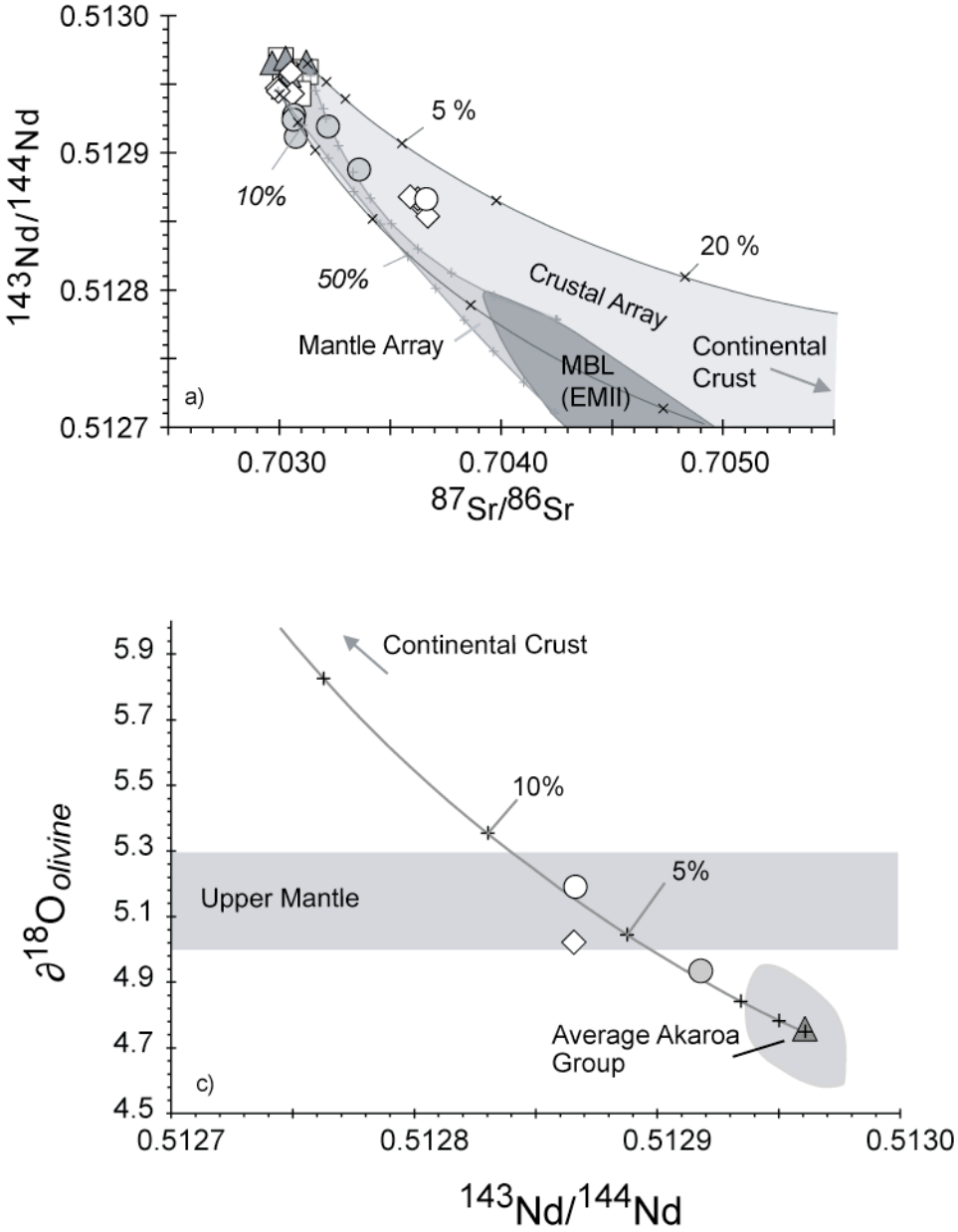

Fig.2.10a - 10b: Sr, Nd and O isotope relationships of mafic (MgO > 4wt%) Banks Peninsula volcanic rocks. Light grey field on the Sr-Nd plot represent the crustal array (based on energy-constraint assimilation and fractionation modelling after Bohrson and Spera, 2001 and Spera and Bohrson, 2001), whereas the grey field represents the mantle array (based on binary mixing calculations between Akaroa lavas and MBL lavas). Black tick marks represent percentage of local continental crust (fb_{CC}) assimilated by Akaroa lavas, whereas the grey tick marks represent the amount of Marie Byrd Land magma (Storey et al, 1999) mixed into the Akaroa lavas. To generate the isotope ratios of the high-silica Lyttelton lavas ~ 1 - ~ 7 % of the local continental crust has to be assimilated into the low-silica Akaroa lavas (dependent on the mixture of asthenospheric Akaroa melts and the lithospheric MBL melts).

The averaged Sr, Nd and Pb isotope ratios (unfortunately there are no Hf isotope data available for the lithospheric EM-type endmember) and $\delta^{18}O$ values of the most enriched Lyttelton group lavas can be modeled by the addition of a crustal EM-type endmember to the averaged isotope ratios by means of the EC-AFC method

(see Table 4 for modeling parameters). As seen in Fig. 2.10b, the continental crust can only be assimilated to a certain degree (~ 50 %), depending on the heat of the ascending melt. For the modeling, an initial temperature of 1280°C has been assumed for the ascending magma, which then has to fuse the surrounding continental crust with a solidus temperature of ~900°C. If the temperature of the ascending (stagnating) low-silica melt drops below the solidus of the assimilant, no further interaction occurs. In the Sr-Nd, Pd-Pb and Nd-O isotope diagrams (Fig.2.10a-2.10c) almost all enriched (EMII-type) signatures of the high-silica Lyttelton volcanics can be generated simply by adding 1-7 % local continental crust into the low-silica Akaroa volcanics. Some of the Lyttelton group volcanics plot slightly outside the modeled crustal array on Pb isotope diagrams (Fig.2.11) and therefore binary mixing between the low-silica Akaroa group melts and the EMII-type lithospheric mantle (based on isotopic composition of Cretaceous Marie Byrd Land dikes; Storey *et al.*, 1999; Fig.2.10a-2.10b) may have also taken place. In conclusion, we propose that the Lyttelton melts represent Akaroa-type asthenospheric melts contaminated in the lithosphere (both subduction-modified mantle and continental crust).

Table 4: EC-AFC Parameters

Thermal Parameters			
Magma liquidus temperature	1280°C	Crystallization enthalpy (J/kg)	396000
Magma initial temperature	1280°C	Isobaric specific heat of magma (J/kg per K)	1484
Assimilant liquidus temperature	1000°C	Fusion enthalpy (J/kg)	270000
Assimilant initial temperature	650°C	Isobaric specific heat of assimilant (J/kg per K)	1370
Solidus Temperature	900°C		
Equilibration Temperature	980°C		

Compositional Parameters

Element	Sr	Nd	Pb	Pb	O
Magma initial concentration (ppm)	1080	38.5	1.64	1.64	
	740	25.1	2.61	2.61	
Bulk D0 in magma	1.0	0.25	0.1	0.1	
Enthalpy of trace element distr. Magma	0	0	0	0	
Assimilant initial concentration	391	21.0	7.67	7.67	
	126	22.8	17.3	17.3	
Bulk D0 in assimilant	0.5	0.25	0.1	0.1	
Enthalpy of trace element distr. Assim.	0	0	0	0	
Isotope ratio/∂ value in magma	0.702998	0.512944	19.88	15.61	4.8
	0.703124	0.512966	19.56	15.58	
Isotope ratio/∂ value in assimilant	0.707680	0.512558	19.50	15.65	8.8*
	0.716264	0.512381	18.90	15.67	

*∂18O value for the assimilant are from Tappenden (2003)

It has been shown that historic tholeiites erupted on the Canaries can be formed by mixing an asthenospheric low-silica melt with a high-silica component to

equal amounts ± 10%, either by diffusive infiltration of alkalies from the basanites into the lithospheric mantle or by direct interaction with the lithosphere incongruently melting-out orthopyroxene (Lundstrom *et al.*, 2003). Similar processes could account for the formation of the high-silica Lyttelton lavas. The rate of interaction may increase as the SiO_2 content of the melts increases, resulting in higher viscosity and subsequently longer stagnation within the continental lithosphere.

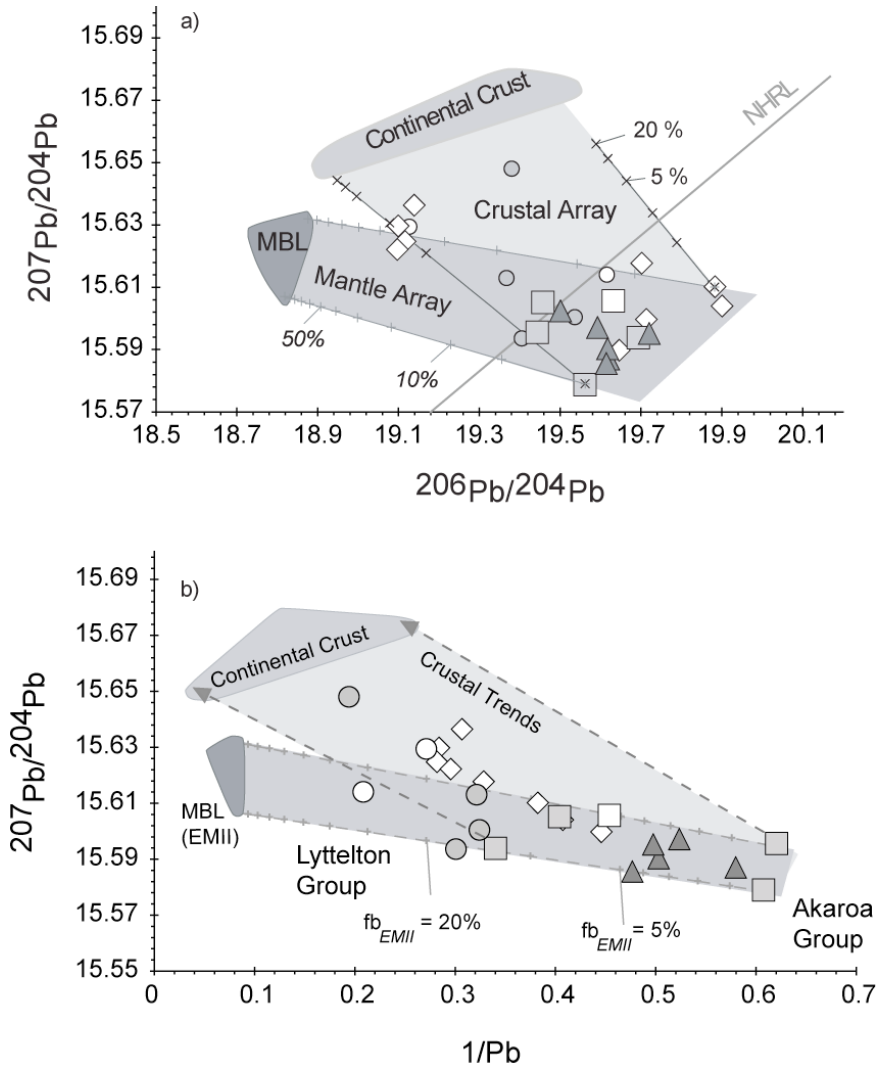

Fig.2.11: $^{206}Pb/^{204}Pb$ versus $^{207}Pb/^{204}Pb$ and 1/Pb versus $^{207}Pb/^{204}Pb$. The mantle array represent mixing calculations between the Akaroa group lavas and those from mafic dikes of Marie Byrd Land, Antarctica, believed to reflect the composition of the lithospheric mantle beneath Zealandia (Storey et al., 1999). Tick marks represent the amount of lithospheric mantle assimilated into the averaged Akaroa group lavas (fb_{EMII}). Dashed arrows indicate the possible field of crustal assimilation. The low 1/Pb and $^{207}Pb/^{204}Pb$ of some Lyttelton group lavas cannot be explained by assimilating continental crust into the ascending low-silica Akaroa group lavas. To lower both ratios interaction of the low-silica Akaroa group lavas with the lithospheric mantle (up to ~ 10 %) is required.

The late stage volcanic rock MSI9A from Lyttelton volcano has distinctly higher incompatible element contents (Fig. 2.3 and 2.4b), compared to the Lyttelton shield stage volcanic rocks, which have high FeO^t, alkalies, incompatible trace element concentrations and $^{206}Pb/^{204}Pb$ but low $^{207}Pb/^{204}Pb$. This suggests lower degrees of partial melting and thus preferential sampling of the eclogite/pyroxenite component towards the end of volcanic activity of the Lyttelton volcano (Fig. 2.5 and 2.6).

2.5.6 High-silica Diamond Harbour Volcanic Group Rocks: Strongest lithospheric signature

The high-silica Diamond Harbour lavas, erupted on the northern flank of the Lyttelton volcano, are transitional tholeiites ($SiO_2 \geq 48$ wt%) with high MgO (> 8wt%). These volcanics show the highest Pb, U, and Th contents (resulting in low Nd/Pb, Nb/(U, Th)), together with the lowest Sr, TiO_2, CaO, FeO^t, $^{143}Nd/^{144}Nd$, $^{206}Pb/^{204}Pb$ found in Banks Peninsula volcanic rocks. More extensive interaction of the low-silica Akaroa group lavas with the enriched (EMII-type) continental lithospheric mantle compared to the high-silica Lyttelton volcanics can explain the geochemical composition of these relatively high MgO magmas. Thus, the high-silica Diamond Harbour Volcanic Group lavas may have been affected most by lithospheric mantle and/or least continental crustal contamination. This is consistent with an age progressive change in the amount of contamination of the Diamond Harbour Volcanic Group lavas erupted at Lyttelton Volcano. The largely uncontaminated Diamond Harbour lavas erupted first at ~ 7.5 Ma and then the strongly contaminated lavas erupted later (between ~ 7 Ma).

2.6 Dynamic Model for the Magmatic Evolution of Banks Peninsula

Zealandia drifted ~ 4000 km to the NW during the Cenozoic. During this time, intraplate volcanism although volumetrically small was widespread and randomly distributed, showing no evidence for long-lived time-progressive volcanic alignments. In addition there is no seismic evidence for a shallow plume-like thermal anomaly beneath Zealandia (e.g. Finn *et al.*, 2005; Priestley & McKenzie, 2006), which strongly agues against the presence of a plume beneath Banks Peninsula. Major extension ceased in the late Cretaceous and only mild extension occurred during the

Cenozoic, which cannot account for the amount of melt required to form a shield volcanoes the size of the Banks Peninsula volcanoes (~1600km^3). Furthermore, there is no evidence for an adequate heat source that could have produced ≥1600 km^2 of melt from the lithospheric mantle through heat conduction.

For Zealandia (the New Zealand micro-continent), lithospheric detachment has been proposed to trigger asthenospheric upwelling and decompression melting (Hoernle *et al.,* 2006). Due to prolonged exposure to subduction-related fluids and melts at the northern margin of Gondwana during the Mesozoic, the lower lithosphere beneath Banks Peninsula (and also Zealandia) has been refertilized, increasing its density with respect to the underlying asthenosphere. This layer therefore represents a layer of gravitational instability, where the lower lithosphere is negatively buoyant, resulting in the formation of Rayleigh-Taylor instabilities. Following lower lithosphere delamination, less dense, hot asthenospheric mantle streams up into the resulting gaps partially melting due to decompression. These melts interact variably with the metasomatized (volatile-rich) lithospheric mantle and local continental crust (Hoernle *et al.,* 2006).

To form the two volcanoes of the Banks Peninsula, we propose multiple delamination events. The first delamination event removed some of the enriched lower lithosphere beneath Lyttelton Volcano causing upwelling of the heterogeneous upper asthenosphere and subsequent decompression melting (Fig.2.12a). The asthenospheric melts triggered low-degree melting of the enriched, volatile-rich lithospheric mantle and interacted extensively with these melts. Lithospheric melting and interaction are most likely in the initial stage of volcanism, when there is extensive enriched lithosphere present, which has not been depleted by melting yet and magma pathways to the surface are not yet well established. After the formation of the Lyttelton Volcano, another major delamination event occurred removing most of the enriched lithosphere beneath Akaroa Volcano (Fig.2.12b).

The more extensive delamination event beneath Akaroa Volcano allowed more upwelling of the upper asthenosphere to shallower depths. This triggered more voluminous partial melting by decompression, resulting in the formation of the much larger Akaroa Volcano. The larger volumes of newly formed magmas presumably ascended more rapidly through the thinner lithosphere beneath Akaroa Volcano, and therefore experienced less lithospheric interaction than the Lyttelton group volcanics.

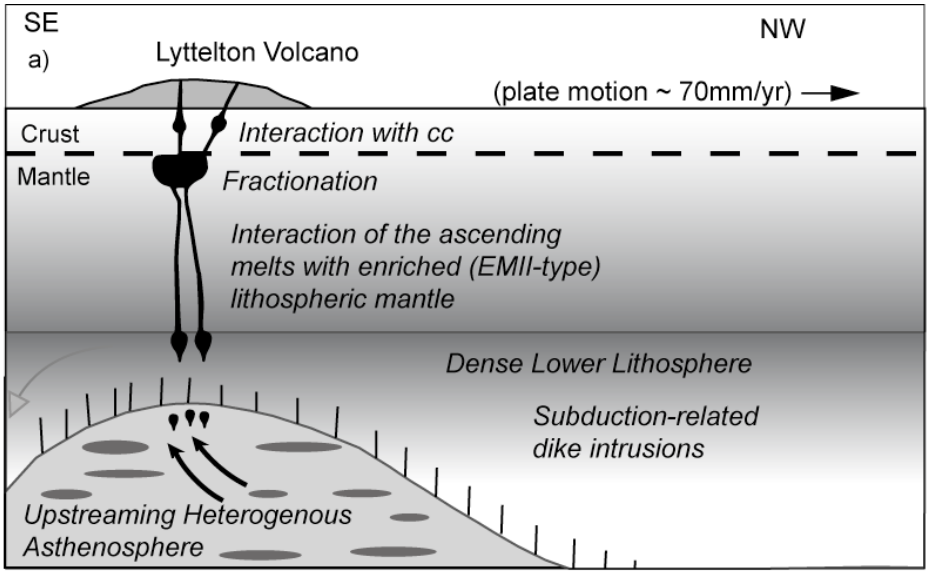
SE
a)
Lyttelton Volcano
NW
(plate motion ~ 70mm/yr)
Crust
Mantle
Interaction with cc
Fractionation
Interaction of the ascending
melts with enriched (EMII-type)
lithospheric mantle
Dense Lower Lithosphere
Subduction-related
dike intrusions
Upstreaming Heterogenous
Asthenosphere

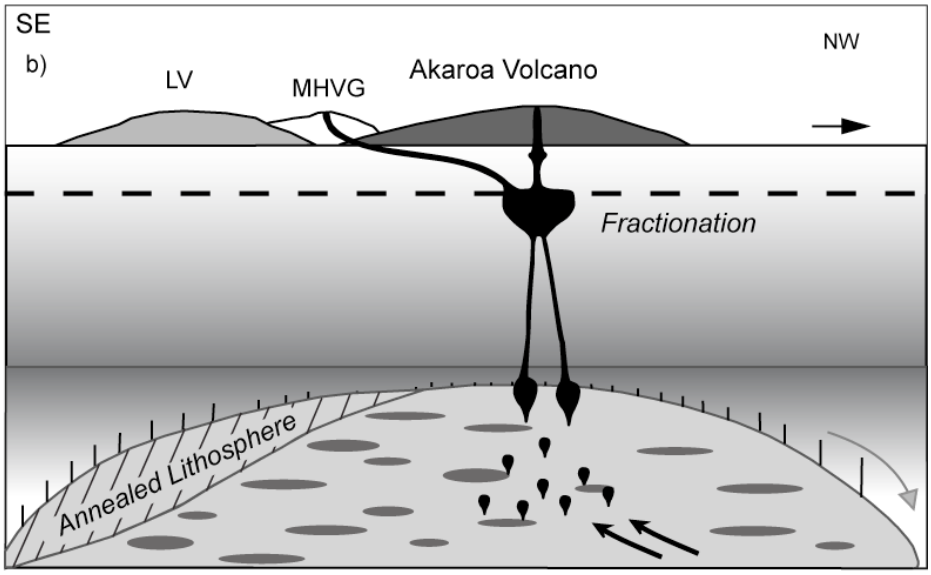
SE
b)
LV
MHVG
Akaroa Volcano
NW
Fractionation
Annealed Lithosphere

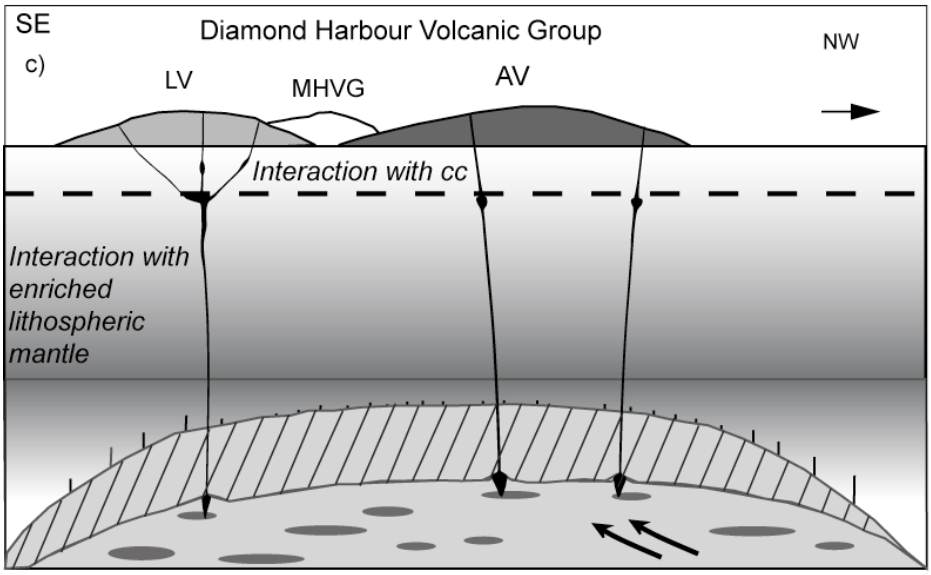
SE
c)
Diamond Harbour Volcanic Group
NW
LV
MHVG
AV
Interaction with cc
Interaction with
enriched
lithospheric
mantle

Fig.2.12a-c: Schematic model to explain the development of intraplate volcanism at Banks Peninsula. Due to prolonged exposure to subduction related activity during the Palaeozoic and Mesozoic at the northern margin of Gondwana (bringing in fluids and melts) the lower lithosphere beneath Zealandia (and Banks Peninsula) was enriched. Basaltic dikes, converted to eclogite, increased the density of the lower lithosphere with respect to the underlying asthenosphere. Therefore, this boundary represents a layer of gravitational instability, where the dense lower lithosphere is negatively buoyant. Detachment of the lower lithosphere results in upwelling of the less dense asthenospheric mantle into the resulting gap, partially melting due to decompression. A first detachment event occurred beneath Lyttelton volcano (Fig.2.12a). Asthenospheric melts interacted with the enriched continental lithosphere (mantle and crust). A second, larger detachment event took place to the SW beneath the Akaroa Volcano (Fig. 2.12b). Late-stage volcanism of the Diamond Harbour Volcanic group formed by continued upwelling as the plate moved to the NW but annealed and thickened (Fig. 2.12c). The duration of late-stage volcanism suggests that it takes ca. 1-3 Ma for the lithosphere to anneal completely and regain at least the thickness at which no further partial melting occurs after a detachment event.

Alternatively the Banks magmatism may have resulted from a delamination event that started beneath Lyttelton and expanded beneath the Akaroa Volcano. Two temporally separated voluminous pulses of volcanic activity however are more easily explained by two separate detachment events or two stages of delamination.

Thicker lithosphere beneath Lyttelton Volcano may have been one of the major factor causing greater lithospheric contamination of the Lyttelton asthenospheric melts. Interestingly, older crustal rocks are exposed at Lyttelton Volcano but not at Akaroa, possibly suggesting a difference in the composition of the crust beneath both volcanoes that may also in part be responsible for the greater observed lithospheric contamination. It is possible, for example, that the crust beneath Akaroa is more mafic than beneath Lyttelton and thus melts at higher temperatures, contributing less to crustal contamination than more evolved (silicic) crust. Similarly the lithospheric mantle beneath Lyttelton Volcano may also have had a different (more enriched) composition than beneath Akaroa Volcano, possibly reflecting local differences in lithospheric metasomatism during subduction along the Gondwana margin.

In addition to the mafic volcanic rocks, more evolved rock types (e.g. trachytes, rhyolites) were erupted contemporaneously with mafic volcanic activity at both volcanoes. This indicates that there are magmatic reservoirs beneath Lyttelton and Akaroa volcanoes where magma was stored, fractionated and assimilated crustal material (Fig.2.12). If considering the duration of volcanism at Banks Peninsula, the entire process of lithospheric removal (detachment/delamination) occurred within < 10 Ma. The prolonged late-stage volcanism at Akaroa Volcano suggests an annealing time of the lower lithosphere of ~ 2 – 3 Ma until the lithosphere is re-thickened so that

no further upwelling and melting occurs. Prolonged melt extraction out of the upper asthenospheric mantle will leave a more depleted peridotitic mantle residue, which requires more thermal energy to melt than eclogite (e.g. Hirschmann, 2003). Therefore partial melting in the upwelling asthenosphere ceases after the eclogitic fragments are melted out and the annealed depleted mantle residue then becomes presumably a part of the lithospheric mantle beneath Banks Peninsula (Jaupart, 2007). This leads to a re-thickening of the lithosphere with time, because of the decreasing upwelling rates of the upper asthenosphere.

Finally, geophysical investigations of the Cenozoic deformation rates due to clockwise rotation of the Pacific Plate have demonstrated increased structural deformation in the early – late Miocene (25 - 8 Ma; Hall *et al.*, 2004). This could have caused mild extension beneath Banks Peninsula in addition to the process of lithospheric detachment and hence resulted in increased melt productivity to form large intraplate volcanoes such as on Banks Peninsula, Dunedin Volcano, Auckland and Campbell Island volcanoes, which formed during the Miocene.

2.7 Conclusion

New Ar/Ar ages provide additional constraints on the temporal evolution of Tertiary volcanism on Banks Peninsula and indicate that activity initiated at ~ 13 Ma and persisted for about 5 Ma. The two large shield volcanoes, Lyttelton and Akaroa, both formed within ~ 1 Ma (Lyttelton ~ 12.3 – 11.5 Ma and Akaroa ~ 9.6 – 8.6 Ma) and each volcano had a period of late stage volcanic activity persisting for 1 - 2.5 Ma.

Mafic (MgO > 4 wt%) intraplate volcanism on the Banks Peninsula, consisting of the Lyttelton Volcano in the NW and the Akaroa Volcano in the SE can be divided into a low-silica Akaroa group (SiO_2 < ~ 48 wt%), primarily occurring at the Akaroa volcano, and a high-silica Lyttelton group (SiO_2 > ~ 48 wt%), restricted to the Lyttelton volcano, with each group displaying distinct geochemical characteristics. All mafic volcanic rocks of Banks Peninsula show ocean island basalt incompatible element patterns on multi-element diagrams, but the low-silica Akaroa group lavas are characterized by more pronounced positive Nb, Ta and negative Pb anomalies, compared to the high-silica Lyttelton volcanics. These characteristics are accompanied by high contents of TiO_2, FeO^t, CaO, Nb, Sr, high ratios of Zr/Hf, Sr/Y, (La, Sm)/Yb, and HIMU-type isotopic signatures, which are consistent with recycled

oceanic crust in the source beneath Banks Peninsula. The high-silica Lyttelton group lavas by contrast have generally lower contents of FeO^t, TiO_2, CaO and incompatible elements (e.g. Sr, Nb etc.), lower Nd/Pb, Nd/La, Nb/Th, Nb/U ratios, reflecting a contribution from subduction-modified lithosphere or the crust with enriched (EMII-type) isotopic signatures.

Since there are no morphologic and geophysical indications of a thermal anomaly and/or of major lithospheric extension beneath the Banks Peninsula, we propose lithospheric removal (detachment/delamination) in order to explain the magmatic activity. In order to form the Lyttelton and Akaroa volcanoes, two detachment events or a two-stage delamination event are required: An initial detachment event allowed upwelling of the heterogeneous asthenospheric mantle (containing recycled oceanic crust) and subsequent decompression melting. These melts interacted with the lithospheric mantle, affected by Mesozoic subduction along the Gondwana margin, and the crust (up to 7 %) before erupting and forming the Lyttelton Volcano. A second, relatively larger detachment event caused greater upwelling, resulting in more voluminous generation of low-silica volcanics (which experienced insignificant lithospheric interaction) forming the Akaroa volcano.

Acknowledgement

I would like to thank F.Hauff, D.Rau, J.Sticklus, S.Hauff and especially J. Fietzke for analytical and technical assistance and M. Portnyagin for fruitful discussions. This project was partially funded by the German Research Foundation (DFG, project HO1833/12-1). All analytical work conducted at IFM-GEOMAR was funded by IFM-GEOMAR.

References

Barley ME, Weaver SD (1988) Strontium isotope composition and geochronology of intermediate-silicic volcanics, Mt Somers and Banks Peninsula, New Zealand. New Zealand Journal of Geology and Geophysics 31, 197-206.

Barth M, McDonough WM, Rudnick R (2000) Tracking the budget of Nb and Ta in the continental crust. Chemical Geology 165, 197-213.

Bindeman IN, Eiler JM, Yogodzinskic GM, Tatsumid Y, Sterne CR, Grove TL, Portnyaging M, Hoernle K, Danyushevsky LV (2005) Oxygen isotope evidence for slab melting in modern and ancient subduction zones. Earth and Planetary Science Letters 235, 480– 496.

Blichert-Toft J, Chauvel C, Albarede F (1997) Separation of Hf and Lu for high-precision isotope analyses of rock samples by magnetic sector-mutiple collector ICP-MS. Contributions to Mineralogy and Petrology 127, 248–260.

Bogaard Pvd (1995) $^{40}Ar/^{39}Ar$ ages of sanidine phenocrysts from Laacher See tephra (12,900yr BP): chronostratigraphic and petrological significance. Earth and Planetary Science Letters 133, 163-174.

Bohrson WA, Spera FJ (2001) Energy-Constrained Open-System Magmatic Processes II: Application of Energy-Constrained Assimilation - Fractional Crystallization (EC-AFC) Model to Magmatic Systems. Journal of Petrology 42, 1019-1041.

Coombs DS, Cas RA, Kawachi Y, Landis CA, McDonough WF, Reay A (1986) Cenozoic Volcanism in North, East and Central Otago. In: IEM Smith (ed.) Cenozoic Volcanism in New Zealand. pp. 278-312. Royal Society of New Zealand.

Dasgupta R, Hirschmann MM, Dellas N (2005) The effect of bulk composition on the solidus of carbonated eclogite from partial melting experiments at 3 GPa. Contributions to Mineralogy and Petrology 149, 288–305.

Dasgupta R, Hirschmann MM, Stalker K (2006) Immiscible Transition from Carbonate-rich to Silicate-rich Melts in the 3 GPa Melting Interval of Eclogite + CO3 and Genesis of Silica-undersaturated Ocean Island Lavas. Journal of Petrology 47, 647-671.

Davy B (2006) Bollons Seamount and early New Zealand–Antarctic seafloor spreading. Geochemistry Geophysics Geosystems 7, Q06021, doi:10.1029/2005GC001191.

Duffield WA, Dalrymple GB (1990) The Taylor Creek Rhyolite of New Mexico: a rapidly emplaced field of lava domes and flows. Bulletin of Volcanology 52, 475-487.

Eberhart-Phillips D, Bannister S (2002) Three-dimensional crustal structure in the Southern Alps region of New Zealand from inversion of local earthquake and active source data. Journal Geophysical Research 107, doi: 10.1029/2001JB000567.

Elkins-Tanton LT (2005) Continental magmatism caused by lithospheric delamination. Geological Society of America Special Paper 388, 449-461.

Garbe-Schönberg C-D (1993) Simultaneous determination of thirty-seven trace elements in twenty-eight international rock standards by ICP-MS. Geostandards Newsletter 17, 81-97.

Geldmacher J, Hanan, BB, Blichert-Toft J, Harpp K, Hoernle K, Fauff F, Werner, R, Kerr A (2003) Hafnium isotopic variations in volcanic rocks from the Caribbean Large Igneous Province and Gala´pagos hot spot tracks. Geochemistry Geophysics Geosystems 4, 1062, doi:10.1029/2002GC000477.

Godfrey NJ, Davey F, Stern TA, Okaya D (2001) Crustal structure and thermal anomalies of the Dunedin Region, South Island, New Zealand. Journal of Geophysical Research 106, 30,835-30,848.

Govindaraju K (1994) Compilation of Working Values and Sample Description for 383 Geostandards. Geostandards Newsletter 18, 1-158.

Green DH, Fallon TJ, Eggins SM, Yaxley GM (2001) Primary magmas and mantle temperatures. European Journal of Mineralogy 13, 437-451.

Hall LS, Lamb SH, Mac Niocaill C (2004) Cenozoic distributed rotational deformation, South Island, New Zealand. Tectonics 23, 1-16.

Herzberg C, O'Hara MJ (2002) Plume-associated ultramafic magmas of Phanerozoic age. Journal of Petrology 43, 1857–1883.

Hirose K, Kushiro I (1993) Partial melting of dry peridotites at high pressures: Determination of compositions of melts segregated from peridotite using aggregates of diamond. Earth Planetary Science Letters 114, 477-489.

Hirschmann MM, Kogiso T, Baker MB, Stolper EM (2003) Alkalic magmas generated by partial melting of garnet pyroxenite. Geology 31, 481-484.

Hoernle K, Tilton G, Schmincke H-U (1991) Sr-Nd-Pb isotopic evolution of Gran Canaria: evidence for shallow enriched mantle beneath the Canary Islands. Earth and Planetary Science Letters 106, 44-63.

Hoernle K, White JDL, et al. (2006) Cenozoic Intraplate Volcanism on New Zealand: Upwelling Induced by Lithospheric Removal. Earth and Planetary Science Letters 248, 335-352.

Hoernle K, Abt DL, Fischer KM, Nichols H, Hauff F, Abers GA, van den Bogaard P, Heydolph K, Alvarado G, Protti M, Strauch W (2008) Arc-parallel flow in the mantle wedge beneath Costa Rica and Nicaragua. Nature, doi: 10.1038/nature06550.

Hoke L, Poreda R, Reay T, Weaver SD (2000) The subcontinental mantle beneath southern New Zealand, characterised by helium isotopes in intraplate basalts and gas-rich springs. Geochimica et Cosmochimica Acta 64, 1489-2507.

Hofmann AW (1988) Chemical differentiation of the Earth: the relationship between mantle, continental and oceanic crust. Earth Planetary Science Letters 90, 297-314.

Houseman GA, Neil E, Kohler MD (2000) Lithospheric Instability in the Transverse Ranges of California. Journal Geophysical Research 105, 16,237 - 16,250.

Jaupart C (2007) Dynamics of continental lithosphere. Geophysical Research Abstracts, 9, 06818, SRef-ID: 1607-7962/gra/EGU2007-A-06818

John T, Scherer EE, Haase K, Schenk V (2004) Trace element fractionation during fluid-induced eclogitization in a subducting slab: trace element and Lu–Hf–Sm Nd isotope systematics. Earth and Planetary Science Letters 227, 441– 456.

Kogiso T, Hirschmann MM (2006) Partial melting experiments of bimineralic eclogite and the role of recycled mafic oceanic crust in the genesis of ocean island basalts. Earth and Planetary Science Letters 249, 188–199.

Kogiso T, Hirschmann MM, Frost DJ (2003) High-pressure partial melting of garnet pyroxenite: possible mafic lithologies in the source of ocean island basalts. Earth and Planetary Science Letters 216, 603-617.

Liggett KA, Gregg DR, (1965) Geology of Banks Peninsula, South Island-Tour D. In: LO Kermode (ed.) New Zealand Volcanology- South Island. pp. 9-25. Department of Scientific and Industrial Research Information Series.

Liu Z, Bird P (2006) Two-dimensional and three-dimensional finite element modelling of mantle processes beneath central South Island, New Zealand. Geophysical Journal International 365, 1003–1028.

Lundstrom CC, Hoernle K, Gill J (2003) U-series disequilibria in volcanic rocks from the Canary Islands: Plume versus lithospheric melting. Geochimica et Cosmochimica Acta 67, doi:10.1016/S0016-7037(03)00308-9, 4153-4177.

Mattey D, Lowry D (1994) Oxygen isotope composition of mantle peridotite. Earth and Planetary Science Letters 128, 231-241.

McKenzie D, O´Nions RK (1995) The Source Regions of Ocean Island Basalts. Journal of Petrology 36, 133-159.

Molnar P, Houseman GA, Conrad CP (1998) Rayleigh-Taylor instability and convective thinning of mechanically thickened lithosphere: effects on non-linear viscosity decreasing exponentially with depth and of horizontal shortening of the layer. Geophysical Journal International 133, 568-584.

Montelli R, Nolet G, Dahlen RA, Masters G (2006) A catalogue of deep mantle plumes: New results from finite frequency tomography. Geochemistry Geophysics Geosystems 7, Q11007, doi:10.1029/2006GC001248.

Morency C, Doin M-P (2004) Numerical simulations of the mantle lithosphere delamination. Journal Geophysical Research 109, doi: 10.1029/2003JB002414.

Morgan WJ (1971) Convection plumes in the lower mantle. Nature 230, 42-43.

Muir RJ, Ireland TR, Weaver SD, Bradshaw JD, Evans JA, Eby GN, Shelley D (1998) Geochronology and geochemistry of a Mesozoic magmatic arc system, Fjordland, New Zealand. Journal of the Geological Society, London 155, 1037-1053.

Panter KS, Blusztain J, Hart SR, Kyle PR, Esser R, McIntosh WC (2006) The Origin of HIMU in the SW Pacific: Evidence from Interplate Volcanism in Southern New Zealand and Subantarctic Islands. Journal of Petrology doi:10.1093/petroogy/eg1024, 1-32.

Pertermann M, Hirschmann MM (2003) Anhydrous Partial Melting Experiments on MORB-like Eclogite: Phase Relations, Phase Compositions and Mineral-Melt Partitioning of Major Elements at 2-3 GPa. Journal of Petrology 44, 2173-2201.

Pertermann M, Hirschmann MM (2003) Partial melting experiments on a MORB-like pyroxenite between 2 and 3 GPa: Constraints on the presence of pyroxenite in basalt source regions from solidus location and melting rate. Journal Geophysical Research 108, doi:10.1029/200JB000118.

Pfänder JA, Münker C, Stracke A, Mezger K (2007) Nb/Ta and Zr/Hf in ocean island basalts — Implications for crust–mantle differentiation and the fate of Niobium. Earth and Planetary Science Letters 254, 158-172.

Rehkämper M, Hofmann, AW (1997) Recycled ocean crust and sediment in Indian Ocean MORB. Earth and Planetary Science Letters 147, 93-106.

Robinson JAC, Wood BJ (1998) The depth of the spinel to garnet transition at the peridotite solidus. Earth and Planetary Science Letters 164, 277-284.

Rudnick RL, Barth M, Horn I, McDonough WF (2000) Rutile-Bearing Refractory Eclogites: Missing Link Between Continents and Depleted Mantle. Science 287, 278-281.

Schott B, Schmeling H (1998) Delamination and detachment of a lithospheric root. Tectonophysics 296, 225-247.

Schmidt MW, Dardon A, Chazot G, Vannucci R (2004) The dependence of Nb and Ta rutile-melt partitioning on melt composition and Nb/Ta fractioning during subduction processes. Earth and Planetary Science Letters 226, 415-432

Sewell, RJ, Weaver SD, Reay, MB (1992). Geology of Banks Peninsula Scale 1:100,000. Institute of Geological & Nuclear Sciences geological map 3. Lower Hutt, New Zealand

Sewell RJ (1988) Late Miocene volcanic stratigraphy of central Banks Peninsula, Canterbury, New Zealand. New Zealand Journal of Geology and Geophysics 31, 41-64.

Shelley D (1988) Radial dikes of Lyttelton Volcano - their structure, form and petrography. New Zealand Journal of Geology and Geophysics 31, 65-75.

Spera FJ, Bohrson WA (2001) Energy-Constrained Open -System Magmatic Processes I: General Model and Energy-Constrained Assimilation and Fractional Crystallization (EC-AFC) Formulation. Journal of Petrology 42, 999-101.

Sprung P, Schuth S, Münker C, Hoke L (2007) Intraplate volcanism in New Zealand: the role of fossil plume material and variable lithospheric properties. Contributions to Mineralogy and Petrology 153, 669-687.

Stern T, Okaya D, Scherwath M (2002) Structure and Strength of a continental transform from onshore-offshore seismic profiling of South Island, New Zealand. Earth Planets Space 54, 1011-1019.

Stipp JJ, Mc Dougall I (1968) Geochronology of the Banks Peninsula volcanoes, New Zealand. New Zealand Journal of Geology and Geophysics 11, 1239-1260.

Storey BC, Leat PT, Weaver SD, Pankhurst RJ, Bradshaw JD, Kelley S (1999) Mantle plumes and Antartica - New Zealand rifting: evidence from mid-Cretaceous mafic dykes. Journal of the Geological Society, London 156, 659-671.

Sutherland R (1995) The Australia-Pacific boundary and Cenozioc plate motions in the SW Pazific: Some constraints from Geosat data. Tectonics 14, 819-831.

Tappenden V (2003) Magmatic response to the evolving New Zealand Margin of Gondwana during the Mid-Late Cretaceous. PhD thesis, University of Canterbury, New Zealand, 261pp..

Todt W, Cliff RA, Hanser A, Hofmann AW (1996) $^{202}Pb + ^{205}Pb$ double spike for lead isotopic analyses. In: A Basu and S Hart (eds.) Earth Processes: Reading the Isotopic Code: Geophysical Monograph vol 95.

Turner S, Tonarini S, Bindeman I, Leeman WP, Schaefer BF (2007) Boron and oxygen isotope evidence for recycling of subducted components over the past 2.5 Gyr. Nature 447, doi:10.1038/nature05898

Waight TE, Weaver SD, Muir RJ (1998) Mid-Cretaceous granitic magmatism during the transition from subduction to extension in southern New Zealand: a chemical and tectonic synthesis. Lithos 45, 469-482.

Weaver SD, Sewell RJ (1986) C2: Cenozoic volcanic geology of the Banks Peninsula. South Island igneous rocks. In: BF Houghton & SD Weaver (eds.). pp. 39-63. New Zealand Geological Survey Record 13.

Weaver SD, Smith IEM (1989) New Zealand Intraplate Volcanism. In: RW Johnson, J Knutson and SR Taylor (eds.) Intraplate volcanism in eastern Australia and New Zealand. pp. 157-188. Cambridge University Press.

Yaxley GM, Green DH (1994) Experimental demonstration of refractory carbonate-bearing eclogite siliceous melt in the subduction regime. Earth and Planetary Science Letters 128, 313-325.

Chapter III

Temporal and Geochemical Evolution of the Cenozoic Intraplate Volcanism of Zealandia

Abstract

In order to constrain better the distribution, age, geochemistry and origin of widespread Cenozoic intraplate volcanism in Zealandia, we report new $^{40}Ar/^{39}Ar$ and geochemical (major and trace element and Sr-Nd-Hf-Pb isotope) data from offshore (Chatham Rise, Campbell and Challenger Plateaus) and onland (North, South, Auckland, Campbell, Chatham and Antipodes Islands of New Zealand) volcanism on Zealandia. The samples include nephelinite, basanite, phonolite, alkali basalt, trachyte/rhyolite, and minor tholeiite and basaltic andesite, all of which have ocean island basalt (OIB)-type trace element signatures and which range in age from 64.8 to 0.17 Ma. Isotope ratios show a wide range in composition ($^{87}Sr/^{86}Sr$ = 0.7027 - 0.7050, $^{143}Nd/^{144}Nd$ = 0.5128 - 0.5131, $^{177}Hf/^{176}Hf$ = 0.2829 - 0.2831, $^{206}Pb/^{204}Pb$ = 18.62 - 20.67, $^{207}Pb/^{204}Pb$ = 15.54 - 15.72 and $^{208}Pb/^{204}Pb$ = 38.27 - 40.34) with samples plotting between mid-ocean-ridge basalts (MORB) and Cretaceous New Zealand intraplate volcanic rocks.

Major characteristics of Zealandia's Cenozoic volcanism include longevity, irregular distribution and lack of age progressions in the direction of plate motion, or indeed any systematic temporal or spatial geochemical variations. We believe these characteristics can be best explained in the context of lithospheric detachment, which causes upwelling and melting of the upper mantle. We propose that a large-scale seismic low velocity anomaly at a depth of > 600 km that stretches from beneath West Antarctica to Zealandia may represent a geochemical reservoir that has been in existence since the Cretaceous, and has been supplying the upper mantle beneath Zealandia with plume type material throughout the Cenozoic.

3.1 Introduction

The origin of intraplate volcanism is a subject of intense debate at present. For continental areas, the classic models for explaining intraplate volcanism either invoke mantle plumes (e.g. Morgan, 1971) or extensive lithospheric thinning often preceding continental rifting (e.g. Weaver and Smith, 1989). Neither of these models however can adequately explain intraplate volcanism in the SW Pacific continent of Zealandia (e.g. Finn et al., 2005; Panter et al., 2006; Hoernle et al., 2006; Sprung et al., 2007; Timm et al., in review). Newer models for Zealandia volcanism can be divided into two groups: low-degree melting of lithosphere metasomatized by earlier subduction and plume-related processes (Finn et al., 2005; Panter et al., 2006; Sprung et al., 2007), or lithospheric removal (detachment) that results in asthenospheric upwelling and melting (Hoernle et al., 2006; Timm et al., in review). Almost all these previous studies were largely based on geochemical results from New Zealand's North and South Islands. Here we present new $^{40}Ar/^{39}Ar$ age and comprehensive geochemical (major and trace elements and Sr-Nd-Hf-Pb isotope) data from more remote parts of Zealandia. These include both offshore samples obtained during RV Sonne SO168 and SO169 cruises from the Challenger and Campbell Plateaus and the Chatham Rise, and onland samples from the North, South, Chatham, and Subantarctic islands. In this paper we combine our spatially more comprehensive data-set with data from the literature, evaluate the temporal and spatial evolution of volcanism on Zealandia, and test and propose models of the origin of this widespread, long-lived and enigmatic intraplate volcanism.

3.2 Tectonic Background of Zealandia since the Late Cretaceous

The mainly submerged continent of Zealandia covers an area of more than 2 million km^2 and is lies between ~ 25° - 56°S and 160°E - 168°W on the Pacific and Antarctic plates (Mortimer, 2004) (Figure 3.1). The submerged parts of Zealandia consist of the Campbell Plateau in the southeast, the Bounty Trough, and Chatham Rise in the east and the Challenger Plateau and Lord Howe Rise in the northwest. The North and South Island of New Zealand, four groups of Subantarctic islands

(Antipodes, Auckland, Campbell and Chatham Islands) and New Caledonia are the only emergent parts of Zealandia.

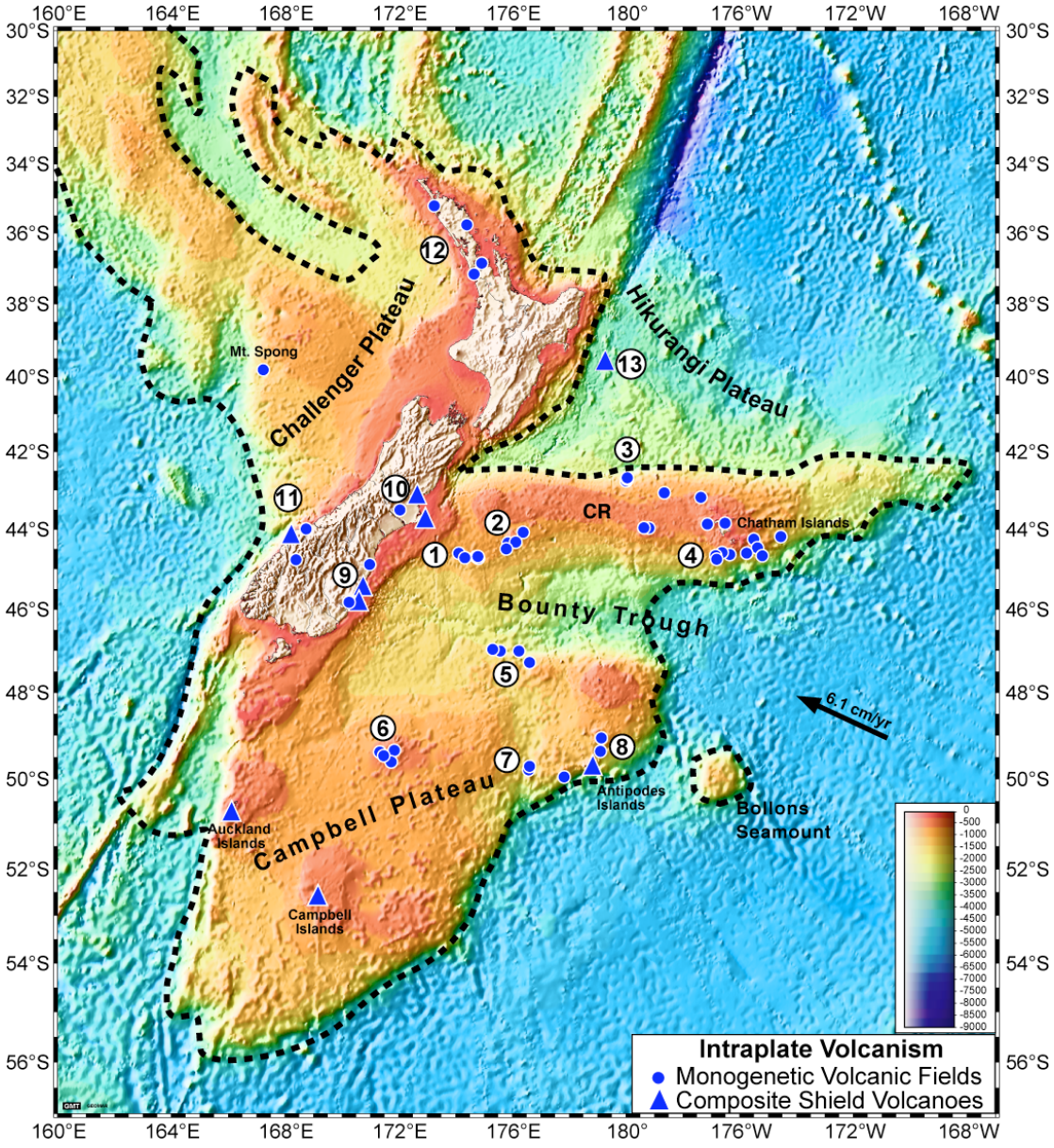

Figure 3.1: Bathymetric map of the mainly submerged continent of Zealandia, outlined by the dashed line, and adjacent areas. Sampling sites are shown by blue dots marking Cenozoic volcanic centers (monogenetic volcanic fields = circles and larger volcanic complexes/fields with ≥100 km^3, including composite shield volcanoes = triangles). Sampling sites are (1) Urry Knolls, (2) Veryan Bank, (3) Graveyard seamounts, (4) western Chatham Rise, (5) northern Campbell Plateau margin, (6) Pukaki Bank, (7, 8) areas north and west of the Antipodes Islands, (9) Otago volcanic fields (including Timaru/Geraldine) and Dunedin Volcano, (10) Canterbury volcanic fields and Banks Peninsula, (11) Westland, (12) Auckland and Northland volcanic fields, (13) Rowling B seamount on the Hikurangi Plateau. Plate motion vector is from Clouard et al. (2005)

Before ~84 million years ago, Zealandia formed a part of the Gondwana super-continent, and was situated at its active eastern continental margin facing subducting proto-Pacific basin plates (e.g. Storey et al., 1999; Mortimer et al., 2006). Marine magnetic and satellite-derived gravity data indicate that the eastern and southeastern margins of the Chatham Rise and the Campbell Plateau were attached to the northern margin of Marie Byrd Land (West Antarctica) (e.g., Larter et al., 2002; Eagles et al., 2004 and references therein). Exhumation of metamorphic complexes, formation of sedimentary basins and rift-related magmatism (e.g. extensive diking) at ~ 110 - 105 Ma were the first responses to separation of Zealandia from West Antarctica (Weaver et al., 1984; Storey et al., 1999) - the final phase of Gondwana breakup. Many models have been proposed to explain the rifting of Zealandia from West Antarctica (Weaver et al., 1994; Storey et al., 1999 and 1995; Mortimer, 2004 and 2006; Finn et al., 2005; Davy and Wood, 1994; Davy, in press). Several authors have proposed that a plume beneath Marie Byrd Land during the late Cretaceous caused the break-up of Zealandia from Gondwana (Weaver, 1994; Storey, 1999, 1995), whereas Waight et al. (1998) related the inception of intraplate volcanism to lithospheric thinning. An alternative model attributed the change from subduction-related to intraplate volcanism to the collision of the Hikurangi Plateau LIP (Figure 3.1) with the paleo-subduction zone at the northern margin of the Chatham Rise, which caused subduction to shut down (Davy and Wood, 1994; Mortimer et al., 2006; Davy, in press). Slab detachment resulted in the formation of a slab window by 97 Ma (Finn et al., 2005; Mortimer et al., 2006), which allowed hot, deeper mantle, some possibly related to a starting plume head (Weaver et al. 1994; Storey et al. 1999) to upwell directly beneath the former Gondwana margin, leading to widespread intracontinental rifting and thinning prior to ocean crust formation between Zealandia and West Antarctica at 84 Ma (Larter et al., 2002; Mortimer et al., 2006; Eagles et al., 2004).

Since 84 Ma Zealandia has drifted north away from Antarctica. Since Antarctica has basically remained stationary in a hotspot reference frame, Zealandia's continental lithosphere has also moved north thousands of km relative to the Earth's subasthenospheric mantle. At ~ 45 Ma, a Pacific-Australia plate boundary propagated through Zealandia (Sutherland, 1995). Initially this boundary was extensional and later strike-slip, causing relative motion between north and south parts of Zealandia. Since ~ 6 Ma, the Pacific and Australian plates have converged within and near

Zealandia, resulting in the uplift of the Southern Alps with subduction zones to the north and south of New Zealand.

Intraplate igneous activity in Zealandia commenced in the Late Cretaceous (~95-100 Ma). Plutonic and volcanic centers characteristically involved small volumes of magma, forming the Tapuaenuku and Mandamus Igneous Complexes on the South Island of New Zealand (Baker et al., 1994; Tappenden, 2003), and a variety of volcanic centers on and around the eastern Chatham Rise, as well as on the Chatham Islands (Grindley et al., 1977; Panter et al., 2006; Mortimer et al., 2006).

The major Cenozoic intraplate volcanic centers are located on the South Island (Coombs et al., 1986; Weaver and Smith, 1989; Hoernle et al., 2006; Panter et al., 2006; Sprung et al., 2007) and on the Campbell Plateau (i.e. Campbell, Auckland and Antipodes Islands; Adams, 1983; Gamble et al., 1986; Weaver and Smith, 1989). On the North Island, volumetrically minor Pleistocene intraplate volcanism in the Auckland and Northland areas has been attributed to melting of lithosphere overprinted by Mesozoic or earlier subduction and plume-related magmatism (Huang et al., 1997; Cook et al., 2004). Submarine intraplate volcanoes have been described from the southern flank of the Chatham Rise (Urry Knolls) (Herzer et al., 1989), from Mt. Spong on the Challenger Plateau (Carey et al., 1991) and from the South Fiji Basin north of the North Island of New Zealand (Mortimer et al., 2007). Geophysical and bathymetric data suggest that intraplate volcanism is common and widespread on submarine portions of Zealandia, which was confirmed during R/V Sonne SO168 and 169 Expeditions (Hoernle et al., 2003, Gohl et al., 2003).

Except for the Dunedin area the heat flow on the continental plateau of Zealandia is ~ 60 mW/m^{-2} similar to the averaged global heat flow (~ 57 mW/m^{-2}), (Godfrey et al., 2001; Sclater et al., 1980). In the Dunedin area, the heat flow is elevated (> 90 mW/m^2) (Godfrey, et al., 2001) and is accompanied by the highest proportions of mantle helium (~ 84 %) (Hoke, et al., 2000) measured in the South Island, suggesting recent magmatic activity in this area. Northward towards Banks Peninsula the heat flow steadily decreases to 'normal' values of continental crust (Godfrey et al., 2001). Based on seismic imaging, the lithospheric thickness beneath Zealandia ranges between 70 and 100 km (Molnar et al., 1999; Stern et al., 2002; Liu and Bird, 2006) with an orogenic root extending up to ~ 140 km beneath the Southern Alps (Stern et al., 2002).

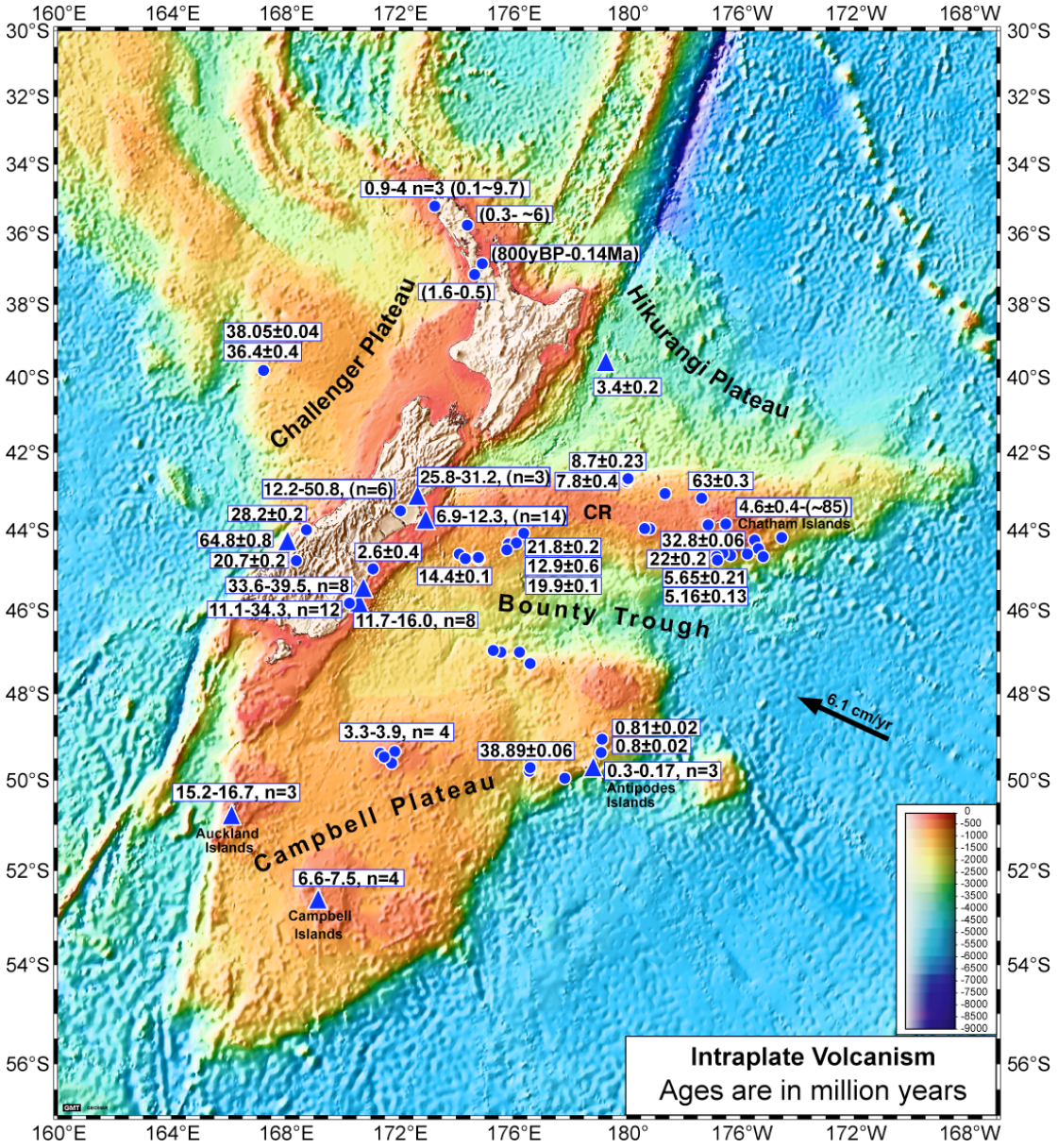

Figure 3.2: Ages of intraplate volcanic centers of Zealandia. The Cenozoic volcanoes (black numbers) are irregularly scattered on the Central and Western Chatham Rise, the Campbell and Challenger Plateaus and the South and North Islands of New Zealand, showing no clear age progressions (symbols as in Figure 3.1).

3.3 Evolution of Cenozoic Magmatism and Sample Background

Since Early Cretaceous subduction ceased off Zealandia, intraplate volcanism has been widespread on the continent (e.g. Figure 3.2, 3.3) (Gamble et al., 1986; Weaver and Smith, 1989). Products of this volcanism are primarily mafic, ranging from quartz tholeiitic to nephelinitic and carbonatitic, but with minor trachyte and

phonolite. Major episodes of volcanism occurred in the Late Cretaceous, Paleocene to Early Eocene, Late Eocene to Early Oligocene and Middle to Late Miocene. Minor activity has been recorded in the Late Oligocene to Early Miocene and Pliocene to Quaternary. The most voluminous volcanism is associated with the Miocene Lyttelton and Akaroa basaltic shield volcanoes (~1800km^3) on Banks Peninsula and the Dunedin Volcano (~600km^3) on the Otago Peninsula.

NORTHERN SOUTH ISLAND. The oldest intraplate volcanic rocks in the northern South Island include the mid-Cretaceous alkaline intrusive Tapuaenuku Complex and its associated mid-Cretaceous to Paleocene (100-60 Ma) basanitic to trachybasaltic radial dike swarm (Baker et al., 1994; Grapes, 1992). In Canterbury, intraplate volcanic products include the mid-Cretaceous alkaline Mandamus Igneous Complex (88-97 Ma) (Tappenden, 2003). The Paleocene to Lower Eocene tholeiitic basalts to basaltic andesites of the View Hill area in Central Canterbury have yielded K/Ar ages of 51.7 ± 2.4 and 47.9 ± 3.6 Ma (Sewell and Gibson, 1988), whereas the tholeiitic to alkaline Cookson Volcanics (≥100 km^3) (McLennan and Weaver, 1984; Morris, 1987) were erupted in the Oligocene. Based on our field studies, the stratigraphically oldest eastern Cookson units are pillow basalts and sheet flows, indicative of submarine volcanic activity, whereas the western Cookson units are characterized by stratigraphically younger conglomerates with large, well-rounded beach cobbles and heavily-oxidized lava flows with top and/or bottom breccias, indicating shallow water to subaerial conditions of emplacement. Therefore we interpret the Cookson Volcanics to likely have been part of an Oligocene shield volcano, which rose above sea-level and formed an island. Based on K/Ar dating, the Oxford volcanics in central Canterbury range in age from 27.1 ± 0.8 - 15.6 ± 1.0 Ma (Sewell and Gibson, 1988). Middle to Late Miocene alkaline to tholeiitic volcanic activity was widespread and produced the large Lyttelton (~350 km^3) and Akaroa (~1200 km^3) composite shield volcanoes on Banks Peninsula (Timm et al., in review; Stipp and McDougall, 1968; Weaver and Smith, 1989). A temporal migration of volcanism on Banks Peninsula from >12 to ~7 Ma towards the southeast corresponds with a compositional evolution to more mafic and Si-undersaturated compositions (from andesites through rhyolites to alkali basalts through trachytes and phonolites to alkali basalts through nephelinites; Timm et al., in review). Pliocene volcanism in northern South Island produced only very low volume transitional basaltic and olivine

and quartz tholeiitic lava flows near Geraldine and Timaru (1.3 km^3) (Duggan and Reay, 1986) with an $^{39}Ar/^{40}Ar$ age of 2.5 ± 0.4 Ma (Hoernle et al., 2006), which agrees well with an previously determined K/Ar age of 2.5 ± 0.7 Ma (Mathews and Curtis, 1966).

SOUTHERN SOUTH ISLAND. The oldest-known volcanic rocks in the Otago region are an ~1 km sequence of Paleocene tuffs drilled offshore (Coombs et al., 1986). The Upper Eocene to Lower Oligocene (40 - 34 Ma) (Hoernle et al., 2006) Waiareka-Deborah volcanics (~100 km^3) were largely erupted under submarine conditions (e.g. pillow lavas in Oamaru), possibly forming a submarine shield volcano. Tholeiitic basalts prevail, but rare alkaline volcanism also occurred (Coombs et al., 1986). The basanitic Kakanui Mineral Breccia, with $^{40}Ar/^{39}Ar$ ages of 33.7 ± 0.3 and 34.1 ± 0.1 on amphibole, is the youngest unit of the Waiareka-Deborah group, (Hoernle et al., 2006). The Waipiata Volcanics (25 - 11 Ma) of eastern and central Otago include alkali basalt to nephelinite, trachyandesite, mugearite and phonolite (Coombs et al., 1986; Hoernle et al., 2006). The Dunedin shield volcano lies within the Waipiata Volcanic Field. Its lavas range in composition from alkali basalt and basanite to trachyte and phonolite. The dominance of alkali basalt, in contrast to primarily basanite of the Waipiata Volcanics, is consistent with generally higher degrees of melting to form the volumetrically larger Dunedin Volcano, which was active for ~4 million years between ~16.0 - ~11.7 Ma (Price and Compston, 1973; McDougall and Coombs, 1973; Hoernle et al., 2006).

WESTERN SOUTH ISLAND. Two episodes of mafic mildly alkaline volcanism have been recognized along the west coast of the South Island in South Westland (Sewell and Nathan, 1987). The Late Cretaceous to Paleocene Arnott Basalt was erupted close to the axis of rifting during the separation of New Zealand and Australia (Smith and Weaver, 1989). The Otitia Basalt was erupted during a period of late Eocene crustal extension (Nathan et al., 1986). Both basalts have intraplate affinities. Although the onshore outcrops of these volcanic episodes are limited, geophysical data from magnetic surveys north of the onshore outcrops and offshore seismic profiles suggests that these volcanic episodes were much more extensive (Weaver and Smith, 1989) and the Arnott Basalt may have been a part of a largely submarine shield volcano. An U/Pb zircon age of 61.4 Ma has been obtained from a rhyolitic clast at Porphyry Point, from a deposit that stratigraphically overlies the

Arnott Basalt (Phillips et al., 2005). The lamprophyric Alpine Dike Swarm extends 110 km southeast from the Alpine Fault. It ranges from nephelinite, basanite and carbonatite to phonolite and trachyte in composition (Cooper, 1986). Cooper et al. (1987) proposed that these dikes intruded into tension fractures and Riedel shears at the initiation of the Alpine dextral wrench fault system. K/Ar whole-rock ages from the Alpine Dike Swarm suggest an unusually large range of 14-846 Ma (Adams, 1980). K/Ar kaersutite ages indicate a much more restricted range of 23-52 Ma (Adams and Cooper, 1996). Rb-Sr and U-Pb age dating produced an age range of 20-25 Ma (Cooper et al., 1987). More recent dating of a dike sample on the southeastern edge of the field gave an $^{40}Ar/^{39}Ar$ age of 20.7 ± 0.2 Ma (Hoernle et al., 2006), younger than any K/Ar kaersutite age.

SUBANTARCTIC ISLANDS. Late Cretaceous to Pleistocene volcanic rocks with intraplate geochemical characteristics occur on four sub-Antarctic island groups. Igneous activity on the Chatham Islands occurred in three phases: Late Cretaceous (85-82 Ma; Southern Volcanics), Eocene-Oligocene (41-35 Ma; Northern Volcanics) and Miocene-Pliocene (~5 Ma; Rangitihi Volcanics) (Panter et al., 2006). With decreasing age, the volcanics became progressively more Si-undersaturated, from ol-rich basalt to basanite. More-voluminous volcanism occurred at the Ross and Carnley Volcanoes at the Auckland Islands (Ar/Ar ages of 15.2 ± 0.2 Ma and 16.7 ± 0.6 were determined for the Ross Volcano), and it was active at a similar time as the Dunedin Volcano (c. 12-16 Ma) (Hoernle et al., 2006). There is some question about the large K/Ar age ranges of 12 - 25 Ma for the Ross Volcano and 17 - 37 Ma for the Carnley Volcano (Adams, 1983). Based on detailed age dating of the younger Banks and Dunedin volcanoes, which are also much better exposed and accessible, we see that these volcanoes generally have a peak in activity over 1 - 2 million years and then low levels of activity for the next 3 - 5 million years. Therefore, if the Ross and Carnley shield volcanoes were formed by similar processes to the shield volcanoes on the South Island, we would expect age ranges for these volcanoes on the order of 4-6 Ma and therefore suspect that some of the K/Ar ages are inaccurate due to alteration of the samples. Two lavas from Campbell Island give $^{40}Ar/^{39}Ar$ ages of 7.5 ± 0.1 to 6.6 ± 0.3 Ma, falling into the K/Ar age range of 6.5 - 8.5 (Adams, 1979). The Antipodes Islands, located on the northeastern edge of the Campbell Plateau consist of Si-undersaturated (basanite to nepheline hawaiite to phonolite) volcanic rocks (Gamble

et al., 1986). Two K/Ar dates of 0.25 and 0.50 Ma suggest that this volcano may have formed in the Pleistocene (Cullen, l969). On the North Island of New Zealand intraplate volcanism was active between ~11 Ma and ~600 yrs ago in the Northland area (Smith et al., 1993), whereas volcanic activity in the South Auckland Volcanic Field occurred between ~2 Ma and 200 yrs ago (Briggs et al., 1994) and thus include the youngest intraplate volcanic rocks known on Zealandia.

The common occurrence of pillow lavas and sheet flows, partly with glassy margins, on the South Island of New Zealand (e.g. within the Waiareka Deborah Formation at Oamaru, the View Hill Basalts etc.) implies that Zealandia was, through most of the Cenozoic, submerged. Only a few volcanic centers emerged above sea-level, such as the Cookson Volcanic Complex, and the Dunedin and Banks Peninsula volcanoes, which began erupting under submarine conditions (e.g. Smith & Weaver, 1989).

OTHER OFFSHORE REGIONS. Submarine intraplate volcanoes have been described from the southern flank of Chatham Rise (Urry Knolls) (Herzer et al., 1989), from Mt. Spong on the Challenger Plateau and from the South Fiji Basin north of the North Island of New Zealand (Mortimer et al., 2007). Geophysical and bathymetric data suggested that intraplate volcanoes were common and widespread on submarine portions of Zealandia, and this was confirmed during R/V Sonne expeditions SO168 and 169 (Hoernle et al., 2003, Gohl et al., 2003).

On the SO168 and 169 expeditions, more than 30 volcanic structures were mapped on or near the Chatham Rise and on the Campbell and Challenger Plateaus using a SIMRAD EM120 multi-beam echo-sounding system. The volcanoes on the central and western Chatham Rise and on the Campbell Plateau rarely exceed 1 - 3 km in basal diameter and some hundreds of meters in height. Their bases are located at water depths of ~1,500 m - 60 m. The volcanism in these regions primarily occurs in localized areas, such as around the Chatham Islands, the Graveyard Seamount area, the Veryan Bank area and at the Urry Knolls on the Chatham Rise, and the Pukaki Bank, north and west of Antipodes Island and the northern margin of the Campbell Plateau (Figure 3.1). Each of the submarine Cenozoic volcanic centers has a distinct morphology. Mount Spong on the Challenger Plateau for instance only rises ~100m above the surrounding ocean floor, but contains two WNW ESE aligned oval-shaped

calderas (overall ~2 x 0.8 km), the floors of which lie at greater depths than the surrounding sea floor (Figure 3.3a).

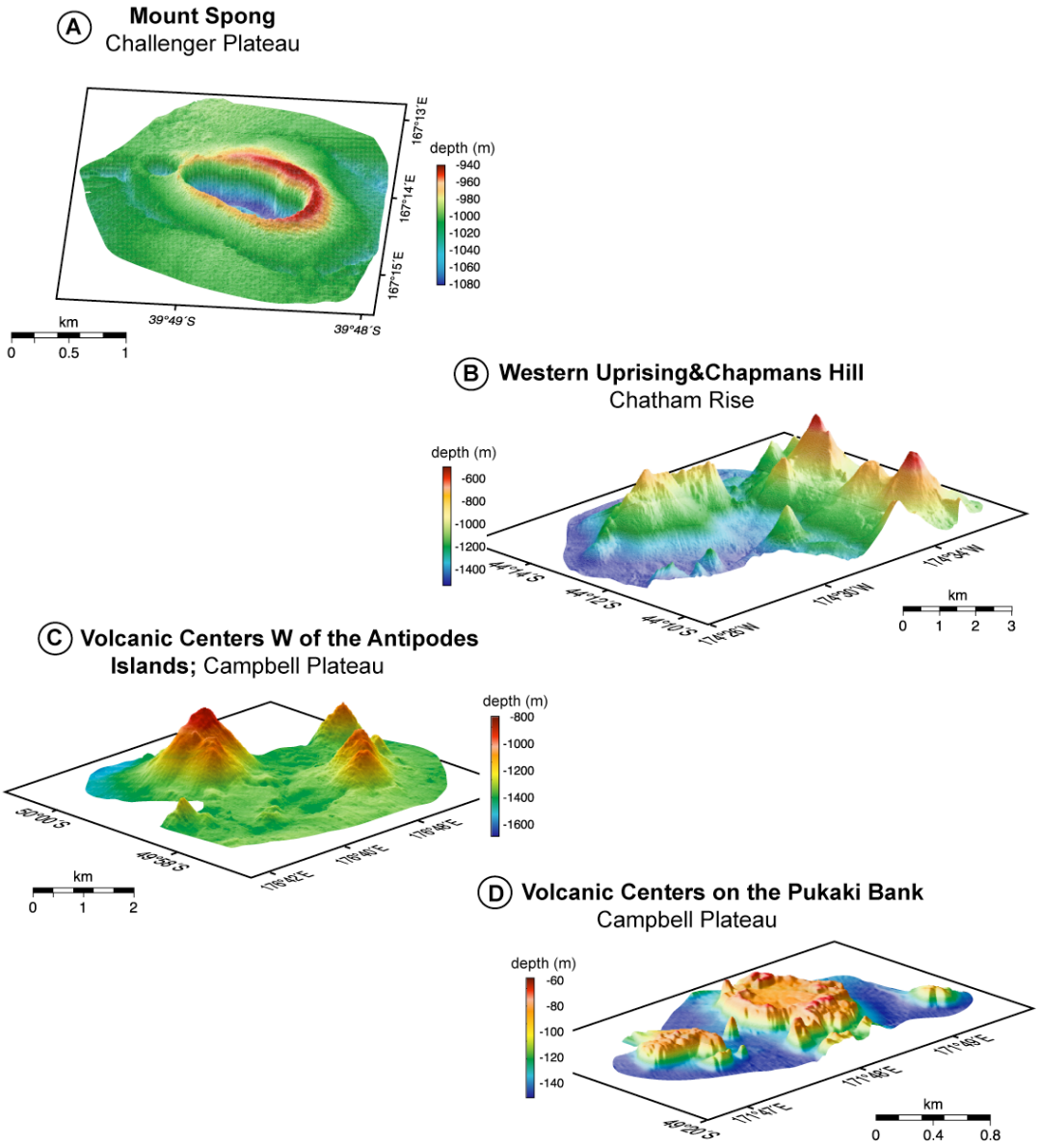

Figure 3.3a-3.3d: Oblique views, derived from multibeam bathymetry, of (A) Mount Spong on the Challenger Plateau, showing two volcanic structures with deep craters, densely-clustered volcanic ridges and cones (B) of the Western Uprising & Chapmans Hill volcanic field on the Western Chatham Rise and (C) west of the Antipodes Islands (B and C represent the dominant volcanic features on the central and western Chatham Rise and the Campbell Plateau respectively), and (D) the Pukaki Bank plateau on the Campbell Plateau.

Probably this structure was higher than 100m in the past, but has been almost entirely buried by Cenozoic sediments. Chapmans Hill and Western Uprising on the Chatham Rise consist, in contrast, of volcanic cones and ridges rising up to 1000m above their bases to ~500 mbsl (Figure 3.3b). North and South of the Antipodes Islands on the Campbell Plateau numerous small volcanic cones were mapped, which show comparable morphologies to those on the Chatham Rise, reaching maximum heights of about 600 m above the seafloor, with basal diameters of ~2 km at their bases at ~1400mbsl (Figure 3.3c). In the central part of the Campbell Plateau, several volcanic structures (~ 1 km in diameter with flat tops located ~60 mbsl are located on the Pukaki Bank. The flat tops of the Pukaki Bank volcanoes may also represent post-eruptive erosional platforms. Voluminous Cenozoic volcanic structures appear to be restricted to the Chatham, Campbell, Auckland, and Antipodes Islands (and possibly the Pukaki Bank). The morphology of the submarine volcanic features overall is comparable to that of volcanic centers on the South Island of New Zealand. There are two volcanic end members - widely distributed monogenetic volcanic fields, and large composite shield volcanoes, which are shown by different symbols in Figure 3.1.

3.4 Sampling and Analytical Methods

For the present study, volcanic rocks were dredged from 26 now submerged volcanoes on the central and western Chatham Rise, 13 locations on the Campbell Plateau, 2 locations from Mount Spong on the Challenger Plateau and 1 location on the Hikurangi Plateau (Figure 3.1). At all dredge sites discussed here, the angular shape of the rocks, freshly broken surfaces, and the homogeneity of rock types indicate an in-situ (not ice-rafted) origin for the dredged rocks. Subaerial volcanic areas of New Zealand were sampled during three field seasons. Sampling localities are summarized in Table 1.

Analyses of $^{40}Ar/^{39}Ar$ were conducted on matrix chips and amphibole and feldspar phenocrysts at the IFM-GEOMAR Tephrochronology Laboratory. The particles were hand-picked from crushed and sieved splits. All separates were cleaned using an ultrasonic disintegrator. Plagioclase and amphibole phenocrysts were additionally etched in 15% hydrofluoric acid for 15 and 10 minutes, respectively. Samples were neutron irradiated at the 5-MW reactor of the GKSS Research Center (Geesthacht, Federal Republic of Germany), with crystals and matrix chips in aluminum trays and

irradiation cans wrapped in 0.7 mm cadmium foil. Age determinations by laser $^{40}Ar/^{39}Ar$ analysis were performed by fusing single crystals of feldspar phenocrysts in a single step and matrix chips by laser step-heating analysis. Purified gas samples were analyzed using a MAP 216 series noble gas mass spectrometer. Raw mass spectrometer peaks were corrected for mass discrimination, background and blank values determined every fifth analysis. The neutron flux was monitored using Taylor Creek Rhyolite Sanidine (TCR-2: 27.87 ± 0.04 Ma) (Lanphere, unpubl. data). Vertical variations in J-values were quantified by a cosine function fit. Corrections for interfering neutron reactions on Ca and K are based on analyses of optical grade CaF_2 and high-purity K_2SO_4 salt crystals that were irradiated together with the samples. Replicate analyses of 8-13 particles from each phase were carried out for statistical reasons in order to calculate mean apparent ages and isochron ages. Internal errors are reported at the 2-sigma confidence level.

Samples selected for geochemistry were first crushed to small pieces, then washed in deionized water and carefully hand-picked under a binocular microscope. Major elements and some trace elements (e.g., Cr, Ni, Zr, Sr) of whole rock samples were determined on fused beads using a Philips X'Unique PW1480 X-ray fluorescence spectrometer (XRF) equipped with a Rh-tube at IFM-GEOMAR. H_2O and CO_2 were analyzed in an infrared photometer (Rosemount CSA 5003). Additional trace elements (e.g., Rb, Ba, Y, Nb, Ta, Hf, U, Th, Pb and all REE) were determined by ICP-MS on a VG Plasmaquad PQ1-ICP-MS at the Institute of Geosciences (University of Kiel) after the methods of Garbe-Schönberg (1993).

Sr-Nd isotope analyses of the submarine samples were carried out on rock powders, leached in 6N HCl at 130°C for up to 24 hours prior to dissolution in a 5:1 mixture of concentrated HF ultra-pure (u.p.) and HNO3 u.p. Hf and Pb isotope analyses used unleached powders and rock chips respectively. The element chromatography followed the methods outlined in Hoernle and Tilton (1993) and Hoernle et al. (2008). Sr-Nd-Pb isotopic ratios were determined on the TRITON and MAT262 RPQ^{2+} thermal ionization mass spectrometers (TIMS) at IFM-GEOMAR with both instruments operating in static multi-collection. Sr and Nd isotopic ratios are normalized within run to $^{86}Sr/^{88}Sr = 0.1194$ and $^{146}Nd/^{144}Nd = 0.7219$, respectively. All Sr isotope data are reported relative to NBS987 $^{87}Sr/^{86}Sr = 0.710250$ with an external $2\sigma = 0.000012$ (N=32) for the MAT262 and $2\sigma = 0.000009$ (N=26) for the TRITON. The Nd isotope data are reported relative to La Jolla $^{143}Nd/^{144}Nd =$

0.511849± 0.00007 (N=33) and to an in-house monitor Spex $^{143}Nd/^{144}Nd$ = 0.511715± 0.00007 (N=26). The long-term NBS 981 (N=125) values are $^{206}Pb/^{204}Pb$ = 16.898± 0.006, $^{207}Pb/^{204}Pb$ = 15.437± 0.007, $^{208}Pb/^{204}Pb$ = 36.527± 0.024 and corrected to the NBS 981 values given in Todt et al. (1996). Total chemistry blanks were <400 pg for Sr, Nd, Hf and Pb and thus considered negligible. Hafnium was separated following a slightly modified two-column procedure as described by Blichert-Toft et al. (1997). Hafnium isotope ratios were carried out on a VG Axiom multi-collector ICPMS (MC-ICPMS). After two days of measuring the in-house spex monitor to stabilize the signal, standards was determined repeatedly every two or three samples to verify the machine performance. To correct the instrumental mass bias $^{176}Hf/^{177}Hf$ was normalized to $^{179}Hf/^{177}Hf$ = 0.7325.

3.5 Results

3.5.1 $^{40}Ar/^{39}Ar$ dating

Our 43 new $^{40}Ar/^{39}Ar$ ages from Cenozoic volcanic rocks across Zealandia range from 64.8 ± 0.4 to 0.17 ± 0.09 (Figure 3.4). A detailed list of all $^{40}Ar/^{39}Ar$ age data and accuracy of the measurements can be found in Table 1. All errors are stated as 2 σ.

Only a few samples yielded early Cenozoic $^{40}Ar/^{39}Ar$ ages between ~ 65 and 40 Ma. On the South Island of New Zealand, a sample of the Arnott Basalt was dated at 64.8 ± 0.4 Ma by $^{40}Ar/^{39}Ar$ step heating of feldspar (fsp), consistent with the U-Pb zircon age of 61.4 Ma obtained from a rhyolitic clast in a deposit that stratigraphically overlies the Arnott Basalt (Phillips et al., 2005). Since the Arnott Basalt is on the Australian Plate, the Arnott Basalt must have been located close to the Auckland Islands when these rocks were erupted. Samples from the View Hill Volcanics in central Canterbury yielded a restricted age range with ages of 50.8 ± 0.3, 49.7 ± 0.6, 49.3 ± 0.6 and 48.9 ± 0.7 Ma (fsp and matrix step heating, within the K/Ar age range of 48-52 Ma) (Sewell and Gibson, 1988). The oldest Cenozoic ages for offshore volcanism are from a volcanic cone on the central Chatham Rise ($^{40}Ar/^{39}Ar$ age of 63.0 ± 0.3 Ma; matrix step heat). Volcanism in the late Eocene and early Oligocene was widespread, occurring at small volcanic centers west of the Antipodes Islands (38.9 ± 0.1 Ma; matrix step heat with a relatively poor plateau of 43%) and on the

central Chatham Rise (Chapmans Hill; 32.8 ± 0.1 Ma; matrix step heat), at Mount Spong (feldspar single fusion $^{40}Ar/^{39}Ar$ ages of 38.1 ± 0.04 and 36.4 ± 0.4; n = 12 and 13, respectively).

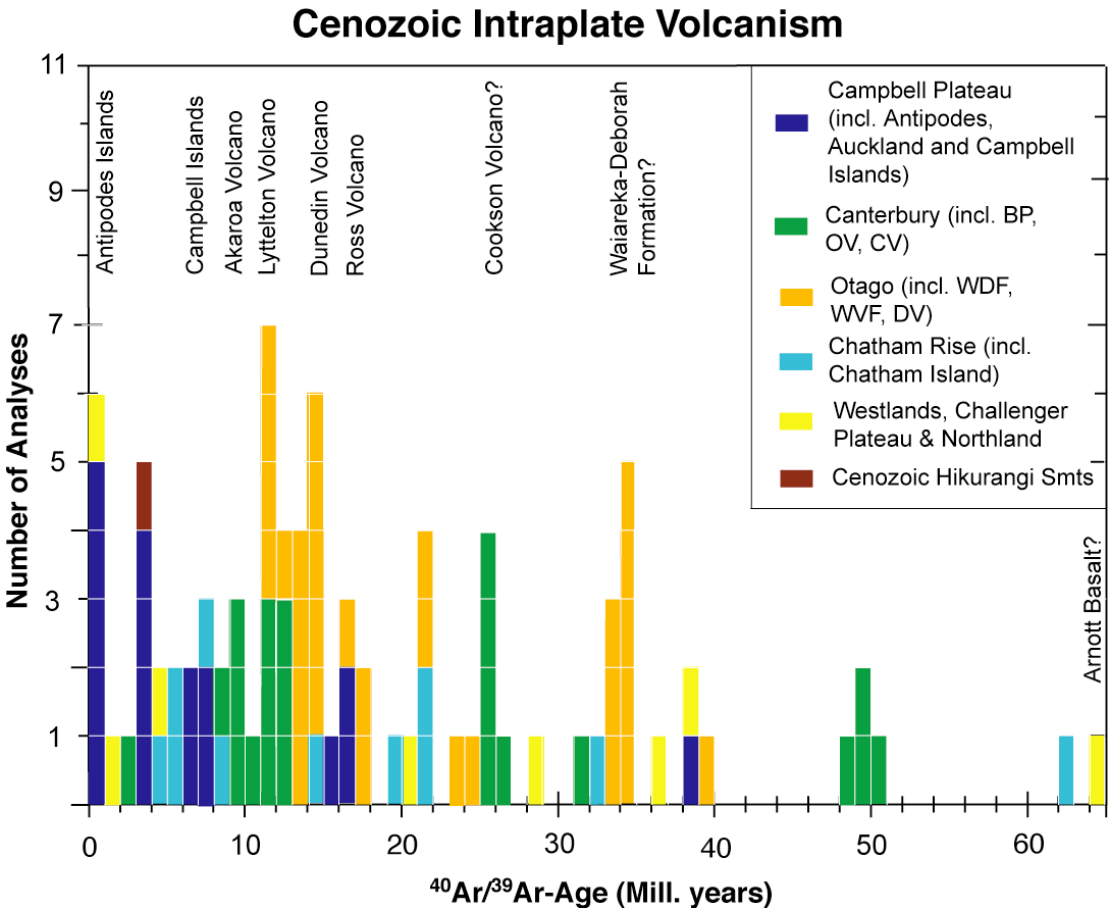

Figure 3.4: Histogram showing a complete compilation of our $^{40}Ar/^{39}Ar$ database. Although the number of analyses reflects to a large extent a sampling bias with younger volcanism being less likely to be eroded or covered with sediments, there does appear to be an increase with time in the abundance of large magmatic events (≥100 km^3), such as composite shield volcanoes (denoted by the vertical text at the time the event primarily took place or shield volcano formed).

On land the Cookson Volcanics in southern to central Canterbury on the South Island gave three matrix step heat $^{40}Ar/^{39}Ar$ ages of 31.2 ± 0.6, 26.6 ± 0.1 and 25.9 ± 0.3 Ma, which overlap with the age of the Otitia Basalts in Westland (28.2 ± 0.2 Ma; matrix step heat). We note that our Late Oligocene age is not consistent with the Otitia basalt having formed during a period of Late Eocene extension as previously proposed (Nathan et al., 1986). Since the Otitia Basalts are, similar to the Arnott Basalt, on the Australian Plate, they were emplaced several hundred kilometers south of the majority

of the South Island located on the Pacific Plate. Two alkali basalts in central Canterbury collected along the Eyre River (Oxford area) yielded late Oligocene $^{40}Ar/^{39}Ar$ ages - identical within error - of 25.6 ± 0.3 and 25.2 ± 0.1 Ma (both matrix step heat), falling at the older end of the K/Ar range determined for the Oxford volcanics (30-11 Ma) (McLennan and Weaver, 1984; Sewell and Gibson, 1988). Early to mid Miocene volcanic activity also took place on the Central Chatham Rise, near the Chatham Islands (Charlton A Seamount, 22 ± 0.2 Ma; matrix step heat), western Chatham Rise (Orton/Vernon Bank and Veryan Bank, 21.8 ± 0.2 and 12.9 ± 0.6 Ma, respectively, both matrix step heat ages) and at the Urry Knolls (Jordan Seamount; 14.4 ± 0.1 Ma; matrix step heat). In southern and central Canterbury (Oxford area) two mid Miocene ages of 12.2 ± 0.5 and 11.5 ± 1.5 Ma (matrix and feldspar step heat, respectively) were determined on lavas of Burnt and Harper Hills and thus overlap the K/Ar range determined by Sewell and Gibson (1988) for the Harper Hill basalt (13.5-11.0 Ma). A sample from the Waipiata Volcanic Field produced a matrix step heat age 23.2 ± 0.2, placing it at the earlier end of the Waipiata volcanism (25-11 Ma) (Hoernle et al., 2006), whereas two additional step heat ages from the and Dunedin Volcano yielded ages of 14.6 ± 0.2 (feldspar) and 11.7 ± 0.6 (feldspar) Ma, also falling within the previous range established for the Dunedin Volcano (~16-12 Ma) (Hoernle et al., 2006). Lavas with late Miocene ages were also found on the northern central Chatham Rise from the Graveyard Seamounts (8.7 ± 0.23 and 7.8 ± 0.4 Ma; both matrix step heat).

Pliocene volcanic rocks are widespread on Zealandia. The youngest volcanic successions on the Chatham Islands yielded an $^{40}Ar/^{39}Ar$ (matrix step heat) of 4.6 ± 0.1 Ma. Samples from Clerk and Perry Seamounts on the central Chatham Rise, near the Chatham Islands, produced a matrix step heat ages of 5.7 ± 0.21 and 5.2 ± 1.13 Ma, whereas a sample from the Urry Knolls on the western Chatham Rise was dated at 2.6 ± 0.6 Ma (matrix step heat age), similar in age to the nearby Timaru and Geraldine volcanic rocks (Mathews and Curtis, 1966; Hoernle et al., 2006) erupted on the coast of the South Island at the end of the Chatham Rise. Two samples from the Pukaki Bank on the Campbell Plateau yielded ages of 3.9 ± 0.09 Ma and 3.3 ± 0.11 Ma (matrix step heat ages). A Pliocene matrix step heat age of 3.4 ± 0.2 was also determined on a volcanic rock from Rowling B seamount, located on the Hikurangi Plateau.

Table 1: Results of step-heating and single-crystal $^{40}Ar/^{39}Ar$ analyzes.

Sample ID	Group	Mean apparent age or plateau age (Ma)		1σ	MSWD	%^{39}Ar in plateau	n	Dated Material and type of analyses
Western and Central Chatham Rise								
SO168-DR91-1	lsg	63.0	±	0.3	1.3	83.1		Matrix Step Heat
SO168-DR74-1	lsg	32.8	±	0.3	0.53	92.3		Matrix Step Heat
SO168-DR80-1	lsg	22.0	±	0.2	1.6	71.1		Matrix Step Heat
SO168-DR97-1	lsg	21.8	±	0.2	1.6	69.8		Matrix Step Heat
SO168-DR99-2	lsg	19.9	±	0.1	1.19	84.8		Matrix Step Heat
SO168-DR101-1	lsg	14.4	±	0.1	0.72	100		Matrix Step Heat
SO168-DR96-1	lsg	12.9	±	0.6	2.3	62.5		Matrix Step Heat
SO168-DR3-1	lsg	8.70	±	0.2	1.5	71.5		Matrix Step Heat
SO168-DR5-1	lsg	7.80	±	0.4	0.59	55.8		Matrix Step Heat
SO168-DR87-6	hsg EMII	5.65	±	0.2	1.2	65.8		Matrix Step Heat
SO168-DR87-4	hsg EMII	5.16	±	0.1	1.5	81.5		Matrix Step Heat
Chatham Islands								
P74894	lsg	4.6	±	0.1	1.4	86.8		Matrix Step Heat
Challenger Plateau								
SO168-DR2-1	lsg	38.05	±	0.0	1.91		12	Feldspar
SO168-DR2-2	lsg	36.4	±	0.4	1		13	Feldspar
Campbell Plateau								
SO169-DR6-1	lsg	38.89	±	0.1	1.4	*42.9*		Matrix Step Heat
SO169-DR11-5	lsg	3.85	±	0.1	1.7	92		Matrix Step Heat
SO169-DR15-1	lsg	3.63	±	0.1	1.3	100		Matrix Step Heat
SO169-DR12-1	lsg	3.60	±	0.1	1.5	65.9		Matrix Step Heat
SO169-DR11-1	lsg	3.34	±	0.1	1.3	98.2		Matrix Step Heat
SO169-DR3-1	lsg	0.80	±	0.0	1.11		18	Feldspar
SO169-DR3-7	lsg	0.81	±	0.0	1.08		18	Feldspar
A105	lsg	0.30	±	0.1	0.88	100		Matrix Step Heat
A8B	lsg	0.19	±	0.0	0.93	99		Matrix Step Heat
A109	lsg	0.17	±	0.1	0.72	99.2		Matrix Step Heat
Canterbury: Cookson Volcanics								
MSI36 A	lsg	31.2	±	0.6	1.6	69.4		Matrix Step Heat
MSIK33 A	lsg	26.6	±	0.1	0.9	72.8		Matrix Step Heat
MSI42 C	lsg	25.8	±	0.3	0.8	57.5		Matrix Step Heat

Table 1 (continued)

Sample ID	Group	Mean apparent age or plateau age (Ma)		1σ	MSWD	%^{39}Ar in plateau	n	Dated Material and type of analyses
Canterbury: Oxford Volcanics								
MSI180 B	hsg EMII	50.8	±	0.3	0.7	73.0		Matrix Step Heat
MSI24	hsg EMII	49.7	±	0.3	0.3	60.5		Fsp Step Heat
MSI23 A	hsg EMII	49.3	±	0.6	0.6	80.1		Fsp Step Heat
MSI25	hsg EMII	48.9	±	0.7	1.3	82.6		Matrix Step Heat
MSI27 A	hsg EMII	25.6	±	0.3	1.6	58.6		Matrix Step Heat
MSI22 B	hsg EMII	25.2	±	0.1	1.1	86.8		Fsp Step Heat
MSI181	hsg EMII	12.2	±	0.5	0.9	95.5		Matrix Step Heat
MSI21 A	hsg EMII	11.5	±	0.8	2.4	76.2		Fsp Step Heat
Westland: Otitia and Arnott Basalts								
MSI65 A	lsg	64.8	±	0.4	1.2	60.1		Fsp Step Heat
MSI63 A	lsg	28.2	±	0.2	1.8	48.0		Matrix Step Heat
Otago: Dunedin Volcano and Waipiata Volcanic Field								
FouldenV2A	lsg	23.2	±	0.2	1.4	92.8		Matrix Step Heat
MSI88 A	lsg	14.6	±	0.2	0.8	49.3		Fsp Step Heat
OU22636	lsg	11.7	±	0.1	1.4	87.0		Fsp Step Heat
Northland								
NZN3	hsg MORB	4.0		0.7	0.7	68.8		Fsp Step Heat
NZN28	hsg MORB	1.97		0.3	1.6	98.1		Fsp Step Heat
NZN32	hsg MORB	0.88		0.3	1.1	100		Fsp Step Heat

Remaining Ar/Ar age data of the Dunedin Volcano, Waipiata Volcanic Field, Waiareka-Deborah Formation, Auckland, Campbell, Antipodes Islands and Banks Peninsula are taken from Hoernle et al., 2006 and Timm et al., in review.
Abbr.: lsg=low-silica group; hsg=high-silica group

In the Quaternary several pulses of volcanism formed volcanic cones around the Antipodes Island giving two identical $^{40}Ar/^{39}Ar$ ages within error of 0.81 ± 0.02 and 0.80 ± 0.02 Ma (feldspar single fusion; both n = 18). Three matrix step heat ages of 0.3 ± 0.1, 0.19 ± 0.1 and 0.17 ± 0.02 Ma were obtained for onland Antipodes Island lavas, extending the 0.25-0.50 Ma K/Ar age range for the Antipodes reported by Cullen (1969) to even younger ages.

In summary, our new $^{40}Ar/^{39}Ar$ data set reveals that Cenozoic intraplate volcanism was widespread across the submerged part of Zealandia, which was unknown before, Our new data also give new and more precise information on the

temporal distribution of intraplate volcanism on the emergent islands of Zealandia (Figure 3.4). They generally confirm the published age data for North, South and Subantarctic islands volcanism where available and add new radiometric ages for areas where none existed before (e.g. Cookson Volcanics; Otitia and Arnott Basalts). The existence of only a few ages between 65 - 40 Ma may or may not indicate true lower levels of volcanic activity in the early Cenozoic; an overall sampling bias may be present due to older rocks having been eroded or covered with sediment. Although large shield-type volcanoes also formed in the early and mid Cenozoic, ~65-25 Ma (e.g. possibly Arnott Basalts including offshore outcrops, Waiareka-Deborah and Cookson volcanics), shield volcanoes, however, appear to become more abundant in the last 25 Ma (e.g. Dunedin, Auckland Island, Banks Peninsula, Campbell Islands in the Miocene, Pukaki Bank volcanoes in the Pliocene and Antipodes Island in the Quaternary).

3.5.2 Geochemistry of Cenozoic intraplate volcanic rocks from Zealandia

3.5.2.1 Major and trace elements

Major and trace element, as well as isotope analyses are given in Tables 2 and 3.
Volcanic rocks from Zealandia range from nephelinite/basanite through phonolite, and from alkali basalt through trachyte to peralkaline rhyolite, with minor occurrences of tholeiites and basaltic andesites (rock classification after Le Maitre et al., 1989; Figure 3.5a). The studied mafic samples (MgO > 5wt%) range from tholeiite-basaltic andesite to alkali basalt–mugearite to basanite-tephrite to nephelinite (Figure 3.5b). On binary diagrams with SiO_2, the samples show moderate to good positive correlations with Al_2O_3, Na_2O, K_2O and negative correlations with TiO_2, FeO^t, CaO, which can be explained by fractional crystallization of the common mineral phases olivine, orthopyroxene, clinopyroxene and plagioclase. Based on SiO_2 content versus alkalies (TAS), the mafic volcanic rocks (MgO > 5 wt%) can be divided into a low-silica (SiO_2 < 46 wt%) and a high-silica (SiO_2 > 46 wt%) group, as defined by Hoernle et al. (2006) (Figure 3.5b). More evolved samples within a group can be derived from more mafic in the group through fractional crystallization. At a given MgO content, the low-silica group generally has higher TiO_2, FeO^t, CaO and Na_2O in

contrast to the high-silica group, but there is almost complete overlap in Al_2O_3 of both groups.

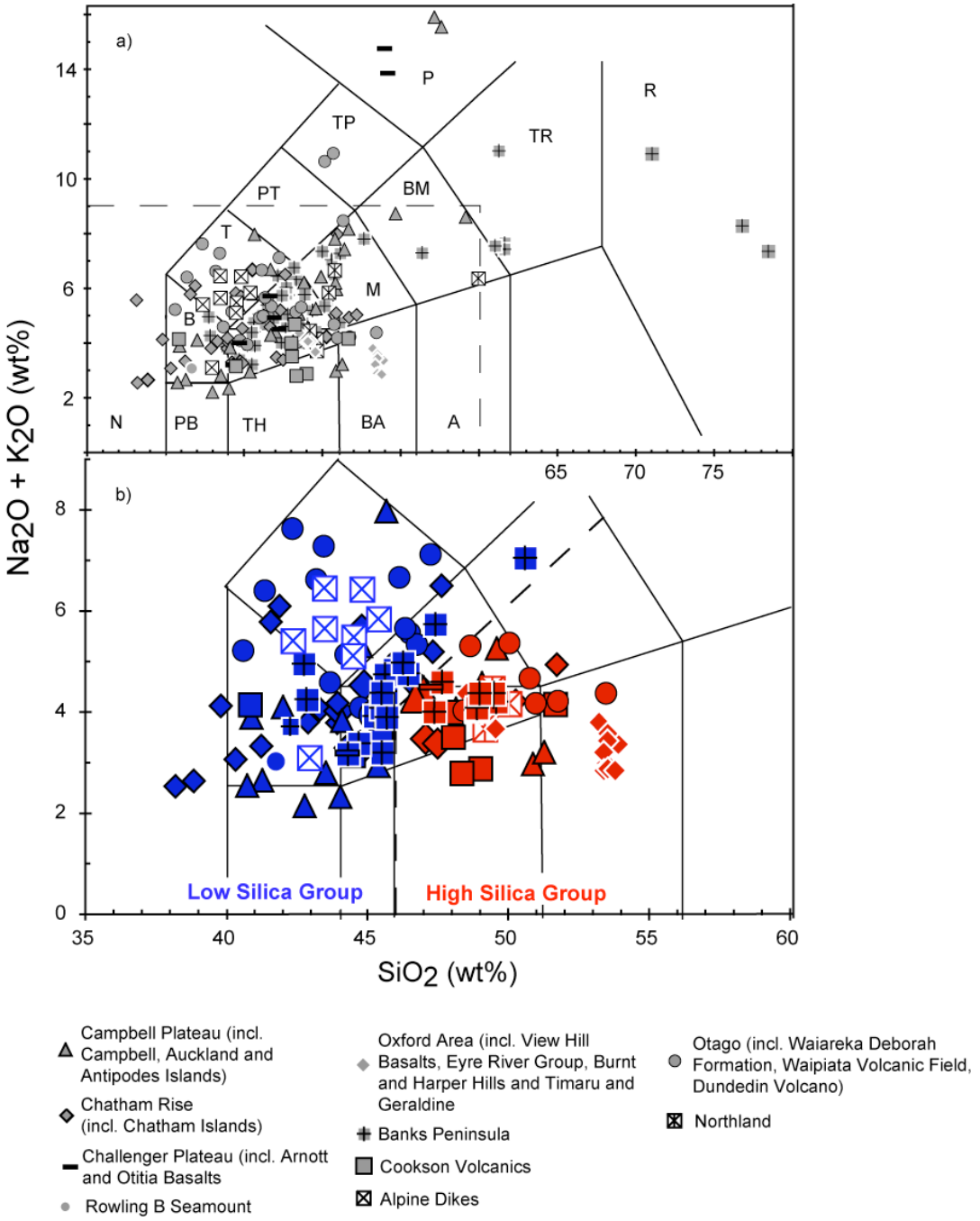

Figure 3.5: SiO_2 vs Total Alkalies (Na_2O+K_2O) normalized to 100% on a volatile-free basis according to rock type classification (LeMaitre, 1989). A) Samples from Zealandia range from tholeiite through basaltic andesite to alkali basalt through trachyte and peralkaline rhyolite to basanite through phonolite to nephelinite (Date from this study and the literature). B) Mafic (MgO > 5 wt%) volcanic rocks from Zealandia from this study are divided into high-silica (red symbols; SiO_2 > 46 wt%) and low-silica (blue; SiO_2 <46 wt%) groups.

Compared to experimentally generated melts of peridotite (Hirose and Kushiro, 1993; Dasgupta et al., 2007), garnet pyroxenite (Hirschmann et al., 2003) and eclogite (Kogiso and Hirschmann, 2006; Dasgupta et al., 2006) the low-silica group almost completely overlaps with the field for eclogite (± garnet pyroxenite) melts, whereas the high-silica rocks generally extend from the field for eclogite to that of peridotite melts.

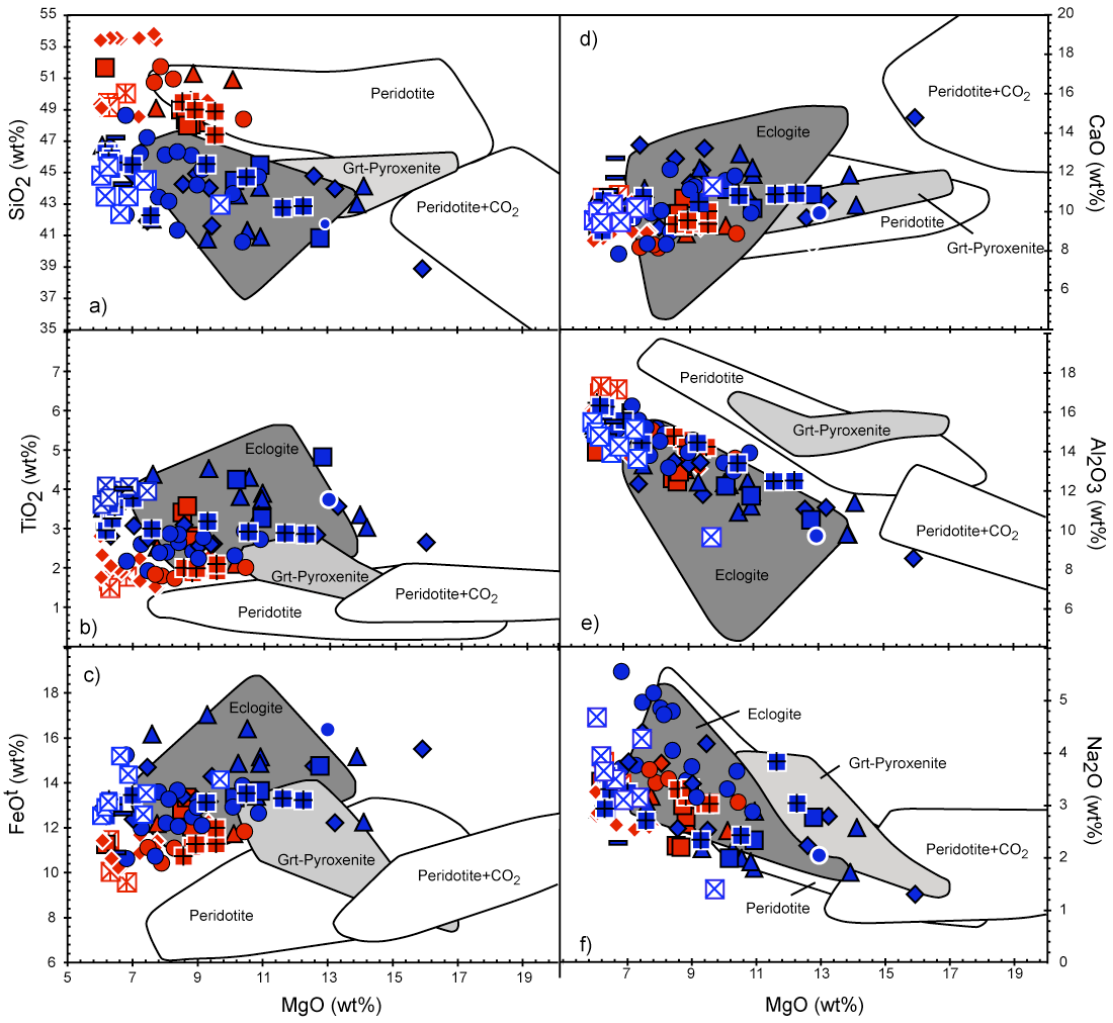

Figure 3.6a-6e: Diagrams showing selected major elements versus MgO for mafic samples (MgO > 6wt%) of the Cenozoic Zealandia volcanic rocks. The following filters were applied to reject strongly altered rocks: H_2O > 3 wt%, CO_2 > 0.8 wt%, MnO > 0.25. All data are normalized to a 100% volatile free basis. The high-silica group rocks have higher SiO_2 (as per definition) but also generally lower TiO_2, FeO^t, CaO and Na_2O relative to MgO. There is almost complete overlap in Al_2O_3 for both groups. The dark grey field represents the compositional range of experimental melts of eclogite (Kogiso and Hirschmann, 2006 and Dasgupta et al., 2006), the light grey field melts of garnet pyroxenite (Hirschmann et al., 2003) and the white fields (Hirose and Kushiro, 1993 and Dasgupta et al., 2007) are melts of peridotite with and without CO_2.

Most mafic volcanic rocks from Zealandia (MgO > 5 wt%) show similar incompatible element characteristics to ocean island basalts (OIB) on multi-element diagrams, with typical negative anomalies at Pb and K and positive anomalies at Nb and Ta (Figure 3.7).

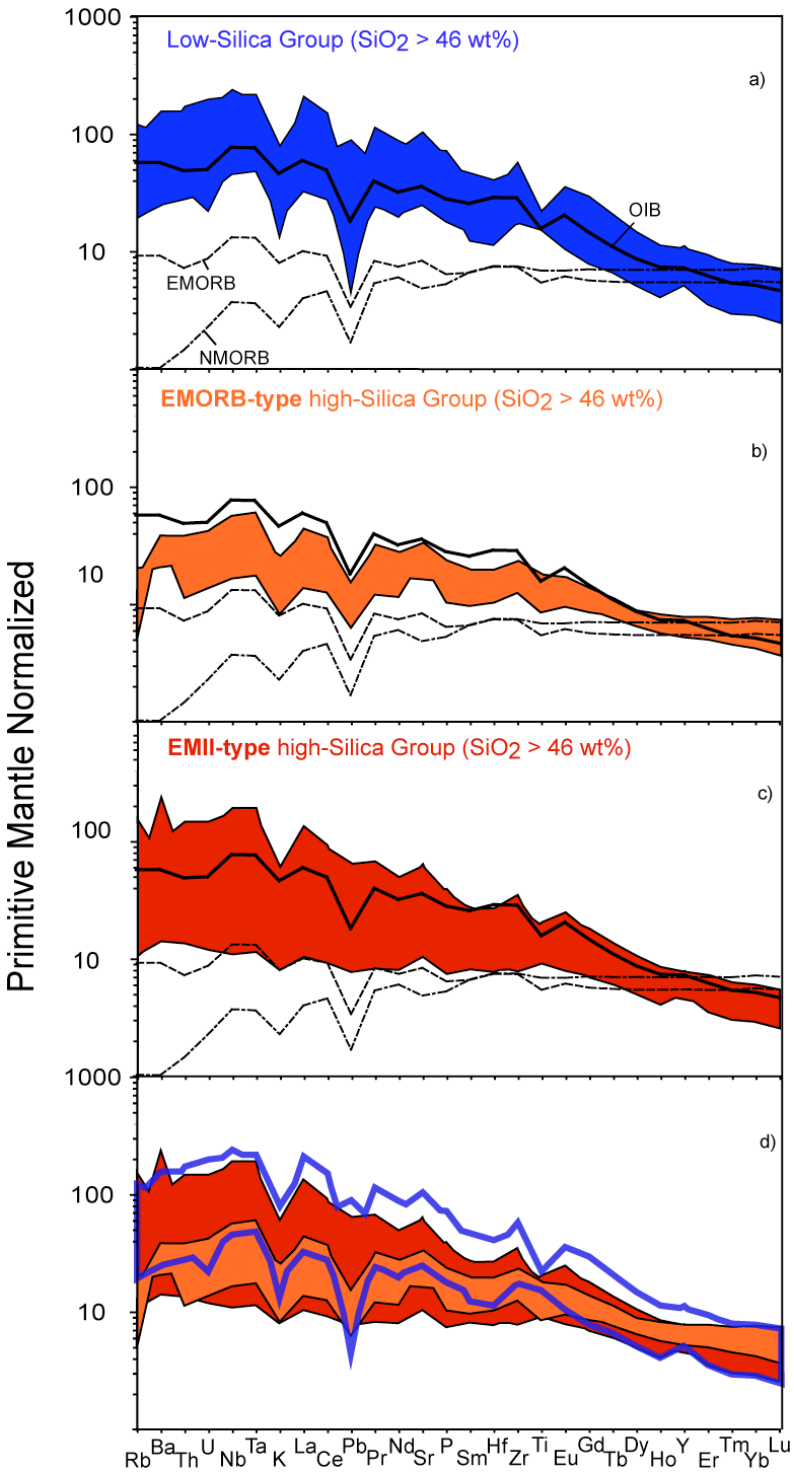

Figure 3.7a-d: Multi-element diagrams normalized to primitive mantle (Hofmann, 1988) of mafic (MgO > 5wt%) Zealandia intraplate lavas. The blue field represents the low-silica group volcanic rocks (SiO_2 < 46wt%; Figure 3.7a), whereas the red and orange fields represent the high-silica group volcanic rocks (SiO_2 > 46 wt%; Figure 3.7b-c). The high-silica group rocks are divided into a depleted (MORB-like; b) and an enriched (EM-like; c) group. For comparison a typical alkali basalt (OIB), EMORB and NMORB pattern (after Sun & McDonough, 1989) are also included.

The anomalies for Nb, Ta, Pb and K generally become more pronounced in rocks with lower silica contents (e.g. higher Nb/La, Nb/K, Ce/Pb and Nd/Pb). The low-silica rocks also have higher Zr/Hf and Nb/Ta. As more silica-rich rocks, the OIB-type patterns are smoother approaching EMORB-type signatures,

except that the HREE elements form steep patterns rather than a flat patterns as is characteristic of enriched (E) MORB. In addition, the high-silica rocks have higher fluid-mobile to less fluid-mobile (e.g. U/La, Rb/Zr, Ba/Y, Sr/Nd, Pb/Nd) and lower more to less incompatible element ratios (e.g. Zr/Hf, (Zr, Hf)/Nb, Zr/Y, (Nb, Ta)/Th, Nb/La, La/Sm, (Sm, Gd)/Yb) ratios.

3.4.2.2 Sr - Nd - Hf - Pb Isotope Data

The mafic Cenozoic volcanics have relatively low to moderate $^{87}Sr/^{86}Sr$ (0.7027 - 0.7050) and moderate to high $^{143}Nd/^{144}Nd$ (0.5128 - 0.5131) and $^{176}Hf/^{177}Hf$ (0.2829 - 0.2831). Lead isotope ratios reveal a broad range: $^{206}Pb/^{204}Pb$ = 18.62 - 20.67, $^{207}Pb/^{204}Pb$ = 15.54 - 15.72 and $^{208}Pb/^{204}Pb$ = 38.27 - 40.34. The range in isotopic composition of the Cenozoic Zealandia intraplate volcanic rocks falls within the range of ocean island basalts. On isotope correlation diagrams, the data largely forms an array extending from E-MORB to HIMU, but a third enriched (EMII)-type component is also required (Figure 3.8 and 3.10).

In comparison to the high-silica volcanic rocks, the low-silica Cenozoic intraplate volcanic rocks on Zealandia are characterized by HIMU-like compositions having radiogenic Pb isotope ratios (e.g. $^{206}Pb/^{204}Pb$ = 18.6-20.7). Almost all low-silica samples have negative Δ7/4Pb, i.e. they plot beneath the Northern Hemisphere Reference Line (NHRL of Hart, 1984) and form a crude array between HIMU and MORB-type mantle components (Figure 3.10a). The high-silica alkali basalts and tholeiites trend towards both E-MORB (e.g. Northland volcanic rocks) and the enriched (EMII-type) isotopic endmember (most other high-silica rocks) on Sr-Nd-Hf-Pb correlation diagrams (Figure 3.8a-b, Figure 3.10a-c). The high-silica rocks trending towards an EMII-like component also show a systematic increase of more- to less-incompatible and more- to less-fluid-mobile trace element ratios as silica content increases. All Cenozoic mafic volcanic rocks, however, generally have less-radiogenic Pb and Sr and more radiogenic Nd and Hf, compared to the Cretaceous volcanic rocks (Tappenden, 2003; Hoernle et al., in prep), but more radiogenic Pb and Sr and less radiogenic Nd and Hf isotopic compositions than Pacific N-MORB. Excluding samples that show evidence of seawater alteration that has primarily affected the Sr isotopic composition, the Cenozoic mafic volcanic rocks could be

explained through mixing of the Cretaceous intraplate volcanic source with the MORB source (i.e. DM, depleted mantle).

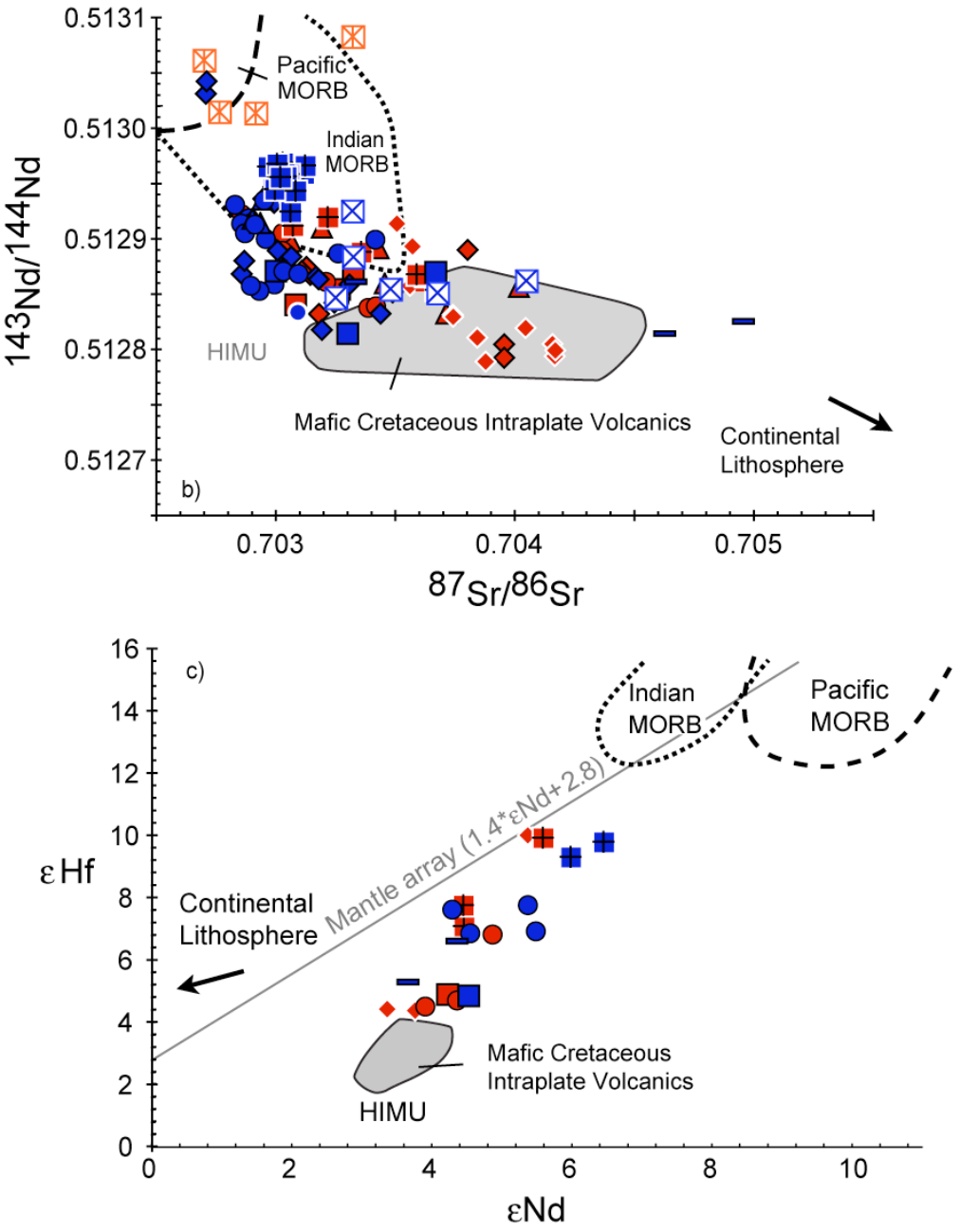

Figure 3.8a-3.8b: On $^{87}Sr/^{86}Sr$ versus $^{143}Nd/^{144}Nd$ (a) and εNd versus εHf (b) diagrams, the mafic (MgO > 5 wt%) Cenozoic volcanic rocks define an array between HIMU and Pacific MORB, with several samples trending off this array towards the EMII-like continental lithosphere. References fields and lines are from Tappenden (2003), Hoernle et al. (in prep), Storey et al., (1999), Zindler and Hart (1986) and Blichert-Toft (1995).

***Table 2**: Sr-Nd-Pb-Hf Isotope data*

Sample Number	Location	Group	$^{87}Sr/^{86}Sr$	$^{143}Nd/^{144}Nd$	$^{206}Pb/^{204}Pb$	$^{207}Pb/^{204}Pb$	$^{208}Pb/^{204}Pb$	$^{176}Hf/^{177}Hf$
Western Chatham Rise								
SO168_DR3-1	Graveyard A Morgue	lsg	0.703492 (2)	0.512852 (2)	19.502 (8)	15.639 (6)	39.438 (16)	
SO168_DR5-4	(Graveyards)	lsg	0.703441 (3)	0.512832 (2)	19.847 (14)	15.642 (11)	39.820 (29)	
SO168_DR74-2	Chapmans Hill	lsg	0.702710 (5)	0.513030 (3)	19.164 (2)	15.553 (1)	38.628 (3)	
SO168_DR74-4	Chapmans Hill	lsg	0.702713 (3)	0.513042 (3)	19.236 (7)	15.557 (4)	38.761 (9)	
SO168_DR80-6	Charlton A	lsg	0.703183 (3)	0.512832 (2)	20.107 (3)	15.667 (6)	39.792 (14)	
SO168_DR81-1	Charlton B	lsg	0.703182 (3)	0.512863 (3)				
SO168_DR83-2	FBI	lsg	0.702809 (2)	0.512990 (12)	18.933 (13)	15.620 (6)	38.651 (29)	
SO168_DR84-2	Gore	lsg	0.703010 (3)	0.512889 (2)	19.540 (6)	15.618 (6)	39.006 (21)	
SO168_DR87-1	Perry	hsg EMII	0.703147 (3)	0.512867 (3)	19.302 (9)	15.623 (5)	39.028 (23)	
SO168_DR87-4	Perry	hsg EMII	0.703132 (3)	0.512874 (3)	19.319 (2)	15.627 (1)	39.057 (3)	
SO168_DR87-6	Perry	hsg EMII	0.703111 (2)	0.512871 (4)	19.317 (3)	15.628 (2)	39.041 (6)	
SO168_DR88-1	Thompson	lsg	0.702950 (2)	0.512936 (3)	19.808 (3)	15.602 (4)	39.382 (2)	
SO168_DR89-4	Clerke A	lsg	0.703068 (2)	0.512883 (3)	19.955 (29)	15.638 (23)	39.820 (58)	
SO168_DR91-1	Manley	lsg	0.703806 (3)	0.512889 (3)	19.291 (22)	15.621 (17)	38.976 (43)	
SO168_DR96-1	Silke	lsg	0.703248 (2)	0.512842 (3)	19.405 (4)	15.645 (3)	39.212 (8)	
SO168_DR97-1	Orton	lsg	0.702861 (2)	0.512868 (3)	20.165 (7)	15.654 (6)	39.888 (14)	
SO168_DR98-2	Gathrey	lsg	0.702871 (2)	0.512880 (3)	20.200 (11)	15.656 (7)	39.766 (34)	
SO168_DR99-1	Anja	lsg	0.702933 (3)	0.512901 (4)	20.094 (18)	15.655 (10)	39.689 (14)	
SO168_DR101-1	Jordan	lsg	0.703968 (3)	0.512804 (3)	18.899 (3)	15.610 (4)	39.072 (20)	
SO168_DR104-1	Forwood	lsg	0.703055 (3)	0.512949 (3)	19.829 (9)	15.632 (14)	39.553 (53)	
SO168_DR105-1	Bootie	lsg	0.702996 (3)	0.512932 (2)	19.513 (4)	15.626 (2)	39.281 (13)	
Chatham Islands								
P75894	The Horns	lsg	0.703171 (4)	0.512865 (3)	20.620 (1)	15.680 (1)	40.279 (2)	0.282949 (7)
P74899	Cape L'Evenque	lsg	0.703023 (5)	0.512874 (2)	19.652 (1)	15.639 (1)	39.192 (2)	
Cenozoic Hikurangi Plateau and Osbourn Crust Seamounts								
SO168_DR19-1	Rowling B Smt.	lsg	0.703088 (4)	0.512832 (3)	19.644 (1)	15.648 (1)	39.307 (1)	0.282949 (7)

***Table 2**: Sr-Nd-Pb-Hf Isotope data (continued)*

Sample Number	Location	Group	$^{87}Sr/^{86}Sr$	$^{143}Nd/^{144}Nd$	$^{206}Pb/^{204}Pb$	$^{207}Pb/^{204}Pb$	$^{208}Pb/^{204}Pb$	$^{176}Hf/^{177}Hf$
Challenger Plateau								
SO168_DR2-1	Mount Spong	lsg	0.703158 (5)	0.512860 (3)	20.421 (1)	15.664 (1)	40.022 (2)	
SO168_DR2-2	Mount Spong	lsg	0.703200 (3)	0.512867 (3)	20.673 (4)	15.713 (3)	40.664 (7)	
Cambell Plateau								
SO169_DR3-1K	N of Antipodes Is.	lsg	0.703116 (3)	0.512900 (3)	20.303 (1)	15.661 (1)	39.613 (3)	
SO169_DR3-7	N of Antipodes Is.	lsg	0.703102 (5)	0.512903 (3)	20.247 (1)	15.658 (1)	39.580 (3)	
SO169_DR6-1	W of Antipodes Is.	lsg	0.703172 (3)	0.512892 (3)	19.253 (2)	15.564 (1)	38.898 (3)	
SO169_DR11-1	Pukaki Bank	lsg	0.703008 (2)	0.512964 (3)	19.774 (3)	15.601 (3)	39.312 (7)	
SO169_DR11-5	Pukaki Bank	lsg	0.703019 (5)	0.512952 (3)	19.755 (1)	15.589 (1)	39.264 (2)	
SO169_DR12-1	Pukaki Bank	lsg	0.703132 (2)	0.512940 (3)	19.649 (2)	15.594 (1)	39.243 (4)	
SO169_DR15-1	Pukaki Bank	lsg	0.703221 (5)	0.512925 (2)	19.584 (1)	15.595 (1)	39.207 (2)	
A105	Antipodes Islands	lsg	0.702939 (3)	0.512914 (3)	20.515 (3)	15.673 (2)	39.787 (6)	
A109	Antipodes Islands	lsg	0.702904 (2)	0.512917 (2)	20.501 (3)	15.660 (2)	39.758 (5)	
Northland								
NZN3	Cable Bay	hsg MORB	0.702918 (5)	0.513013 (3)	18.910 (1)	15.585 (1)	38.586 (2)	
NZN28	Near Lake Omapeu	hsg MORB	0.703315 (5)	0.512963 (3)	18.810 (1)	15.592 (1)	38.584 (1)	
NZN29	Tuanui Quarry	hsg MORB	0.702767 (4)	0.513014 (3)	19.002 (1)	15.577 (1)	38.592 (2)	
NZN30	NW of Kerikeri	hsg MORB	0.702702 (5)	0.513061 (2)	18.781 (1)	15.544 (1)	38.409 (2)	
NZN31	East side of Kerikeri	hsg MORB	0.703324 (5)	0.513082 (3)	18.625 (2)	15.537 (1)	38.269 (3)	
NZN32	East side of Kerikeri	hsg MORB	0.703281 (20)	0.512962 (3)	18.891 (1)	15.596 (1)	38.623 (2)	
Marlborough: Graseed Volcanics								
P 50272 B	Grasseed Volcanics	lsg	0.703800 (3)	0.512853 (3)	19.918 (2)	15.668 (1)	39.531 (4)	0.282874 (5)
Canterbury: Oxford Area								
MSI 21A	Harper Hill	hsg EMII	0.703509 (2)	0.512913 (2)	19.460 (1)	15.613 (1)	39.204 (2)	0.283054 (11)
MSI 22B	Acheron Gabbro	hsg EMII	0.703845 (3)	0.512810 (2)	19.003 (1)	15.640 (1)	38.816 (2)	0.282896 (12)
MSI 23A	View Hill	hsg EMII	0.704161 (3)	0.512805 (3)	19.052 (1)	15.629 (1)	38.905 (2)	
MSI 25	View Hill	hsg EMII	0.704169 (2)	0.512794 (3)	18.988 (2)	15.624 (2)	38.843 (4)	
MSI 27A	View Hill	hsg EMII	0.703880 (5)	0.512788 (3)	19.136 (1)	15.648 (1)	38.925 (2)	
MSI 180A	View Hill	hsg EMII	0.704172 (3)	0.512799 (3)	19.047 (2)	15.632 (1)	38.923 (4)	

***Table 2**: Sr-Nd-Pb-Hf Isotope data (continued)*

Sample Number	Location		$^{87}Sr/^{86}Sr$	$^{143}Nd/^{144}Nd$	$^{206}Pb/^{204}Pb$	$^{207}Pb/^{204}Pb$	$^{208}Pb/^{204}Pb$	$^{176}Hf/^{177}Hf$
Canterbury: Oxford Area (continued)								
MSI 181	Burnt Hill	hsg EMII	0.704048 (3)	0.512819 (3)	19.072 (1)	15.632 (1)	38.890 (3)	
Canterbury: Cookson Volcanics								
MSIK 33A	Little Lottery River	lsg	0.703001 (5)	0.512871 (3)	20.175 (3)	15.658 (2)	39.687 (6)	
MSI 36A	Main Lottery River	lsg	0.703084 (3)	0.512840 (3)	19.991 (5)	15.676 (4)	39.647 (10)	
MSI 41B	Waiau River	lsg	0.703301 (5)	0.512814 (3)	20.403 (1)	15.718 (1)	40.092 (2)	
MSI 42C	Mason River	lsg	0.703670 (5)	0.512870 (2)	19.582 (1)	15.634 (1)	39.235 (3)	0.282910 (8)
MSI 45A	Lowermost Unit	hsg	0.703267 (3)	0.512854 (2)	19.339 (1)	15.636 (1)	39.055 (2)	0.282910 (9)
NZS14	Lowermost Unit	hsg	0.703325 (5)	0.512871 (3)	19.337 (1)	15.642 (1)	39.073 (2)	
Canterbury: Timaru and Geraldine Basalt								
MSI 6A	Timaru basalt	hsg EMII	0.703744 (3)	0.512831 (3)	18.858 (2)	15.611 (1)	38.711 (4)	0.282895 (8)
MSI 8A	Geraldine basalt	hsg	0.703575 (5)	0.512893 (2)	19.169 (1)	15.614 (1)	38.928 (2)	
Otago: Dunedin Volcano								
30-10-02-1	Aramoana	lsg	0.702858 (5)	0.512922 (3)	19.977 (1)	15.635 (1)	39.447 (2)	
12-11-02-3	Mt. Holmes Organ Pipes	lsg	0.702888 (4)	0.512919 (3)	19.849 (1)	15.640 (1)	39.389 (2)	0.282967 (6)
30-11-02-1	Pilot Point	lsg	0.702900 (4)	0.512915 (2)	20.231 (1)	15.656 (1)	39.697 (3)	
OU22636	Mt. Cargill	lsg	0.702949 (3)	0.512897 (2)	19.980 (1)	15.641 (1)	39.511 (1)	
OU22855*	St. Clair beach	lsg	0.702913 (5)	0.512913 (5)	20.074 (1)	15.658 (1)	39.598 (3)	0.282992 (7)
LSI22*	Allans beach	lsg	0.703032 (6)	0.512871 (8)	20.189 (3)	15.664 (2)	39.802 (5)	0.282967 (7)
MSI 87	Cape Saunders rd	lsg	0.703029 (5)	0.512905 (2)	19.925 (1)	15.649 (1)	39.416 (2)	
MSI 90A	Taiaroa Head	lsg	0.702855 (5)	0.512914 (3)	20.146 (1)	15.637 (1)	39.596 (1)	
MSI 95	Mt. Cargill rd	lsg	0.702986 (5)	0.512902 (4)	20.098 (1)	15.646 (1)	39.563 (1)	
Otago: Waipiata Volcanic Field								
OU54926*	Lookout Bluff	lsg	0.703261 (7)	0.512887 (7)	19.253 (2)	15.618 (2)	38.935 (3)	0.282965 (7)
LST1*	Conical Hill	lsg	0.702895 (8)	0.512858 (9)	20.349 (5)	15.644 (3)	40.101 (7)	0.282988 (7)
Otago: Waiareka - Deborah Formation								
LSI7*	Bridge Point	hsg EMII	0.703387 (4)	0.512838 (3)	18.999 (1)	15.628 (1)	38.735 (2)	0.282899 (7)
OU54929*	1 km SE of Maheno	hsg EMII	0.703210 (7)	0.512861 (6)	19.248 (2)	15.636 (1)	38.888 (4)	0.282905 (8)

***Table 2**: Sr-Nd-Pb-Hf Isotope data (continued)*

Sample Number	Location		$^{87}Sr/^{86}Sr$	$^{143}Nd/^{144}Nd$	$^{206}Pb/^{204}Pb$	$^{207}Pb/^{204}Pb$	$^{208}Pb/^{204}Pb$	$^{176}Hf/^{177}Hf$
Westland: Otitia Basalt								
MSI 63A	Otitia Basalt	lsg	0.704956 (2)	0.512825 (2)	19.730 (2)	15.625 (1)	39.739 (3)	0.282921 (7)
MSI 63E	Otitia Basalt	lsg	0.704627 (5)	0.512814 (3)	19.794 (2)	15.629 (1)	39.716 (4)	
Westland: Arnott Basalt								
MSI 65A	Along the coastline	lsg		0.512866 (2)	20.214 (3)	15.648 (2)	39.937 (5)	
MSI 66	Along the coastline	lsg	0.703335 (3)	0.512861 (2)	20.340 (3)	15.643 (3)	40.027 (6)	0.282960 (11)
Westland: Alpine Dike Swarm								
MSI 69B	Alpine Dike Swarm	lsg	0.703253 (3)	0.512846 (2)	20.616 (1)	15.657 (1)	40.337 (1)	
MSI 70B	Alpine Dike Swarm	lsg	0.703679 (2)	0.512851 (2)	20.170 (1)	15.649 (1)	39.929 (1)	
MSI 71A	Alpine Dike Swarm	lsg	0.703483 (5)	0.512854 (3)	20.443 (1)	15.651 (1)	40.163 (1)	
Lake Hawea 3	Alpine Dike Swarm	lsg	0.704050 (2)	0.512862 (2)	20.221 (1)	15.650 (1)	39.976 (2)	

* Sr, Nd, Pb Isotope data were taken from Hoernle et al., 2006

**Corresponding P sample numbers are P67436, P67437, P67439-P, P67439-X, P67440, P67455-G, P67455-S and P67456

Sr, Nd, Pb, Hf isotope data from Banks Peninsula are available from Timm et al., in review

Remaining data used were taken from Hoernle et al., 2006

All sample numbers of SO168DR and SO169 are working names

Abbr.: lsg =low-silica group; hsg=high silica group

3.6 Discussion

We begin by reviewing the Late Cretaceous volcanism on Zealandia and the adjacent Hikurangi Plateau and then discuss the Cenozoic volcanism.

3.6.1 Late Cretaceous Volcanism of Zealandia

Late Cretaceous magmatism on Zealandia has been attributed primarily to the end of subduction (Waight et al., 1998; Tappenden, 2003) and subsequent development of an extensional regime (Barley and Weaver, 1988; Weaver et al., 1994). For the period 110 - 95 Ma a transition from igneous source I-type to alkaline A-type intrusive rocks, together with the emplacement of mafic dikes, is reflected in rocks of Zealandia and Marie Byrd Land, and has been interpreted to record the transition from subduction to an extensional tectonic regime (e.g. Waight et al., 1998; Storey et al., 1999).

Igneous activity linked to continental rifting (ie. after subduction but before sea floor spreading) lasted for ~ 15 million years with an apparent peak in activity between 100 and 90 Ma represented by intrusions of the Tapuaenuku and Mandamus Igneous Complexes (Tappenden, 2003; Baker et al., 1994) and large seamounts on the adjacent Hikurangi Plateau (Hoernle et al., 2003, in prep.). These Late Cretaceous igneous rocks have HIMU-like trace element and isotopic compositions (Tappenden, 2003; Panter et al., 2006). Decompression melting of asthenosphere upwelling beneath the thinned lithosphere is a possible mechanism for generating volcanism beneath areas that underwent major continental extension during the Late Cretaceous. Separation of Zealandia from eastern Australia and West Antarctica began at ~84 Ma, as reflected by the formation of oceanic crust, coinciding with the emplacement of the Hohonu Dike Swarm (Waight et al., 1998). The HIMU-type geochemical characteristics of the entire age range of Late Cretaceous volcanism (c. 100-79 Ma) on the Hikurangi Plateau, South Island and Chatham Island has been attributed to a Gondwana breakup HIMU plume beginning at c. 107 Ma, proposed to have been located beneath Marie Byrd Land (Weaver et al., 1994; Hart et al., 1997; Storey et al., 1999; Panter et al., 2000, 2006; Hoernle et al., in prep.).

3.6.2 Cenozoic volcanism

Cenozoic volcanism was widespread and essentially continuous across Zealandia and generally characterized by low volumes and predominantly alkaline composition. The frequency of larger volcanic centers (≥100 km^3) with primarily tholeiitic to alkali basaltic compositions, in many cases forming composite shield volcanoes, appears to have crudely increased throughout the Cenozoic: Arnott Basalt Event (c. 65 Ma), Waiareka-Deborah Volcanic Event (c. 40-36 Ma), Cookson Volcanic Event (31-26 Ma), Auckland Islands Volcanoes (c. 17-15 Ma), Dunedin Volcano (c. 16-12 Ma), Lyttelton Volcano (c. 12-10 Ma), Akaroa Volcano (9-6 Ma), Campbell Volcano (c. 8-7 Ma), Antipodes Volcano (<1 Ma) (Figure 3.4). As is clear from a detailed study of the well-exposed Banks Peninsula Volcanoes (Lyttelton and Akaroa), volcanic activity formed the voluminous composite shield volcanoes generally over less than 2 million years, followed by prolonged late-stage, small-volume, phases (Timm et al., in review). Interestingly the volcanoes of Dunedin and Banks Peninsula were formed towards the end of the diffuse volcanic activity of the Waipiata Volcanic Field and widespread Miocene volcanism in the Oxford area, respectively, which possibly suggests an accumulation of partial melts leading up to the final activity within these two fields, which culminated in voluminous eruptions that formed the large volcanic edifices (composite shield volcanoes) (Hoernle et al., 2006; Timm et al., in review).

We can now demonstrate that volcanism with intraplate geochemical compositions occurred over much, if not most, of the Cenozoic in several different locations on Zealandia (Figure 3.2). In Canterbury, volcanic activity at View Hill took place between ~53 - 48 Ma, the Cookson Volcanics were erupted between ~31 and 26 Ma, volcanism in the Oxford area ranges in age from ~25 Ma to ~12 Ma (this study and Sewell and Gibson, 1988), Banks Peninsula shield volcanoes were active between ~12.5-7 Ma (Timm et al., in review) and volcanism at Timaru and Geraldine occurred at ~2.5 Ma. In Otago, Paleocene volcanic activity has been recorded at the Endeavor 1 site just off shore of Oamaru. On land, the oldest Waiareka-Deborah volcanism is Late Eocene (~40 -34 Ma), followed by the Waipiata Volcanic Field volcanism, which was low-volume but almost continuous between ~25 and ~11 Ma (this study and Hoernle et al., 2006). The Dunedin Volcano (~16 -12 Ma) formed at the end and possibly in the center of the Waipiata field, if offshore volcanism is also included.

The Alpine dike swarm in Westland on the Pacific Plate (west of Otago) overlaps in age with the older part of the Waipiata volcanism and may be an extension of this volcanism. The part of Westland on the Australian Plate only forms a thin silver of land between the Southern Alps mountain range and the coast but records at least two volcanic episodes, in addition to the Alpine Dikes, which are difficult to age date due to their metamorphosed nature. The early Paleozoic Arnott Basalts, which may have formed a shield volcano in particular if it is accepted that the submarine volcanism offshore of the Arnott Basalts were formed during the same event, and the Late Oligocene Otitia basalts. Due to the occurrence of these volcanic rocks on the Australian Plate, they are likely to have formed as much as 500 km to the south of the part of Westland on the Pacific Plate. On the North Island of New Zealand in the Northland and Auckland areas, volcanism with intraplate geochemical compositions occurred from the mid Miocene to Recent (~10 Ma to ~500 years ago; this study and see summary in Cook et al., 2004).

On the western and central Chatham Rise volcanism has been recorded over most of the Cenozoic. The oldest volcanism on the central Chatham Rise, northwest of the Chatham Islands, was dated at 63 Ma. Our age of 32.8 ± 0.06 Ma from submarine volcanism just south of the Chatham Islands is within error of the age of 36.0 ± 4.2 Ma obtained for the intermediate episode of volcanism on the Chatham Islands (Panter et al., 2006). Another volcanic center south of the Chatham Islands yielded an age of 22 Ma and two additional centers south of the Chatham Islands produced ages of 5.2-5.7 Ma, falling within the range of the youngest episode of volcanism on the Chatham Islands (4.3-7.3 Ma) (Panter et al., 2006, and this study). Volcanism on the western Chatham Rise ranges from Early Miocene through Pliocene with different volcanic fields yielding ages of c. 22, 20, 14, 13, 9, 8 and 3 Ma. Combined age data from the central and western Chatham Rise shows that volcanism occurred in the Paleocene Late Eocene/Early Oligocene and then was nearly continuous over the last 22 Ma with the largest gap in age dates being ~6 Ma during this time interval. The sparser record of sampled Paleocene through Oligocene volcanism could well represent the increased difficulty in obtaining samples from these older units due to more extensive sediment cover.

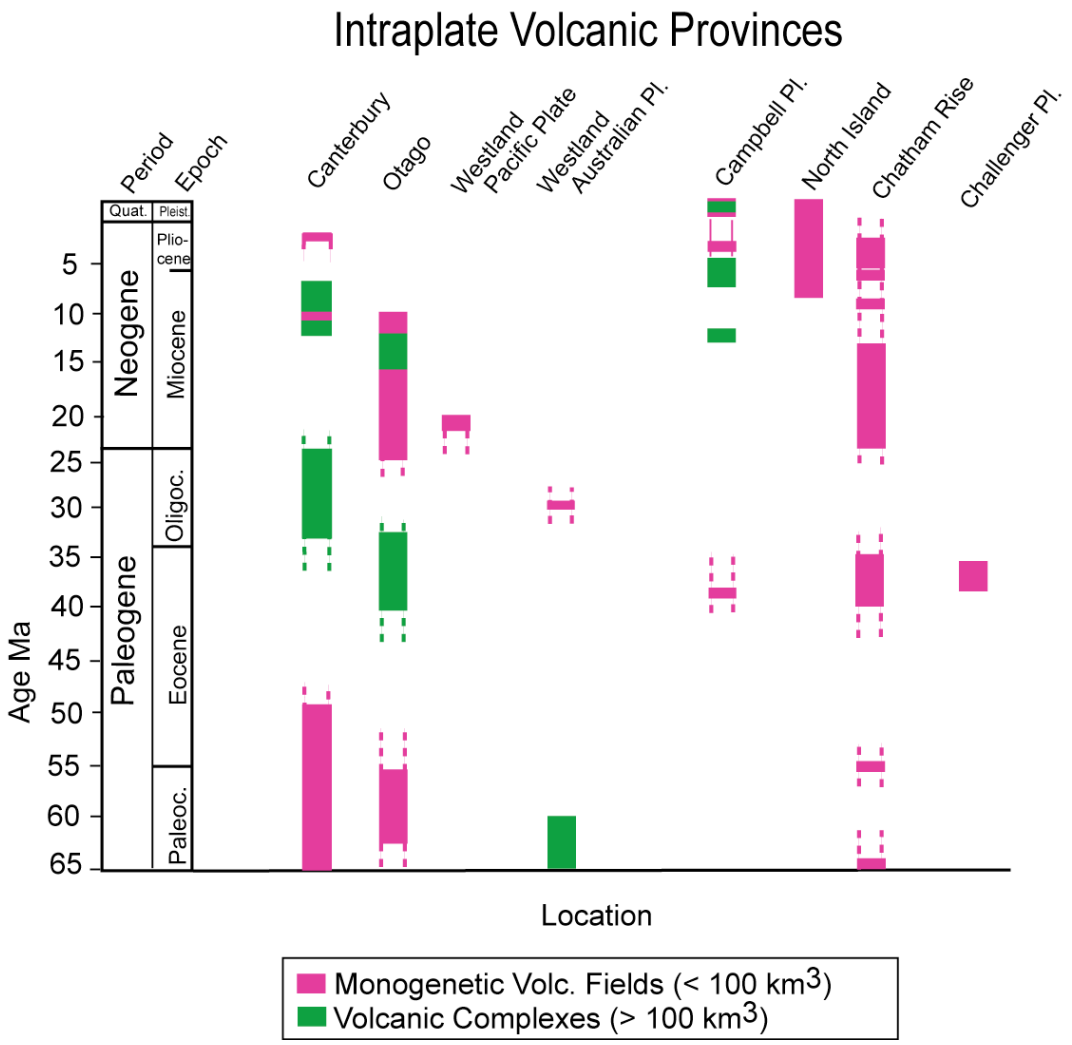

Figure 3.9: Age distribution of the intraplate volcanic centers, based $^{40}Ar/^{39}Ar$ age data from Panter et al. (2006), Hoernle et al. (2006) and this study and <10 Ma K/Ar data from compilation in Cook et al. (2004). The closed areas represent the dated $^{40}Ar/^{39}Ar$ age range; dashed lines connect volcanism with gaps of ≤ 5 Ma and indicate an extended age range determined by the K/Ar, Rb/Sr and U/Pb methods (see text for details).

The Campbell and Challenger Plateaus have not been sampled in as great a detail as the Chatham Rise. Nevertheless, volcanism on the Campbell Plateau occurred at least at c. 39, 17-15, 8-7, 4-3, 0.8-0.2 Ma, overlapping largely with Late Eocene to Quaternary volcanism on the Chatham Rise. The only dated volcanism from the Challenger Plateau from Mt. Spong gives an age range of 38-36 Ma, overlapping within errors with volcanism in Otago (Waireka-Deborah volcanism, c. 40-34 Ma), on and south of the Chatham Islands (c. 36-33 Ma) and on the Campbell Plateau west of the Antipodes Islands (39 Ma). Finally, it is important to note that Cenozoic intraplate volcanism also took place on the Hikurangi Plateau (Rowling Seamount), which similar to intraplate volcanism on Zealandia is also located on

thickened lithosphere, and from seamounts directly adjacent to the northern margin of the Hikurangi Plateau, and thus where there is a major change in lithospheric thickness.

In conclusion, volcanism within a given region on Zealandia not only occurred during much of the Cenozoic, but also, at a given age, volcanism occurred over much of the micro-continent. These observations are clearly not consistent with a plume hypothesis or with large-scale extension being the cause of the Cenozoic intraplate volcanism. As an alternative to these models, melting of volatile-rich lower lithosphere due to heat conduction from a hotter than normal asthenosphere has also been proposed to explain the intraplate volcanism on Zealandia and surrounding areas (Finn et al., 2005; Panter et al., 2006; Sprung et al., 2005). Although diffuse, low-volume volcanic activity forming monogenetic volcanic centers and fields and restricted dike and intrusive events could possibly be explained by lithospheric melting, such a model is not consistent with the generation of large volumes of melts in relatively short time periods (several million years) as required to explain the larger magmatic events and composite shield volcanoes, such the Arnott Basalts, seamounts adjacent to the Hikurangi Plateau, Waiareka-Deborah and Cookson Volcanics, and the Dunedin, Lyttelton, Akaroa, Antipodes and possibly the Ross, Carnley and Campbell Volcanoes. Finally the geochemical similarity in major elements, trace elements and isotopes between the basalts of the composite shield volcanoes and those from monogenetic centers indicates that these two basic types of Cenozoic volcanism (e.g. Hoernle et al., 2006) must be derived from a similar source and therefore places into question a primarily lithospheric origin for the Cenozoic intraplate volcanism.

The cause of the Cenozoic intraplate volcanism on Zealandia remains controversial, and will therefore be evaluated in more detail in the following section.

3.6.3 Source characteristics of intraplate volcanic rocks Zealandia

Although major and trace element and $^{206}Pb/^{204}Pb$ isotopic compositions of the mafic Cretaceous and Cenozoic intraplate volcanic rocks (MgO > 5 wt%) largely overlap, the Cenozoic lavas generally have less radiogenic $^{87}Sr/^{86}Sr$, $^{207}Pb/^{204}Pb$ and $^{208}Pb/^{204}Pb$ but more radiogenic Nd and Hf isotopic compositions, plotting between the

field for the Cretaceous volcanic rocks and Pacific N-MORB. Therefore the Cenozoic volcanic rocks could be at least in part explained by mixing of these two reservoirs.

As noted above, the mafic volcanic rocks from Zealandia are can be divided into high- (SiO_2 > 46 wt%) and a low-silica (SiO_2 < 46 wt%) groups. Compared to the high-silica group, the low-silica volcanic rocks generally have higher TiO_2, FeO^t, CaO, higher abundances of incompatible elements (e.g., Nb, Ta, Zr, Hf, Rb, Sr, U), higher more- to less-incompatible-element ratios (La/Sm, (Sm, Gd)/Yb, (Nb, Zr)/Y, Th/(Nb, Ta), Nb/(Zr, Hf), Nb/La), higher Zr/Hf and Nb/Ta and lower fluid-mobile to fluid-immobile element ratios (U/La, Ba/Zr, Rb/Nd, (K, Pb, Sr)/Nb). On isotope correlation diagrams, the low-silica group rocks form an array between MORB and the HIMU mantle endmember and have the most HIMU-like compositions of the Cenozoic volcanic rocks. The high-silica lavas generally have less radiogenic Pb isotope ratios and trend towards a MORB (DMM)-like or an enriched (EMII-type) component (Figure 3.10). The high-silica rocks with the most depleted isotopic compositions (highest Nd and Hf isotope ratios) also have the most depleted incompatible element compositions, while the high-silica samples trending towards an EMII-type component are also characterized by higher fluid-mobile to fluid-immobile element abundances (e.g. U/La, Ba/Zr, Rb/Nd, (K, Pb, Sr)/Nb) and higher Hf/Nb, Zr/Nb and Th/Ta but lower Sm/Yb. In summary, the geochemistry of Cenozoic volcanic rocks throughout Zealandia requires the presence of at least three components (see Figure 3.8a and 3.10a,b): 1) HIMU-type component (low-silica rocks), 2) MORB (or DMM)-like component (high silica rocks), and 3) EMII-type component (some high-silica rocks) (data from this study and Barreiro and Cooper, 1987; Price et al., 2003; Cook et al., 2004; Hoernle et al., 2006; Panter et al., 2006; Sprung et al., 2006; Timm et al., in review). These systematic differences in geochemical composition suggest fundamental differences in the formation of the two groups, which will be evaluated in the following.

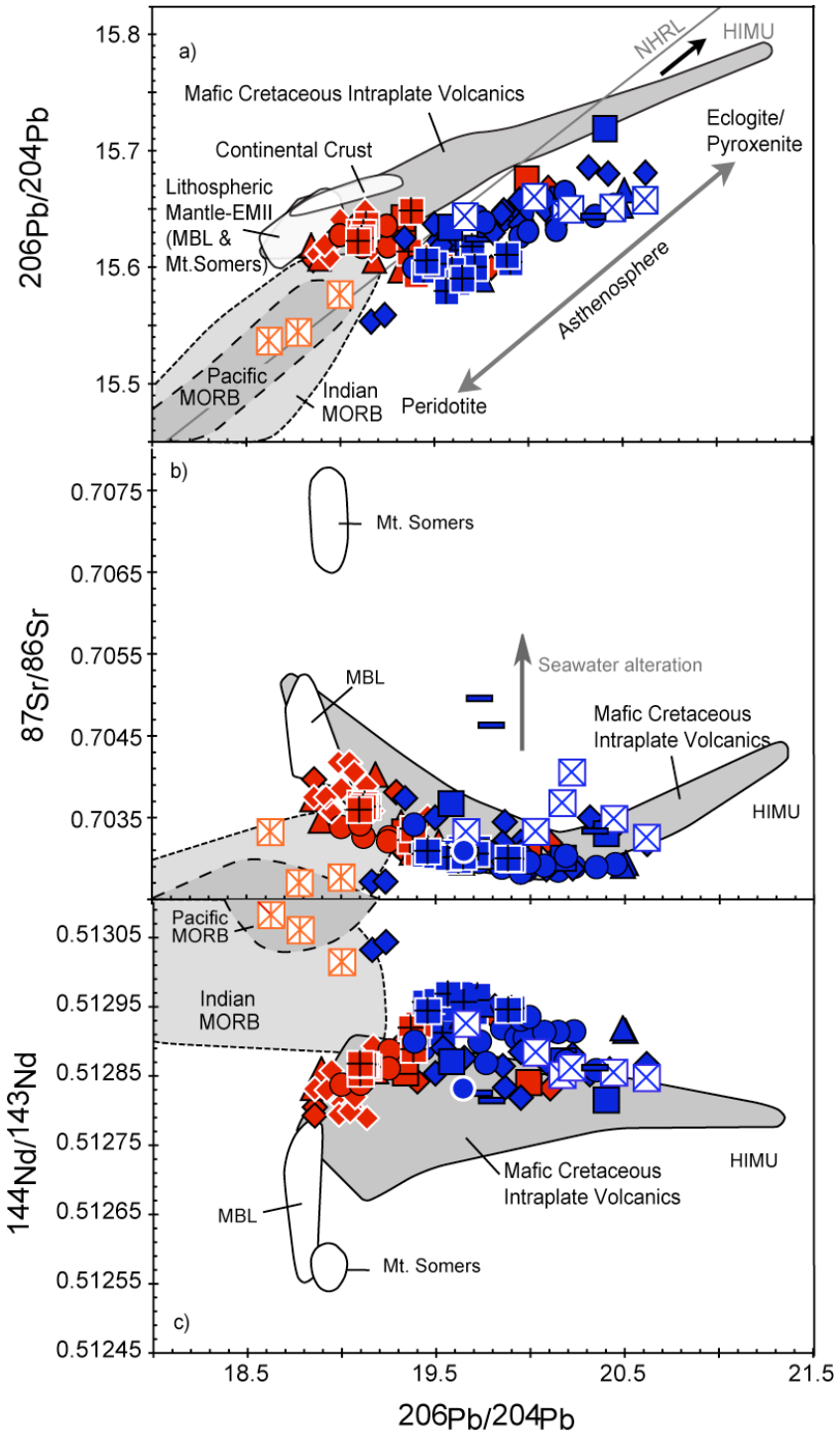

Figure 3.10a-3.10c: $^{206}Pb/^{204}Pb$ versus $^{207}Pb/^{204}Pb$, $^{87}Sr/^{86}Sr$ and $^{143}Nd/^{144}Nd$ isotope correlation diagrams for mafic (MgO < 5 wt. %) Zealandia samples (including data from Hoernle et al., 2006 and Timm et al., in review). The low-silica group samples are characterized by the most radiogenic Pb but intermediate Sr and Nd isotopic compositions, whereas the high-silica group extends from the low-silica volcanic rocks to relatively unradiogenic Pb isotopic ratios. The high-silica samples form two groups: 1) a depleted group with unradiogenic Sr but radiogenic Nd isotope ratios with compositions similar to E (enriched) MORB and 2) an enriched (EM II-type) group with relatively radiogenic Sr but unradiogenic Nd, which trends towards the composition expected of the Zealandia lithosphere (similar in composition to subduction-related rocks from Mt. Somers and Cretaceous mafic dikes from Marie Byrd Land, Antarctica; Tappenden, 2003; Storey et al., 1999). The field for mafic Cretaceous Zealandia intraplate volcanic rocks are from Tappenden (2003) and Hoernle et al. (in prep.).

3.6.3.1 Low-silica mafic volcanic rocks - partial melting of upwelling heterogeneous asthenosphere

The isotopic compositions of the low-silica Cenozoic intraplate volcanic rocks from Zealandia clearly indicate that they are largely derived from different sources than the high-silica volcanic rocks. The low-silica volcanic rocks are characterized by HIMU-like compositions having radiogenic Pb isotope ratios (e.g. $^{206}Pb/^{204}Pb$ = 18.6-20.7) and form a crude array between HIMU (or Cretaceous intraplate volcanic rocks on Zealandia) and MORB-type mantle components. Below we discuss what the major and trace element and isotopic compositions of these rocks can tell us about their origins.

The generally high FeO^t, high ratios of LREE/(MREE, HREE) in the low silica group volcanic rocks suggests a deep-seated (> 85 km after Robinson and Wood, 1998) and fertile source containing residual garnet. The high Zr/Hf and Nb/Ta (Figure 3.10) suggest the presence of pyroxenitic/eclogite domains in the source beneath Zealandia (Pfänder et al., 2007; Pertermann and Hirschmann, 2004). The presence of CO_2-rich eclogite is also suggested by comparing our major element data with experimentally determined melts of peridotite, pyroxenite and eclogite (Dasgupta et al., 2006, 2007; Hirschmann et al., 2003; Kogiso and Hirschmann, 2006; Hirose and Kushiro, 1993). Pure peridotite melts (even in the presence of CO_2) cannot account for the high TiO_2 and FeO^t in most of the mafic lavas from Zealandia but carbonated eclogite can. Therefore it appears that almost all Zealandia volcanic rocks were derived from sources with some carbonated eclogite. Since almost all mafic major element data from Zealandia plot between melts of peridotite and carbonated eclogite, they are likely to represent a mixture of these two components (also proposed by Hoernle et al., 2006). The garnet pyroxenite melts (Hirschmann et al., 2003) generally have intermediate compositions between eclogite and peridotite and thus may also have been present in the sources of some of these rocks. Bimineralic eclogite (Kogiso and Hirschmann, 2006) also overlaps with the Zealandia data but has lower MgO than the carbonated eclogite and therefore cannot explain the composition of the more mafic Zealandia melts.

Sobolev et al. (2007) showed that when eclogite derived melts react with peridotite a reaction pyroxenite is formed, which occurs in similar proportion to the

amount of initial eclogite. The typical quantity of reaction pyroxenite from eclogite (recycled oceanic crust) contributing to partial melting beneath thin (< 70 km) continental crust is ~ 60%, which can increase to 100 % beneath thick (> 70 km) continental crust. These results imply a greater contribution of pyroxenite and thus eclogite to melts formed as lithospheric thickness increases, as was previously proposed for Zealandia by Hoernle et al. (2006). Increasing involvement of pyroxenite/eclogite with increasing thickness of the lithosphere beneath Zealandia could also correspond to increasing melting depth with increasing Zr/Hf, Nb/Ta $^{206}Pb/^{204}Pb$, $(Sm/Yb)_N$, FeO^t and decreasing SiO_2. Therefore, we conclude that the low-silica Zealandia lavas, which have the highest FeO^t, TiO_2 and, highly and moderately incompatible element contents and $^{206}Pb/^{204}Pb$ and $^{208}Pb/^{204}Pb$ isotope ratios and lowest SiO_2, $^{143}Nd/^{144}Nd$, $^{176}Hf/^{177}Hf$, $^{87}Sr/^{86}Sr$, and $^{207}Pb/^{204}Pb$ represent the smallest melt fraction with the highest proportion of pyroxenite/eclogite component involved in melt generation.

In order to produce silica-undersaturated lavas, CO_2 plays an important role during melting (Dasgupta et al. 2005; 2006; 2007), which is consistent with CO_2 fluid inclusions found in plagioclase in alkalic volcanic rocks (e.g. Kakanui Mineral Breccia) (Coombs et al., 1986), (Alpine Dike Swarm) (Cooper, 1986). The most HIMU-type volcanic rocks were sampled at the Waipiata Volcanic Field, the Dunedin Volcano, the Cookson Volcanics, the Alpine dike swarm and the Chatham and Antipodes Islands (Barreiro et al., 1987; Panter et al., 2006; Hoernle et al., 2006; this study). Some samples of the Alpine Dike Swarm trend towards the enriched (EMII-type) endmember (more radiogenic Sr and Nd isotopes, although less pronounced than in the high-silica group rocks), which suggests that interaction with the continental lithosphere (mantle and crust) may also play a role in some lavas of the low-silica group. This contamination, however, is not as obvious in the low-silica rocks, due in part to the higher concentrations of incompatible elements in these rocks.

Intraplate volcanic rocks erupted on the North Island of New Zealand (Auckland and Northland Volcanic Fields), together with two samples from central Chatham Rise (Chapmans Hill) in contrast have the most depleted MORB-like signatures on Sr-Nd and Pb isotope diagrams (Figure 3.8 and 3.10) suggesting the least influence of HIMU- and enriched (EMII) type components beneath these

regions. Magmatism here has been attributed to low degrees of partial melting (1.5 - 3.5 %) (Huang et al., 1997) of the asthenospheric and lithospheric mantle caused by extension (e.g. Biggs and McDonough, 1990, Cook et al., 2004, Huang et al., 2000).

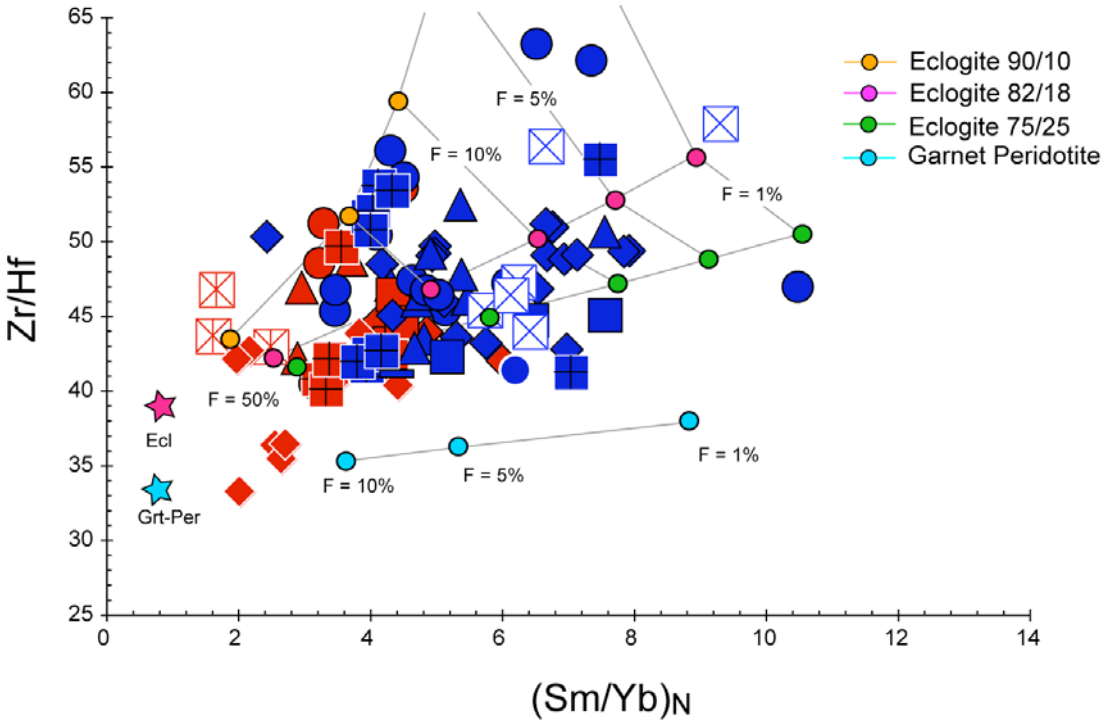

Figure 3.11: $(Sm/Yb)_N$ versus Zr/Hf of mafic (MgO > 6 wt%) Cenozoic volcanic rocks. The turquoise dots indicate the composition of smaller degree partial melts of garnet peridotite. The parental composition is denoted by the turquoise star. The green, pink and orange curves represent increasing degrees of partial melting of eclogite with different clinopyroxene (first number) and garnet (number after the slash) mineral modes (in wt. %), as indicated in the legend. The parental composition is denoted by the pink star. The gray lines indicate the fraction (F) of melt produced. Increasing $(Sm/Yb)_N$ ratios reflect increasing garnet signature. Zr/Hf instead displays an increasing contribution of pyroxenite and/or eclogite to the partial melt. Modeling parameters are taken from Pertermann and Hirschmann (2004), except for slightly higher Zr (75 ppm) for the eclogite and slightly lower Zr (8 ppm) for the garnet peridotite composition. After our model, high degrees of partial melts (up to 50%) of eclogite are required to explain the Zr/Hf and $(Sm/Yb)_N$ ratios of mafic and silica-deficient lavas from Zealandia.

Generally, the geochemical and isotopic composition of the low-silica volcanic rocks from the monogenetic volcanic fields and from the shield volcanoes are comparable, but the lavas forming the shields tend towards higher silica and lower abundances of highly and moderately incompatible elements, indicating the formation through higher degrees of partial melting and therefore an increasing contribution of peridotite melts. It is problematic to obtain reliable information about melting pressure for the Cenozoic volcanic rocks from Zealandia, since pyroxenite/eclogite played an important role in the formation of all mafic low-silica rocks. In addition, the

low-silica lavas were presumably formed under the presence of CO_2, similar to the situation proposed by Herzberg and Asimow (in review). Taking into account that most of the volcanic rocks contain garnet in the source, partial melting occurred at least beneath ~45 km (Hirschmann and Stolper, 1996). As Dasgupta et al., 2006 pointed out, different mantle components (e.g. peridotite, pyroxenite and eclogite) will melt out at different mantle depth and temperatures. In accordance with the models of Hoernle et al. (2006) and Dasgupta et al. (2006), we also propose that incipient melting occurred in the upper heterogeneous asthenosphere, containing pyroxenitic and/or eclogitic domains.

In conclusion, since all mafic Cenozoic volcanic rocks plot between the field for Cretaceous volcanism on Zealandia and the Hikurangi Plateau and Pacific MORB, binary mixing of the Cretaceous lavas' mantle source with a Pacific MORB-like mantle source could explain the Sr-Nd-Hf-Pb isotopic composition of the mafic Cenozoic volcanic rocks. The pyroxenitic and or eclogite component(s) could reflect plume-related material that remained in the mantle after formation of the Cretaceous volcanic rocks that has mixed with depleted upper mantle peridotite. Both of these components contribute to the formation of the Cenozoic melts to varying degrees based on how radiogenic the Pb isotopic are.

3.6.3.2 High-silica mafic volcanic rocks – contribution of the lithosphere (mantle and crust)

Whereas mafic low-silica volcanic rocks (basanites, nephelenites and some alkali basalts) primarily have HIMU-type isotopic signatures, mafic (MgO > 5 wt%) high-silica (SiO_2 > 46 wt%) volcanic rocks (some alkali basalts, tholeiites and basaltic andesites) extend to more E-MORB-or EMII-type isotopic signatures. The mafic high-silica volcanic rocks also generally have lower FeO^t, TiO_2, incompatible element concentrations and higher more- to less–incompatible and fluid-immobile to fluid-mobile element ratios (e.g. (Zr, Hf)/Nb, Sm/Yb, U/La, Th/Ta; Figure 3.11 and 3.12).

Some previous studies proposed that the high-silica rocks were likely derived from a sublithospheric source with depleted (similar to E-MORB) compositions that were then contaminated in the lithospheric mantle geochemically enriched during subduction when Zealandia was part of the Gondwana margin in the Mesozoic

(Hoernle et al., 2006; Timm et al., in review). Original derivation from a depleted (E-MORB-type) sublithospheric source, however, was not actually observed but only inferred from the incompatible element and isotope systematics.

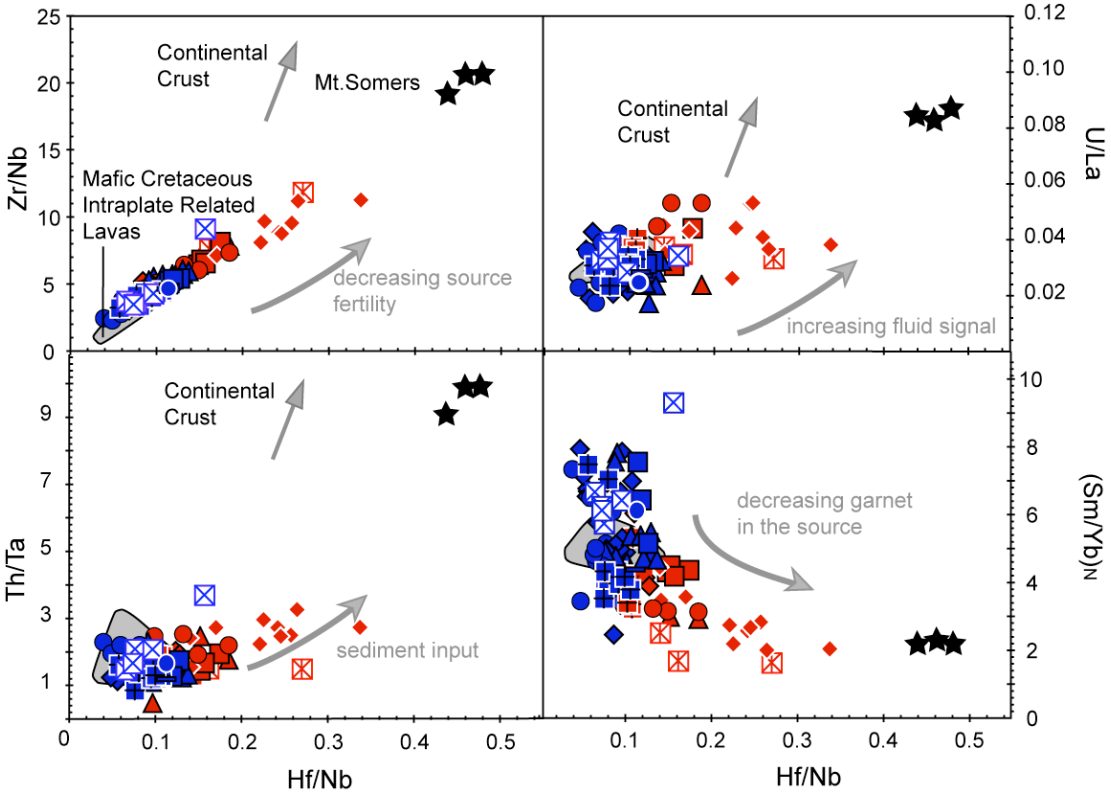

Figure 3.12a-3.12d: Hf/Nb versus (a) Zr/Nb, (b) Th/Ta, (c) U/La and (d) $(Sm/Yb)_N$ of mafic (MgO > 5wt%) Cenozoic Zealandia intraplate lavas illustrate that the high-silica group display greater amounts of lithospheric contamination than the low-silica group lavas and that the low-silica group overlap largely in composition with the Cretaceous intraplate volcanic rocks on Zealandia. The Cretaceous subduction-related lavas of the Mount Somers Volcanic Group (data are taken from Tappenden, 2003) serve as a possible endmember for assessing the composition of the lithospheric mantle enriched by subduction, when Zealandia formed part of the Gondwana margin. The increasing imprint of a subduction component from lithospheric interaction or direct melting of the lithosphere on the asthenospheric intraplate melts is indicated by decreasing Nb, whereas Zr and Hf remain relatively unchanged, resulting in an increase in Zr/Nb and Hf/Nb ratios. Increasing sediment and fluid contribution in some areas is displayed by increasing Th/Ta (increasing Th together with decreasing Ta) and U/La ratios. Decreasing $(Sm/Yb)_N$ reflects decreasing quantities of garnet in the source. Combined with increasing Hf/Nb the decreasing $(Sm/Yb)_N$ displays a change from OIB to a more depleted, subduction-related source.

For example, Timaru basaltic andesites had the lowest incompatible element abundances (similar to E-MORBs) in the previously-studied mafic Cenozoic volcanic rocks. Since both crystal fractionation and lithospheric contamination (mantle and crustal) would have increased the abundances of the incompatible elements, the incompatible element abundances in the parental melts must have been even lower,

leading to the interpretation that the parental melts were derived through high degrees of melting of a depleted peridotitic source (Hoernle et al., 2006). In addition, it was shown that lithospheric interaction could explain the enriched isotopic compositions of high-silica melts from Timaru and the Waiareka-Deborah formation if the asthenospheric melts had E-MORB-like isotopic compositions. E-MORB-type isotopic compositions, however, were not actually observed in any of the studied rocks. The data from Northland volcanic rocks, however, confirm the presence of depleted high-silica rocks with enriched E-MORB-type isotopic compositions, strengthening the model that the enriched high-silica volcanic rocks were formed by high degrees of melting of depleted peridotite and then contaminated in the lithosphere.

In order to test further if the enriched (EMII-type) signatures of most high-silica rocks could reflect lithospheric interaction, we use the composition of the Late Cretaceous (c. 90-98 Ma) Mt. Somers Volcanic Group (data from Tappenden, 2003; Mortimer et al., 2006) as a potential endmember for the composition of the lithospheric mantle, enriched by subduction, when Zealandia formed part of the Gondwana margin. These lavas have high incompatible element ratios characteristic of subduction-zone volcanic rocks (e.g. Figure 3.12). High Th/Ta and U/(La, Nb) are indicative of source enrichment by hydrous fluids/melts from subducted altered oceanic crust and marine sediments, while high (Zr, Hf, La)/Nb ratios reflect Nb depletion relative to other highly to moderately incompatible elements in the melts. Low $(Sm/Yb)_N$), on the other hand, reflect lower amounts of garnet in the source. The trace element composition of the Cenozoic high-silica rocks trend towards the Mt. Somers trace element compositions suggesting greater amounts of interaction of these magmas with lithosphere affected by Gondwana subduction. In order to explain the decreasing source fertility (lower FeO^t), the flatter HREE patterns, lower Zr/Hf and generally lower incompatible element abundances, however, a more depleted, peridotitic source and a shallower depth of partial melting are also required.

Although the low-silica rocks have trace element and isotopic compositions, which overlap with the field for Cretaceous intraplate volcanic rocks extending towards MORB, the high-silica rocks require the presence of an additional enriched component (Figure 3.10 and 3.12), with a composition similar to the subduction-derived Late Cretaceous Mt. Somers volcanic rocks and/or local sediments. Since

subduction has not occurred beneath most of Zealandia since the Late Cretaceous and Zealandia has drifted thousands of kilometers away from the former Gondwana subduction margin in the Cenozoic, we interpret the subduction signature in the high-silica rocks to be derived through lithospheric interaction (similar to Hoernle et al., 2006). It is difficult if not impossible to distinguish between in most cases whether the lithospheric contamination occurred within the crust or lithospheric mantle, because melts with compositions similar to Mt. Somers lavas must have also metasomatized the lithospheric mantle on their way to the surface or stagnated and crystallized directly within the lithospheric mantle.

The lavas from the Timaru area, View Hill, Waiareka-Deborah Formation and Lyttelton Volcano show the greatest influence of an enriched (EMII-type) subduction-related lithospheric component. The presence of crustal xenoliths in lavas from these areas (e.g. Coombs et al., 1986; Duggan and Reay, 1986; Timm et al., in review) suggests that crustal interaction has occurred even in the high-silica rocks with the lowest incompatible element concentrations. Sewell and Gibson (1988) pointed out that the entire Canterbury volcanics (incl. View Hill, Oxford volcanics and Timaru basalt) show a crustal imprint. On the other hand, the presence of hydrous minerals, like kaersutite and phlogopite in mantle xenoliths of the Waiareka - Deborah Formation (Reay and Sipiera, 1987), suggest source metasomatism and thus the ascending lavas are also likely to have experienced interaction with such a metasomatized lithospheric mantle. Timm et al. (in review) show that combined O-Sr-Nd-Hf-Pb isotope data for the tholeiitic rocks from Lyttelton Volcano on Banks Peninsula support extensive crustal interaction, especially of the oldest lavas. It has also been shown that the enriched signature in the lavas of Banks Peninsula cannot simply be created by assimilating continental crust, but also requires significant interaction with the lithospheric mantle (Timm et al., in review). In conclusion, since the lithospheric mantle will no doubt have enriched domains with similar compositions to Cretaceous and older subduction-zone lavas, it is extremely difficult, if not impossible, to distinguish between lithospheric mantle and crustal contamination. Even combined studies of O and radiogenic isotopes such as Sr-Nd-Pb-Hf cannot always unambiguously distinguish between contamination in these two parts of the lithosphere, since eclogitic components in the asthenosphere (derived

from recycled oceanic crust) contributing to the formation of the parental magmas can have variable and lower $\delta^{18}O$ than the ambient peridotitic MORB source mantle.

Finally we conclude that both, the low and high-silica groups are derived from a similar asthenospheric mantle containing domains of fertile pyroxenitic material (most likely of plume origin associated with the continental breakup of Zealandia from Gondwana) in a depleted (peridotitic) upper asthenosphere.

3.6.4 Evaluation of previously proposed models for the origin of the Cenozoic intraplate volcanism on Zealandia

The new $^{40}Ar/^{39}Ar$ age data clearly contradict the crude WNW to ESE age progression in volcanism postulated by Adams (1981) and show that there is considerably more overlap between the age ranges of the individual volcanic fields than previously recognized (Figure 3.4). This, as well as the longevity of the Cenozoic volcanism, argues against an origin involving relative movement of Zealandia over a linear mantle region of upwelling asthenosphere as proposed by Adams (1981) or Farrar and Dixon (1984).

Another conceivable source of the HIMU-type component in the Cenozoic magmas is a plume swarm. The occurrence of volcanism in a very restricted region on the Chatham Rise, Marlborough, Otago (Hoernle et al., 2006) and in Canterbury for more than 60 million years on a fast moving plate (~60 mm/year) is, however, incompatible with the classic hotspot hypothesis, which should generate chains of volcanoes that become progressively older in the direction of plate motion (Figure 3.2, 3.4, 3.9 and 3.13. Although the classic model is for hotspots fixed relative to plate motions, it has been shown that mantle plumes are not necessarily stationary and can move large distances over tens of millions of years. The Hawaiian plume, for example, moved more than 1000 km over ~40 million years (Tarduno et al., 2003; Steinberger et al., 2004). Multiple plumes that moved more than ~4000 km with the Zealandia micro-continent since ~ 60 Ma, however, would be required beneath a fast-moving Zealandia as well as beneath an essentially stationary West Antarctica, which does not appear to be feasible based on our present knowledge of plume motions. Alternatively there could be tens or hundreds of small plumelets located beneath the region over which Zealandia has passed (~4000 km) since the Cretaceous. There is,

however, no seismic evidence for widespread shallow thermal anomalies (low S and P wave velocities) (Finn et al., 2005; Priestley and McKenzie, 2006, Montelli, et al., 2006, Nolet et al., 2006 and Li et al., 2008) beneath Zealandia. Therefore, we conclude that the HIMU-type component in the Cenozoic magmas of Zealandia is not directly derived from deep mantle plumes upwelling to the base of the Zealandia lithosphere.

Although volcanic rocks with intraplate geochemical characteristics can be generated in areas of continental rifting and extensional tectonics, major continental rifting between Zealandia and Antarctica ceased in the Late Cretaceous. Even though localized extensional tectonics events on New Zealand may have facilitated the rise of some magmas to the surface and even be responsible for generating some low-level volcanic activity (Weaver and Smith, 1989), for example isolated monogenetic volcanoes or even volcanic fields, OIB-type volcanism occurred in Zealandia both in times of extension (Cretaceous), passive drift (Paleogene) and compression (Neogene) and it is difficult to explain large volumes of, for example, composite shield volcanism through localized extensional events. Moreover, our new age data suggest that the intensity of intraplate volcanism on Zealandia may have even increased during the period of compressional tectonics (i.e. since ~22 Ma; Cooper et al., 1987; see Figure 3.4), excluding major extensional tectonics as the controlling factor in generating Cenozoic intraplate volcanism on Zealandia.

Finn et al. (2005) proposed that catastrophic slab detachment along the Gondwana margin in the Late Cretaceous induced upward mantle flow in a broad region of the upper asthenosphere to the base of the metasomatized lower subcontinental lithosphere. They proposed that the increased temperature beneath Zealandia, Australia and Antarctica causes partial melting in the base of the lithosphere. The mixing of metasomatized subcontinental lithospheric mantle with warm Pacific asthenosphere explains the diversity of mantle sources (HIMU, EM and MORB) of a huge diffuse alkaline magmatic province (DAMP) now dispersed on both sides of the Tasman Sea and Southern Ocean. Although we agree that the EM and HIMU components may be located in the lithospheric mantle metasomatized by subduction zone fluids and sediment melts, we do not agree that volcanism associated with the formation of the composite shield volcanoes can be derived solely from melting of the lithospheric mantle beneath Zealandia. A universal characteristic of

subduction zone volcanism (excluding minor backarc volcanism) is trace element signatures characterized by relative depletions in Nb and Ta and the lack of relative depletion in Pb; this signature is found in the Cretaceous Gondwana subduction lavas, for example in the Mount Somers volcanic group (Tappenden, 2003; Mortimer et al., 2006). Subduction zone trace element signatures also show large enrichments in fluid-mobile elements versus fluid-immobile elements.

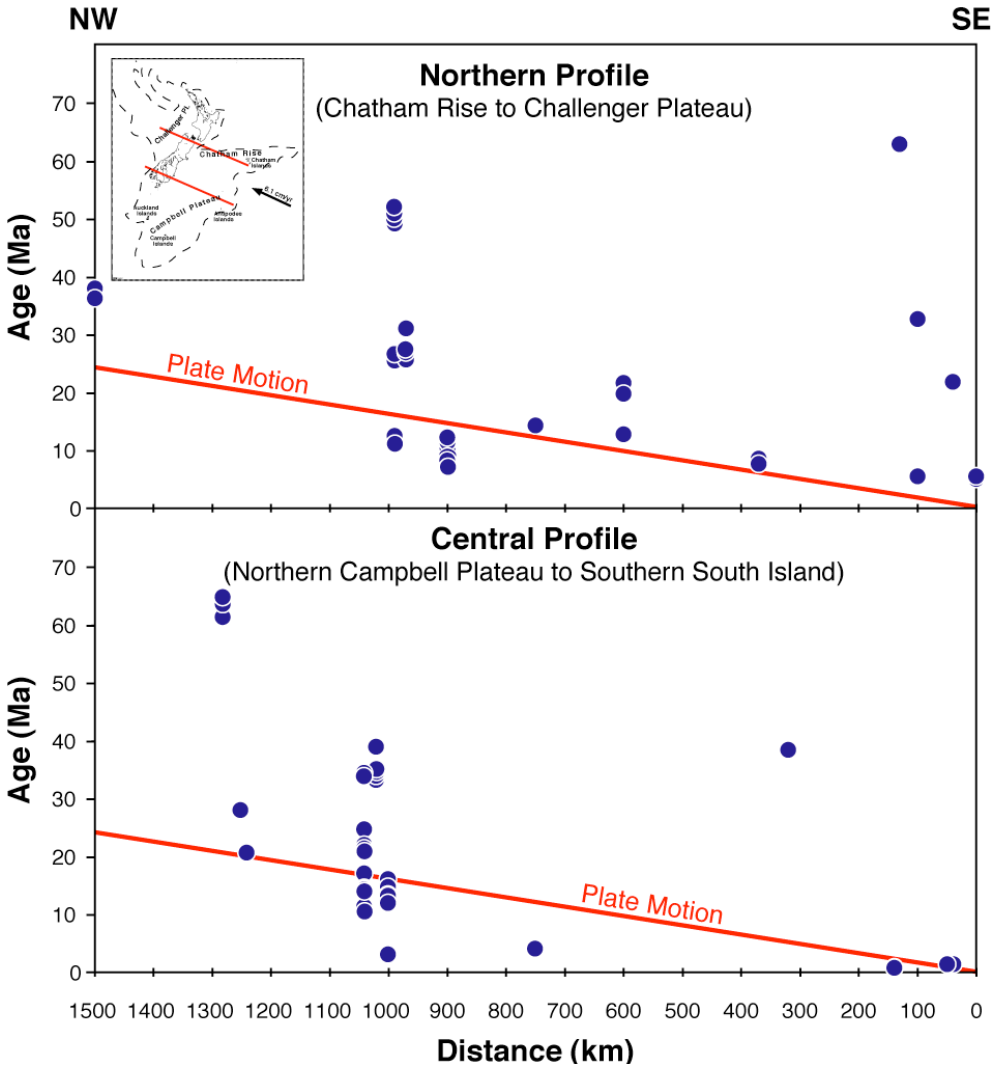

Figure 3.13: Ages of volcanism have been projected onto two profiles in the direction of plate motion (after Clouard, 2005) in the inset, demonstrating that there are no systematic age progressions in the direction of plate motion on the northern and central parts of Zealandia. The red lines on the distance versus age diagrams represent possibly age progressive trends, assuming current plate velocity of 6.1cm/yr (see Figure 3.1 for ages). The red lines representing possible age progressions can be moved vertically (without changing the slope of the line), but clear age progressions are not observed, because volcanism occurs episodically at individual locations throughout the Cenozoic.

None of these characteristics are observed in the silica-undersaturated Cenozoic

basalts from Zealandia and we therefore rule out derivation of the Cenozoic basanites and some alkali basalts from subduction-modified lithospheric mantle.

Coombs et al. (1986) noted the similarity in Sr and Nd isotopic composition of Cenozoic basalts on the South Island of New Zealand to 1) volcanic rocks from St. Helena and Tubuai (type localities for the HIMU component in ocean island basalts) and 2) basalts from Marie Byrd Land, Antarctica and Australia. They point out that the areas having volcanism with HIMU-type Sr and Nd isotopic compositions on these three continental blocks were contiguous prior to 100 Ma but rifted apart at c. 80 Ma, suggesting that this volcanism was derived from a common, probably lithospheric, source. Later authors have expanded on this idea proposing that a fossil HIMU plume head, involved in the last breakup phase of Gondwana (Weaver et al., 1994; Storey et al., 1999), is located at the base of the lithosphere beneath these formerly connected areas (Hart et al., 1997; Panter et al., 2000, 2006).

Panter et al. (2006) and Sprung et al. (2007) suggest that different mixing proportions of a degassed upper asthenosphere having a MORB-like composition with HIMU-signature melts that metasomatized the lower MORB-like lithospheric mantle, can melt to generate the isotopic relationships of the Cenozoic lavas. It remains unclear, however, why some of the same lithospheric domains would repeatedly melt throughout the Cenozoic. We also again note that it may be possible to explain some of the low level (monogenetic) volcanism through lithospheric melting as a result of conductive heating from the asthenosphere but not the larger (>100 km^3) events, in particular the formation of composite shield volcanoes, such as the Akaroa Volcano, with volumes of up to 1200 km^3 that largely formed within 1-2 Ma (Timm et al., in review). Conductive heating is an inefficient process for production of large amounts of melt (e.g. Elkins-Tanton, 2006).

A number of studies have investigated the process of delaminating dense lower lithosphere (e.g. Conrad and Molnar, 1997; Houseman and Molnar, 1997; Neil and Houseman, 1999; Jull and Kelemen, 2001), which may, for example, have caused the formation of the Transverse Ranges in Colorado (Houseman et al., 2000) and Cenozoic intraplate basalt volcanism in Mongolia (Barry et al., 2003). Lithospheric detachment has also been proposed to explain minor younger (at ~90 Ma) volcanism on the Ontong Java Plateau (Korenaga, 2005). In accordance with this model, detachment of dense lithosphere, containing eclogite, garnet-pyroxenite and Fe-rich

garnet-lherzolite, beneath the plateau drives convective currents, which can possibly even cause detached mantle to upwell locally and melt. Hoernle et al., (2006) and Timm et al. (in review) have proposed lithospheric removal (detachment) as an alternative model for triggering partial melting beneath Zealandia. Prolonged exposure to the passage of subduction-related and possibly also plume-related magmas during the Mesozoic fertilized the lower lithospheric mantle, increased its density with respect to the underlying asthenospheric mantle and thereby produced a negatively buoyant, gravitationally unstable layer. In response to detachment and sinking of domains of dense lower lithosphere, less-dense upper asthenosphere streams up and partially melts by decompression. The HIMU-type component would be linked to the presence of pyroxenite/eclogite in a depleted peridotitic matrix within the upper asthenospheric mantle.

3.6.5 Towards a combined model to explain the Cenozoic intraplate volcanism on Zealandia

In the Cenozoic, Zealandia drifted ~4000 km to the north/northwest, but low-volume intraplate volcanism was widespread over the entire micro-continent. As discussed above, there is no evidence for belts of age-progressive volcanism or seismic evidence for shallow low-velocity anomalies beneath Zealandia, which would be expected if fixed plumes were involved in generating this intraplate volcanism (Finn et al., 2005; Priestley and McKenzie, 2006). There is also little evidence for major lithospheric extension and thinning during the Cenozoic on the different parts of Zealandia. Local minor extensional events, or lithospheric melting due to heat conduction from the asthenosphere, are furthermore not sufficient to generate the extensive partial melting necessary to account for the amount of magma required to form composite shield volcanoes (Hoernle et al., 2006; Timm et al., in review). For these reasons and the problems with other models discussed above, we favor lithospheric removal as the major (but not necessarily exclusive) trigger for causing partial melting beneath Zealandia, primarily decompression melting of the upper asthenosphere but also some melting of lithospheric material. Even though the HIMU-type trace element and isotopic compositions of the low-silica Zealandia intraplate basalts are believed to be derived from the asthenosphere, they are not characteristic of an upper MORB-type mantle. In order to explain the HIMU-type

composition of the basalts, Hoernle et al. (2006) proposed that young recycled oceanic crust in the form of pyroxenite/eclogite was present in the upper asthenosphere. We note, however, that this interpretation does not explain why the Sr-Nd-Pb-Hf isotopic composition of the Cenozoic low-silica intraplate volcanism forms arrays extending from the field of the Cretaceous intraplate volcanism to MORB, which imply that the Cenozoic volcanism could be explained by mixing of the Cretaceous volcanic source with the depleted upper mantle.

As noted above, large volumes of Cretaceous (99-89 Ma) HIMU-type volcanism have been found on the Hikurangi Plateau (Hoernle et al., 2005; Hoernle et al., in prep) and on the South Island of New Zealand (e.g. Tapuaenuku Igneous Complex) (Baker et al., 1994), (Mandamus) (Tappenden, 2003). This Cretaceous intraplate volcanism may give us the best idea of the composition of the Cretaceous plume head, since these melts would have avoided interaction with the Gondwana mantle wedge and continental lithosphere (Hoernle et al., in prep.). Both P and S wave seismic tomographic studies show that a large-scale, deep-seated low-velocity zone is present between depths of ~600 -1450 km, extending from beneath the Chatham Rise to beneath western Antarctica margin, shallowing to ~300 km beneath some areas (Montelli et al., 2006; Nolet et al., 2006; Li et al., 2008). If this tomographic anomaly represents the source of the Cretaceous volcanism (Hoernle et al., in prep.), we speculate that it may have extensively polluted the uppermost asthenosphere with HIMU-type material, enriched in an eclogitic component derived from recycled ancient ocean crust (Figure 3.14). As a result the uppermost asthenosphere could reflect a mixture of HIMU-type eclogitic and depleted MORB-source-type peridotitic mantle. Our conclusion is supported by a study of $^{3}He/^{4}He$ isotope ratios on fluid inclusions in mantle xenocrysts and basalt phenocrysts from the South Island which point to a more degassed upper MORB-like mantle source beneath Zealandia, containing remnants of plume material (Hoke et al., 2000).

Subduction throughout the Mesozoic along the Gondwana margin may have overprinted the Zealandia lithosphere not only with an EM-type geochemical signature, but with subduction-related melts that froze in the lower lithosphere forming eclogite and ultramafic cumulates, e.g. garnet pyroxenite. These dense rocks would have significantly increased the density of the lowermost lithosphere (Elkins-

Tanton, 2006), pre-conditioning it for later lithospheric detachment in response to continental extension and break-up at the end of the Cretaceous.

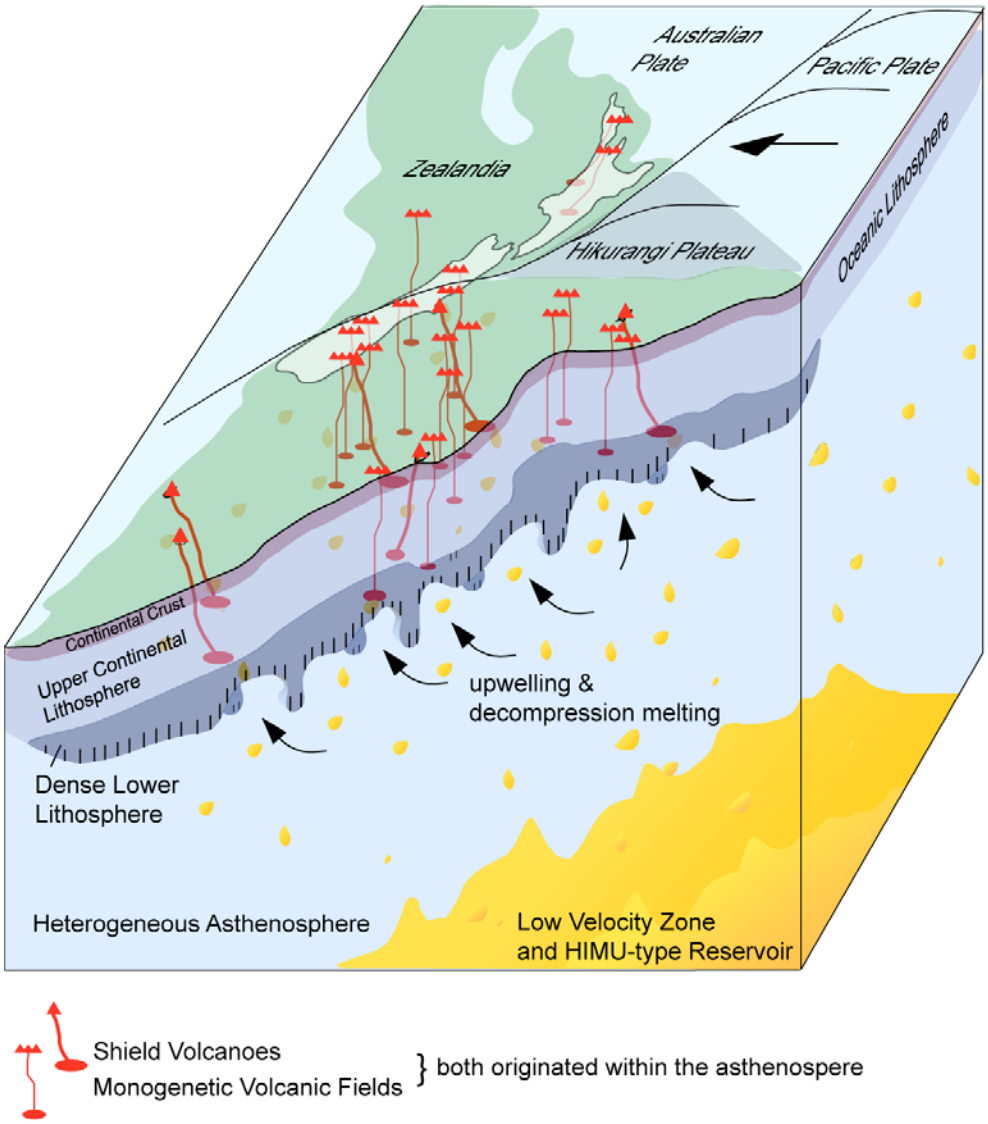

Figure 3.14: Schematic box model to explain melt generation beneath Zealandia. A large-scale hot thermal anomaly was identified beneath the Chatham Rise by seismic tomography at ~ 600 km depth (P- and S-waves) (Montelli, 2006; Nolet, 2006; Li et al., 2008). If this thermal anomaly represents the source of Cretaceous HIMU-plume-type volcanic rocks (Hoernle et al., in prep.), we propose that it pollutes the upper asthenosphere with carbonated eclogitic (recycled ancient ocean crust) plume material with a HIMU-type composition. Based on Montelli et al. (2006) and Li et al. (2008), the velocity anomaly below ~ 600 km can be traced to the south all the way to Antarctica. We invoke lithospheric detachment to trigger melting, which induces partial melting of carbonated eclogite within depleted upper asthenospheric peridotite. The mixing proportion between eclogite and peridotite melts controls the extent of the HIMU-type signature found in the Cenozoic lavas erupted on Zealandia. The extent of melting is controlled by the extent of lithospheric detachment, which in turn controls the degree of upwelling and the amount of decompression melting. Low-silica melts are formed by low degrees of melting primarily sampling carbonated eclogite, while larger degrees of melting preferentially sample peridotite producing high-silica melts with depleted compositions. Lithospheric interaction shows up preferentially in the depleted high-silica melts, generating enriched (EMII-type) incompatible element and isotope ratios.

As Zealandia drifted northwards, detachment of the dense lithospheric root led to localized upwelling, melting and volcanism. Small-scale detachment events could generate minor upwelling and low-degree melting, preferably of eclogite to form low-silica magmas (Hoernle et al., 2006). If these events occurred repeatedly, low levels of volcanism could be maintained over long periods of time or re-occur regularly at the same locations on the moving continental mass. On the other hand detachment of larger bodies, or a rapid succession of small ones, could generate more extensive upwelling and melting to form shield volcanoes. More extensive melting of the upwelling asthenosphere would exhaust the eclogitic component, resulting in melts with higher silica and more depleted compositions. More extensive melting would also result in the greater transfer of heat to the lithosphere by larger volumes of ascending melts, causing areas enriched during Gondwana subduction to melt, resulting in larger amounts of lithospheric interaction. Greater lithospheric interaction with the more depleted (low in incompatible element abundances), larger-degree, largely peridotitic melts would result in more noticeable contamination by subduction-related EM-type components in the lithosphere. Peridotitic melts, for example in Northland, that have depleted (E-MORB-type) isotopic compositions could have ascended through areas of thinner lithosphere and possibly through lithosphere that was not as extensively affected by Gondwana subduction. This model explains both the depleted (E-MORB)- and enriched (EM)-type compositions of the high-silica melts.

3.7 Conclusions

1) Cenozoic intraplate volcanism is widespread on both the presently emergent and submerged parts of Zealandia, and occurred throughout much of the Cenozoic. No age progressions in the direction and at the rate of plate motion or close correlation with local extensional events are observed, confirming that the plume hypothesis and continental rifting/extension are not adequate models for explaining the origin of this intraplate volcanism.

2) The geochemical data confirm that three different types of mantle source components are required to explain the composition of the Cenozoic volcanism on Zealandia: 1) HIMU-type component (characterized by $^{206}Pb/^{204}Pb$ = 19.2-20.6) that dominates in mafic low-silica (SiO_2 < 46 wt. %) volcanic rocks, 2) depleted (E-

MORB-type) component (characterized by $^{206}Pb/^{204}Pb$ = 18.6-19.0 and $^{143}Nd/^{144}Nd$ = 0.51279-0.51293) that dominates in high-silica ($SiO_2 \geq 46$ wt. %) volcanic rocks from Northland and 3) enriched (EMII-type) component (characterized by $^{206}Pb/^{204}Pb$ = 18.9-19.6 and $^{143}Nd/^{144}Nd$ = 0.51296-0.51308) that dominates in all the other high-silica rocks. Although the presence of a depleted (E-MORB-type) component was previously postulated, it was not previously identified.

3) The distribution, ages and geochemical composition of the Cenozoic intraplate volcanism throughout Zealandia can be best explained by the process of lithospheric removal and subsequent decompression melting of upwelling heterogeneous asthenospheric mantle as proposed by Hoernle et al. (2006). We conclude that the heterogeneous asthenospheric mantle consists of eclogite/pyroxenite with HIMU-type isotopic composition within a depleted (MORB-type) peridotitic matrix. Interaction of the depleted high-silica melts with the lithosphere, enriched to various degrees by a subduction-related component as represented by the Late Cretaceous Mt. Somers volcanic rocks (within both the mantle and crustal parts of the lithosphere) and crustal rocks could generate the EMII-type signatures of most of the high-silica rocks.

4) The Cenozoic volcanic rocks can be explained by mixing of sources for Cretaceous intraplate volcanism (interpreted to result from the interaction of a HIMU plume with the Gondwana mantle wedge and lithosphere) and MORB. We propose that a deep-seated large-scale low velocity zone between 650 – 1450 km, presumably associated with the Cretaceous volcanism, polluted the depleted upper MORB-source peridotitic asthenosphere with carbonated eclogite domains, having HIMU-type trace element and isotopic compositions. Low-degree, decompression melting of the primarily carbonated eclogite (representing recycled ancient ocean crust) produces low-silica melts with primarily HIMU-type trace element and isotopic compositions. At greater degrees of decompression melting, the eclogitic component in the melts decrease and the peridotitic component increases resulting in the generation of high-silica melts with depleted (E-MORB-type) trace element and isotopic compositions. Contamination within portions of the lithosphere enriched during subduction along the Gondwana margin and by non-volcanic crustal rocks primarily affects the composition of the depleted high-silica melts, due to their low incompatible element contents.

Acknowledgements

Dagmar Rau, Jan Fietzke and Silke Hauff are thanked for their technical assistance with the major element and isotopic analyses. We are grateful to K. Gohl, chief scientist of cruise SO 169, and the SO168 and SO169 captain's, crews and shipboard scientists for their expert support. B. Davy and R. Herzer provided a variety of maps, data and other invaluable information for the marine sampling. We are especially grateful to D. Coombs, T. Reay, D. Lee and A. Cooper from Otago University, H. Campbell from the GNS in Dunedin and S. Weaver and V. Tappenden from Canterbury University for providing us samples out of the OU, P and UC catalogues and/or for helpful advice and enlightening discussions. M. Großman and M. Thorman helped with processing of the SIMRAD data. K. Heydolph and M. Rehder are thanked for sample preparation and S. Duggen for stimulating discussions. The German Ministry of Education and Research (BMBF; Grants SO168 Zealandia and SO169 CAMP) and the DFG (Grant HO18/12-1 and 2) and IFM-GEOMAR are gratefully acknowledged for providing funding for this project. Several figures were prepared with GMT public domain software (Wessel and Smith, 1995).

References

Adams, C. J., 1981. Migration of late Cenozoic volcanism in the South Island of New Zealand and the Campbell Plateau. Nature 294, 153-155.

Adams, C. J., 1983. Age of the volcanoes and granite basement of the Auckland Islands, Southwest Pacific. New Zealand Journal of Geology and Geophysics 26, 227-237.

Baker, J., Gamble J. A., Graham, I. J., 1994. The age, geology, and geochemistry of the Tapuaenuku Igneous Complex, Marlborough, New Zealand. New Zealand Journal of Geology and Geophysics 37, 249-268.

Barreiro, B. A., Cooper, A., 1987. A Sr, Nd, and Pb isotope study of alkaline lamprophyres and related rocks from Westland and Otago, South Island, New Zealand. Geological Society of America Special Paper 215, 115-125.

Barley, M.E., Weaver, S. D., 1988. Strontium isotope composition and geochronology of intermediate-silicic volcanics, Mt Somers and Banks Peninsula, New Zealand. New Zealand Journal of Geology and Geophysics 31, 197-206.

Barry, T.L., Saunders, A.D., Kempton, J.D., Windley, B.F., Pringle, M.S., Dorjnamjaa, D., Saandar, S., 2003. Petrogenesis of Cenozoic Basalts from Mongolia: Evidence for the Role of Asthenosphere versus Metasomatized Lithospheric Mantle Sources. Journal of Petrology 44(1), 55-91.

Blichert-Toft, J., Chauvel C., Albarede, F., 1997. Separation of Hf and Lu for high-precision isotope analyses of rock samples by magnetic sector-multiple collector ICP-MS. Contributions to Mineralogy and Petrology 127, 248–260.

Briggs, R.M., McDonough W.F., 1990. Contemporaneous Convergent Margin and Intraplate Magmatism, North Island, New Zealand. Journal of Petrology 31 (4), 813-851.

Briggs, R.M., Okada, T., Itaya, T., Shibuya, H., Smith I. E. M., 1994. K-Ar ages, paleomagnetism, and geochemistry of the South Auckland volcanic field, North Island, New Zealand. New Zealand Journal of Geology and Geophysics 37, 143-153.

Carey, C., Mortimer, N., Uruski, C., Wood R., 1991. Fire and brimstone on the western Challenger Plateau: further evidence from Mount Spong and Megabrick. New Zealand Geological Survey Record 43, 123-128.

Clouard, V., Bonneville A., 2005. Ages of seamounts, islands and plateaus and plateaus on the Pacific plate, in: G.R. Foulger, J.H. Natland, D.C. Presnall, D.L. Anderson (Eds.), Plates, Plumes, and Paradigms. Geological Society of America Special Paper, vol. 388, Geological Society of America, 2005, 71–90.

Conrad, C.P., Molnar P., 1997. The growth of Rayleigh-Taylor-type Instabilities in the lithosphere for various rheological and density structures, Geophysical Journal International 129, 95-112.

Cook, C., Briggs, R. M., Smith I. E. M., Maas R., 2004. Petrology and geochemistry of intraplate basalts in the South Auckland Volcanic Field, New Zealand: Evidence for two coeval magma suites from distinct sources. Journal of Petrology 46, 473-503.

Coombs, D.S., Cas, R.A., Kawachi, Y., Landis, C. A., McDonough W. M., Reay A., 1986. Cenozoic Volcanism in North, East and Central Otago. Cenozoic Volcanism in New Zealand. I. E. M. Smith, Royal Society of New Zealand - Bullentin 23, 278-312.

Cooper, A.F. (1986), A carbonatitic lamprophyre dike swarm from the Southern Alps, Otago and Westland. Late Cenozoic Volcanism in New Zealand. I. E. M. Smith, Royal Society of New Zealand – Bulletin 23, 313-336.

Cooper, A.F., Barreiro, B. A., Kimbrough D. L., Mattinson J. M., 1987. Lamprophyre dike intrusion and the age of the Alpine fault, New Zealand. Geology 15, 941-944.

Cullen, D.J., 1969. Quaternary volcanism at the Antipodes Islands: its bearing on the

structural interpretation of the southwest Pacific. Journal of Geophysical Research 74, 4213–4220.

Dasch, E. J., Evans, A. L., Essene, E., 1970. Radiometric and petrologic data from eclogites and megacrysts of the Kakanui Mineral Breccia, New Zealand. Geological Society American Abstract Program 7, 532–533.

Dasgupta, R., Hirschmann, M. M., Dellas, N., 2005. The effect of bulk composition on the solidus of carbonated eclogite from partial melting experiments at 3 GPa. Contributions Mineralogy Petrology 149, 288–305.

Dasgupta, R., Hirschmann, M. M., Stalker, K., 2006. Immiscible Transition from Carbonate-rich to Silicate-rich Melts in the 3 GPa Melting Interval of Eclogite + CO3 and Genesis of Silica-undersaturated Ocean Island Lavas. Journal of Petrology 47(4), 647-671.

Dasgupta, R., Hirschmann, M. M., Smith, N. D., 2007. Partial Melting Experiments of Peridotite + CO2 at 3 GPa and Genesis of Alkalic Ocean Island Basalts. Journal of Petrology 48(11), 2093-2124.

Davy, B., Wood, R., 1994. Gravity and magnetic modelling of the Hikurangi Plateau. Marine Geology 118, 139-151.

Davy, B., Hoernle, K., Werner, R., XXXX. The Hikurangi Plateau - crustal structure, rift formation and Gondwana subduction history. Geochemistry Geophysics Geosystems xxx.

Duggan, M. B., Reay, A., 1986. The Timaru Basalt. Royal Society of New Zealand - Bulletin 23, 246–277.

Elkins-Tanton, L.T., 2005. Continental magmatism caused by lithospheric delamination, in: G.R. Foulger, J.H. Natland, D.C. Presnall, D.L. Anderson (Eds.), Plates, Plumes, and Paradigms, Geological Society of America Special Paper 388, Geological Society of America, 449–461.

Eagles, G., Gohl, K., Larter, R. D., 2004. High-resolution animated tectonic reconstruction of the South Pacific and West Antarctic Margin. Geochemistry Geophysics Geosystems 5(7), 21.

Farrar, E., Dixon, J. M., 1984. Overriding of the Indian-Antarctic Ridge: Origin of Emerald Basin and migration of late Cenozoic volcanism in Southern New Zealand and Campbell Plateau. Tectonophysics 104, 243-256.

Finn, C.A., Mueller, R. D., Panter, K. S., 2005. A Cenozoic diffuse alkaline magmatic province (DAMP) in the southwest Pacific without rift or plume origin. Geochemistry Geophysics Geosystems 6, Q02005, doi:10.1029/2004GC000723.

Funnell, R.H., Allis, R. G., 1996. Hydrocarbon maturation potential of offshore Canterbury and Great South Basins. New Zealand Petroleum Conference, Wellington, Publicity Unit, N. Z.

Gamble, J.A., Morris P. A., Adams, C. J., 1986. The Geology, Petrology and Geochemistry of Cenozoic Volcanic Rocks from the Campbell Plateau and Chatham Rise. Late Cenozoic Volcanism in New Zealand. J. Smith, The Royal Society of New Zealand, 344-365.

Garbe-Schönberg, C.-D., 1993. Simultaneous determination of thirty-seven trace elements in twenty-eight international rock standards by ICP-MS. Geostandards Newsletter 17, 81-97.

Godfrey, N.J., Davey, F., Stern, T., and Okaya, D., 2001. Crustal structure and thermal anomalies of the Dunedin Region, South Island, New Zealand. Journal of Geophysical Research 106(B12), 30,835-30,848.

Gohl, K., Davey, F. Davy, B., Barker, D., and Uenzelmann-Neben, G., 2003. The Campbell Plateau (New Zealand) and its Rifted Margin: A history of its break-up process. Geophysical Research Abstracts 5, 2.

Grapes, R.H., Lamb, S. H., Adams, C. J., 1992. K-Ar ages of basanitic dikes, Awatere Valley, Marlborough, New Zealand. New Zealand Journal of Geology and Geophysics 35, 415-419.

Grindley G.W., C. J. Adams, J. T. Lumb and W. A. Watters (1977), Paleomagnetism, K-Ar dating and tectonic interpretation of upper Cretaceous and Cenozoic volcanic rocks of the Chatham Islands, New Zealand, New Zealand Journal of Geology and Geophysics 20, 425-467.

Hart, S.R., Blusztajn, J., Craddock, C., 1997. Hobbs Coast Cenozoic volcanism: Implications for the West Antarctic rift system. Chemical Geology 139, 223-248.

Herzberg, C., Zhang J., 1996. Melting experiments in anhydrous peridotite KLB-1: compositions of magmas in the upper mantle and transition zone. Journal of Geophysical Research 101(B4), 8271-8295.

Herzberg, C., Asimow, P. D., in review. Petrology of some Oceanic Island Basalts: PRIMELT2.XLS software for Primary Magma Calculation. Geochemistry Geopysics Geosystems (in review).

Herzer, R.H., Challis, G. A., Christie, R. H. K., Scott G. H., Watters, W. A., (1989), The Urry Knolls, late Neogene alkaline basalt extrusives, southwestern Chatham Rise. Journal of the Royal Society of New Zealand 19(2), 181-193.

Hirose, K., Kushiro, I., 1993. Partial melting of dry peridotites at high pressures: Determination of compositions of melts segregated from peridotite using aggregates of diamond. Earth Planetary Science Letters 114, 477-489.

Hirschmann, M.M., Stolper, E. M., 1996. A possible role for garnet pyroxenite in the origin of the “garnet signature” in MORB. Contribution to Mineralogy and Petrology 124,185–208.

Hirschmann, M.M., Kogiso, T, Baker, M. B., and Stolper, E. M., 2003. Alkalic magmas generated by partial melting of garnet pyroxenite. Geology 31, 481-484.

Hoernle, K., Mortimer, N., Werner, R., Hauff, F., 2003. Fahrtbericht/Cruise Report SO 168 Zealandia (causes and effects of plume and rift-related Cretaceous and Cenozoic volcanism on Zealandia). G. R. 133, 1-127+app.

Hoernle, K., White, J. D. L., Bogaard, P.v.d., Hauff, F., Coombs, D. S., Werner, R., Timm, C., Garbe-Schönberg, C.-D., Reay, A., Cooper, A. F., 2006. Cenozoic Intraplate Volcanism on New Zealand: Upwelling Induced by Lithospheric Removal. Earth and Planetary Science Letters 248, 335-352.

Hoernle, K., Abt, D. L., Fischer, K. M., Nichols, H., Hauff, F., Abers, G. A., Bogaard, P. van den, Heydolph, K., Alvarado, G., Protti, M., Strauch, W., 2008. Arc-parallel flow in the mantle wedge beneath Costa Rica and Nicaragua. Nature, doi: 10.1038/nature06550.

Hoke, L., Poreda, R. Reay, A., Weaver, S. D., 2000. The subcontinental mantle beneath southern New Zealand, characterised by helium isotopes in intraplate basalts and gas-rich springs. Geochimica et Cosmochimica Acta 64(14), 2489-2507.

Houseman, G. A., Molnar P., 1997. Gravitational (Rayleigh-Taylor) instability of a layer with non-linear viscosity and convective thinning of the continental lithosphere. Geophysical Journal International 128, 125-150.

Houseman, G.A., Neil, E., Kohler, M. D., 2000. Lithospheric Instability in the Traverse Ranges of California. Journal Geophysical Research 105(B7), 16,237 - 16,250.

Huang, Y., Hawkesworth, C., van Calsteren., P., Smith, I., Black, P., 1997. Melt generation models for the Auckland volcanic field, New Zealand: constraints from U -Th isotopes. Earth and Planetary Science Letters 149, 67-84.

Huang, Y., Hawkesworth, C., Smith, I., van Calsteren., P., Black, P., 2000. Geochemistry of late Cenozoic basaltic volcanism in Northland and Coromandel, New Zealand: implications for mantle enrichment processes. Chemical Geology 164, 219-238.

Jull, M. and Kelemen, P.B., 2001. On conditions for lower crustal convective instability. Journal Geophysical Research 106, 6423-6446.

Kogiso, T., and Hirschmann, M.M., 2006. Partial melting experiments of bimineralic eclogite and the role of recycled mafic oceanic crust in the genesis of ocean island basalts. Earth and Planetary Science Letters 249, 188–199.

Korenaga, J., 2005. Why did not the Ontong Java Plateau form subaerially? Earth and Planetary Science Letters 234, 385–399.

Larter, R.D., Cunningham, A.P., Barker, P.F., Gohl. K., Nitsche, F.O., 2002. Tectonic evolution of the Pacific margin of Antactica 1. Late Cretaceous tectonic reconstructions. Journal of Geophysical Research 107(B12), 19.

Le Maitre, R.W., Bateman, P., Dudek., A., Keller, J., Lameyre, J., La Bas, M.J., Sabine, P.A., Schmidt R., Sörensen, H., Streckeisen, A., Wooley, A.R., Zanettin, B., 1989. A classification of igneous rocks and glossary of terms. Blackwell Scientific Publications.

Li, C., van der Hilst, R, D., Engdahl, E. R., Burdick, S., 2008. A new global model for P wave speed variations in Earth's mantle. Geochemistry Geopysics Geosystems 9 (5), Q05018, doi:10.1029/2007GC001806.

Liu, Z. and Bird, P., 2006. Two-dimensional and three-dimensional finite element modelling of mantle processes beneath central South Island, New Zealand. Geophysical Journal International 365, 1003–1028.

Mathews, W.H., Curtis, G.H., 1966. Date of the Pliocene-Pleistocene boundary in New Zealand. Nature 212, 979-980.

McDougall, I., Coombs, D.S., 1973. Potassium-Argon ages for the Dunedin Volcano and outlying volcanics. New Zealand Journal of Geology and Geophysics 16 (2), 179-188.

McLennan, J.M., Weaver, S.D., 1984. Olivine-nephelinite at Mounseys Creek, Oxford, Canterbury (Note). New Zealand Journal of Geology and Geophysics 27, 389-390.

Molnar, P., Anderson, H.J., Audoine, E., Eberhart-Phillips, D., Gledhill, K.R., Klosko, E.R:, McEvilly, T.V., Okaya, D., Savage, K,M., Stern, T., Wu, F.T., 1999. Continuous deformation versus faulting through the continental lithosphere of New Zealand. Science 286, 516-519.

Montelli, R., Nolet, G., Dahlen, R.A., Masters, G., 2006. A catalogue of deep mantle plumes: New results from finite frequency tomography. Geochemistry Geophysics Geosystems 7(11), Q11007, doi:10.1029/2006GC001248.

Morgan ,W.J., 1971. Convection plumes in the lower mantle. Nature 230, 42-43

Morris, J. C. 1987: The stratigraphy of the Amuri Limestone group, east Marlborough, New Zealand. Unpublished Ph.D. thesis, lodged in the Library, University of Canterbury. 388 p.

Mortimer, N., 2004. New Zealand's geological foundations. Gondwana Reasearch 7(1), 261-272.

Mortimer, N., Hoernle, K., Hauff, F., Palin, J.M., Dunlap, W.J., Werner, R., Faure, K., 2006. New constraints on the age and evolution of the Wishbone Ridge, southwest Pacific Cretaceous microplates, and Zealandia–West Antarctica breakup. Geology 34 (3), 185-188.

Mortimer, N., Herzer, R.H., Gans, P.B., Laporte-Magoni, C., Calvert, A.T., Bosch, D., 2007. Oligocene–Miocene tectonic evolution of the South Fiji Basin and Northland Plateau, SW Pacific Ocean: Evidence from petrology and dating of dredged rocks. Marine Geology 237, 1-24.

Nathan, S., Anderson, H.J., Cook, R.A., Herzer, R.H., Hoskins, R.H., Raine, J.I., Smale, D., 1986. Cretaceous and Cenozoic sedimentary basins of the West Coast Region, South Island, New Zealand. New Zealand Geological Survey Basin Studies 1, 9-18.

Neil, E. and Houseman G.A., 1999. Rayleigh-Taylor instability of the upper mantle and its role in intraplate orogeny. Geophysysical Journal International 138, 89-107.

Nolet, G., Karato, S.-I., Montelli, R., 2006. Plume fluxes from seismic tomography. Earth and Planetary Science Letters 248, 685-699.

Panter, K. S., Blusztain, J., Hart, R.S., Kyle, P.R., Esser, R., McIntosh, W.C., 2006. The Origin of HIMU in the SW Pacific: Evidence from Interplate Volcanism in Southern New Zealand and Subantarctic Islands. Journal of Petrology doi:10.1093/petroogy/eg1024, 1-32.

Panter, K.S., Hart, R.S., Kyle, P.R., Blusztain, J., Wilch, T., 2000. Geochemistry of Late Cenozoic basalts from the Crary Mountains: Characterisation of mantle sources in Marie Byrd Land, Antarctica. Chemical Geology 165, 215-241.

Pertermann, M., M. M. Hirschmann, et al. (2004). Experimental determination of trace element partitioning between garnet and silica-rich liquid during anhydrous partial melting of MORB-like eclogite. Geochemistry Geopysics Geosystems 5(5): Q05A01 DOI 10.1029/2003GC000638.

Pfänder, J. A., Münker, C., Stracke, A., Mezker, K., 2007. Nb/Ta and Zr/Hf in ocean island basalts — Implications for crust–mantle differentiation and the fate of Niobium. Earth and Planetary Science Letters 254, 158-172.

Phillips, C.J., Cooper, A.F., Palin, J.M., Nathan, S., 2005. Geochronological constraints on Cretaceous–Paleocene volcanism in South Westland, New Zealand, New Zealand Journal of Geology and Geophysics 48, 1–14.

Price, R.J., Compston, W., 1973. The Geochemistry of the Dunedin Volcano: Strontium Isotope Chemistry. Contributions to Mineralogy and Petrology 42, 55-61.

Price, R.C., Cooper, A.F., Woodhead, J.D., Cartwright, I.A.N., 2003. Phonolitic diatremes within the Dunedin Volcano, South Island, New Zealand, J. Petrol. 44, 2053–2080.

Priestley, K. and McKenzie, D., 2006. The thermal structure of the lithosphere from shear wave velocities. Earth and Planetary Science Letters 244, 285-301.

Reay, A. and Sipiera, P.P., 1987. Mantle xenoliths from the New Zealand region. Mantle Xenoliths. P. H. Nixon, John Wiley & Sons Ltd, 347-358.

Robinson, J.A.C. and Wood, B.J., 1998. The depth of the spinel to garnet transition at the peridotite solidus. Earth and Planetary Science Letters 164, 277-284.

Scherwath, M., Stern, T., Melhuish, A., Molnar, P., 2002. Pn anisotropy and distributed upper mantle deformation associated with a continental transform fault. Geophysical Research Letters 29(8), 161 - 164.

Sclater, J.G., Jaupart, C., Galson, D., 1980. The heat flow through oceanic and continental crust and the heat loss of the Earth. Reviews of Geophysics and Space Physics 18, 269-311.

Sewell, R.J. and Gibson, I.L., 1988. Petrology and geochemistry of Tertiary volcanic rocks from inland Central and South Canterbury, South Island, New Zealand. New Zealand Journal of Geology and Geophysics 31, 477-492.

Sewell, R.J., Nathan, S., 1987. Geochemistry of Late Cretaceous an Early Tertiary basalts from south Westland, New Zealand Geological Survey Record 18, 87–94.

Smith, I.E.M., Okada, T., Itaya, T., Black, P.M., 1993. Age relationships and tectonic implications of late Cenozoic basaltic volcanism in Northland, New Zealand. New Zealand Journal of Geology and Geophysics 36, 385-393.

Sobolev, A.V., Hofmann, A.W. Kuzmin, D. V., Yaxley, G. M., Arndt, N. T., Chung, S.-L., Danyushevsky, L. V., Elliott, T., Frey, F. A., Garcia, M. O., Gurenko, A. A., Kamenetsky, V. S., Kerr, A. C., Krivolutskaya, N. A., Matvienkov, V. V., Nikogosian, I. K., Rocholl, A., Sigurdsson, I. A., Sushchevskaya, N. M., Teklay, M., 2007. The Amount of Recycled Crust in Sources of Mantle-Derived Melts. Science 10.1126/science.1138113.

Sprung, P., Schuth, S., Münker, C., Hoke, L., 2007. Intraplate volcanism in New Zealand: the role of fossil plume material and variable lithospheric properties. Contributions Mineralogy Petrology 153, 669-687.

Steinberger, B., Sutherland, R. O'Connell, R.J., 2004. Prediction of Emperor-Hawaii seamount locations from a revised model of global plate motion and mantle flow. Nature 430, 167-173.

Stern, T., Okaya, D., Scherwarth, M., 2002. Structure and Strength of a continental transform from onshore-offshore seismic profiling of South Island, New Zealand. Earth Planets Space 54, 1011-1019.

Stipp, J.J., McDougall, I., 1968. Geochronology of the Banks Peninsula volcanoes, New Zealand. New Zealand Journal of Geology and Geophysics 11, 1239-1260.

Storey, B.C., 1995. The role of mantle plumes in continental breakup: case histories from Gondwanaland. Nature 377, 301-308.

Storey, B.C., Leat, P.T., Weaver, S.D., Pankhurst, R.J., Bradshaw, J.D., Kelley, S., 1999. Mantle plumes and Antartica - New Zealand rifting: evidence from mid-Cretaceous mafic dykes. Journal of the Geological Society, London 156, 659-671.

Sutherland, R. (1995). The Australia-Pacific boundary and Cenozioc plate motions in the SW Pazific: Some constraints from Geosat data. Tectonics 14(4), 819-831.

Tappenden, V. (2003). Magmatic response to the evolving New Zealand Margin of Gondwana during the Mid-Late Cretaceous. Department of Geological Sciences Christchurch, University of Canterbury. PhD, 250.

Tarduno, J.A., Duncan, R.A., Scholl. D.W., Cottrell, R.D., Steinberger, B., Thordason, T., Kerr, B.C., Neal, C.R., Frey, F.A., Torii, M., Carvallo, C., 2003. The Emperor Seamounts: Southward Motion of the Hawaiian Hotspot Plume in Earth's Mantle. Science 301, 1064-1069.

Timm, C., Hoernle, K., Bogaard, P.v.d., Bindemann, I., Weaver, S.D., in review. Geochemical evolution of intraplate volcanism at Banks Peninsula; New Zealand: mantle melts versus crustal contamination. Journal of Petrology, xxx-xxx

Thirlwall, M.F. 1997. Pb isotopic and elemental evidence for OIB derivation from young HIMU mantle. Chemical Geology 139, 51-74.

Todt, W., Cliff, R.A., Hanser, A., Hofmann, A.W., 1996. $^{202}Pb + ^{205}Pb$ double spike for lead isotopic analyses. In: A Basu and S Hart (eds.) Earth Processes: Reading the Isotopic Code: Geophysical Monograph vol 95

Waight, T.E., Weaver, S.D. Maas, R., Eby, G.N., 1998. French Creek Granite and Hohonu Dyke Swarm, South Island, New Zealand: Late Cretaceous alkaline magmatism and the opening of the Tasman Sea. Australian Journal of Earth Sciences 45, 823-835.

Waight, T.E., Weaver, S.D., Muir, R.J., 1998. Mid-Cretaceous granitic magmatism during the transition from subduction to extension in southern New Zealand: a chemical and tectonic synthesis. Lithos 45, 469-482.

Weaver, S.D. and Pankhurst, R.J., 1991. A precise Rb-Sr age for the Mandamus Igneous Complex, North Canterbury, and regional tectonic implications. New Zealand Journal of Geology and Geophysics 34.

Weaver, S.D. and Smith, I.E.M., 1989. New Zealand Intraplate Volcanism. Intraplate volcanism in eastern Australia and New Zealand. R. W. Johnson, J. Knutson and S. R. Taylor, Cambridge University Press. Chapter 4, 157-188.

Weaver, S.D., Storey, B.C., Pankhurst, R.J., Mukasa, S.B., DiVenere, V.J., Bradshaw, J.D., 1994. Antarctica-New Zealand rifting and Marie Byrd Land lithospheric magmatism linked to ridge subduction and mantle plume activity. Geology 22, 811-814.

Wright, J.B., 1968. Contributions to the Volcanic Succession and Petrology of the Auckland Islands, New Zealand: 3. Minor Intrusives on the Ross Volcano. Transactions of the Royal Society Of New Zealand, Geology 6(1), 1-11.

***Table 3**: Major and Trace element compositions*

	Western and Central Chatham Rise					
	P63478	**P63483**	**P63485**	**P63527**	**SO168-DR3-1**	**SO168-DR5-1**
Location	Hardcastles Dory Tow	Lambton Quay	Elm Street	Lucky Hill	Graveyard A	Morgue (Graveyards)
Latitude	44°41.448´S	44°45.000 S	44°74.546´S	44°23.760´S	42°45.088'S	42°42.687'S
Longitude	182°89.272´W	186°.06.000´E	185°43.002´E	194°23.724´E	179°59.092'W	179°57.049'W
Group	lsg	lsg	lsg	lsg	lsg	lsg
Major elements in wt%						
SiO_2	50.14	43.97	41.01	40.54	36.76	33.55
TiO_2	1.98	2.78	2.68	2.54	4.13*	4.11*
Al_2O_3	16.58	10.78	12.00	11.42	8.00	8.26
FeO^t	10.28	13.03	12.94	12.52	13.19	12.15
Fe^2O^3	1.15	1.46	1.45	1.41	1.48	1.36
MnO	0.26	0.19	0.17	0.18	0.49	0.11
MgO	2.45	12.38	7.32	9.23	15.08	7.22
CaO	6.14	9.48	13.07	12.86	13.96	19.79
Na_2O	5.77	2.17	4.28	4.05	1.21	0.98
K_2O	2.06	1.10	1.68	1.58	1.29	1.25
P_2O_5	1.27	0.60	1.01	0.88	2.05*	5.33*
H_2O	0.85	1.43	1.26	1.23	2.50	3.26
CO_2	0.31	0.54	0.09	0.48	0.29	0.57
Total	99.24	99.91	98.96	98.92	100.43	97.94
Trace elements in parts per million (ppm)						
Li	12.1	8.82	14.5	19.2	14.4	10.4
Sc	5.91	24.3	19.9	18.8	24.2	28.0
V	41.2	253	272	255	327	326
Cr	1.31	574	213	220	597	514
Co	14.8	63.4	51.8	59.3	104	49.4
Ni	2.26	407	100	166	490	114
Cu	5.25	56.7	35.0	35.7	81.9	24.2
Zn	121	127	151	136	139	115
Ga	22.5	20.0	23.5	22.0	16.8	17.0
Rb	48.2	23.1	45.7	46.2	37.0	35.5
Sr	1219	638	890	912	773	883
Y	43.9	27.0	30.1	28.0	29.4	35.6
Zr	453	259	235	223	256	250
Nb	118	54.5	83.0	76.8	97.2	19.1
Mo	4.90	1.02	1.51	1.10	4.13	1.45
Sn	1.87	1.78	1.74	1.59	1.53	n.a.
Sb	0.16	0.06	0.18	0.08	1.19	n.a.
Cs	0.30	0.21	0.67	0.92	0.36	0.51
Ba	648	293	600	604	512	617
La	88.4	36.7	55.8	51.6	56.9	90.5
Ce	178	77.0	105	100	113	165
Pr	20.6	9.33	12.6	11.6	13.4	19.6
Nd	76.6	37.1	48.7	44.9	51.5	75.3
Sm	13.2	7.62	9.74	8.97	9.71	13.8
Eu	3.98	2.38	2.87	2.62	2.80	4.21
Gd	10.2	6.60	8.39	7.68	7.88	11.9
Tb	1.52	0.98	1.22	1.13	1.10	1.48
Dy	7.77	5.11	6.04	5.56	5.30	7.21
Ho	1.41	0.88	0.99	0.91	0.89	1.20
Er	3.69	2.14	2.30	2.10	2.14	2.64
Tm	0.50	0.27	0.27	0.25	0.27	0.34
Yb	3.25	1.64	1.56	1.42	1.59	1.95
Lu	0.47	0.22	0.20	0.18	0.22	0.26
Hf	8.59	5.22	4.78	4.38	5.46	4.07
Ta	5.91	3.11	4.38	4.00	5.56	0.32
Tl	0.05	0.02	0.12	0.08	1.28	0.41
Pb	4.15	2.25	4.77	4.17	15.5	9.16
Th	8.27	4.39	7.35	6.84	6.21	8.61
U	1.39	1.19	1.71	1.47	2.41	9.47

***Table 3**: Major and Trace element compositions (continued)*

	Western and Central Chatham Rise (continued)					
	SO168-DR5-4	**SO168-DR74-2**	**SO168-DR74-4**	**SO168-DR79-1**	**SO168-DR80-1**	**SO168-DR80-6**
Location	Morgue (Graveyards)	Chapmans Hill	Chapmans Hill	Howson D	Charlton A	Charlton A
Latitude	42°42.687'S	44°09.080'S	44°09.080'S	43°57.195'S	44°11.634'S	44°11.634'S
Longitude	179°57.049'W	174°32.850'W	174°32.850'W	175°18.889'W	175°27.948'W	175°27.948'W
Group	lsg	lsg	lsg	lsg	lsg	lsg
	Major elements in wt%					
SiO_2	38.41	41.31	43.09	36.02	35.93	44.79
TiO_2	3.88*	2.75	3.01	3.28	1.96	2.26
Al_2O_3	9.05	11.96	13.05	12.55	11.17	12.08
FeO^t	12.84	10.99	11.73	10.86	9.01	10.46
Fe^2O^3	1.44	1.23	1.32	1.22	1.01	1.17
MnO	0.14	0.14	0.15	0.14	0.12	0.10
MgO	9.31	8.27	8.35	9.45	4.64	10.32
CaO	15.68	14.61	12.34	14.20	20.42	10.04
Na_2O	1.58	2.21	2.47	1.91	2.57	2.39
K_2O	1.52	0.79	0.74	0.83	0.89	0.91
P_2O_5	2.39*	0.73	0.87	1.15	0.53	0.41
H_2O	3.01	2.6	2.45	5.93	1.56	3.79
CO_2	0.19	3.23	0.6	2.54	9.68	0.91
Total	99.44	100.82	100.17	100.08	99.49	99.63
	Trace elements in parts per million (ppm)					
Li	9.88	55.2	31.1	28.1	n.a.	56.1
Sc	26.8	25.7	23.4	23.9	n.a.	22.8
V	324	322	267	287	n.a.	225
Cr	523	450	356	294	n.a.	420
Co	53.8	108	44.3	61.2	n.a.	46.1
Ni	187	282	118	137	n.a.	310
Cu	39.0	46.4	43.4	83.4	n.a.	80.6
Zn	129	175	145	140	n.a.	109
Ga	17.8	18.5	21.1	18.4	n.a.	18.1
Rb	43.2	15.3	10.4	7.62	n.a.	21.2
Sr	935	384	1139	680	n.a.	349
Y	32.3	43.2	29.0	32.2	n.a.	20.2
Zr	311	192	218	270	n.a.	138
Nb	130	42.3	52.4	68.8	n.a.	30.9
Mo	2.46	6.60	2.15	1.48	n.a.	0.91
Sn	2.52	1.50	1.75	1.91	n.a.	1.28
Sb	0.90	2.27	0.20	0.34	n.a.	0.17
Cs	0.62	0.56	0.19	0.06	n.a.	0.43
Ba	589	154	342	131	n.a.	204
La	79.8	40.3	30.4	55.6	n.a.	26.8
Ce	150	56.6	61.5	117	n.a.	54.0
Pr	17.8	8.83	7.97	14.1	n.a.	6.70
Nd	67.3	37.9	33.2	54.4	n.a.	26.6
Sm	12.2	8.51	7.70	10.33	n.a.	5.62
Eu	3.55	2.91	2.49	3.35	n.a.	1.79
Gd	9.63	8.35	7.15	8.66	n.a.	5.05
Tb	1.34	1.19	1.07	1.25	n.a.	0.76
Dy	6.28	6.23	5.56	6.09	n.a.	3.93
Ho	1.01	1.10	0.93	1.00	n.a.	0.67
Er	2.38	2.67	2.22	2.32	n.a.	1.62
Tm	0.29	0.33	0.28	0.28	n.a.	0.21
Yb	1.65	1.97	1.61	1.60	n.a.	1.23
Lu	0.22	0.28	0.21	0.21	n.a.	0.17
Hf	6.29	4.13	4.73	5.52	n.a.	3.14
Ta	6.75	2.30	2.96	3.87	n.a.	1.66
Tl	0.19	0.33	0.02	0.05	n.a.	0.02
Pb	6.93	5.18	1.49	2.39	n.a.	1.84
Th	8.27	3.20	3.49	5.73	n.a.	2.97
U	2.88	1.77	0.72	1.13	n.a.	0.75

***Table 3**: Major and Trace element compositions (continued)*

	Western and Central Chatham Rise (continued)					
	SO168-DR81-1	**SO168-DR83-2**	**SO168-DR84-2**	**SO168-DR84-4**	**SO168-DR87-1**	**SO168-DR87-4**
Location	Charlton B	FBI	Gore	Gore	Perry	Perry
Latitude	44°13.780'S	44°40.833'S	44°36.673'S	44°36.673'S	44°38.581'S	44°38.581'S
Longitude	175°27.100'W	175°12.754'W	175°45.024'W	175°45.024'W	176°49.498'W	176°49.498'W
Group	lsg	lsg	lsg	lsg	hsg	hsg
Major elements in wt%						
SiO_2	36.14	30.20	31.49	41.46	50.75	49.06
TiO_2	2.45	1.65	3.24	3.54	2.50	2.59
Al_2O_3	9.63	11.82	9.92	13.10	14.96	15.47
FeO^{i}	13.15	12.33	15.03	13.67	8.95	9.34
$Fe^{2}O^{3}$	1.48	1.39	1.69	1.53	1.01	1.05
MnO	0.18	0.12	0.09	0.13	0.16	0.16
MgO	11.93	1.46	4.26	4.12	5.10	4.47
CaO	12.94	16.87	15.05	9.59	9.11	8.60
Na_2O	2.40	2.74	1.33	2.87	3.70	3.61
K_2O	1.34	1.66	1.72	2.55	1.14	1.29
P_2O_5	1.33	9.92*	6.81*	2.73*	0.53	0.56
H_2O	3.98	4.58	3.19	n.a.	1.6	2.39
CO_2	2.51	1.61	0.3	n.a.	0.1	0.12
Total	99.46	96.35	94.12	95.29	99.61	98.71
Trace elements in parts per million (ppm)						
Li	22.5	9.46	13.9	n.a.	10.6	13.2
Sc	21.5	21.2	23.1	n.a.	18.7	16.3
V	185	256	299	n.a.	211	190
Cr	329	262	406	n.a.	165	83.6
Co	50.6	66.4	28.3	n.a.	43.5	32.4
Ni	315	163	106	n.a.	145	82.6
Cu	45.6	59.4	60.0	n.a.	48.4	46.8
Zn	153	236	177	n.a.	132	125
Ga	20.9	19.9	18.7	n.a.	23.5	24.2
Rb	24.5	21.5	46.0	n.a.	20.7	24.2
Sr	713	939	1063	n.a.	668	661
Y	37.6	244	66.2	n.a.	26.5	26.7
Zr	319	122	263	n.a.	196	198
Nb	124	10.2	39.5	n.a.	35.7	40.1
Mo	1.50	2.35	2.74	n.a.	2.28	2.17
Sn	2.46	0.64	0.89	n.a.	1.67	1.93
Sb	0.27	7.01	4.17	n.a.	0.10	0.11
Cs	0.85	0.95	1.24	n.a.	0.48	0.93
Ba	480	150	528	n.a.	312.7	316
La	94.4	122	63.6	n.a.	27.2	29.5
Ce	180	49.8	90.2	n.a.	55.7	60.3
Pr	21.6	21.8	13.6	n.a.	7.16	7.82
Nd	81.4	93.8	54.2	n.a.	29.7	32.3
Sm	15.0	18.5	10.6	n.a.	6.85	7.46
Eu	4.42	5.42	3.18	n.a.	2.20	2.42
Gd	13.5	23.9	9.74	n.a.	6.37	7.48
Tb	1.66	3.38	1.39	n.a.	0.96	1.04
Dy	8.13	21.6	7.52	n.a.	5.12	5.52
Ho	1.34	4.90	1.43	n.a.	0.88	0.96
Er	3.16	13.9	3.80	n.a.	2.16	2.35
Tm	0.38	1.90	0.50	n.a.	0.28	0.30
Yb	2.26	11.9	3.12	n.a.	1.66	1.82
Lu	0.30	1.89	0.46	n.a.	0.22	0.25
Hf	6.50	2.35	5.06	n.a.	4.31	4.74
Ta	6.04	0.54	1.87	n.a.	1.98	2.06
Tl	0.06	0.09	0.15	n.a.	0.12	0.07
Pb	5.42	43.6	2.91	n.a.	2.65	2.86
Th	11.5	2.40	4.35	n.a.	3.35	3.57
U	1.76	6.66	3.50	n.a.	0.94	1.06

***Table 3**: Major and Trace element compositions (continued)*

	Western and Central Chatham Rise (continued)					
	SO168-DR87-6	**SO168-DR88-1**	**SO168-DR89-4**	**SO168-DR91-1**	**SO168-DR96-1**	**SO168-DR97-1**
Location	Perry	Thompson	Clerke A	Manley	Manley	Orton
Latitude	44°38.581'S	44°44.268'S	43°52.375'S	43°22.090'S	43°22.090'S	44°21.020'S
Longitude	176°49.498'W	176°48.072'W	177°07.473'W	177°22.456'W	177°22.456'W	176°11.400'E
Groups	hsg	lsg	lsg	lsg	hsg	lsg
Major elements in wt%						
SiO_2	50.91	44.78	41.19	40.50	47.01	41.63
TiO_2	2.57	1.93	2.36	2.26	2.58	3.81*
Al_2O_3	15.56	16.37	10.74	9.74	14.16	11.99
FeO^t	9.00	8.46	11.29	10.78	11.27	12.81
Fe^2O^3	1.01	0.95	1.27	1.21	1.27	1.44
MnO	0.12	0.13	0.17	0.09	0.09	0.18
MgO	4.36	7.63	12.44	12.09	5.94	9.00
CaO	8.35	8.70	13.30	9.15	9.73	11.73
Na_2O	3.60	3.57	2.33	1.86	2.93	2.37
K_2O	1.30	1.34	1.32	1.02	1.06	1.22
P_2O_5	0.55	0.57	0.63	0.56	0.68	0.71
H_2O	2.75	5.64	1.63	6.58	2.59	2.04
CO_2	0.06	0.57	1.32	4.2	0.24	1.13
Total	100.14	100.64	99.99	100.04	99.55	100.06
Trace elements in parts per million (ppm)						
Li	6.2	44.9	8.37	36.3	30.1	6.44
Sc	18.1	31.4	25.6	17.4	17.5	23.3
V	196	262	243	127	179	315
Cr	109	308	492	283	227	359
Co	36.4	40.9	58.3	32.5	27.8	68.4
Ni	94.1	175	282	155	91.8	256
Cu	49.1	46.1	68.0	38.2	36.1	62.9
Zn	125	85.3	111	119	99.1	145
Ga	23.7	18.9	17.9	18.7	16.7	22.9
Rb	25.6	18.7	25.0	14.4	28.1	23.1
Sr	667	373	661	199	450	976
Y	26.6	27.5	24.2	19.6	21.4	24.1
Zr	197	180	203	163	141	281
Nb	39.7	41.2	66.7	35.1	25.5	58.4
Mo	2.37	0.86	3.19	0.39	0.93	2.70
Sn	1.91	1.19	1.82	1.59	1.21	1.83
Sb	0.12	0.16	0.13	0.13	0.30	0.07
Cs	0.64	0.30	0.40	0.41	2.60	0.27
Ba	334	234	383	526	164	346
La	28.9	26.0	43.3	26.0	22.3	42.7
Ce	59.0	51.7	86.7	56.5	44.8	91.4
Pr	7.71	6.33	10.8	7.18	5.67	11.6
Nd	31.9	24.6	42.1	30.0	23.2	46.2
Sm	7.41	5.13	8.50	6.69	5.15	9.10
Eu	2.38	1.62	2.56	1.93	1.71	2.89
Gd	7.38	4.80	7.89	6.38	4.76	7.41
Tb	1.04	0.79	1.03	0.83	0.73	1.04
Dy	5.53	4.53	5.21	4.19	3.89	5.02
Ho	0.96	0.88	0.89	0.70	0.68	0.80
Er	2.34	2.39	2.11	1.64	1.68	1.85
Tm	0.30	0.34	0.27	0.20	0.22	0.22
Yb	1.82	2.25	1.58	1.19	1.34	1.24
Lu	0.25	0.33	0.22	0.16	0.18	0.16
Hf	4.70	3.55	4.72	3.89	3.16	5.69
Ta	2.02	2.33	3.39	1.79	1.39	3.42
Tl	0.13	0.02	0.05	0.06	0.02	0.18
Pb	2.89	1.48	2.70	2.79	2.95	2.19
Th	3.51	3.29	5.33	2.75	2.80	4.38
U	1.22	0.92	1.56	0.73	0.71	1.33

***Table 3**: Major and Trace element compositions (continued)*

	Western and Central Chatham Rise (continued)					
	SO168-DR97-2	**SO168-DR98-2**	**SO168-DR99-1**	**SO168-DR101-1**	**SO168-DR104-1**	**SO168-DR104-4**
Location	Orton	Gathrey	Anja	Jordan	Forwood	Forwood
Latitude	44°21.020'S	44°24.135'S	44°30.479'S	44°45.326'S	44°45.900'S	44°45.900'S
Longitude	176°11.400'E	175°55.220'E	175°51.062'E	174°52.612'E	174°23.907'E	174°23.907'E
Groups	lsg	lsg	lsg	hsg	lsg	lsg
Major elements in wt%						
SiO_2	46.24	39.74	41.18	49.44	44.27	43.51
TiO_2	2.65	3.85*	2.94	2.72	2.52	2.57
Al_2O_3	15.59	12.56	15.84	15.35	13.05	13.53
FeO^t	10.42	12.24	10.66	9.17	11.66	11.22
Fe^2O^3	1.17	1.37	1.20	1.03	1.31	1.26
MnO	0.16	0.16	0.08	0.10	0.16	0.16
MgO	5.21	7.61	1.19	5.42	8.91	6.50
CaO	8.33	12.79	10.69	10.26	11.27	12.13
Na_2O	4.23	2.52	3.93	3.24	3.34	3.43
K_2O	2.07	1.20	2.10	0.91	1.12	1.36
P_2O_5	0.68	0.99	4.86*	0.50	0.75	1.00
H_2O	2.81	2.43	2.57	1.59	1.6	2.25
CO_2	0.28	2.24	0.62	0.05	0.13	0.53
Total	99.84	95.85	97.86	99.78	100.09	99.45
Trace elements in parts per million (ppm)						
Li	17.0	19.6	6.68	9.60	14.7	n.a.
Sc	16.2	20.2	14.3	28.4	23.3	n.a.
V	191	273	160	277	261	n.a.
Cr	163	240	22.9	433	245	n.a.
Co	35.1	54.8	16.8	37.8	52.9	n.a.
Ni	81.6	158	31.4	119	163	n.a.
Cu	36.7	59.4	15.5	54.6	71.3	n.a.
Zn	145	144	115	124	124	n.a.
Ga	26.2	24.1	23.0	24.0	20.6	n.a.
Rb	54.6	23.7	28.9	7.95	24.8	n.a.
Sr	970	987	1325	553	692	n.a.
Y	37.7	31.8	36.6	30.7	28.3	n.a.
Zr	491	363	225	216	202	n.a.
Nb	94.8	73.3	6.08	36.8	51.8	n.a.
Mo	5.97	2.71	1.20	1.26	2.34	n.a.
Sn	2.16	2.25	0.09	1.64	1.55	n.a.
Sb	0.18	0.11	1.15	0.15	0.09	n.a.
Cs	0.64	0.41	0.65	0.08	0.49	n.a.
Ba	624	388	585	270	398	n.a.
La	79.6	53.4	61.1	28.1	41.3	n.a.
Ce	139	116	143	58.7	81.6	n.a.
Pr	15.8	14.3	17.4	7.56	9.63	n.a.
Nd	56.8	56.3	70.4	31.0	37.3	n.a.
Sm	10.3	11.1	13.5	7.07	7.69	n.a.
Eu	2.97	3.38	4.67	2.29	2.38	n.a.
Gd	8.52	9.05	12.2	6.70	6.83	n.a.
Tb	1.28	1.29	1.50	1.04	1.03	n.a.
Dy	6.61	6.35	7.59	5.69	5.34	n.a.
Ho	1.18	1.05	1.28	1.01	0.91	n.a.
Er	2.99	2.47	3.07	2.49	2.22	n.a.
Tm	0.40	0.30	0.38	0.32	0.28	n.a.
Yb	2.46	1.78	2.22	1.95	1.66	n.a.
Lu	0.34	0.23	0.30	0.26	0.22	n.a.
Hf	8.02	6.94	3.89	4.73	4.11	n.a.
Ta	5.18	4.18	0.19	2.11	2.77	n.a.
Tl	0.10	0.20	0.04	0.02	0.05	n.a.
Pb	4.84	2.43	6.89	3.47	3.37	n.a.
Th	10.5	5.62	4.80	4.05	5.39	n.a.
U	2.51	1.63	5.66	0.75	1.38	n.a.

***Table 3**: Major and Trace element compositions (continued)*

			Chatham Islands		Challenger Plateau	
	SO168-DR104-7	**SO168-DR105-1**	**P74894**	**P74899**	**SO168-DR2-1**	**SO168-DR2-2**
Location	Forwood	Bootie	The Horns	Cape L'Evenque	Mount Spong B	Mount Spong B
Latitude	44°45.900'S	44°36.121'S	44°07.174'S	44°07.306'S	39°48.814'S	39°48.502'S
Longitude	174°23.907'E	174°14.770'E	176°37.674'E	176°37.949'E	167°14.291'E	167°14.397'E
Groups	lsg	hsg	lsg	lsg	lsg	lsg
Major elements in wt%						
SiO_2	42.64	46.09	44.30	43.35	51.76	52.31
TiO_2	2.51	2.77	3.03	3.51	0.53	0.53
Al_2O_3	12.93	14.44	15.47	10.90	21.40	20.54
FeO^{i}	11.47	11.62	12.24	12.06	4.86	4.80
$Fe^{2}O^{3}$	1.29	1.30	1.37	1.35	0.55	0.54
MnO	0.14	0.16	0.20	0.16	0.36	0.30
MgO	9.09	6.26	6.96	13.07	0.92	1.58
CaO	11.70	10.59	10.11	10.35	1.44	1.58
Na_2O	2.81	3.39	3.76	2.73	8.03	8.92
K_2O	1.08	1.13	1.87	1.39	5.21	5.38
P_2O_5	1.00	0.79	0.64	0.78	0.18	0.15
H_2O	2.5	1.25	1.38	1.39	4.32	3.34
CO_2	0.23	0.06	0.04	0.05	0.1	0.07
Total	99.39	99.85	101.37	101.09	99.66	100.04
Trace elements in parts per million (ppm)						
Li	32.2	11.3	6.17	6.93	29.7	20.9
Sc	23.2	21.0	19.8	19.9	0.63	0.78
V	267	262	257	245	20.3	13.6
Cr	241	128	120	400	1.02	1.05
Co	51.3	45.1	42.1	58.8	2.78	2.26
Ni	168	86.4	57.5	327	10.9	2.57
Cu	67.2	76.9	44.7	48.9	2.15	3.52
Zn	130	127	106	118.5	201	202
Ga	20.6	23.4	19.7	19.3	35.3	35.8
Rb	25.3	23.1	42.6	16.1	151	142
Sr	638	634	876	946	685	678
Y	28.8	29.2	28.4	24.6	61.0	60.8
Zr	207	216	271	247	858	838
Nb	52.9	43.2	71.9	53.0	272	267
Mo	2.39	1.84	3.05	2.67	2.20	4.48
Sn	1.58	1.86	1.67	1.76	2.51	2.58
Sb	0.14	0.14	0.08	0.06	0.74	0.44
Cs	0.80	0.51	0.50	0.27	5.41	4.33
Ba	331	292	519	532	910	706
La	42.2	32.9	50.2	41.8	239	222
Ce	84.0	67.6	103	89.4	369	350
Pr	9.79	8.44	12.1	11.2	33.7	33.1
Nd	37.9	33.8	47.2	46.8	96.7	95.2
Sm	7.78	7.25	9.08	9.81	13.4	13.4
Eu	2.47	2.25	2.84	3.11	3.28	3.39
Gd	6.94	6.64	8.28	8.79	10.1	10.4
Tb	1.04	1.01	1.15	1.18	1.72	1.72
Dy	5.41	5.41	5.96	5.75	9.30	9.41
Ho	0.93	0.95	1.08	0.96	1.82	1.84
Er	2.25	2.34	2.71	2.19	5.13	5.24
Tm	0.29	0.31	0.36	0.26	0.75	0.77
Yb	1.69	1.85	2.24	1.51	4.89	5.03
Lu	0.23	0.25	0.32	0.20	0.68	0.70
Hf	4.21	4.45	6.00	5.77	11.4	11.5
Ta	2.83	2.37	4.02	2.93	7.60	7.75
Tl	0.07	0.08	0.01	0.02	0.94	0.87
Pb	4.48	3.04	3.78	2.46	15.0	14.5
Th	5.55	4.36	6.20	4.28	31.6	30.9
U	1.32	0.95	1.60	1.30	2.11	1.81

***Table 3**: Major and Trace element compositions (continued)*

	Campbell Plateau					
	SO169-DR3-1K	**SO169-DR3-7**	**SO169-DR6-1**	**SO169-DR11-1**	**SO169-DR11-5**	**SO169-DR12-1**
Location	North of Antipodes Island	North of Antipodes Island	West of Antipodes Island	Pukaki Bank	Pukaki Bank	Pukaki Bank
Latitude	49°31.240´S	49°31.240´S	49°59.350´S	49°10.200´S	49°10.200´S	49°14.120´S
Longitude	178°51.860´E	178°51.860´E	179°40.300´E	171°51.590´E	171°51.590´E	171°46´360´E
Groups	lsg	lsg	lsg	lsg	lsg	lsg
Major elements in wt%						
SiO_2	56.24	56.09	50.17	45.30	40.55	49.35
TiO_2	0.10	0.10	1.83	2.73	2.53	1.91
Al_2O_3	19.84	19.54	17.96	16.59	16.21	16.92
FeO^t	4.16	4.13	8.16	9.84	10.14	9.00
Fe^2O^3	0.47	0.46	0.92	1.11	1.14	1.01
MnO	0.30	0.31	0.11	0.20	0.17	0.18
MgO	0.44	0.41	1.25	3.34	5.28	2.54
CaO	0.86	0.88	6.78	9.73	9.30	6.62
Na_2O	10.77	10.25	5.06	4.85	3.64	5.51
K_2O	4.87	4.88	2.86	1.63	1.24	2.06
P_2O_5	0.16	0.15	1.67	1.40	2.54	1.73
H_2O	0.87	1.32	1.52	1.71	5.07	2.47
CO_2	0.03	0.07	0.23	1.34	1.29	0.15
Total	99.11	98.59	98.52	99.77	99.10	99.45
Trace elements in parts per million (ppm)						
Li	29.8	30.4	11.1	12.5	38.9	14.8
Sc	3.02	2.71	12.0	6.56	6.46	7.59
V	2.78	3.40	194	96.3	72.6	24.2
Cr	1.06	1.05	77.8	1.22	1.48	7.36
Co	4.29	2.68	14.4	24.2	20.8	10.4
Ni	13.6	11.7	45.3	4.33	4.58	4.26
Cu	8.54	7.78	19.0	21.4	17.7	11.3
Zn	261	193	151	143	124	143
Ga	48.1	47.3	29.8	26.1	25.4	25.9
Rb	189	198	50.8	32.9	18.7	36.5
Sr	195	229	1081	1109	1057	1107
Y	66.0	64.4	38.9	34.3	49.0	63.7
Zr	1628	1528	448	351	302	397
Nb	327	331	65.7	74.6	68.0	73.2
Mo	4.70	4.97	1.75	3.71	1.65	3.65
Sn	12.6	12.9	1.98	2.12	n.a.	1.99
Sb	0.51	0.56	2.12	0.10	n.a.	0.13
Cs	1.18	1.98	0.14	0.40	0.35	0.45
Ba	86.9	102	677	417	713	535
La	206	211	74.3	55.4	77.3	88.0
Ce	359	367	138	111	138	161
Pr	36.6	37.3	16.4	14.0	17.2	20.6
Nd	105	106	58.3	54.3	68.9	80.6
Sm	15.7	15.9	10.1	10.7	13.4	15.5
Eu	2.54	2.56	2.78	3.33	4.24	4.86
Gd	11.6	11.7	8.20	9.28	12.7	13.7
Tb	2.04	2.06	1.21	1.33	1.68	1.98
Dy	11.4	11.3	6.29	6.74	8.78	10.3
Ho	2.14	2.09	1.15	1.15	1.56	1.83
Er	6.08	5.94	3.00	2.75	3.54	4.55
Tm	0.95	0.92	0.41	0.35	0.48	0.59
Yb	6.49	6.35	2.63	2.07	2.81	3.56
Lu	0.93	0.92	0.38	0.27	0.40	0.51
Hf	37.5	36.1	9.39	6.99	6.73	8.06
Ta	30.9	31.1	3.97	4.32	3.61	3.99
Tl	0.28	0.26	0.06	0.07	0.17	0.08
Pb	16.3	16.4	6.03	3.40	2.82	3.57
Th	35.1	35.2	8.35	7.14	6.13	6.33
U	11.3	10.9	1.80	1.97	1.53	2.26

***Table 3**: Major and Trace element compositions (continued)*

	Campbell Plateau (Antipodes Islands)					
	SO169-DR15-1	**A2**	**A5**	**A6**	**A8B**	**A23a**
Location	Pukaki Bank	Antipodes Island	Antipodes Island	Antipodes Island	Antipodes Island	Antipodes Island
Latitude	49°19.650´S	49°40.485´S	49°40.689´S	49°40.566´S	49°42.000´S	49°92.534´S
Longitude	171°48.790´E	178°48.852´E	178°48.438´E	178°48.558´E	178°46.200´E	178°44.496´E
Group	lsg	lsg	lsg	lsg	lsg	lsg
Major elements in wt%						
SiO_2	47.41	45.13	39.41	42.34	53.16	43.09
TiO_2	2.45	2.89	3.75	3.29	1.14	3.77
Al_2O_3	16.84	14.77	11.42	9.55	17.43	12.08
FeO^t	11.14	12.40	14.61	14.93	9.93	14.72
Fe^2O^3	1.25	1.39	1.64	1.68	1.12	1.65
MnO	0.12	0.20	0.18	0.18	0.24	0.17
MgO	2.52	4.99	10.56	13.72	1.48	10.17
CaO	5.51	8.98	11.43	11.65	4.59	11.55
Na_2O	4.17	5.82	2.76	1.67	5.70	2.12
K_2O	1.92	2.04	0.99	0.50	2.78	0.66
P_2O_5	1.40	1.24	0.96	0.41	0.46	0.43
H_2O	4.86	0.23	1.06	0.64	1.16	0.56
CO_2	0.06	0.01	0.65	0.01	0.04	0.03
Total	99.65	100.09	99.42	100.57	99.23	101.00
Trace elements in parts per million (ppm)						
Li	21.0	8.47	5.79	3.50	15.9	5.45
Sc	3.30	9.71	24.0	33.9	3.44	32.0
V	53.5	160	280	340	2.12	417
Cr	-	48.3	291	532	1.90	323
Co	16.9	38.0	69.0	82.7	8.16	74.7
Ni	2.26	52.6	239	268	1.20	159
Cu	11.9	35.3	61.8	32.9	11.4	29.9
Zn	133	201	153	131	190	135
Ga	22.5	29.4	23.4	18.1	30.9	22.1
Rb	35.7	53.7	25.3	9.87	62.9	14.2
Sr	1018	1382	905	428	871	531
Y	43.6	39.1	30.9	22.4	49.1	24.1
Zr	325	501	293	170	643	187
Nb	75.9	95.7	65.1	29.7	124	33.2
Mo	2.06	5.77	2.06	1.28	4.94	0.93
Sn	2.56	1.74	1.76	1.31	4.44	1.55
Sb	0.28	0.12	0.08	0.03	0.16	0.03
Cs	0.66	0.64	0.27	0.11	0.54	0.14
Ba	335	554	334	141	670	171
La	59.3	94.2	50.8	23.5	92.5	25.2
Ce	124	188	111	50.7	179	54.1
Pr	16.1	22.6	13.9	6.76	21.7	7.04
Nd	67.1	84.0	55.8	28.3	77.8	29.1
Sm	13.8	15.3	11.2	6.28	13.8	6.39
Eu	4.41	4.58	3.47	2.06	3.91	2.10
Gd	12.6	12.2	9.32	5.73	11.3	5.81
Tb	1.75	1.70	1.32	0.85	1.72	0.87
Dy	9.10	7.99	6.38	4.45	9.00	4.60
Ho	1.59	1.28	1.03	0.77	1.60	0.79
Er	3.84	2.97	2.34	1.83	4.14	1.92
Tm	0.50	0.36	0.28	0.23	0.57	0.25
Yb	2.95	2.10	1.59	1.40	3.53	1.46
Lu	0.41	0.27	0.21	0.19	0.49	0.19
Hf	7.22	8.77	5.78	3.91	12.4	4.06
Ta	3.81	4.88	3.68	1.82	7.42	1.98
Tl	0.19	0.02	0.00	0.01	0.07	0.01
Pb	3.59	4.71	2.11	0.93	5.07	1.52
Th	5.81	11.1	5.12	2.38	10.6	2.61
U	1.40	3.12	1.33	0.66	3.06	0.42

***Table 3**: Major and Trace element compositions (continued)*

	Campbell Plateau (Antipodes Islands)					**Northland**
	A102	**A105**	**A108**	**A109**	**A112**	**NZN3**
Location	Antipodes Island	Antipodes Island	Antipodes Island	Antipodes Island	Antipodes Island	Cable Bay
Latitude	49°40.860´S	49°42.000´S	49°42.804´S	49°42.000´S	49°42.000´S	35°16.331'S
Longitude	178.46.098´E	178°46.200´E	178°45.336´E	178°46.200´E	178°46.200´E	173°56.623'E
Group	lsg	lsg	lsg	lsg	lsg	hsg MORB
Major elements in wt%						
SiO_2	41.19	40.75	43.19	45.22	39.60	50.82
TiO_2	4.29	4.24	3.67	3.75	4.39	2.68
Al_2O_3	12.95	10.66	10.90	15.82	11.99	16.57
FeO^t	15.85	16.19	14.57	13.29	16.55	10.57
Fe^2O^3	1.78	1.82	1.64	1.49	1.86	1.19
MnO	0.20	0.18	0.16	0.19	0.20	0.18
MgO	7.47	10.42	10.73	4.89	9.06	4.21
CaO	10.92	12.74	11.97	9.04	11.84	8.02
Na_2O	2.95	1.94	1.74	4.28	2.09	4.68
K_2O	1.07	0.68	0.55	1.46	0.39	1.20
P_2O_5	0.85	0.64	0.37	0.95	0.78	0.67
H_2O	0.76	0.52	0.7	0.38	1.68	0.38
CO_2	0.09	0.04	0.04	0.01	0.12	0.03
Total	100.37	100.82	100.23	100.77	100.55	101.20
Trace elements in parts per million (ppm)						
Li	6.02	4.11	3.40	7.44	5.76	12.4
Sc	23.6	33.9	35.4	12.7	28.3	23.2
V	384	468	411	184	416	266
Cr	190	379	318	18.9	284	20.2
Co	69.4	77.7	72.0	35.9	72.2	32.0
Ni	119	162	155	13.3	160	18.5
Cu	78.0	27.7	29.9	16.8	61.3	47.2
Zn	165	147	126	161	160	118
Ga	25.2	22.6	20.2	26.7	23.5	22.4
Rb	26.2	15.8	10.7	31.6	6.64	17.6
Sr	943	641	433	1009	768	366
Y	35.7	27.9	19.9	39.8	31.5	39.6
Zr	324	226	158	354	264	266
Nb	57.4	37.4	26.7	65.0	46.4	39.2
Mo	2.73	1.54	1.17	2.69	1.75	1.89
Sn	2.09	1.73	1.39	2.50	1.67	2.16
Sb	0.06	0.04	0.03	0.07	0.04	0.05
Cs	0.21	0.14	0.11	0.25	0.09	0.28
Ba	304	190	143	347	242	220
La	47.7	31.6	18.9	48.6	40.0	28.0
Ce	106	70.1	42.0	106	85.9	60.6
Pr	13.1	9.26	5.56	13.8	11.2	7.73
Nd	52.5	38.7	23.3	56.4	45.6	33.0
Sm	10.7	8.25	5.33	11.7	9.44	7.70
Eu	3.37	2.66	1.82	3.78	3.01	2.44
Gd	9.18	7.34	4.93	10.3	8.31	8.06
Tb	1.35	1.07	0.75	1.50	1.20	1.28
Dy	6.86	5.44	3.93	7.64	6.16	7.62
Ho	1.17	0.92	0.68	1.31	1.05	1.53
Er	2.83	2.20	1.62	3.14	2.51	4.09
Tm	0.36	0.27	0.20	0.40	0.32	0.59
Yb	2.13	1.62	1.22	2.36	1.88	3.86
Lu	0.29	0.21	0.16	0.31	0.25	0.57
Hf	6.17	4.90	3.68	6.79	5.52	5.57
Ta	3.39	2.25	1.63	3.88	2.79	2.31
Tl	0.03	0.01	0.01	0.03	0.01	0.03
Pb	2.17	1.29	1.52	2.22	0.73	2.85
Th	4.44	2.77	2.14	4.54	3.57	3.11
U	1.15	0.74	0.61	1.27	0.96	0.88

***Table 3**: Major and Trace element compositions (continued)*

	Northland (continued)					**Marlborough**
	NZN28	**NZN29**	**NZN30**	**NZN31**	**NZN32**	**P 50269**
Location	Near Lake Omapeu	Tuanui Quarry	NW of Kerikeri	East side Kerikeri	East side Kerikeri	Graseed Volcanics
Latitude	35°21.782'S	35°28.728'S	35°09.244'S	35°12.012'S	35°20.758'S	42°07.195'S
Longitude	173°49.119'E	173°48.144'E	173°53.355'E	173°57.836'E	173°53.803'E	173°36.150'E
Group	hsg MORB	hsg MORB	hsg MORB	hsg MORB	hsg MORB	lsg
Major elements in wt%						
SiO_2	59.75	50.04	49.44	49.18	50.72	38.81
TiO_2	1.06	1.79	1.68	1.50	2.46	4.65
Al_2O_3	17.64	17.06	16.85	17.20	16.86	12.67
FeO^t	5.32	8.61	10.29	9.04	10.93	12.69
Fe^2O^3	0.60	0.97	1.16	1.01	1.23	1.43
MnO	0.10	0.14	0.18	0.16	0.19	0.19
MgO	2.86	6.82	6.28	6.32	3.48	5.84
CaO	5.70	10.86	9.79	10.73	6.42	13.98
Na_2O	4.63	3.39	3.81	3.42	4.80	3.47
K_2O	1.70	0.78	0.66	0.25	1.84	1.17
P_2O_5	0.29	0.32	0.34	0.22	0.92	1.48
H_2O	0.56	0.38	0.7	0.99	0.87	3.47
CO_2	0.37	0.03	0.04	0.71	0.03	0.03
Total	100.58	101.19	101.22	100.73	100.75	99.88
Trace elements in parts per million (ppm)						
Li	16.4	6.71	8.84	5.06	16.7	9.52
Sc	14.4	27.5	29.9	29.3	21.4	14.8
V	113	216	211	196	237	470
Cr	29.5	187	105	173	8.47	7.65
Co	19.0	36.2	40.6	40.3	25.5	44.84
Ni	24.8	65.6	57.1	69.1	9.36	58.7
Cu	29.2	41.1	59.1	69.5	17.4	114
Zn	76.9	78.5	84.0	75.5	122	143
Ga	19.3	18.6	18.3	16.8	24.4	24.6
Rb	51.3	9.84	10.6	2.64	28.4	42.4
Sr	269	452	295	445	337	1893
Y	48.0	20.5	30.4	24.8	45.0	34.9
Zr	261	133	167	121	310	337
Nb	21.4	22.0	22.0	10.2	48.4	87.1
Mo	1.64	1.01	0.99	0.34	3.39	2.32
Sn	3.01	1.27	1.44	1.17	1.66	1.58
Sb	0.23	0.04	0.04	0.03	0.06	0.07
Cs	2.66	0.22	0.16	0.18	0.23	0.51
Ba	229	123	136	234	329	565
La	26.7	15.4	16.0	8.40	42.4	73.8
Ce	51.2	32.4	35.2	20.1	90.7	151
Pr	6.01	4.16	4.57	2.89	11.1	19.2
Nd	23.8	17.8	19.8	13.5	45.0	74.7
Sm	5.15	4.30	4.89	3.71	9.78	13.9
Eu	1.42	1.53	1.66	1.38	2.82	4.01
Gd	6.06	4.53	5.35	4.35	9.74	11.2
Tb	1.02	0.72	0.91	0.74	1.51	1.53
Dy	6.72	4.14	5.61	4.63	8.79	7.27
Ho	1.53	0.80	1.16	0.95	1.74	1.18
Er	4.50	2.07	3.22	2.59	4.62	2.72
Tm	0.69	0.29	0.48	0.37	0.66	0.33
Yb	4.58	1.84	3.13	2.44	4.33	1.88
Lu	0.74	0.26	0.47	0.36	0.64	0.24
Hf	5.69	3.09	3.56	2.76	6.63	7.04
Ta	1.41	1.32	1.27	0.61	2.60	4.94
Tl	0.23	0.02	0.02	0.03	0.03	0.13
Pb	7.31	1.44	1.58	1.08	5.29	3.95
Th	6.39	1.78	1.90	0.91	4.79	6.69
U	1.81	0.57	0.55	0.28	1.46	2.08

***Table 3**: Major and Trace element compositions (continued)*

	Marlborough	**Canterbury (Oxford Area)**				
	P 50272 A	**P 50272 B**	**MSI 21A**	**MSI 22A**	**MSI 22B**	**MSI 23A**
Location	Graseed Volcanics	Graseed Volcanics	Oxford Area – Harper Hill	Oxford Area – Acheron Gabbro	Oxford Area – Acheron Gabbro	Oxford Area – View Hill
Latitude	42°11.047'S	42°11.047'S	43°29.198'S	43°31.140'S	43°31.140'S	43°19.530'S
Longitude	173°31.246'E	173°31.246'E	171°57.497'E	171°39.510'E	171°39.510'E	172°02.323'E
Group	lsg	lsg	hsg EMII	hsg EMII	hsg EMII	hsg EMII
Major elements in wt%						
SiO_2	41.41	39.40	48.66	47.86	48.51	53.02
TiO_2	3.43	3.23	2.77	2.21	2.04	1.65
Al_2O_3	10.78	9.94	15.82	12.56	11.51	15.08
FeO^t	10.44	10.43	11.38	11.82	11.35	9.40
Fe^2O^3	1.17	1.17	1.28	1.33	1.27	1.06
MnO	0.60	0.63	0.15	0.13	0.15	0.13
MgO	7.29	6.35	5.95	9.02	12.66	5.77
CaO	14.35	16.75	9.27	8.84	8.21	9.67
Na_2O	2.29	2.18	3.19	2.30	2.83	2.81
K_2O	1.37	1.63	0.82	1.24	1.15	0.50
P_2O_5	2.00	0.93	0.49	0.38	0.39	0.18
H_2O	2.42	5.65	0.72	2.82	1.12	2.46
CO_2	2.89	1.96	0.03	0.09	0.05	0.29
Total	100.44	100.25	100.53	100.60	101.24	102.02
Li	24.6	16.2	5.84	n.a.	20.6	8.56
Sc	21.7	20.5	21.1	n.a.	19.5	22.6
V	320	334	227	n.a.	183	171
Cr	266	309	88.6	n.a.	497	249
Co	56.2	53.8	56.2	n.a.	60.8	33.0
Ni	150	158	123	n.a.	377	81.7
Cu	185	96.0	61.6	n.a.	59.8	74.5
Zn	206	145	120	n.a.	134	89.7
Ga	26.0	23.4	21.2	n.a.	18.5	20.0
Rb	15.1	19.0	15.2	n.a.	33.5	12.5
Sr	603	535	522	n.a.	447	271
Y	46.5	27.9	26.4	n.a.	20.7	18.4
Zr	245	251	179	n.a.	170	102
Nb	39.3	40.5	31.0	n.a.	30.0	10.8
Mo	1.44	1.40	1.43	n.a.	1.87	n.a.
Sn	1.77	1.87	1.59	n.a.	1.86	1.04
Sb	0.18	0.41	0.05	n.a.	0.11	0.03
Cs	0.29	0.17	0.30	n.a.	2.61	0.22
Ba	211	215	217	n.a.	288	120
La	56.6	32.1	23.4	n.a.	25.4	10.4
Ce	102	69.2	49.5	n.a.	53.2	22.7
Pr	14.9	9.07	6.38	n.a.	6.74	3.01
Nd	62.6	37.4	27.5	n.a.	27.7	13.5
Sm	12.4	8.04	6.44	n.a.	6.20	3.82
Eu	3.90	2.56	2.27	n.a.	1.98	1.41
Gd	11.3	7.17	6.61	n.a.	5.98	4.37
Tb	1.48	1.05	0.99	n.a.	0.86	0.68
Dy	7.28	5.34	5.41	n.a.	4.50	3.95
Ho	1.24	0.90	0.99	n.a.	0.79	0.73
Er	2.94	2.13	2.45	n.a.	1.91	1.78
Tm	0.36	0.26	0.32	n.a.	0.25	0.24
Yb	2.07	1.54	1.99	n.a.	1.50	1.45
Lu	0.28	0.20	0.28	n.a.	0.20	0.20
Hf	5.56	5.28	4.41	n.a.	4.20	2.77
Ta	2.40	2.38	1.84	n.a.	1.73	0.63
Tl	0.03	0.03	0.07	n.a.	0.13	0.04
Pb	1.44	1.58	2.22	n.a.	11.4	1.94
Th	3.40	3.30	2.82	n.a.	4.17	1.56
U	1.48	1.10	0.81	n.a.	1.14	0.42

***Table 3**: Major and Trace element compositions (continued)*

	Canterbury (Oxford Area continued)					
	MSI 25	**MSI 27A**	**MSI 180A**	**MSI 180B**	**MSI 181**	**MSI 183B**
Location	Oxford Area – View Hill	Oxford Area – View Hill	Oxford Area – View Hill	Oxford Area – View Hill	Oxford Area – Burnt Hill	Oxford Area – Browns Rock
Latitude	43°16.603'S	43°17.740'S	43°17.382'S	43°17.382'S	43°22.305'S	42°22.713'S
Longitude	172°02.148'E	172°02.353'E	171°57.288'E	171°57.288'E	172°09.453'E	172°05.213'E
Group	hsg EMII	hsg EMII	hsg EMII	hsg EMII	hsg EMII	hsg EMII
Major elements in wt%						
SiO_2	52.29	52.01	52.36	52.46	52.77	48.23
TiO_2	1.85	2.18	1.93	2.01	1.74	2.23
Al_2O_3	14.40	15.25	14.51	14.67	14.95	15.31
FeO^t	10.01	9.39	10.00	10.39	11.31	10.79
Fe^2O^3	1.12	1.05	1.12	1.17	1.27	1.21
MnO	0.11	0.11	0.10	0.09	0.13	0.16
MgO	6.52	5.43	6.42	6.22	5.98	7.18
CaO	9.32	9.11	8.65	8.47	8.43	10.41
Na_2O	2.54	2.95	2.94	2.78	2.74	3.18
K_2O	0.38	0.76	0.56	0.59	0.43	1.16
P_2O_5	0.20	0.36	0.19	0.20	0.24	0.52
H_2O	1.17	2.35	2.07	1.8	1.54	0.45
CO_2	0.76	0.15	0.08	0.09	0.02	0.01
Total	100.67	101.10	100.93	100.94	101.55	100.84
Li	11.8	8.68	11.8	n.a.	6.36	n.a.
Sc	24.5	19.5	26.0	n.a.	21.7	n.a.
V	200	192	208	n.a.	185	n.a.
Cr	236	148	276	n.a.	193	n.a.
Co	49.4	35.1	48.2	n.a.	39.6	n.a.
Ni	187.0	78.7	187	n.a.	174	n.a.
Cu	86.0	43.7	85.2	n.a.	96.7	n.a.
Zn	106	95.2	106	n.a.	120	n.a.
Ga	19.5	21.3	20.4	n.a.	18.5	n.a.
Rb	7.90	17.4	12.9	n.a.	13.0	n.a.
Sr	277	489	284	n.a.	265	n.a.
Y	20.3	22.1	19.3	n.a.	29.4	n.a.
Zr	112	167	110	n.a.	113	n.a.
Nb	12.7	23.6	12.6	n.a.	13.9	n.a.
Mo	1.02	n.a.	0.92	n.a.	0.73	n.a.
Sn	1.34	1.63	1.25	n.a.	1.35	n.a.
Sb	0.05	0.07	0.04	n.a.	0.05	n.a.
Cs	0.31	0.66	0.13	n.a.	0.43	n.a.
Ba	94.3	211	132	n.a.	163	n.a.
La	11.4	23.2	10.2	n.a.	18.7	n.a.
Ce	24.7	48.8	22.4	n.a.	27.7	n.a.
Pr	3.29	6.15	3.01	n.a.	4.89	n.a.
Nd	14.6	25.6	13.7	n.a.	21.7	n.a.
Sm	4.08	5.87	4.00	n.a.	5.60	n.a.
Eu	1.46	1.92	1.49	n.a.	1.86	n.a.
Gd	4.71	5.80	4.60	n.a.	6.43	n.a.
Tb	0.75	0.85	0.73	n.a.	1.00	n.a.
Dy	4.33	4.72	4.25	n.a.	5.75	n.a.
Ho	0.81	0.86	0.78	n.a.	1.08	n.a.
Er	2.01	2.11	1.92	n.a.	2.66	n.a.
Tm	0.27	0.29	0.26	n.a.	0.36	n.a.
Yb	1.70	1.77	1.61	n.a.	2.20	n.a.
Lu	0.24	0.25	0.22	n.a.	0.30	n.a.
Hf	3.09	4.03	3.11	n.a.	3.09	n.a.
Ta	0.82	1.38	0.79	n.a.	0.86	n.a.
Tl	0.04	0.08	0.05	n.a.	0.07	n.a.
Pb	2.76	4.84	2.15	n.a.	2.30	n.a.
Th	2.21	3.73	1.94	n.a.	1.92	n.a.
U	0.60	0.99	0.54	n.a.	0.48	n.a.

***Table 3**: Major and Trace element compositions (continued)*

	Canterbury (Cookson Volcanics)					
	MSIK 33A	**MSI 36A**	**MSI 41B**	**MSI 42C**	**MSI 45A**	**MSI 49A**
Location	Cookson Volcanics	Cookson Volcanics	Cookson Volcanics	Cookson Volcanics	Cookson Volcanics	Cookson Volcanics
Latitude	42°31.970'S	42°31.882'S	42°37.958'S	42°30.423'S	42°30.687'S	41°52.917'S
Longitude	173°02.172'E	173°03.113'E	172°46.363'E	173°08.837'E	173°10.235'E	174°02.143'E
Group	lsg	hsg	lsg	lsg	hsg	lsg
Major elements in wt%						
SiO_2	39.90	50.46	43.49	44.14	47.04	45.78
TiO_2	4.71	2.85	4.15	3.17	2.76	4.01
Al_2O_3	10.20	13.56	11.89	11.33	12.87	15.21
FeO^t	14.43	11.00	13.06	13.25	11.81	11.50
Fe^2O^3	1.62	1.23	1.47	1.49	1.33	1.29
MnO	0.18	0.15	0.18	0.17	0.16	0.14
MgO	12.48	6.03	9.93	10.61	8.64	3.89
CaO	10.61	8.86	10.87	9.86	10.46	8.89
Na_2O	2.69	3.35	1.93	2.25	2.70	2.73
K_2O	1.36	0.71	1.15	1.26	0.74	1.71
P_2O_5	0.79	0.48	0.80	0.72	0.50	0.77
H_2O	1.9	1.93	1.61	2.11	1.91	2.26
CO_2	0.08	0.26	0.13	0.1	0.09	2.4
Total	100.95	100.87	100.66	100.46	101.01	100.58
Trace elements in parts per million (ppm)						
Li	5.02	4.25	12.7	11.1	15.7	21.8
Sc	21.5	20.5	26.7	19.7	24.4	17.4
V	317	193	302	239	255	266
Cr	318	216	437	292	311	2.00
Co	75.5	47.0	55.3	60.9	50.0	33.8
Ni	338	167	185	261	148	14.4
Cu	70.8	50.0	71.2	60.9	63.4	20.0
Zn	135	125	118	134	119	124
Ga	22.5	22.7	19.9	22.0	21.5	24.7
Rb	34.0	12.0	26.2	23.3	8.86	29.7
Sr	898	572	700	882	520	834
Y	26.7	25.9	30.1	24.1	23.5	32.3
Zr	330	321	286	296	222	373
Nb	63.5	39.55	53.1	55.3	34.5	59.1
Mo	n.a.	n.a.	1.77	n.a.	n.a.	2.80
Sn	2.03	2.56	1.64	2.27	1.83	2.86
Sb	0.09	0.10	0.10	0.08	0.06	0.13
Cs	0.37	0.32	0.46	0.30	0.30	0.44
Ba	433	250	337	337	229	449
La	51.4	33.1	46.7	38.0	25.2	51.1
Ce	110	68.9	102	80.9	54.6	113
Pr	13.8	8.59	12.8	10.3	7.10	14.3
Nd	55.6	35.3	52.5	42.6	30.1	58.2
Sm	11.3	7.90	10.5	9.17	6.98	11.7
Eu	3.48	2.58	3.14	2.91	2.27	3.52
Gd	9.89	7.48	9.56	8.39	6.79	10.3
Tb	1.31	1.07	1.31	1.13	0.97	1.40
Dy	6.49	5.72	6.67	5.76	5.25	7.09
Ho	1.07	1.01	1.16	0.95	0.92	1.24
Er	2.38	2.43	2.82	2.15	2.19	3.04
Tm	0.29	0.32	0.36	0.26	0.29	0.39
Yb	1.60	1.94	2.19	1.53	1.74	2.42
Lu	0.20	0.26	0.30	0.20	0.24	0.33
Hf	7.32	6.90	6.77	6.60	5.14	8.79
Ta	3.72	2.49	3.07	3.28	2.10	3.51
Tl	0.02	0.09	0.02	0.26	0.16	0.10
Pb	2.45	3.06	2.79	2.77	2.68	6.74
Th	4.97	4.84	5.35	4.15	3.11	6.81
U	1.52	1.45	1.49	1.18	0.85	1.90

***Table 3**: Major and Trace element compositions (continued)*

	Canterbury (Cookson Volcanics continued)			**Canterbury (Timaru/Geraldine)**		**Otitia Basalt**
	P 44830 A	**P 44830 B**	**NZS14**	**MSI 6A**	**MSI 8A**	**MSI 63A**
Location	Cookson Volcanics	Cookson Volcanics	Cookson Volcanics	Timaru Basalt	Geraldine Basalt	Otitia Basalt
Latitude	42°15.842'S	42°15.842'S	42°30.455'S	44°24.960'S	44°05.268'S	43°13.913'S
Longitude	173°37.048'E	173°37.048'E	173°10.112'E	171°15.838'E	171°14.328'E	169°48.923'E
Group	hsg	lsg	hsg	hsg EMII	hsg EMII	lsg
Major elements in wt%						
SiO_2	46.16	45.43	48.00	52.69	47.93	45.85
TiO_2	3.22	3.36	2.71	1.48	2.27	3.44
Al_2O_3	11.81	11.61	12.86	13.51	15.56	14.25
FeO^t	12.07	12.54	12.37	11.25	11.15	10.58
Fe^2O^3	1.35	1.41	1.39	1.26	1.25	1.19
MnO	0.15	0.16	0.16	0.16	0.14	0.61
MgO	8.02	8.14	8.72	7.66	5.94	6.31
CaO	9.32	9.31	9.21	8.86	9.93	10.74
Na_2O	2.08	2.05	2.98	2.56	2.76	2.98
K_2O	0.64	0.58	1.02	0.25	1.20	1.39
P_2O_5	0.51	0.55	0.50	0.12	0.55	0.53
H_2O	1.92	2.1	1.69	0.49	1.44	2.65
CO_2	3.09	3.41	0.03	0.01	0.04	0.25
Total	100.34	100.86	101.64	100.30	100.16	100.77
Trace elements in parts per million (ppm)						
Li	21.6	n.a.	13.2	4.91	11.2	59.7
Sc	22.6	n.a.	22.9	23.7	24.0	32.1
V	246	n.a.	252	173	236	329
Cr	271	n.a.	281	288	233	142
Co	53.8	n.a.	55.2	46.8	33.8	52.1
Ni	199	n.a.	187	190	95.3	99.6
Cu	61.7	n.a.	69.0	59.6	46.7	72.5
Zn	140	n.a.	131	106	103	117
Ga	22.3	n.a.	21.9	18.2	20.6	19.6
Rb	13.7	n.a.	22.8	5.72	31.1	25.5
Sr	608	n.a.	435	187	560	1160
Y	28.3	n.a.	24.2	19.3	23.3	27.0
Zr	227	n.a.	217	75.1	176	265
Nb	33.4	n.a.	33.1	6.69	48.5	53.8
Mo	1.16	n.a.	1.37	0.57	n.a.	1.13
Sn	1.70	n.a.	1.98	1.02	1.52	2.23
Sb	0.13	n.a.	0.08	0.04	0.06	0.04
Cs	0.64	n.a.	0.30	0.17	1.07	1.22
Ba	175	n.a.	232	84.5	409	1427
La	27.1	n.a.	26.0	6.33	31.6	41.0
Ce	59.6	n.a.	56.0	14.6	60.5	85.1
Pr	7.82	n.a.	7.14	1.98	7.55	10.4
Nd	32.8	n.a.	30.6	9.47	30.4	42.3
Sm	7.54	n.a.	7.07	3.11	6.43	8.70
Eu	2.49	n.a.	2.30	1.21	2.15	2.77
Gd	6.98	n.a.	6.94	3.82	6.26	8.09
Tb	1.05	n.a.	1.02	0.65	0.90	1.15
Dy	5.57	n.a.	5.48	3.89	4.95	6.12
Ho	0.97	n.a.	0.96	0.74	0.89	1.09
Er	2.33	n.a.	2.33	1.88	2.19	2.68
Tm	0.30	n.a.	0.30	0.26	0.29	0.36
Yb	1.80	n.a.	1.81	1.64	1.79	2.17
Lu	0.25	n.a.	0.25	0.23	0.25	0.30
Hf	5.09	n.a.	5.19	2.26	4.01	6.42
Ta	2.01	n.a.	1.98	0.40	2.70	3.26
Tl	0.08	n.a.	0.19	0.03	0.04	0.07
Pb	1.71	n.a.	2.86	1.34	3.85	2.69
Th	2.90	n.a.	3.30	1.09	4.46	4.84
U	0.83	n.a.	0.89	0.24	1.08	0.87

***Table 3**: Major and Trace element compositions (continued)*

		Arnott Basalt			Alpine Dike Swarm	
	MSI 63E	**MSI 65A**	**MSI 66**	**MSI 67**	**MSI 69B**	**MSI 70B**
Location	Otitia Basalt	Arnott Basalt	Arnott Basalt	Arnott Basalt	Alpine Dike Swarm	Alpine Dike Swarm
Latitude	43°13.913'S	43°42.508'S	43°42.728'S	43°42.718'S	44°36.130'S	44°32.242'S
Longitude	169°48.923'E	169°14.233'E	169°13.717'E	169°13.783'E	168°53.962'E	168°53.387'E
Group	lsg	lsg	lsg	lsg	lsg	lsg
Major elements in wt%						
SiO_2	45.78	44.07	43.13	43.65	43.17	40.52
TiO_2	3.99	4.03	3.91	4.31	3.48	3.81
Al_2O_3	16.50	18.44	15.04	15.47	14.85	13.24
FeO^t	10.95	8.15	12.32	12.74	12.09	14.55
Fe^2O^3	1.23	0.91	1.38	1.43	1.36	1.63
MnO	0.28	0.64	0.15	0.19	0.20	0.24
MgO	4.81	1.80	6.54	5.28	5.83	6.35
CaO	9.45	10.33	12.38	11.03	9.20	9.90
Na_2O	2.79	3.77	2.21	2.64	4.49	3.33
K_2O	2.01	1.63	0.91	1.27	1.70	1.84
P_2O_5	0.63	1.29	0.57	0.78	1.00	1.45
H_2O	2.77	2.51	2.25	2.18	2.86	2.07
CO_2	0.09	3.38	0.46	0.28	0.68	1.33
Total	101.28	100.95	101.25	101.25	100.91	100.26
Trace elements in parts per million (ppm)						
Li	57.7	20.3	17.5	23.2	25.4	40.8
Sc	24.1	17.5	29.3	24.2	15.2	14.7
V	334	265	354	361	264	245
Cr	29.3	60.3	251	66.9	54.4	3.78
Co	41.1	37.1	44.5	41.2	38.5	42.7
Ni	27.9	37.2	101	50.7	50.6	27.4
Cu	34.8	25.8	60.2	51.5	58.3	41.6
Zn	118.8	146	110	123	143	171
Ga	24.3	21.3	20.5	21.9	27.9	26.0
Rb	41.3	30.0	14.7	21.0	30.4	40.8
Sr	1506	1293	677	884	848	1284
Y	30.5	35.9	28.0	33.1	35.7	41.8
Zr	319	391	251	315	446	475
Nb	62.5	74.1	54.1	65.4	128	111
Mo	n.a.	2.05	n.a.	1.24	2.15	5.00
Sn	2.08	0.93	1.81	1.33	1.97	1.29
Sb	0.06	0.06	0.08	0.13	0.21	0.08
Cs	2.98	1.06	0.32	1.25	3.25	0.76
Ba	673	551	258	417	520	914
La	44.7	66.3	37.6	54.1	102	116
Ce	95.2	137	81.8	115	196	229
Pr	11.9	16.9	10.5	14.0	22.4	27.4
Nd	48.2	68.1	43.2	56.1	82.3	103
Sm	9.84	13.1	9.02	10.9	14.2	17.8
Eu	3.08	4.15	2.85	3.39	4.17	5.14
Gd	8.92	11.6	8.28	9.98	12.1	15.1
Tb	1.25	1.58	1.15	1.37	1.58	1.93
Dy	6.70	8.17	6.20	7.13	7.73	9.34
Ho	1.20	1.46	1.11	1.28	1.34	1.59
Er	2.92	3.60	2.71	3.18	3.36	3.89
Tm	0.39	0.47	0.36	0.42	0.43	0.49
Yb	2.37	2.91	2.20	2.59	2.65	2.97
Lu	0.33	0.41	0.31	0.36	0.36	0.40
Hf	7.18	8.50	6.08	7.30	9.82	10.8
Ta	3.71	3.60	3.21	3.74	6.67	5.65
Tl	0.12	0.08	0.02	0.03	0.15	0.09
Pb	2.59	2.73	1.94	2.20	5.11	5.79
Th	4.91	7.35	3.79	5.77	13.9	11.8
U	1.38	2.14	1.06	1.58	3.97	3.25

***Table 3**: Major and Trace element compositions (continued)*

	Alpine Dike Swarm				**Otago (Dunedin Volcano)**	
	MSI 71A	**MSI 72A**	**MSI 73**	**Lake Hawea 3**	**30-10-02-1**	**12-11-02-3**
Location	Alpine Dike Swarm	Alpine Dike Swarm	Alpine Dike Swarm	Alpine Dike Swarm	Aramoana	Mount Holmes
Latitude	44°32.185'S	44°30.492'S	44°30.585'S		45°46.733'S	45°48.983'S
Longitude	168°53.362'E	168°45.148'E	168°45.013'E		170°42.183'E	170°34.633'E
Group	lsg	lsg	lsg	lsg	lsg	lsg
Major elements in wt%						
SiO_2	41.97	42.34	43.48	41.43	45.50	45.12
TiO_2	3.95	3.68	3.63	3.88	2.93	2.37
Al_2O_3	14.38	14.32	14.06	13.51	15.83	14.20
FeO^t	12.49	12.00	12.60	13.70	12.22	12.23
Fe^2O^3	1.40	1.35	1.42	1.54	1.37	1.37
MnO	0.19	0.15	0.18	0.19	0.19	0.18
MgO	5.97	7.00	6.01	6.56	5.43	8.64
CaO	9.64	9.69	9.00	9.02	9.32	9.46
Na_2O	3.78	2.98	3.48	2.94	4.05	3.38
K_2O	2.44	1.88	2.11	2.44	1.40	1.45
P_2O_5	1.34	0.80	0.90	1.23	0.76	0.59
H_2O	2.5	2.39	3.45	1.2	1.2	1.41
CO_2	0.27	2.3	1.02	0.07	0.07	0.03
Total	99.63	99.68	99.63	97.71	100.27	100.43
Trace elements in parts per million (ppm)						
Li	35.3	n.a.	n.a.	38.8	8.55	7.27
Sc	17.3	n.a.	n.a.	17.1	17.8	22.4
V	294	n.a.	n.a.	290	223	242
Cr	21.0	n.a.	n.a.	12.0	68.1	304
Co	40.6	n.a.	n.a.	46.7	38.9	53.8
Ni	35.1	n.a.	n.a.	36.8	51.4	168
Cu	68.6	n.a.	n.a.	44.2	41.2	62.4
Zn	141.8	n.a.	n.a.	157	132	118
Ga	24.1	n.a.	n.a.	25.3	24.7	20.1
Rb	52.4	n.a.	n.a.	50.0	30.7	32.1
Sr	1151	n.a.	n.a.	1044	811	728
Y	36.8	n.a.	n.a.	34.8	33.7	26.0
Zr	452	n.a.	n.a.	457	283	242
Nb	130	n.a.	n.a.	133	69.0	56.5
Mo	n.a.	n.a.	n.a.	2.35	3.08	2.60
Sn	2.57	n.a.	n.a.	2.84	2.00	1.68
Sb	0.08	n.a.	n.a.	0.46	0.07	0.06
Cs	12.6	n.a.	n.a.	1.43	0.50	0.40
Ba	836	n.a.	n.a.	934	411	404
La	98.6	n.a.	n.a.	100	47.0	38.5
Ce	196	n.a.	n.a.	1941	95.9	78.2
Pr	23.2	n.a.	n.a.	22.4	11.6	9.20
Nd	87.9	n.a.	n.a.	84.9	44.6	35.0
Sm	15.4	n.a.	n.a.	14.9	8.78	6.80
Eu	4.47	n.a.	n.a.	4.42	2.75	2.07
Gd	12.8	n.a.	n.a.	12.4	7.65	5.87
Tb	1.64	n.a.	n.a.	1.64	1.16	0.90
Dy	8.28	n.a.	n.a.	8.08	6.14	4.74
Ho	1.42	n.a.	n.a.	1.39	1.10	0.84
Er	3.40	n.a.	n.a.	3.38	2.80	2.13
Tm	0.44	n.a.	n.a.	0.43	0.37	0.28
Yb	2.64	n.a.	n.a.	2.60	2.32	1.77
Lu	0.36	n.a.	n.a.	0.35	0.32	0.25
Hf	9.55	n.a.	n.a.	9.83	5.47	4.79
Ta	7.08	n.a.	n.a.	7.56	3.83	3.10
Tl	0.14	n.a.	n.a.	0.12	0.04	0.04
Pb	7.03	n.a.	n.a.	5.51	2.82	2.69
Th	11.5	n.a.	n.a.	12.5	5.10	4.47
U	3.25	n.a.	n.a.	3.67	1.37	1.20

***Table 3**: Major and Trace element compositions (continued)*

	30-11-02-1	**OU22636**	**MSI 87**	**MSI 90A**	**MSI 95**	**SO168DR19-1**
Location	Long Beach	Mt. Cargill	Otago Peninsula	Otago Peninsula	Otago Peninsula	Rowling B Smt.
Latitude	45°46.233'S		45°51.342'S	45°47.032'S	45°18.188'S	39°33.650'S
Longitude	170°40.450'E		170°43.180'E	170°43.448'E	170°34.443'E	179°13.660'E
Group	lsg	lsg	lsg	lsg	lsg	lsg
Major elements in wt%						
SiO_2	48.97	49.93	45.31	46.12	50.08	41.35
TiO_2	1.50	1.26	2.3	1.89	1.72	3.70
Al_2O_3	16.95	19.05	18.03	15.12	17.51	16.21
FeO^t	8.77	8.32	9.08	10.87	9.53	14.57
Fe^2O^3	0.99	0.93	1.02	1.22	1.07	1.64
MnO	0.20	0.18	0.17	0.20	0.21	0.27
MgO	4.58	2.48	3.95	7.29	3.26	12.85
CaO	5.53	5.54	9.23	8.01	6.19	11.05
Na_2O	7.51	7.58	3.20	4.83	5.53	2.02
K_2O	2.88	3.19	1.62	2.12	2.73	0.99
P_2O_5	0.41	0.61	0.69	0.88	0.56	0.78
H_2O	0.59	2.03	1.6	1.15	1.56	1.89
CO_2	0.27	0.04	3.72	0.06	0.08	0.04
Total	99.15	101.14	99.92	99.76	100.03	100.07
Trace elements in parts per million (ppm)						
Li	26.2	13.8	10.7	n.a.	18.3	5.98
Sc	10.8	6.68	10.8	n.a.	8.40	19.1
V	112	76.4	145	n.a.	95.5	240
Cr	129	26.6	22.7	n.a.	27.8	362
Co	27.8	18.0	28.3	n.a.	21.7	69.1
Ni	91.7	25.7	28.8	n.a.	22.0	375
Cu	30.0	29.4	30.8	n.a.	26.8	87.0
Zn	180	114	98.6	n.a.	135	175
Ga	32.5	25.1	22.3	n.a.	26.4	21.3
Rb	124	78.2	40.8	n.a.	99.3	19.6
Sr	1072	1488	841	n.a.	620	596
Y	39.6	30.8	26.4	n.a.	35.6	43.2
Zr	780	446	257	n.a.	557	303
Nb	171	120	70.8	n.a.	125	65.1
Mo	10.2	6.19	n.a.	n.a.	n.a.	3.08
Sn	5.55	3.19	2.18	n.a.	4.84	2.57
Sb	0.47	0.13	0.13	n.a.	0.26	0.41
Cs	1.54	1.46	2.14	n.a.	2.30	0.48
Ba	591	1118	498	n.a.	430	286
La	107	82.0	48.1	n.a.	85.4	59.6
Ce	175	147	92.8	n.a.	148	117
Pr	17.4	15.4	10.8	n.a.	15.4	16.3
Nd	56.0	53.3	40.6	n.a.	53.0	66.6
Sm	9.51	9.13	7.71	n.a.	9.27	14.1
Eu	2.63	3.10	2.49	n.a.	2.57	4.47
Gd	7.81	8.15	6.95	n.a.	8.37	13.6
Tb	1.27	1.15	0.98	n.a.	1.21	1.79
Dy	6.84	6.09	5.41	n.a.	6.89	9.13
Ho	1.23	1.13	1.00	n.a.	1.32	1.53
Er	3.26	2.97	2.56	n.a.	3.56	3.55
Tm	0.45	0.42	0.36	n.a.	0.53	0.43
Yb	2.76	2.66	2.26	n.a.	3.33	2.45
Lu	0.36	0.38	0.32	n.a.	0.46	0.33
Hf	12.1	8.34	5.12	n.a.	9.82	7.32
Ta	10.6	6.63	4.07	n.a.	8.05	3.83
Tl	0.19	0.10	0.23	n.a.	0.10	1.00
Pb	13.3	7.79	4.26	n.a.	9.33	5.98
Th	30.5	13.9	6.73	n.a.	19.7	6.41
U	7.08	3.89	1.95	n.a.	5.33	1.48

*Presumably strongly affected by seawater alteration

Chapter IV

Melting processes by Rayleigh-Taylor instabilities beneath Continents: Evidence from Cenozoic intraplate volcanism on Zealandia, SW Pacific

Abstract

On the New Zealand micro-continent, Zealandia, intraplate volcanism was widespread and continuous throughout the Cenozoic, erupting predominantly low volumes of alkaline lava. The absence of linear chains of volcanoes, which become older in the direction of plate motion (combined with the lack of anomalously hot mantle or large extensional structures) is inconsistent with the presence of a single or multiple stationary thermal anomalies beneath Zealandia. A possible mechanism that can explain this diffuse intraplate volcanism is lithospheric removal through Rayleigh-Taylor instabilities. In order to better understand non-plume and non rift-related intraplate volcanism, we performed two-dimensional modeling using the finite element method. We show that removal of the lower lithosphere by Rayleigh-Taylor instabilities and subsequent upwelling of the upper asthenosphere can trigger intraplate volcanism beneath Zealandia, but the degree of melting is of course strongly dependent on the composition and H_2O content of the upwelling mantle. The presence of slightly hydrated asthenosphere, containing pyroxene-bearing plume-related fragments, is supported by the geological history of Zealandia, which was situated above an active subduction zone in the Mesozoic and affected by plume activity in the Late Cretaceous while separating from Gondwana. We also considered the effects of edge driven convection to generate a more realistic picture of asthenospheric mantle flow beneath Zealandia

4.1 Introduction

The reason why volcanic activity occurs within tectonic plates is a matter of active debate. Stationary upwelling of hot mantle material (thermal plume) originating in the

deep mantle was assumed as one of the major processes for the cause of intraplate volcanism (e.g. Morgan, 1971). A second model involves a substantial thinning of the lithosphere and the subsequent upwelling of shallow mantle, causing pressure release melting (e.g. Weaver and Smith, 1989). Major extension and plume activity generally lead to extensive volcanic activity and are therefore contrary to diffusively and continuously occurring low-volume Cenozoic intraplate volcanism on the New Zealand micro-continent, Zealandia (e.g. Coombs et al., 1986; Cooper et al., Weaver and Smith, 1989). For Zealandia, it has been proposed that a gravitationally unstable lower lithosphere was subjected to multiple delamination events during the Cenozoic (Panter et al., 2006; Hoernle et al., 2006; Timm et al., in review) causing upwelling of the upper asthenosphere and subsequent decompression melting. The concept of an anomalously dense lower lithosphere is supported by the geological history of Zealandia. Located at the NW margin of Gondwana, Zealandia was exposed to subduction-related volcanism during the Mesozoic (e.g. Muir et al., 1995). Whereas the influx of subduction-related fluids and hydrous melts from the subducting Phoenix plate is likely to have metasomatized the Zealandia lithosphere adding hydrous phases, subduction-related melts may also have re-fertilized the subcontinental lithosphere with basaltic veins, now turned into eclogite, and thereby further increased its density with respect to the underlying asthenospheric mantle. In addition, plume-related melts, associated with the separation of Zealandia from Gondwana, the froze in the lower lithosphere, would also have contributed to the density increase and presumably weakened this layer, which as a result became negatively buoyant and more susceptible to the process of lithospheric removal by Rayleigh-Taylor instabilities. Using finite element modeling, we will test Rayleigh-Taylor type removal of a dense layer at the base of the lithosphere as a melting trigger beneath Zealandia.

4.2 Geological and Geochemical Background of Zealandia

Major continental rifting associated with voluminous volcanism ended with the final separation of Zealandia from the former super-continent Gondwana ~ 85 million years ago. This late Cretaceous volcanic activity was attributed to plume activity (e.g. Weaver et al., 1994; Storey et al., 1999). Since then, the micro-continent drifted ~

6000 km to the NW. While drifting, widespread diffuse but continuous volcanic activity of predominately alkaline character formed two volcanic endmembers throughout the Cenozoic: monogenetic volcanic fields (e.g. Waipiata Volcanic Field, Oxford Volcanics, Alpine Dike Swarm, Urry Knolls, Orton and Veryan Banks) and larger volcanic fields including composite shield volcanoes (e.g. Banks Peninsula and Dunedin volcanoes on the South Island of New Zealand, the Auckland, Campbell, Antipodes Islands on the Campbell Plateau and; see Timm et al., in review, for more detailed information about the sample locations).

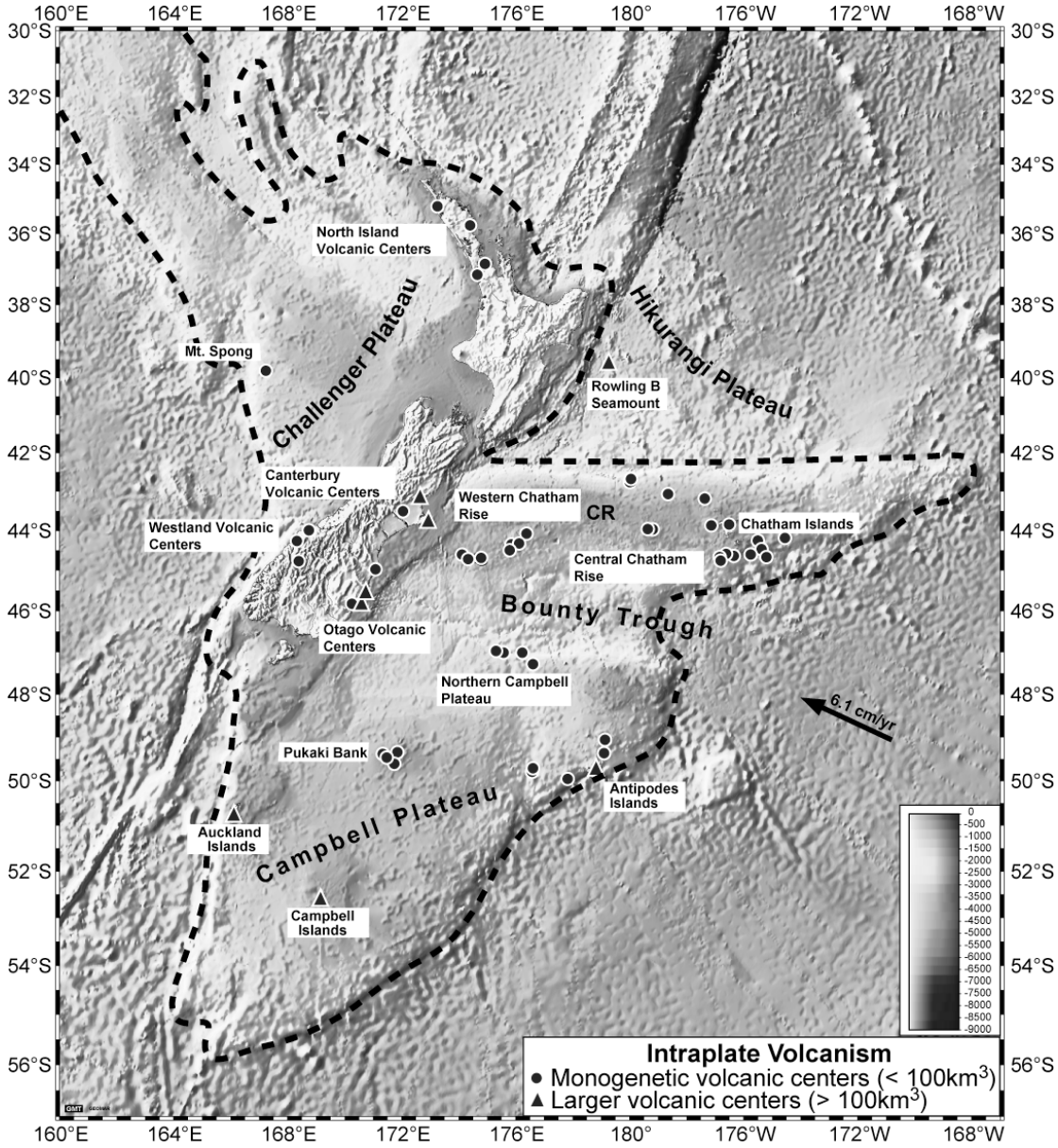

Fig. 4.1: Schematic map of the New Zealand micro-continent Zealandia. Black circles represent locations of the monogenetic volcanic fields, whereas the black triangles mark the locations of larger volcanic centers.

The monogenetic volcanic fields represent low-volume volcanism (< 100 km^3), which occurred episodically over up to ~20 Ma (e.g. Hoernle et al., 2006; Panter et al., 2006). The composite shield volcanoes instead form single volcanic complexes, having volumes >100 km^3 of up to ~ 1600 km^3 (in case of Banks Peninsula). Composite shield volcanoes on the South Islands (Dunedin, Lyttelton and Akaroa) were largely formed within 4 Ma (Hoernle et al., 2006; Timm et al., in review).

The absence of linear chains of volcanoes becoming progressively older in direction of plate motion is inconsistent with the classical theory of a stationary thermal anomaly beneath Zealandia (Fig. 4.1). In addition, no shallow, unusually warm asthenospheric mantle material, displayed by low velocity zones was imaged by seismic tomography. (Montelli et al., 2006; Nolet et al., 2006; Priestley and McKenzie, 2005), although a deep-seated low velocity zone (~600 – 1450 km) extends from beneath the Chatham Rise to Antarctica (Montelli et al., 2006; Li et al., 2008), which has been interpreted as thermal anomaly (Nolet et al., 2006). Multiple small-scale structures less than 100 km in diameter, however, are unlikely to be resolved in global tomographic studies. Major continental rifting ended with the final separation of Zealandia from Gondwana. Since then, the tectonic regime allowed only minor rifting events (Weaver et al., 1989), which cannot adequately account for the larger volumes of magma required to form for example shield volcanoes, such as Banks Peninsula (~ 1600 km^3).

All mafic Cenozoic intraplate volcanic rocks from Zealandia (MgO > 6 wt%) range from basanite through alkali basalt to tholeiites and resemble oceanic island basalts (OIB), having positive Nb and Ta and negative K and Pb anomalies on multi-element diagrams. Furthermore, based on FeOt vs. SiO2; Figure 2.7 the depth of partial melting ranges between ~70-100 km. These depth estimates are in good agreement with calculated mantle temperatures of ~ 1320 - ~1400°C (after Herzberg et al., 2007), falling into the range of common upper asthenospheric mantle temperatures (Green and Falloon, 2001; Herzberg et al., 2007). The super-chondritic Zr/Hf ratios, together with high FeO^t, TiO_2, Nb/Ta, $(Sm/Yb)_N$ Sr/Y, $^{206}Pb/^{204}Pb$, $^{208}Pb/^{204}Pb$ (> 19.5 and 39.3, respectively) and low SiO_2, $^{87}Sr/^{86}Sr$ (< 0.7040), εNd (< 6) and εHf (< 8) indicates a HIMU-type source component, derived by partial melting of garnet pyroxenite and/or eclogite (Hoernle et al., 2006; Timm et al., in review). It has been experimentally demonstrated, that carbonated eclogite and/or garnet

pyroxenite can act as source material for the generation of silica-undersaturated volcanic rocks, such as basanite to alkali basalts (e.g. Pertermann et al., 2004; Hirschmann et al., 2003; Kogiso et al., 2006; Dasgupta et al., 2006). The formation of more silica-saturated EMII-type volcanics emplaced on Zealandia has been predominantly attributed to extensive interaction between the low silica asthenospheric melts and the continental lithosphere, whereas higher silica content and MORB-like composition reflect partial melting of a more depleted source as described in Hoernle et al., 2006. Since lithospheric thickness beneath Zealandia range today from ~ 70 - 100 km, which increases to ~ 140 km beneath the Southern Alps (Stern et al., 2002; Molnar et al., 1998) a minimal melting depth of ~85 km (suggested by the presence of garnet and based on FeO^t vs. SiO_2; Figure 2.7) is generally consistent with initial partial melting in the upper asthenosphere.

The formation of the monogenetic volcanic fields are attributed to low degree melting of predominantly carbonated garnet pyroxenite and/or eclogite (e.g. Hoernle et al. 2006, Timm et al., in review), whereas the shield lavas of the larger volcanoes are slightly more depleted in composition and therefore reflect generally higher degrees of partial melting of a similar heterogeneous upper asthenosphere involving higher quantities of garnet peridotite. This requires larger cavities at the lithospheric base beneath the shield volcanoes than beneath the monogenetic volcanic fields, resulting in different melting columns heights and therefore generally more depleted MORB-like composition of shield lavas. The Dunedin Volcano and the composite shield volcanoes of Banks Peninsula are located within the center of monogenetic volcanic fields, the Waipiata Volcanic Field and the Oxford Volcanics, respectively and became active towards the end of volcanic activity of the fields. This implies that the cavities that form in response to the removal process develop in a time progressive fashion, resulting in diffuse volcanism first followed by greater outpourings of magma.

4.3 Lithospheric removal (delamination)

In this section we focus on ductile delamination (removal) by density contrasts, created by changing compositions and varying phase assemblages. It has been shown that the lower lithosphere can form instabilities at their base at thickened convergent

continental plates margins, e.g. through thermal contraction and phase changes increasing the density of the lower lithosphere (e.g. Conrad and Molnar, 1997; Kay and Kay, 1993) and convective thinning (e.g. Molnar et al., 1998; Houseman et al., 2000). Melts coming from an active subduction zone may intrude the subcontinental lithosphere and freeze as eclogite veins, and therefore increase its density with respect to the underlying mantle. It has been found, that ~10% eclogite will increase the density by ~1% (Kay & Kay, 1993), which is consistent with the findings of Jull & Kelemen (2001), who proposed that mantle compositions derived from arc magmatism are 1 - 5% denser than "unmodified" mantle. A density contrast of ~1% between a dense lower lithosphere above a less dense asthenosphere is sufficient to drive gravitational instabilities at the interface (Conrad and Molnar, 1996). Gravitational instabilities without thermal diffusion at the base of the lithosphere can be approximated as Rayleigh-Taylor instabilities (Conrad and Molnar, 1996). Rayleigh-Taylor instabilities develop dominant wavelengths that depend mainly on the relative thickness of the unstable layer and the viscosity contrast. These relations can be analyzed using linear stability analysis (e.g. Turcotte and Schubert, 2001, Kaus, 2004). Figure 4.2a shows that the dominant wavelength decreases with decreasing layer size. A thin layer, for instance, results in a higher frequency of the perturbations and subsequently in the formation of more instabilities with lower growth rates (Fig.4.2a). A thicker layer results in the formation of a longer wavelength and consequently less abundant faster growing instabilities (after Kaus, 2004). The viscosity contrast (μ_2/μ_1) mainly affects the growth rate of the instabilities but also has some control on wavelength. Figure 4.2b shows that high viscosity contrasts result in lower growth rates. The Formation and evolution of Rayleigh-Taylor instabilities is therefore mainly controlled by the thickness of the unstable layer and the relative viscosity contrast.

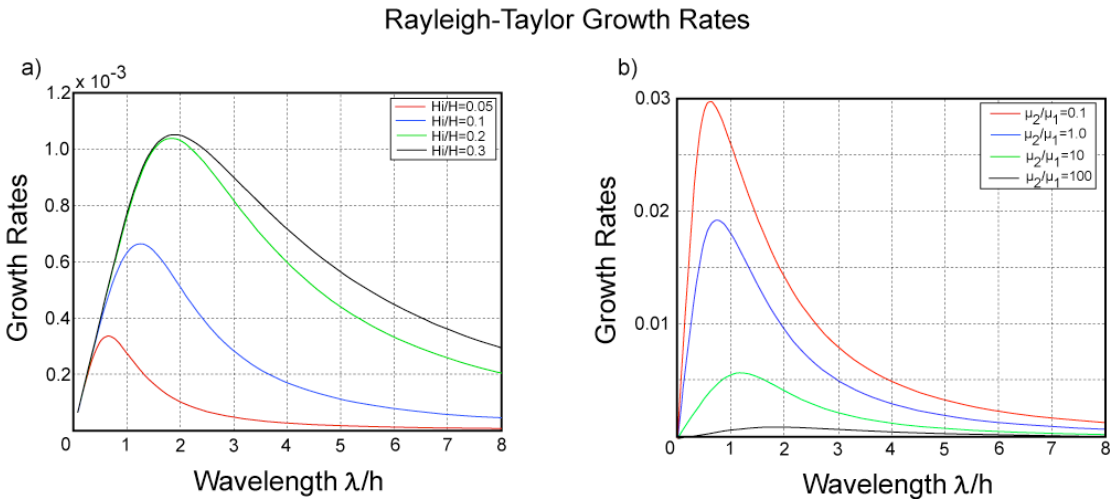

Fig.4.2a-2b: Results from linear stability analysis following Kaus (2004). In (a) the dependence of the dominant wavelength on layer thickness is shown; (b) illustrates how the growth rate is controlled by the relative viscosity contrast.

Conrad and Molnar, 1996 demonstrated that a typical wavelength of a Rayleigh Taylor instability is ~100 – 200 km. Since this perturbation is similar to the thickness of the lithosphere, topographic changes (tens of meters) above down- and upwelling of the lower lithosphere and upper asthenosphere, respectively, are insignificant (Conrad and Molnar, 1996; Elkins-Tanton, 2007) form.

The concept of a dense and gravitationally unstable lower lithosphere forming Rayleigh-Taylor instabilities was proposed to be a mechanism to explain continental intraplate volcanism by several studies (e.g. Kay and Kay, 1993; Elkins-Tanton, 2005 and 2007; Korenaga, 2005). Elkins-Tanton (2007 and 2005) showed the general possibility to generate melts by Rayleigh-Taylor instabilities at the interface of a dense lower lithosphere and a less dense upper asthenosphere by decompression and possible devolatization of the down-welling lithosphere. Korenaga (2005) attributed the formation of younger (~90 Ma) volcanism on the Ontong Java plateau to detachment of dense lower lithosphere beneath the plateau, containing eclogitic and garnet-pyroxenitic components and Fe-rich garnet lherzolite, which drive local convection currents. Consequently, the detached lower lithosphere upwells locally and partially melts by decompression. Elkins-Tanton and Hager (2000) proposed lithospheric delamination as a trigger for extensive volcanism, forming the Siberian flood basalt province, which represents the largest preserved continental flood basalt event on Earth. Barry et al. (2006) attributed the formation of diffusively occurring basaltic Cenozoic intraplate volcanism in Mongolia to partial melting through lithospheric delamination as also recognized for other diffuse Cenozoic basalt

provinces in NE China (e.g. Menzies, 1993) and Vietnam (Hoang and Flower, 1998). Molnar and Jones (2004) demonstrated that lithospheric removal took place beneath the Sierra Nevada between ~10 and 3 Ma as Rayleigh-Taylor like instabilities formed through convection. In order to better understand the generation of intraplate volcanism on the Zealandia micro-continent, we applied a viscous flow model as summarized below.

4.4 Model Setup

We use a thermal convection model to simulate lithospheric removal beneath Zealandia. The mantle flow model is based on the equations for incompressible viscous flow, which are solved with the finite element method. We use a seven-velocity node triangular element with linear pressure variations. Viscosity can either be constant or temperature dependent. In order to accurately track material boundaries, we use a Lagrangian mesh. If the computational mesh becomes too distorted during the calculations, it is automatically remeshed. The temperature evolution is also computed with the finite element method.

Figure 4.3 shows the model set-up and a low-resolution mesh. The size of the modeling domain is 1800 km by 600 km. Zealandia is approximated by a 30 km crustal layer (ρ_0 = 2800 kg/m^3; red), a 40 km layer of normal lithospheric mantle (ρ_1 = 3250 kg/m^3; yellow), and a 35 km thick layer of slightly more enriched and consequently denser lithospheric mantle layer (ρ_3 = 3300+1.5% kg/m^3; cyan). Each layer has its distinct material properties. The upper mantle (ρ_4 = 3300 kg/m^3; blue) has a temperature dependent viscosity that exponentially increases from 1e20 [Pa s] at 1700°C to 1e24 [Pa s] at the surface. The enriched lithospheric mantle layer has a viscosity of 5e20 [Pa s], the normal lithospheric mantle a viscosity of 1e22 [Pa s], and the crust a viscosity of 1e23 [Pa s].

The mechanical boundary conditions are no flow at the top and bottom and symmetry at the sides. The thermal boundary conditions are constant temperature at the top and bottom and zero heat flow at the sides.

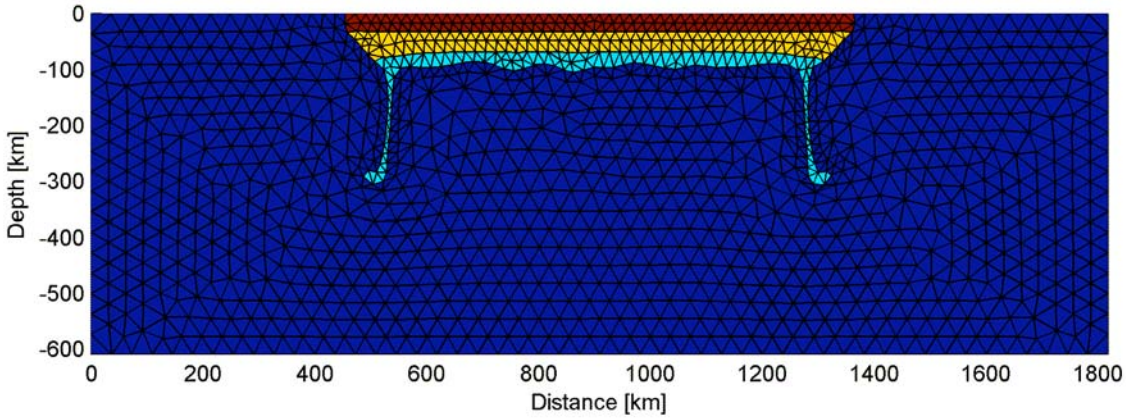

Fig. 4.3: Model setup as described above. For the model runs a high-resolution mesh with about 60.000 elements was used.

4.5 Results

4.5.1 Temporal and spatial development of the Rayleigh-Taylor instabilities

Figure 4.4 and 4.5 show the result of a reference model run. After ~10 Ma the upper asthenosphere has already begun to develop large convection cells (~400 km in diameter) at both sides of the continental lithosphere. These cells develop in the first few million years and develop independently of the chosen viscosities (see section above). The convection cells accelerate the growth of gravitational instabilities at both edges of the continental lithosphere significantly, compared to the development of these instabilities at the base beneath the continental lithosphere. The first instabilities, therefore develop at the edges on the continental lithosphere in the first 10 Ma (Fig. 4.4a). In the following ~10 Ma, the tips of the outer instabilities reach a depth of ~200 km, which result in the development of additional smaller convection cells at the inner sides of the instabilities. The downwelling rate of the lower subcontinental lithosphere at the edges is therefore ~10 km Ma^{-1} in the first 20 Ma (Fig. 4.3b). For a thickness of the lower unstable lithosphere of ~35 km, nine "subcontinental" perturbations with wavelength of ~80 – 100 km and a maximum downwelling of ~30 - 80 km (resulting in a maximum height of ~ 20 km above the initial position of the lower lithosphere) formed after ~30 Ma (Fig.4.4c). Meanwhile the outer anchor-shaped instabilities descended to ~500km, which is a velocity increase by the factor 2, compared to the downwelling rate in the first 20 Ma. The increased downwelling rate is consistent

with stronger convection, as indicated in Fig.4.4c. The inner perturbations become increasingly affected by the large-scale convection formed at the inner parts of the "edge instabilities", resulting in the formation of instabilities at the both sides of the continent bent slightly towards the outer continental edges (Fig. 4.4c-d).

After ~40 Ma three larger (up to 100 km) instabilities are developed from nine initial perturbations, with maximum heights of ~25 -30 km between the two convection driven instabilities at the edge of the continent, which reached the transition zone and flow laterally to both sides (Fig. 4.4d). In response to the large-scale edge-driven convection and due to mass balance, the lower (> 600 km) warmer asthenospheric mantle (1700°C) starts to stream up locally.

After ~50 Ma four large ~150 - 200 km wide by ~50 km high cavities were formed at the base of the lithosphere, similar to those proposed by Conrad and Molnar (1996). The instabilities beneath the central part of the micro-continent develop inverted mushroom-like shapes at their lower tips with thin connections of ~5-10 km in diameter extending to the lowermost lithosphere, reaching maxim depths of ~250 km after ~50 Ma. The lateral edge driven flow along the transition zone forms viscous folding structures that are recycled back into the upper asthenosphere through the upwelling of hot asthenosphere. With the growth of "subcontinental" instabilities, smaller-scaled convection cells develop at the sides of all instabilities, accelerating the downwelling of the lower lithosphere and the subsequent upwelling of the upper asthenosphere.

The change in the convective flow results in the widening of the right "subcontinental" cavities by moving the instabilities away from each other, which can be observed after ~60 Ma running time. The progressive downwelling of the lower lithospheric mantle results in increasing upwelling at both sides of the continent and in the middle beneath the lithosphere. The middle upwelling ascended within the following 10 Ma, reaching its base at ~70 Ma (Fig.4.4g).

After ~79 Ma most of the unstable lithosphere is removed and partly recycled back into the upper asthenosphere through the upwellings at ~600 km (Fig.4.4h). This is consistent with more voluminous volcanism towards later stages in the Cenozoic, as already suggested by Timm et al., in review; Figure 3.4.

4.5.2 Partial melting by Rayleigh-Taylor instabilities and the influence of H_2O

The occurrence of partial melting by decompression is strongly dependent on the temperature, source composition (e.g. fertility of peridotite, eclogite, pyroxenite) and probably most important on the presence of H_2O and CO_2 in the source, which can lower the solidus of dry mantle rocks significantly. The presence of H_2O and CO_2 in the source beneath Zealandia are likely, because is the subduction-metasomatized lower lithosphere sinks, pressure increases, which leads to the devolatilization of the lower lithosphere, releasing its fluids to the surrounding upper asthenosphere. There is evidence for water that the larger degrees of melting with more involvement of a peridotitic source (high-silica volcanic rocks; e.g. Hoernle et al., 2006; Timm et al., in review. Volcanic rocks with lower silica content are generally attributed to partial melting of eclogite/pyroxenite partly in the presence of CO_2 (Hoernle et al., 2006; Timm et al., in review). In our model, however only the influence water in melt generation has been considered. In addition to the parameterization for dry peridotite and pyroxenite melting (Hirschmann, 2000 and Pertermann, 2003), we included the parameterization of hydrous melting after Katz et al., 2003 in our model. Unless extreme, rather unrealistic conditions are set ($T \geq 1500°C$; ~45 km of lithosphere removed), no partial melting of dry peridotite takes place. Since the downwelling lithospheric instability may release water into the surrounding asthenosphere mantle through increasing temperature, the solidus of the asthenospheric mantle material may be lower than that of a dry mantle rock. Similarly, if a drip sinks slowly and heats conductively it may also melt itself and thus contribute to melt generation in the asthenosphere. After Katz et al. (2003) the presence of 0.1 bulk wt% H_2O lowers the temperature of the solidus at a given pressure about 200°C. Geochemical studies on basalts, glasses and olivines from oceanic islands suggests the presence of 300–1000 ppm in the source (e.g. Dixon and Clague, 2001; Dixon et al., 2002; Jamtveit et al., 2001), whereas a content of 50–200 ppm were determined in the source of mid ocean ridge basalts (MORB; e.g. Saal et al., 2002). The storage capacity of H_2O in the upper mantle above the transition zone inferred from olivine and wadsleyite H_2O storage capacity is ~0.5 and 1-2 wt %, respectively (Hirschmann et al., 2005). For the Hawaiian source regions a water content of 525 ± 75 ppm and 450 ± 190 ppm were estimated (e.g. Dixon et al., 1997 and Wallace, 1998).

As noted above, the geochemical composition of the volcanic rocks erupted on Zealandia also indicate the presence of a pyroxene-bearing source component, such as garnet pyroxenite. Although less well constrained the storage capacity of pyroxene (and garnet) is even higher compared to olivine (Hirschmann, 2006). If mantle material ascends adiabatically, pyroxenite begins to melt by decompression ~30 - 50 km deeper than peridotite (Pertermann and Hirschmann, 2003). To model the solidus of hydrous pyroxenite melting, we apply the same parameterization as used for the peridotite solidus (Katz et al., 2003).

Assuming a H_2O content of ~ 300 - 600 ppm in the source beneath Zealandia, similar to the estimates of water content in the Hawaiian source regions, the first locations where partial melting of pyroxenite (containing ~330 ppm H_2O) occurs in our models are at the outer edge of the lithosphere due to fast removal of the dense lower layer predominately by convection. After a model running time of ~20-25 Ma, partial melting also occurs beneath the interior of the continent. In the following ~10 Ma, larger cavities develop as the instabilities grow beneath the continent, allowing the asthenospheric upwelling and hence to partial melting by decompression. The growth of the instabilities changes the upper convective mantle flow and forces melting at regions, where increased convective upwelling occur. After ~ 40 Ma sufficient mantle has been removed to allow higher degrees of pyroxenite melting (plus some peridotite melts with ~600 ppm H_2O) in the cavities at the base of the lithosphere. The amount of melt increases in the following 10 Ma, whereas at ~60 Ma the productivity is decreased through local changes in the convective mantle flow. After ~65 – 70 Ma the small-scale hot asthenospheric upwelling (~1500 °C) arrived at the base of the lower lithosphere, increasing the productivity significantly through temperature increase.

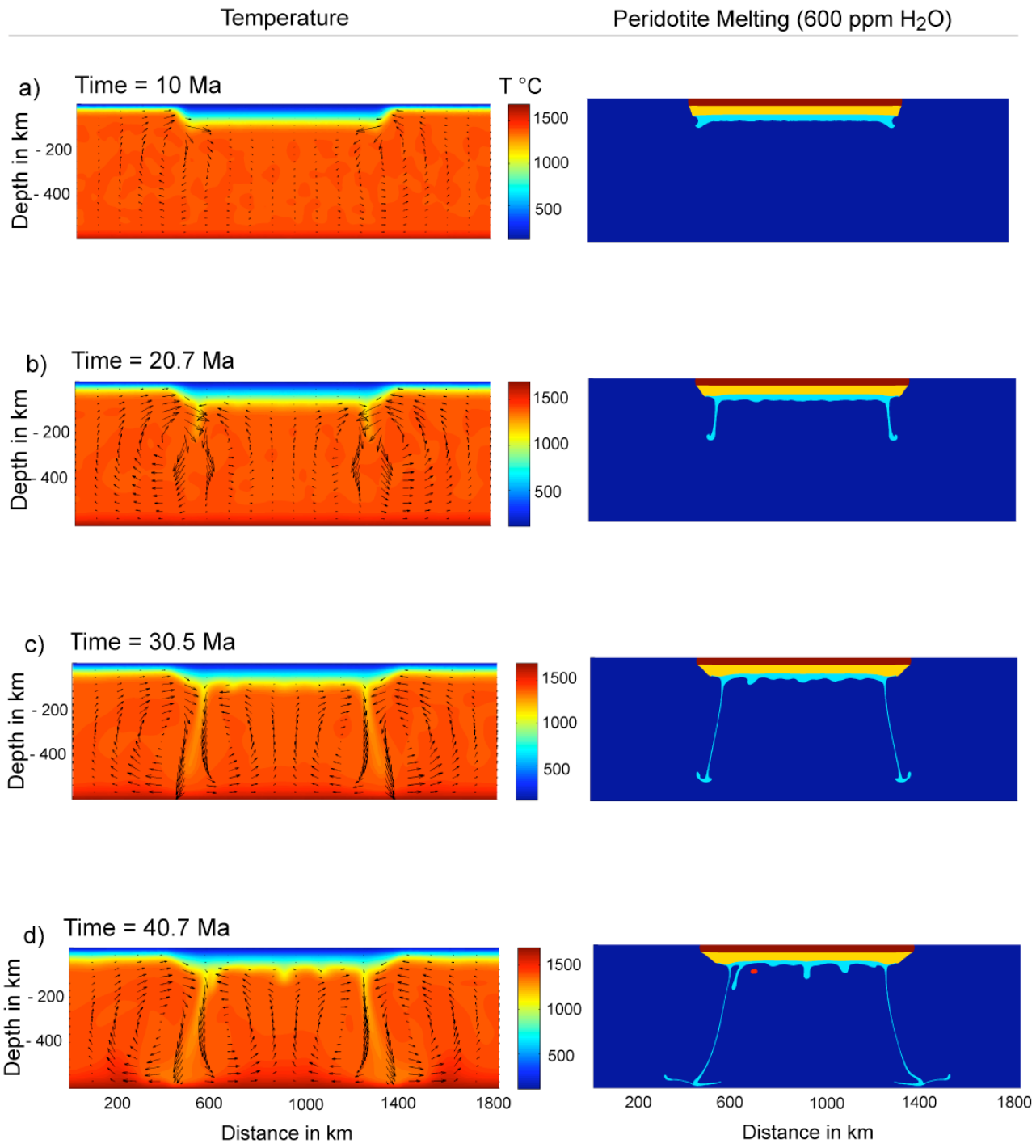

Fig. 4.4a-d: Temperature distribution and melt locations of peridotite (parameterization after Katz et al., 2003) containing 600 ppm water. The x-axis display the length of the cross section in km and the y-axis show depth in km. Black arrows visualize the direction of the mantle flow. The right panels show four layers of different phases as described above.

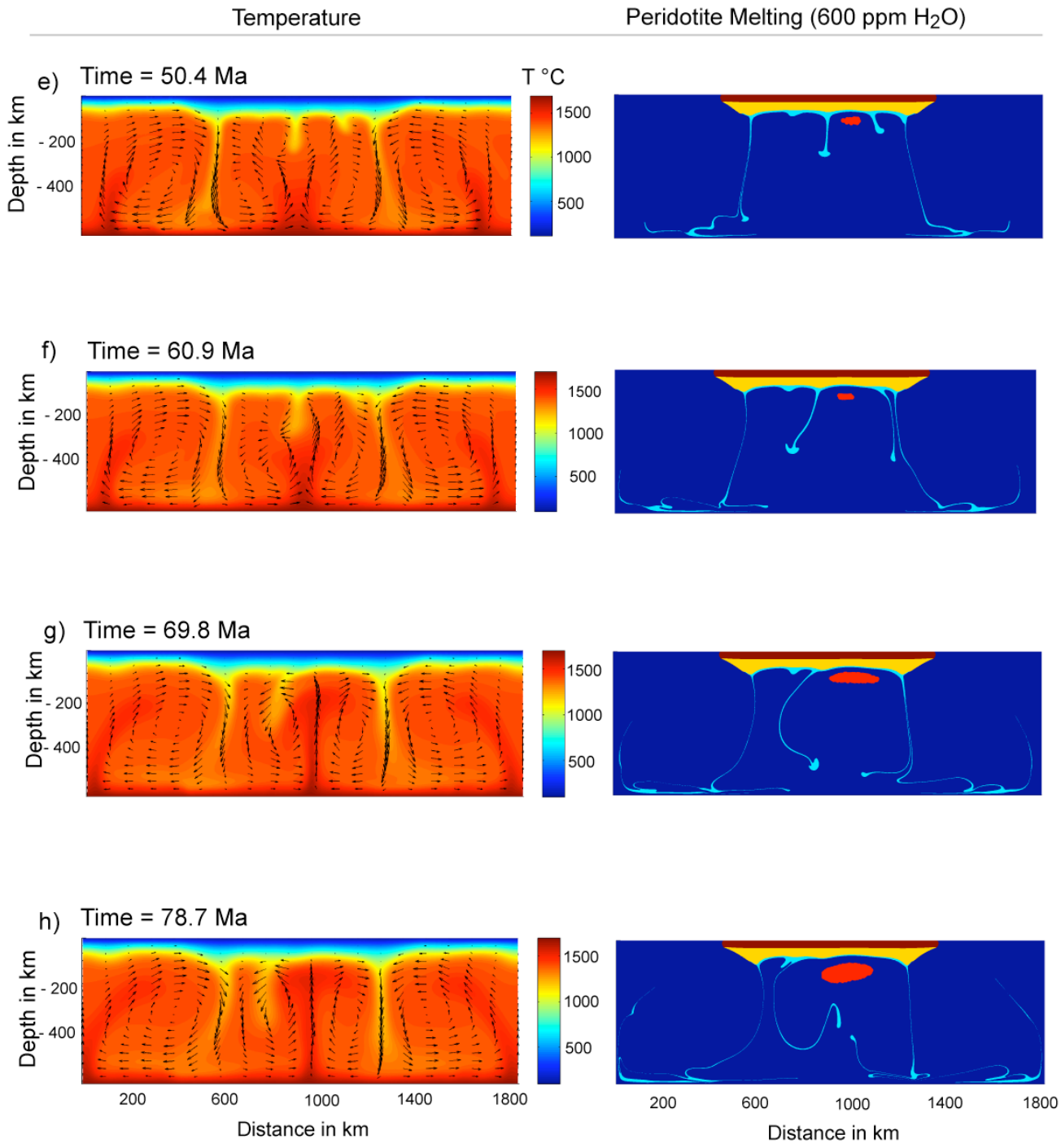

Fig. 4.4e-h: Temperature distribution and melt locations of peridotite (parameterization after Katz et al., 2003) containing 600 ppm water. Note that only regions of mantle melting are shown that are located beneath the continent. The x-axis display the length of the cross section in km and the y-axis show depth in km. Black arrows visualize the direction of the mantle flow. The right panels show four layers of different phases as described above.

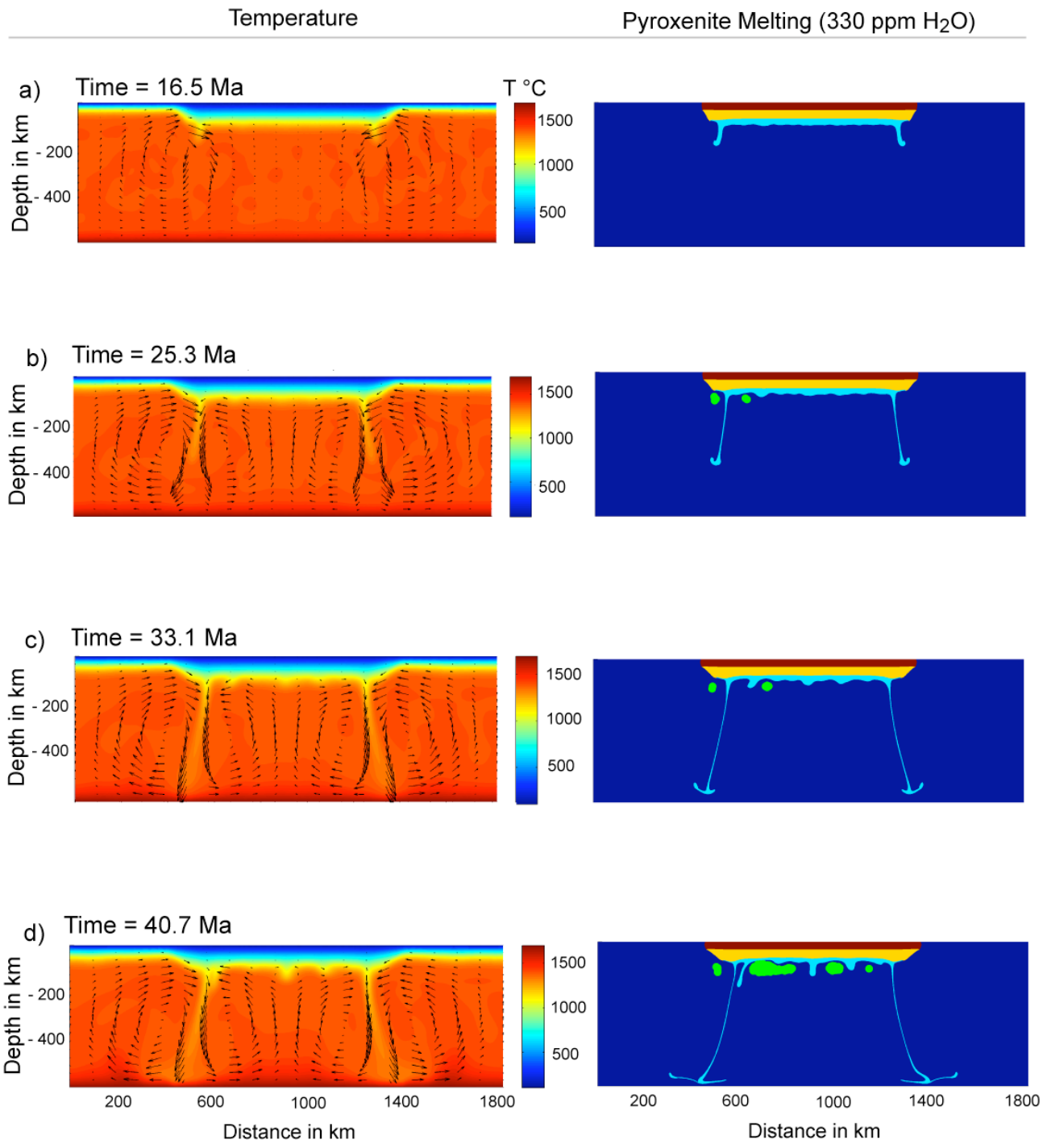

Fig. 4.5a-d: Temperature distribution and melt locations of pyroxenite (parameterization after Katz et al., 2003) containing 330 ppm water. The x-axis display the length of the cross section in km and the y-axis show depth in km. Black arrows visualize the direction of the mantle flow. The right panels show four layers of different phases as described above.

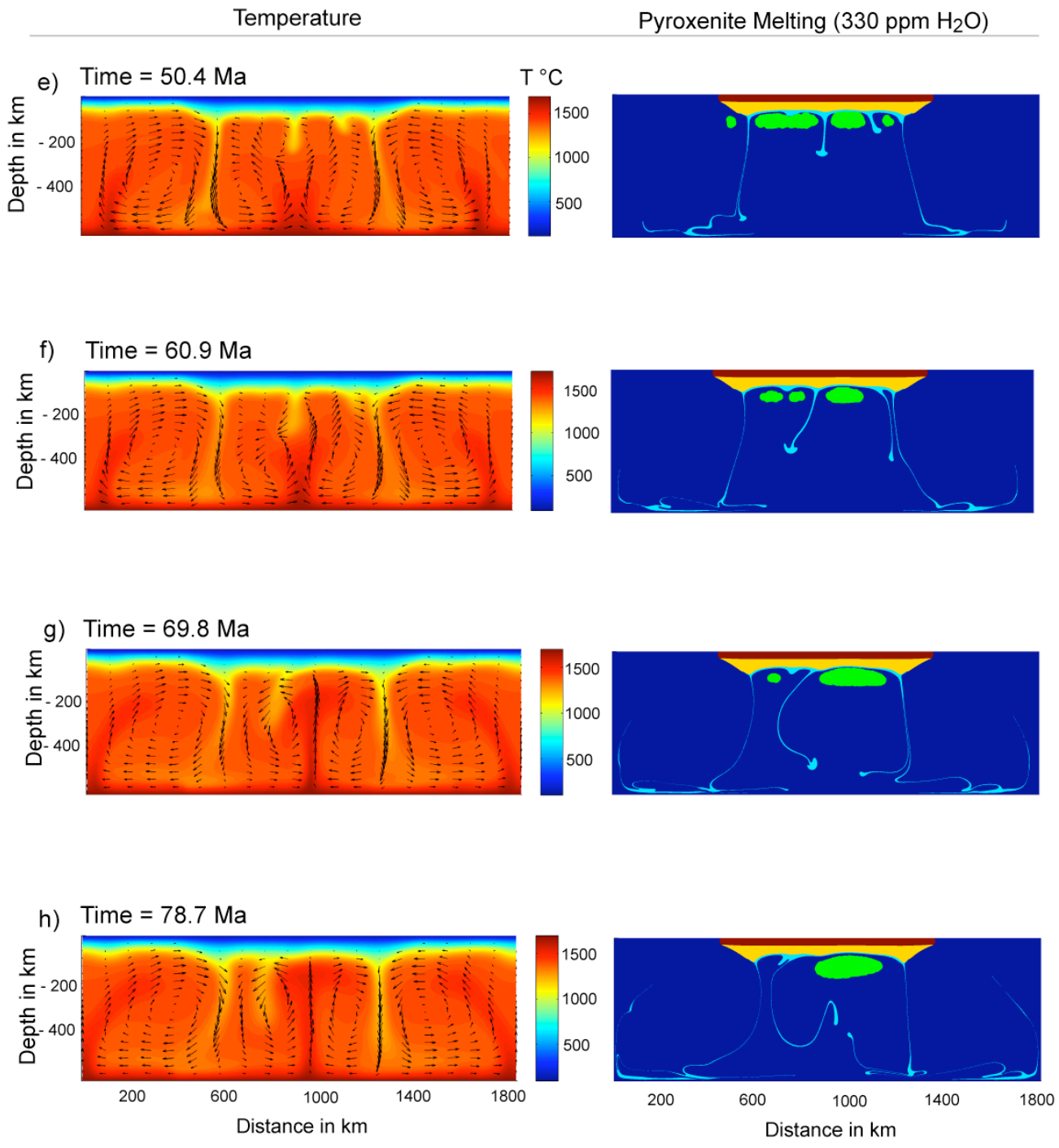

Fig. 4.5e-h: Temperature distribution and melt locations of pyroxenite (parameterization after Katz et al., 2003) containing 330 ppm water. The x-axis display the length of the cross section in km and the y-axis show depth in km. Black arrows visualize the direction of the mantle flow. The right panels show four layers of different phases as described above.

4.6 Discussion

4.6.1 Melting beneath continents triggered by Rayleigh-Taylor instabilities: the Zealandia synthesis

As noted before, the assumption of a damp mantle source beneath Zealandia is supported by the geological history of the micro-continent. Consequently, the lower lithosphere beneath Zealandia presumably contains a considerable amount of H_2O and CO_2. In our simulation, the earliest melts of damp pyroxenite (containing ~330 ppm H_2O) occur along the edges of the continental lithosphere after ~15 to 20 Ma, which would be around 65 Ma considering that separation of the parts of Zealandia from western Antarctica began at ~85 Ma. The results are consistent with the formation of the Arnott basalts, located at the edge of Zealandia at the time of their formation, at ~65 Ma. As noted above the first larger instabilities (resulting in larger cavities at the bottom of the lithosphere and presumably in increasing devolatilisation of the sinking lithosphere) form after ~35 Ma running time, forming the first "intracontinental" melts of a similar pyroxenitic component, which is broadly comparable with the onset of volcanic activity in central Canterbury at ~50 Ma (View Hill basalts).

As noted above three larger "intracontinental" instabilities develop, resulting in the formation of three major cavities. The location where partial melting occurs within an area of broad upwelling is dependent on the source composition (and possibly volatile content) and temperature variations in the asthenosphere rather than simply on the topography of the interface between lithosphere and asthenosphere. Along a cross section from the South Island of New Zealand to the eastern margin of the Chatham Rise (which is a W-E distance of ~1000 km) the western cavity would include the volcanic centers in Canterbury until the western end of the Chatham Rise, whereas the middle region of asthenospheric mantle upwelling comprise the volcanic centers on Central Chatham Rise and the eastern part would include the Chatham Islands and the surrounding volcanic centers. The occurrence of larger amounts of partial melting after ~40 Ma is broadly consistent with the increase of volcanic activity on Zealandia, where several volcanic centers were active at 30 – 40 Ma (e.g. Waiareka Deborah Formation and Cookson Volcanics; see Chapter III; Figure 3.4).

The continuous removal of the lower lithosphere results in increasing rates of upwelling, generally resulting in the formation of more depleted residues, whose density decrease with time, because fertile pyroxenitic lithologies generally melt at lower temperatures and therefore produced the first magma (e.g. Hirschmann, 2000). The density decrease (because of melting out the fertile domains) and the simultaneous increase of required temperature to melt a more depleted (and thus more buoyant) peridotitic mantle will lead to continuous cessation of magmatism with time, which may be a reason why the lithosphere regains some of its thickness (Jaupart, 2007).

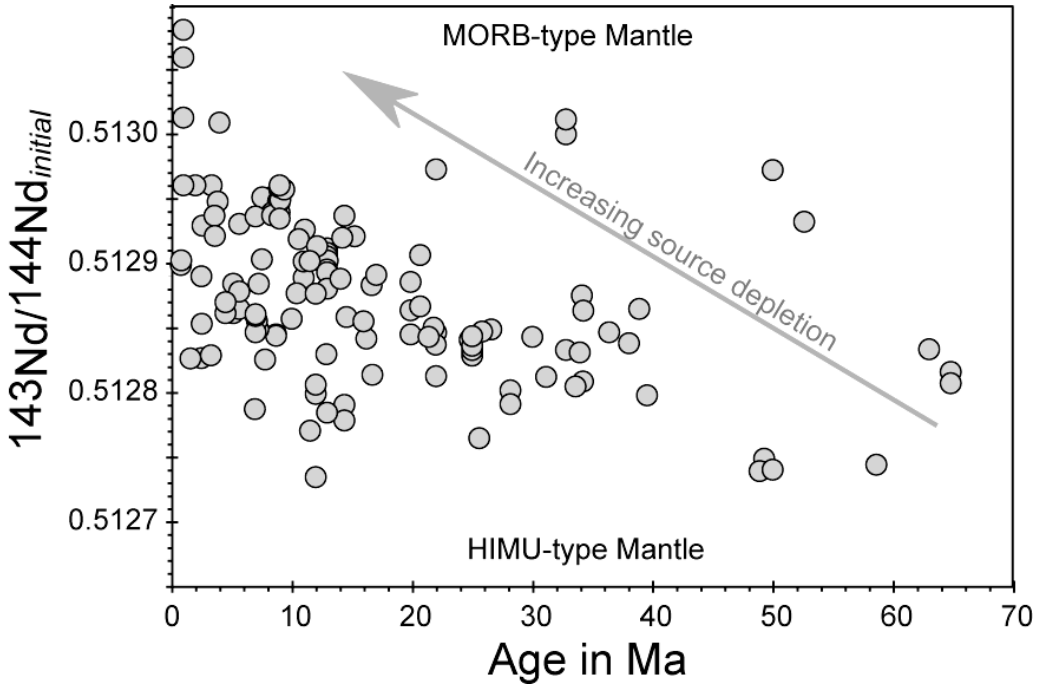

Fig.4.6: Age versus $^{143}Nd/^{144}Nd_{initial}$ of the volcanic centers on Zealandia. For undated volcanic rocks, the age was inferred from dated lavas of the same volcanic center. For a better comparison of the Nd isotopes data, their initial value, presenting the isotope ratios at the time of their formation was calculated. Nd is a conservative element and are therefore most likely unaffected by fluid processes.

A general trend (although there is a huge scatter, due to regional compositional changes and different melting conditions) towards more depleted mantle compositions with decreasing age beneath Zealandia is displayed in the $^{143}Nd/^{144}Nd$ versus age diagram (Fig.4.6). The increasing depletion with time supports the model, where the lower lithosphere is continuously removed, resulting in continuous melting and thus

the decrease of the plume (HIMU-type) component (which melts first) through time (change from fertile pyroxenitic to more depleted peridotitic source compositions), which is consistent with increasing degrees of partial melting as the lower lithosphere is continuously removed, forming longer melting columns. In addition Zealandia moved ~4000 km in the Cenozoic and therefore drifted continuously over new, presumably fertile mantle. The lateral motion of the lithosphere presumably also contributes to the mantle flow into the cavities and melting through decompression as indicated by Hoernle et al., 2006. Small-scale thermal plumes of deeper origin (below 600 km) could have continuously enhanced the melt productivity throughout the Cenozoic, since the deep-seated thermal anomaly was present at least since the late Cretaceous (see Chapter III). Our model shows that lithospheric removal by Rayleigh-Taylor instabilities is a large-scale feature (maximum "finger-spacing" of ~300 km), rather than producing local upwelling of ≤ 50 km. The influx of a small-scaled thermal plume may therefore also play an important role for generating melts and in particular on the formation of larger composite shield volcanoes. Another conceivable scenario is the presence of several thin layers at the base of the lithosphere, which vary laterally in density (and viscosity). In response, smaller and localized (by density) instabilities may form smaller cavities and therefore more localized upwelling of warm mantle in order to form composite shield volcanoes, such as Banks Peninsula (Timm et al., in review).

In summary, our model can explain prolonged (~80 Ma) occurrence of intraplate volcanism. Some uncertainties, however, remain, since our melting model does not incorporate the compositional change of the residue after melt extraction, which shifts the solidus towards higher temperatures at given pressures and therefore clearly overestimates the amount of partial melting, especially after long running times (≥ 50 Ma). Unfortunately, there is no high-resolution seismic tomography available for the mantle beneath Zealandia, which could resolve such small-scale thermal upwelling. In Central Europe, however several cylindrical thermal anomalies have been identified by tomographic imaging (e.g. Wilson, in press; Ritter et al., 2001; Goes et al., 1999; Granet et al., 1995), which are believed to have contributed to the formation of Cenozoic intraplate volcanic centers, such as the Eifel, Massif Central and the Bohemian Massif. The lateral movement of Zealandia, however will cut off from the deeper parts of the convective system caused by Rayleigh-Taylor

instabilities. Since the deep-seated thermal anomaly beneath Zealandia presumably contributed localized upwelling of hot mantle material, it will promote or contribute to partial melting beneath Zealandia.

4.7 Conclusion

Our new model shows that the continuous non-plume and non-rifting related intraplate volcanism on the New Zealand micro-continent, Zealandia can be explained by lithospheric removal through Rayleigh Taylor instabilities. The process of lithospheric removal therefore, may be an important process in explaining diffusively occurring low-volume intraplate volcanism on continents.

In particular, our model generally matches the temporal and spatial evolution of the volcanic centers on Zealandia, although small amounts of water need to be involved to produce partial melts. Unless rather unrealistic conditions, such as high initial temperatures, which exceed the values for common upper mantle or large-scale lithospheric removal are applied no melting of dry peridotite occurs. The presence of a small amount of water in the upper mantle beneath Zealandia, however is supported by the geological history of the micro-continent, which, while a part of the northwestern continental margin of Gondwana, was located above an active subduction zone during the Mesozoic and therefore experienced prolonged subduction-related (wet) volcanism. Downwelling of such modified lower lithosphere most likely leads to devolatilisation during the growth of the instability, releasing the hosted volatiles into the surrounding asthenosphere. The typical wavelengths of Rayleigh-Taylor instabilities at the base of the lithosphere are around 100 – 300 km, independent of their initial perturbation and consequently form large cavities. The formation of these large cavities results in broad upwelling of the upper asthenosphere and subsequent partial melting by decompression, which can adequately explain the intraplate volcanism on New Zealand and possibly at other areas of continental intraplate volcanism on earth.

Acknowledgements

My special thank goes to the PGP Team at the University of Oslo around Yuri Podladchikov, which made this work possible and for partly funding my stay in Oslo. The German Ministry of Education and Research (BMBF; Grants SO168 Zealandia and SO169 CAMP) and the DFG (Grant HO1833/12-1 and 2) and IFM-GEOMAR are gratefully acknowledged for providing funding for this project.

References:

Baker, J.A., Gamble, J.A., Graham, I.J., 1994. The age, geology, and geochemistry of the Tapuaenuku Igneous Complex, Marlborough, New Zealand. New Zealand Journal of Geology and Geophysics 37: 249-268.

Conrad, C.P., and Molnar, P., 1996. The growth of Rayleigh-Taylor instabilities in the lithosphere for various rheological and density structures. Geophysical Journal International 129, 95-112.

Conrad, C.P., and Jones, C., 2004. A testof laboratory based rheological parameters of olivine from an analysis of late Cenozoic convective removal of mantle lithosphere beneath the Sierra Nevada, Calofornia, USA. Geophysical Journal International 156, 555-564.

Coombs, D.S., Cas, R.A., Kawachi, Y., Landis, C.A., McDonough, W.M., Reay, A., 1986. Cenozoic Volcanism in North, East and Central Otago. Cenozoic Volcanism in New Zealand. I. E. M. Smith, Royal Society of New Zealand, 278-312.

Cooper, A. F. (1986). A carbonatitic lamprophyre dike swarm from the Southern Alps, Otago and Westland. Late Cenozoic Volcanism in New Zealand. I. E. M. Smith, Royal Society of New Zealand – Bulletin. 23: 278-312.

Dasgupta, R., Hirschmann, M.M., Stalker, K., 2006. Immiscible Transition from Carbonate-rich to Silicate-rich Melts in the 3 GPa Melting Interval of Eclogite + CO_2 and Genesis of Silica-undersaturated Ocean Island Lavas. Journal of Petrology 47, 647-671.

Dixon, J.E., Clague, D.A., Wallace, P., Poreda, R., 1997. Volatiles in alkali basalts from the Nirth Arch Volcanic Field, Hawaii: extensive degassing of deep submarine-erupted alkalic series lavas. Journal of Petrology 38, 911-939.

Dixon, J.E., Clague, D.A., 2001. Volatiles in basaltic glasses from Loihi Seamount, Hawaii: evidence for a relatively dry plume component. Journal of Petrology 42, 627-654.

Dixon, J.E., Leist, L., Langmuir, C.H., Schilling, J.-G., 2002. Recycled dehydrated lithosphere observed in plume influenced mid-ocean-ridge basalts. Nature 420, 385-389.

Elkins-Tanton, L.T., 2005. Continental magmatism caused by lithospheric delamination, in: G.R. Foulger, J.H. Natland, D.C. Presnall, D.L. Anderson (Eds.), Plates, Plumes, and Paradigms, Geological Society of America Special Paper 388, Geological Society of America, 449–461.

Elkins-Tanton, L.T., 2007. Continental magmatism, volatile recycling, and heterogeneous mantle caused by lithospheric gravitational instabilities. Journal of Geophysical Research 112, B03405, doi: 10.1029/2005JB004072.

Elkins-Tanton, L.T. and Hager, B.H., 2000. Melt intrusion as a trigger for lithospheric foundering and the eruption of the Siberian flood basalt. Geophysical Research Letters 27, 3937-3940.

Finn, C.A., Mueller R.D., Panter, K.S., 2005. A Cenozoic diffuse alkaline magmatic province (DAMP) in the southwest Pacific without rift or plume origin. Geochemistry Geophysics Geosystems 6, Q02005, doi:10.1029/2004GC000723.

Goes, S., Spakman, W., Bijwaard, H., 1999. A lower mantle source for central European volcanism. Science 286, 1928-1931.

Granet, M., Wilson M., Achauer, U., 1995. Imaging a mantle plume beneath the Massif Central. Earth and Planetary Science Letters 136, 281-296.

Green, D.H., Fallon, T.J., Eggins, S.M., Yaxley, G.M., 2001. Primary magmas and mantle temperatures. European Journal of Mineralogy 13, 437-451.

Herzberg, C. and Zhang, J., 1996. Melting experiments in anhydrous peridotite KLB-1: compositions of magmas in the upper mantle and transition zone. Journal of Geophysical Research 101(B4), 8271-8295.

Herzberg, C., P. D. Asimow, N. Arndt, Y. Niu, C. M. Lesher, J. G. Fitton, M. J. Cheadle, and A. D. Saunders (2007), Temperatures in ambient mantle and plumes: Constraints from basalts, picrites, and komatiites, Geochemistry Geophysics Geosystems 8, Q02006, doi:10.1029/2006GC001390.

Hirschmann, M.M., 2000. Mantle solidus: Experimental constraints and the effects of peridotite composition. Geochemistry Geophysics Geosystems 1, 2000GC000070.

Hirschmann, M.M., Kogiso, T., Baker, M.B., Stolper, E.M., 2003. Alkalic magmas generated by partial melting of garnet pyroxenite. Geology 31, 481-484.

Hirschmann, M.M., Aubard, C., Withers, A.C., 2005. Storage capacity of H_2O in nominally anhydrous minerals in the upper mantle. Earth and Planetary Science Letters 236, 167-181.

Hirschmann, 2006. Water, Melting and the Deep Earth H_2O Cycle. Annual Reviews of Earth and Planetary Sciences 34, 629-653.

Hirth, G., and Kohlstedt, D.L., 1996. Water in the oceanic upper mantle.: Implication for rheology, melt extraction, and the evolution of the lithosphere. Earth and Planetary Science Letters 144, 93-108.

Hoernle, K., White, J.D.L., Bogaard, P.v.d., Hauff, F., Coombs, D.S., Werner, R., Timm, C., Garbe-Schönberg, C.-D., Reay. A., Cooper, A.F., 2006. Cenozoic Intraplate Volcanism on New Zealand: Upwelling Induced by Lithospheric Removal. Earth and Planetary Science Letters 248, 335-352.

Houseman, G.A., Neil, E., Kohler, M.D., 2000. Lithospheric Instability in the Traverse Ranges of California. Journal Geophysical Research 105(B7), 16,237 - 16,250.

Hoang, N., Flower, M., 1998. Petrogenesis of Cenozoic Basalts from Vietnam: Implication for the Origins of a "Diffuse Igneous Province". Journal of Petrology 39 (3), 369-395.

Jamtveit, B., Brooker, R., Brooks, K., Larsen, L.M., Pedersen, T., 2001. The water content of olivines from the North Atlantic Volcanic Province. Earth and Planetary Science Letters 186, 401-415-

Jaupart, C., 2007. Dynamics of continental lithosphere. Geophysical Research Abstracts, 9, 06818, SRef-ID: 1607-7962/gra/EGU2007-A-06818

Jull, M. and Kelemen, P.B., 2001. On conditions for lower crustal convective instability. Journal Geophysical Research 106, 6423-6446.

Kaus, B.J.P., 2004. Modelling approaches to geodynamic processes. PhD. Thesis. ETH Zurich.

Katz, R., Spiegelmann, M., Langmuir, C.H., 2003. A new parameterization of hydrous mantle melting. Geochemistry Geophysics Geosystems 4(9), doi: 10.1029/2002GC000433.

Kay, R.W. and Kay, S.M., 1993. Delamination and delamination magmatism. Tectonophysics 219, 177-189.

Kogiso, T., Hirschmann, M.M., 2006. Partial melting experiments of bimineralic eclogite and the role of recycled mafic oceanic crust in the genesis of ocean island basalts. Earth and Planetary Science Letters 249, 188–199.

Korenaga, J., 2005. Why did not the Ontong Java Plateau form subaerially? Earth and Planetary Science Letters 234, 385–399.

Li, C., van der Hilst, R.D., Engdahl, E.R., Burdick, S., 2008. A new global model for P wave speed variations in Earth's mantle. Geochemistry Geophysics Geosystems 9(5), Q05018, doi:10.1029/2007GC001806

Menzies, M.A., Fan, W., Zhang, M., 1993. Paleozoic and Cenozoic lithoprobes and the loss of > 120 km of Archean lithosphere; Sino-Korean craton, China. In: Prichard, H.M., Alabaster, T., Harris., N.B.W., Neary, C.R., (eds): Magmatic Processes and Plate Tectonics. Geological Society, London, Special Publications 76, 71-81.

Molnar, P., Anderson, H.J., Audoine, E., Eberhart-Phillips, D., Gledhill, K.R., Klosko, E.R:, McEvilly, T.V., Okaya, D., Savage, K,M., Stern, T., Wu, F.T., 1999. Continuous deformation versus faulting through the continental lithosphere of New Zealand. Science 286, 516-519.

Molnar P., Houseman, G.A., Conrad, C.P., 1998. Rayleigh-Taylor instability and convective thinning of mechanically thickened lithosphere: effects of non-linear viscosity decreasing exponentially with depth and of horinzontal shortening of the layer. Geophysical Journal International 133, 568-584.

Molnar, P. and Jones, C.H., 2004. A laboratory test based rheological parameters of olivine from an analysis of late Cenozoic convective removal of mantle lithosphere beneath the Sierra Nevada, California, USA. Geophysical Journal International 156, 555-564, doi: 10.1111/j.1365-246X.2004.02138.x.

Montelli, R., Nolet, G., Dahlen, R.A., Masters, G., 2006. A catalogue of deep mantle plumes: New results from finite frequency tomography. Geochemistry Geophysics Geosystems 7(11), Q11007, doi:10.1029/2006GC001248.

Morgan, W.J., 1971. Convection plumes in the lower mantle, Nature 230, 42–43.

Muir, R.J., Ireland, T.R., Weaver, S.D., Bradshaw, J.D., Evans, J.A., Eby, G.N., Shelley, D., 1998. Geochronology and geochemistry of a Mesozoic magmatic arc system, Fjordland, New Zealand. Journal of the Geological Society, London 155, 1037-1053.

Nolet, G., Karato, S.-I., Montelli, R., 2006. Plume fluxes from seismic tomography. Earth and Planetary Science Letters 248, 685-699.

Panter, K. S., Blusztain, J., Hart, R.S., Kyle, P.R., Esser, R., McIntosh, W.C., 2006. The Origin of HIMU in the SW Pacific: Evidence from Interplate Volcanism in Southern New Zealand and Subantarctic Islands. Journal of Petrology doi:10.1093/petroogy/eg1024, 1-32.

Pertermann, M., Hirschmann, M. M., 2003. Partial melting experimats on a MORB-like pyroxenite between 2 and 3 GPa: Constraints on the presence of pyroxenite in basalt source regions from solidus location and melting rate. Journal Geophysical Research 108, doi: 10.1029/2000JB000118.

Pertermann, M., Hirschmann, M. M., Hametner, K., Günther, D., Schmidt, M.W., 2003. Experimental determination of trace element partitioning between garnet and silica-rich liquid during anhydrous partial melting of MORB-like eclogite. Geochemistry Geopysics Geosystems 5(5), Q05A01 DOI 10.1029/2003GC000638.

Pfänder, J. A., Münker, C., Stracke, A., Mezker, K., 2007. Nb/Ta and Zr/Hf in ocean island basalts — Implications for crust–mantle differentiation and the fate of Niobium. Earth and Planetary Science Letters 254, 158-172.

Priestley, K. and McKenzie, D., 2006. The thermal structure of the lithosphere from shear wave velocities. Earth and Planetary Science Letters 244, 285-301.

Ritter, J.R.R., Jordan, M., Christensen, U.R., Achauer, U., 2001. A mantle plume below the Eifel volcanic fields, Germany. Earth and Planetary Science Letters 186 (1), 7-14.

Saal, A.E., Hauri, E.H., Langmuir, C.H., 2002. Vapour undersaturation in primitiva mid-ocean-ridge basalt and the volatile content of Earth's upper mantle. Nature 419, 451-455.

Scherwath, M., Stern, T., Melhuish, A., Molnar, P., 2002. Pn anisotropy and distributed upper mantle deformation associated with a continental transform fault. Geophysical Research Letters 29(8), 161 - 164.

Sprung, P., Schuth, S., Münker, C., Hoke, L., 2007. Intraplate volcanism in New Zealand: the role of fossil plume material and variable lithospheric properties. Contributions Mineralogy Petrology 153, 669-687.

Stern, T., Okaya, D., Scherwarth, M., 2002. Structure and Strength of a continental transform from onshore-offshore seismic profiling of South Island, New Zealand. Earth Planets Space 54, 1011-1019.

Storey, B.C., Leat, P.T., Weaver, S.D., Pankhurst, R.J., Bradshaw, J.D., Kelley, S., 1999. Mantle plumes and Antartica - New Zealand rifting: evidence from mid-Cretaceous mafic dykes. Journal of the Geological Society, London 156, 659-671.

Turcotte D.L., and Schubert, G., 2001. Geodynamics, second edition. Cambridge University Press.

Waight, T.E., Weaver, S.D., Muir, R.J., 1998. Mid-Cretaceous granitic magmatism during the transition from subduction to extension in southern New Zealand: a chemical and tectonic synthesis. Lithos 45, 469-482.

Wallace, P., 1998. Water and partial melting in mantle plumes: inferences from the dissolved H_2O concentrations of Hawaiian basaltic magmas. Geophysical Research Letters 25, 3639-3642.

Weaver, S.D. and Smith, I.E.M., 1989. New Zealand Intraplate Volcanism. Intraplate volcanism in eastern Australia and New Zealand. R. W. Johnson, J. Knutson and S. R. Taylor, Cambridge University Press. Chapter 4, 157-188.

Weaver, S.D., Storey, B.C., Pankhurst, R.J., Mukasa, S.B., DiVenere, V.J., Bradshaw, J.D., 1994. Antarctica-New Zealand rifting and Marie Byrd Land lithospheric magmatism linked to ridge subduction and mantle plume activity. Geology 22, 811-814.

Wilson, M. and Downes, H., in press. Tertiary-Quaternary intra-plate magmatism in Europe and its relation to mantle dynamics. In: Stephenson, R & Gee, D. (eds.) European Lithosphere Dynamics. Geological Society Memoir.

Appendices:

I.I XRF-Standards

Standard (wt%)	JB-2 Lit.*	JB-2 (n=5)	*Dev. (%)*	JB-3 Lit.*	JB-3 (n=4)	*Dev. (%)*	JA-2 Lit.*	JA-2 (n=4)	*Dev. (%)*	JR-1 Lit.*	JR-1 (n=10)	*Dev. (%)*
SiO_2	53.20	53.25	*0.1*	51.04	51.08	*0.1*	56.18	55.96	*-0.4*	75.41	74.69	*-1.0*
TiO_2	1.19	1.17	*-1.7*	1.45	1.41	*-3.1*	0.67	0.67	*0.0*	0.10	0.11	*-10.0*
Al_2O_3	14.67	14.94	*1.9*	16.89	17.50	*3.6*	15.32	15.49	*1.1*	12.89	12.81	*-0.6*
Fe_2O_3	14.34	14.25	*-0.6*	11.88	11.94	*0.5*	6.14	6.37	*3.7*	0.96	0.90	*-6.5*
MnO	0.20	0.21	*5.0*	0.16	0.17	*7.8*	0.11	0.11	*0.0*	0.10	0.10	*0.0*
MgO	4.66	4.69	*0.7*	5.20	5.21	*0.1*	7.68	7.91	*2.9*	0.09	0.12	*30.6*
CaO	9.89	9.89	*0.0*	9.86	9.79	*-0.8*	6.48	6.26	*-3.5*	0.63	0.70	*10.7*
Na_2O	2.03	2.06	*1.4*	2.82	2.74	*-2.9*	3.08	3.01	*-2.4*	4.10	4.03	*-1.7*
K_2O	0.42	0.42	*0.0*	0.78	0.77	*-1.9*	1.80	1.76	*-2.5*	4.41	4.45	*0.9*
P_2O_5	0.10	0.10	*0.0*	0.29	0.30	*2.6*	0.15	0.16	*5.0*	0.02	0.02	*0.0*

* Working values are taken from Govindaraju, 1994

I.II: ICPMS-Standards

Standard ppm	BHVO-1 Lit.#	Avrg. n=4	Stdev. (abs)	*Diff. (%)*	AGV-1 Lit.#	Avrg. n=4	Stdev. (abs)	*Diff. (%)*
Li	4.60	4.49	0.16	*-2.4*	12	10.0	1.32	*-16.4*
Sc	31.8	31.1	0.87	*-2.1*	12.2	11.7	0.32	*-3.9*
V	317	315	3.87	*-0.4*	121	121	0.65	*-0.1*
Cr	289	277	6.00	*-4.3*	10.1	8.4	1.14	*-17.0*
Co	45.0	43.2	0.82	*-4.1*	15.3	14.9	0.29	*-2.8*
Ni	121	116	2.95	*-3.8*	16	15.0	0.69	*-6.2*
Cu	136	124	5.67	*-8.5*	60	57.4	1.77	*-4.3*
Zn	105	102	2.08	*-2.6*	88	85.7	1.71	*-2.6*
Ga	21.0	20.7	0.22	*-1.4*		20.2	0.19	
Rb	9.05	8.97	0.18	*-0.9*	67.3	65.7	1.07	*-2.4*
Sr	395	395	4.22	*0.1*	672	656	11.43	*-2.4*
Y	27.6	24.7	1.39	*-10.4*	20	18.7	0.90	*-6.5*
Zr	179	168	5.69	*-6.3*	227	226	2.94	*-0.4*
Nb	17.1	17.1	0.04	*-0.1*	15	13.7	0.86	*-8.7*
Sn	2.10	1.70	0.17	*-19.3*	4.2	4.14	0.04	*-1.3*
Sb	0.160	0.107	0.02	*-33.23*	4.3	4.20	0.08	*-2.4*
Cs	0.130	0.099	0.01	*-23.8*	1.28	1.26	0.01	*-1.8*
Ba	139	135	2.10	*-2.6*	1203	1200	3.98	*-0.2*
La	15.8	14.89	0.40	*-5.8*	37.6	37.5	0.20	*-0.5*
Ce	39.0	36.7	0.99	*-5.9*	67	67.4	0.30	*0.6*
Pr	5.70	5.34	0.16	*-6.4*	7.6	8.20	0.40	*8.0*
Nd	25.2	24.5	0.41	*-3.0*	33	32.0	0.65	*-2.4*
Sm	6.20	6.09	0.08	*-1.8*	5.9	5.81	0.07	*-1.5*
Eu	2.06	2.06	0.02	*0.1*		1.60	0.01	
Gd	6.40	6.19	0.10	*-3.3*	5	4.97	0.07	*-0.6*
Tb	0.960	0.945	0.02	*-1.6*	0.7	0.676	0.02	*-3.5*
Dy	5.20	5.31	0.07	*2.1*	3.6	3.58	0.03	*-0.5*
Ho	0.990	0.976	0.02	*-1.4*	0.67	0.668	0.01	*-0.4*
Er	2.40	2.41	0.03	*0.5*	1.7	1.75	0.03	*2.8*
Tm	0.330	0.324	0.00	*-1.8*	0.34	0.273	0.04	*-19.6*
Yb	2.02	1.99	0.02	*-1.7*	1.72	1.66	0.04	*-3.7*
Lu	0.291	0.273	0.01	*-6.0*	0.27	0.251	0.01	*-7.1*
Hf	4.38	4.38	0.03	*0.0*	5.1	5.07	0.04	*-0.6*
Ta	1.10	1.07	0.02	*-3.11*	0.9	0.810	0.06	*-10.0*
Tl	0.058	0.020	0.02	*-65.0*	0.34	0.319	0.01	*-6.1*
Pb	2.08	1.58	0.22	*-24.1*	36	36.1	0.34	*0.4*
Th	1.08	1.20	0.05	*-11.1*	6.5	6.28	0.15	*-3.4*
U	0.420	0.410	0.01	*-2.3*	1.92	1.88	0.03	*-2.2*

*Working values are taken from Garbe-Schönberg, 1990

References

Govindaraju K (1994) Compilation of Working Values and Sample Description for 383 Geostandards. Geostandards Newsletter 18, 1-158.

Garbe-Schönberg C-D (1993) Simultaneous determination of thirty-seven trace elements in twenty-eight international rock standards by ICP-MS. Geostandards Newsletter 17, 81-97.

II. Selected Conference Abstracts

Goldschmidt Conference, Melbourne, 2006 (Talk)

A Mantle Origin for the Enriched Signature in Basalts from Banks Peninsula, New Zealand

C. Timm[1] , K. Hoernle[1], F. Hauff[1], Paul van den Bogaard[1] and S. Weaver[2]

[1] IFM-GEOMAR, Wischhofstr. 1-3, 24148 Kiel, Germany (ctimm@ifm-geomar.de)
[2] Department of Geological Sciences, University of Canterbury, Private Bag 4800, Christchurch, NZ

Intraplate volcanism has occurred nearly continuously throughout the Cenozoic on the South Island of New Zealand. The most prominent Cenozoic intraplate volcanism (~2500 km^3) on the South Island formed Banks Peninsula, which includes the two large composite Lyttelton and Akaroa shield volcanoes. New $^{40}Ar/^{39}Ar$ age data give the following age ranges: 11.6-10.6 Ma for Lyttelton Volcano; 9.1-8.3 Ma for Mt. Herbert; 8.8 Ma for Akaroa Volcano and 7.6-6.8 Ma for the Diamond Harbour Volcanic Group on Banks Peninsula, agreeing well with previous K/Ar age results [1]. Rock types studied thus far from Banks Peninsula range from basanite through tephrite to alkali basalt through peralkaline rhyolite to tholeiite. Two end member groups can be defined in the mafic volcanic rocks (with MgO >3 wt. %) based on SiO_2 content: a low-Si group with <47 wt% SiO_2 and high-Si group with >47 wt% SiO_2. Mafic Banks Peninsula volcanic rocks have ocean-island-basalt (OIB)-type trace element signatures with enriched highly to moderately incompatible element contents with peaks at Nb and Ta on multi-element diagrams. Compared to the high-Si group, the low-Si group has higher incompatible element abundances, such as Rb, Ba, U, Th, Nb, Ta and LREE and higher ratios of more to less incompatible elements, such as La/Yb, La/Sm and Th/Lu. Ratios of fluid-mobile elements to less fluid-mobile elements are higher in the high-Si group. The mafic volcanic rocks have distinct isotopic compositions from normal MORB (e.g. $^{206}Pb/^{204}Pb$ = 19.1-19.9) with the high-Si group generally having higher $^{87}Sr/^{86}Sr$ and $^{207}Pb/^{204}Pb$ but lower $^{143}Nd/^{144}Nd$ and $^{206}Pb/^{204}Pb$, i.e. more enriched mantle (EMII)-type, isotopic compositions than the low-Si group, which has more high time-integrated U/Pb (HIMU)-type isotopic compositions. Differences in trace element and isotopic composition could either indicate (1) crustal assimilation or (2) mantle heterogeneity. Mixing calculations indicate that up to 50% crust must be assimilated by the high-SiO_2 group rocks to explain their more enriched (EMII)-type isotopic compositions, which is unrealistic based on the major element compositions of these samples. Therefore, we conclude that the different isotopic (and possibly some of the trace element) characteristics reflect mantle heterogeneity. Furthermore, we propose that the low-SiO_2 group is derived from melting of asthenospheric mantle containing gt pyroxenite/eclogite and that the high-SiO_2 group melts are derived from or contaminated within the lithospheric mantle, possibly enriched by subduction-related melts and fluids when Zealandia was part of the Gondwana supercontinent.

References

[1] Weaver, S. and Smith, I.E.M. (1989). In R. W. Johnson, J. Knutson, S. R. Taylor (eds), Cambridge University Press, 157-188.

European Geoscience Union, Wien 2007 (Talk)

Crustal Assimilation vs. Mantle Melts in Lavas from Banks Peninsula, NZ

C. Timm [(1)], K. Hoernle [(1)], F. Hauff [(1)], Paul van den Bogaard [(1)] and S. Weaver [(2)]

[(1)] IFM-GEOMAR, Wischhofstr. 1-3, 24148 Kiel, Germany (ctimm@ifm-geomar.de)
[(2)] Department of Geological Sciences, University of Canterbury, Private Bag 4800, Christchurch, NZ

Intraplate volcanism was active continuously throughout the Cenozoic on the South Island of New Zealand producing two volcanic end members: 1) widely dispersed volcanic fields and 2) shield volcanoes. The Banks Peninsula represents the latter consisting of ~ 2500 km^2 lavas erupted at two composite shield volcanoes – the older Lyttelton and the younger Akaroa volcano. Volcanic activity on Banks Peninsula persists ~ 6 Ma and can be divided into four different phases. The first eruption of the Lyttelton volcano took place ~ 12 Ma ago. Volcanic activity at the Lyttelton volcano proceeds until ~ 10 Ma ago. Afterwards the center of volcanism shifts towards the SE by erupting the lavas of the Mount Herbert volcanic group, which gave two $^{40}Ar/^{39}Ar$ ages of 9.1 and 8.3 Ma. These ages overlap with volcanic activity at the Akaroa volcano ~ 8.8 Ma ago, which was preceded by another shift of the main volcanic activity to the SE. The Diamond Harbour Volcanic Group occurring mainly at the outer flanks of the Lyttelton Volcano represents late stage volcanism (7.6 – 6.8 Ma). Mafic volcanic rocks sampled (MgO > 4 wt%) range from basanites trough alkali basalts to tholeiites and can be divided by their silica content into a low silica group having SiO_2 < 48.5 wt% and a high silica group with SiO_2 concentration > 48.5 wt%. Trace element pattern of the volcanic rocks analyzed are akin to those of ocean islands basalts. Volcanic rocks of the low silica group show more pronounced peaks in Nb and Ta and troughs for Pb and K on a multi-element diagram, which becomes less pronounced in the high silica group. This is accompanied by increased ratios of fluid to less fluid mobile elements (e.g. Pb/Ce U/Nb, Ba/La etc.) lower concentrations of incompatible elements, like Rb, Ba, Nb, La etc. in the high silica group compared to the low silica group. Isotope ratios measured on mafic volcanic rocks are enriched with the low silica group having higher $^{206}Pb/^{204}Pb$, $^{143}Nd/^{144}Nd$ and $^{176}Hf/^{177}Hf$ ratios and lower $^{87}Sr/^{86}Sr$, Δ 7/4 and $\partial^{18}O$ values reflecting a HIMU-type source and a EMII-type source for the high silica group. Therefore, there are apparently two different types of sources beneath Banks Peninsula volcanoes 1) HIMU-type and 2) EMII-type source that could either imply mantle heterogeneity or the EMII-type signature being created by crustal assimilation. Energy-constraint assimilation-fractional crystallization (EC-AFC) calculations require ~ 8 % of crustal material to be assimilated into uncontaminated the HIMU-type samples to generate a similar Emtype signature as observed in our samples, which is plausible and underlined by trace element modelling. But how are the melts generated? In context of melt generation on the New Zealand micro continent, revealing no morphologic or

geophysical indication of a thermal anomaly and/or extensional tectonism beneath Banks Peninsula an alternative process has to be introduced to trigger melting. A possible mechanism to produce melts stationary over ~ 6 Ma is lithospheric detachment.

Goldschmidt, Köln 2007 (Poster)

Melting processes by Rayleigh-Taylor instabilities beneath Continents: Evidence from Cenozoic intraplate volcanism on Zealandia, SW Pacific

C. Timm[1], L.Rüpke[2], K. Hoernle[1]

[1] IFM-GEOMAR, Wischhofstr. 1-3, 24148 Kiel, Germany (ctimm@ifm-geomar.de)
[2] Physics of Geological Processes, University of Oslo, PO BOX 1048 Blindern, Norway

Intraplate volcanism is mainly attributed to upwelling and subsequent partial melting of hot mantle material. However, the origin of these hot mantle material is still a matter of an active debate (e.g. www.mantleplume.org). On the New Zealand micro continent Zealandia (consisting ~ 90 % of submerged continental crust) intraplate volcanism occurs widespread and nearly continuously since the initial separation activity from Gondwana about 100 Ma ago. Voluminous volcanism was associated with the Cretaceous rifting of Zealandia from Gondwana. In contrast, only scattered, low volume eruptives were produced in the Cenozoic. Two volcanic endmembers can be defined in the Cenozoic: 1) diffuse but widespread monogenetic volcanic and dike fields (e.g. Waipiata Volcanic Field, Pukaki Bank, Alpine dike swarm) and 2) shield volcanoes (e.g. Banks Peninsula, Dunedin Volcano, and Chatham Islands).
The geological processes responsible for this intraplate magmatism remain enigmatic. A mantle plume origin appears unlikely as there is no age progression in the erupted lavas in direction of plate motion, although Zealandia drifted ~ 6,000 km to its present position. This combined with the absence of an anomalous hot mantle or large extensional structures requires an alternative process to trigger partial melting beneath Zealandia. It has been proposed that the gravitationally unstable lower lithosphere was subjected to multiple delamination events during the Cenozoic. Using finite element modeling, we will test two alternative mechanisms: Rayleigh-Taylor type delamination of a dense layer at the base of the lithosphere and edge driven convection. The concept of an anomalously dense lower lithosphere is supported by the geological history of Zealandia. Located at the NW margin of Gondwana it was exposed to subduction for hundreds of million of years. Influx of subducting plate derived fluids and melts may have re-fertilized and thereby densified the lower lithosphere making it gravitationally unstable with respect to the underlying asthenospheric mantle. In addition, the relatively small lateral dimensions of Zealandia might make it particularly vulnerable to erosion by edge driven convection. We will present the conditions under which these two processes are viable explanations for the intraplate volcanism in Zealandia.

European Geoscience Union, Wien 2008 (Invited Talk)

The Origin of Intraplate Volcanism on Zealandia

C. Timm [(1)], K. Hoernle [(1)], R. Werner [(1)], F. Hauff [(1)], P. van den Boogard [(1)], J. White [(2)], N. Mortimer [(3)]

[(1)] IFM-GEOMAR, Wischhofstr. 1-3, 24148 Kiel
[(2)] Geology Department, University of Otago, PO Box 56, Dunedin 9015, NZ
[(3)] Institute of Geological and Nuclear Sciences, PO Box 31-312, Lower Hut, NZ

The origin of intraplate volcanism on continents is generally attributed to mantle plumes or continental rifting. Widespread intraplate volcanism has occurred on the primarily submarine New Zealand micro-continent Zealandia almost continuously since its separation from Gondwana approx. 100 Ma ago. This volcanism cannot be directly related to continental rifting and occurred during local periods of both extension and compression. The lack of extended volcanic belts with age progressions in the direction and at the rate of plate motion is not consistent with the plume hypothesis. Voluminous HIMU-type volcanism was associated with the Cretaceous rifting of Zealandia from Gondwana, consistent with suggestions that a mantle plume or plume head may have been involved in causing the separation of Zealandia from Gondwana (Story et al., 1999). After the "break-up" 84 Ma ago, Zealandia drifted 6,000 km to the NW. In contrast, lower volumes of eruptives were produced in the Cenozoic. Most mafic (MgO > 5 wt%) Cenozoic lavas define an array between the Cretaceous HIMU-type lavas and Pacific MORB on Sr, Nd, Pb and Hf isotope correlation diagrams, suggesting the involvement of the residual HIMU-type plume-type material and the depleted MORB source. Seismic tomography reveals a large low-velocity (presumably hot) body beneath the Chatham Rise between 600 and 1450 km depth, which can be traced beneath Antarctica (Montelli et al., 2006). We propose that the deep-seated thermal anomaly caused the final continental break-up of Gondwana and could still contribute to post-breakup volcanism on Zealandia, possibly in the form of small, short-lived upwellings similar to those that have been imaged beneath Central Europe (e.g., Granet et al., 1995). A possible mechanism for triggering such upwelling may be lithospheric detachment (Hoernle et al., 2006).

References:

1) K. Hoernle et al., 2006. EPSL, 248, 335-352.
2) R. Montelli et al., 2006. G3 7, Q11007, doi:10.1029/2006GC001248.
3) M. Granet et al., 1995. EPSL, 136, 281-296

III. CV

Christian Timm wurde am 08.12.1977 in Rendsburg geboren. 1997 schloss er seine Schulbildung mir dem Abitur an der Freien Waldorfschule in Rendsburg ab. Nach einem Jahr Zivildienst in der Behindertenbetreuung, folgte das Studium der Geowissenschaften an der Christian-Albrechts-Universität zu Kiel ab 1998. 2002 folgte das Vordiplom und 2004 das Diplom in Geologie-Paläontologie an der Christian-Albrechts-Universität zu Kiel. Seit 2004 arbeitet Christian Timm als wissenschaftlicher Angestellter am Leibniz Institut für Meereswissenschaften; IFM-GEOMAR, woraus diese Arbeit entstand.